# Development of new centrifugal microfluidic functions

Adam P. Bouchard

Faculty of Science
Department of Chemistry
McGill University
Montreal
December 2015

A thesis submitted to McGill University
in partial fulfilment of the requirements of the degree of
Doctor of Philosophy

# Abstract

Concern for the economic and environmental impact of chemical analysis has been a driving force behind the miniaturization of analytical analysis. Complex techniques require multiple procedures, highly qualified personnel, sample collection, preparation, reagent storage, waste management and equipment maintenance. The high material, monetary and time costs make the benefits of miniaturization substantial. In addition, the miniaturization of chemical experiments advances analytical chemistry, biochemistry, medicine and environmental science. Shorter diffusion times, the potential for parallelism and the conservation of reagents and samples all contribute to the motivations of microfluidic development.

However, smaller experimental volumes create many challenges that must be overcome. Seemingly easy steps on a macro-scale can become unwieldy and inaccurate when applied to microfluidics. This thesis presents the development of several new functions to overcome limitations native to small volumes in centrifugal microfluidics (CM).

CM is unique in using centrifugal force to drive liquid flow on a preparative or analytical device. The benefits of CM over traditional microfluidics are numerous. CM does not require outside connections for pumps or place limitations on the properties of the reagents in order to use electric or osmotic forces. CM can function in a larger range of volumes and is highly parallel. However, most of the benefits of CM require the constant rotation of the device. This thesis demonstrates several new functions that do not require the device to stop rotating.

Included in this thesis are; (1) a synchronized spectrometer for the measurement of visible light spectra while the device is in motion, (2) a configuration for the generation of small aliquots, (3) a modified passive valve for restricting liquid flow, (4) a liquid deposition method for reagents to a single outlet, (5) two designs for modular development of CM experiments.

# Abrege

Une préoccupation croissante pour l'impact économique et environnemental de l'analyse chimique a été une force motrice derrière la miniaturisation de l'analyse analytique. Des techniques complexes nécessitent de multiples procédures, du personnel hautement qualifié, la collecte d'échantillon, une préparation, le stockage de réactif, une gestion des déchets, et l'entretien du matériel. Ce matériel de haute complexité avec des coûts financiers conséquents rendent les avantages de la miniaturisation importants. En outre, la miniaturisation des expériences chimiques font progresser la chimie analytique, la biochimie, la médecine et la science de l'environnement. Les réductions du temps de diffusion, le potentiel de parallélisme, la conservation des réactifs et des échantillons contribuent tous aux motivations du développement microfluidique.

Cependant, de plus petits volumes expérimentaux créent de nombreux défis qui doivent être surmontés. Apparemment les étapes faciles sur une macro-échelle peuvent devenir lourdes et imprécises lorsqu'elles sont appliquées au microfluidiques. Cette thèse présente le développement de plusieurs nouvelles fonctions pour surmonter les limitations originaires de petits volumes en centrifuges microfluidique (CM).

CM est unique en utilisant la force centrifuge pour conduire l'écoulement de liquide sur un dispositif de préparation ou d'analyse. Les avantages de la CM surla microfluidique traditionnelle sont nombreux. CM ne nécessite pas de connexions externes pour les pompes, ou placer des limites sur les propriétés desréactifs afin d'utiliser les forces électriques ou osmotiques. CM peut fonctionner dans une gamme plus large de volumes et est hautement parallèle. Cependant, tous les avantages exigent de la rotation constante de l'appareil. Cette thèse présente plusieurs nouvelles fonctions qui ne nécessitent pas quel'appareil arrête de tourner.

Inclus dans cette thèse sont; un spectromètre de synchronisation pour la mesure des spectres de la lumière visible tandis que le dispositif est en mouvement; une configuration pour la génération de petites fractions aliquotes; une valve passive modifiée pour restreindre l'écoulement de liquide; un procédé de dépôt de liquide pour les réactifs à une sortie unique; deux modèles pour développement modulaire d'expériences CM.

# Contributions to Original Knowledge

1. Electrical assemblies were developed to supplement a servo-motor CM testing platform for facilitating synchronized spectroscopy: the collection of spectroscopic data from a CM device while it is in motion. The equipment allowed experiments that required spectroscopic measurements to continue without having to stop the rotation of the disk.
2. A novel method for reproducibly and repeatedly adding sub-microliter volumes of reagent to an experimental chamber was developed and demonstrated.
3. An improvement in the construction of CM devices was made through modifying the design of passive adhesive valves to include movement perpendicular (axial) to the plane of the device. These three dimensional (3D) valves were then paired with a compression valve that restricted air from venting and in order to increase the burst frequency.
4. A novel design for liquid distribution was demonstrated that allowed the addition of liquid to a single CM experiment on a device. Open microfluidics were explored for the creation of a Coriolis switch. The switch allowed for the addition of reagents and the subsequent wash solutions to an experiment.
5. Two methods of designing modular CM devices were developed. The first used a single experimental layer segmented into wedges for quick prototyping of multi-step experiments. The second used multiple layers where each was responsible for a single experimental step and could perform several iterations in parallel.

# Contributions of Authors

All instrumental work, experimental work and manuscripts presented in this thesis were developed under the guidance of Professor Eric D. Salin of McGill University.

The French abstract was graciously translated by Bernard Krebs.

All experimental work presented in this thesis was designed, tested and optimized by the author (Bouchard), with some exceptions in Chapter 2. The work of Chapter 2 was aided by the early contributions from Ling Yi Tam who assembled CM devices to test the Synchronized Spectrometer setup and then troubleshoot electrical issues. The data analysis of Chapter 2 was completed using a MATLAB GUI program designed and written by the author (Bouchard). The program was optimized and made more robust in collaboration with Alexei Kazarine. Additionally, Erin Templeton used the setup and MATLAB GUI in her publication regarding filtering and sedimentation of samples. A figure from her results is included and referenced in Chapter 2 with her permission.

# Acknowledgements

The writing of this thesis was only possible because of the support and encouragement of my girlfriend, Brittany Rocque. Thank you for listening to every project idea, editing all that I wrote and being here for me every day.

I would like to thank my supervisor, Professor Eric D. Salin, and my committee members, Professor Cameron D. Skinner and Professor Janine Mauzeroll, for keeping the projects focused. Also, I would like to express my gratitude to Professor Butler who edited this Thesis for submission.

It was a great opportunity to be a part of this lab and to work with David Duford (writing), Ling Yi Tam (spectroscopy), Alexei Kazarine (MATLAB), Matthew Kong (pumping) and Erin Templeton (sedimentation). I wish you all great careers.

Additionally, I would like thank Bernard Krebs who translated the abstract of this thesis to French.

I am also thankful that my parents, Wanda and Lucien Bouchard, were always available to be a part of this process.

# Table of Contents

# LIST OF FIGURES

**CHAPTER 5.**



**CHAPTER 6.**



**APPENDIX 1.**

# LIST OF TABLES

# LIST OF EQUATIONS

# CHAPTER 1: Introduction

## Concepts and Literature Review

Analytical chemistry techniques for the evaluation of liquid samples are well established and have benefitted greatly from the availability of increasingly affordable instrumentation. Amongst that instrumentation optical setups are a staple of quantitative analysis and have improved the ability to identify analytes in a sample. Instrumentation based on optical analysis can collect a large amount of data from a sample in a very short period of time. Despite these advantages, the analytical technique still requires a time-consuming process of preparing samples and standards. The technical capability of the user is also paramount to ensure that all of the preparative work for an analysis is conducted with minimal error. Preparation time and analyst proficiency are just some of the limitations that exist across all analytical systems and should be considered when designing new analytical tools.

Consolidation and minimization of preparative steps in analysis is of particular interest with respect to instrumentation research and development because of the benefits of reducing procedural steps and the costs associated with large volume benchtop experiments. Therefore, development of systems capable of both preparation and analysis is an aspiration in the improvement of instrumental analysis techniques. This approach expands the role of the instrumentation beyond the generation of a data point into the role of manipulating the sample through the necessary preparative steps without having a technician perform the task. In order to design this type of all-encompassing instrument the volumes of the samples would ideally be sufficiently small to enhance affordability and ease of instrumental maintenance.

The use of much smaller volumes has become a central objective of analytical development. Moreover, the reduction of sample size and reagent use has lowered both cost and time in order to facilitate the development of high-throughput analysis. In addition, the advantages to reduction of analytical volume include increased portability for performing analysis outside of a laboratory setting, as well as the opportunity to develop systems which conduct parallel analysis on a single sample. Parallel analysis enables multiple samples and/or experimental conditions to be examined. Owing to all of the theoretical advantages of small volume analysis, such as diffusion time, the development of traditional microfluidics has advanced considerably.

# Traditional Microfluidics

## Microfluidics

Analytical analysis of aqueous solutions requires the careful manipulation of solutions to produce accurate and precise results. Often, quantitative analysis requires the prudent transfer of reagents and analytes to process the sample. In a benchtop analysis the volumes of analyte required are often large and require extensive infrastructure and waste management. By using large volumes the ability to perform an analysis in parallel is limited by the cost of reagents, glassware and technicians to perform the experiment. The transition to smaller volumes creates the opportunity to reduce waste and introduce parallelism to analytical analysis.

The use of smaller volumetric glassware continues the progress towards a reduction of waste and cost, but still requires the same level of technical ability. Additionally, traditional glassware requires that every parallel process to generate replicates increases the work required of the person performing the analysis. Therefore, a technique for producing a parallel methodology needed to be developed. Specifically, in order to move towards lower volumes and

less waste it was necessary to adopt a technique for the construction of micro-scale components to control liquid volumes and movement on the scale of microfluidics. In traditional microfluidics photolithography has been predominately used for the generation of the small channels and chambers, or the generation of the design negatives which have been used for micro-molding.

## Production and Prototyping

The application of photolithography to the production of liquid-handling components has made the mass production of high aspect ratio devices possible. A high aspect ratio describes the ratio between the height and width of a feature on a device (i.e., the height is very large compared to the width). In microfabrication techniques, high aspect ratios are considered to be the goal of construction as they allow the development and incorporation of more complex features. The ability of photolithography to mass produce components with high aspect ratios has enabled greater control of liquid movement in the development of microfluidic devices.

The modern development of photolithography has been driven by the semi-conductor industry where etched designs are used in the creation of microprocessors; the technology has been adapted for use in microfluidics. Photolithography is the process of writing extremely small features onto a substrate using an electron-beam (e-beam) or laser and can be applied to microfluidics in two ways. The first is direct photolithography where the design of the microfluidic system is written onto the substrate of the device by a writing tool, either an e-beam or laser. The second method is indirect and is achieved by writing the negative of the design onto a preliminary substrate, which is then used as a high aspect ratio micro-mold for the mass production of the final device. Both methods employ a chemical process to mediate the etching of the device in a controlled manner. The control of the etching process is determined by a

chemical layer of resist that is modified by a writing tool. The writing tool will chemically alter the layer of resist to determine the etching pattern in the substrate of the device. The resist will always act as a protective layer while dry etching the substrate with plasma or wet etching with acid. The design etched features are either a positive or negative image of the intended device depending on the resist used.

The difference between the two types of resist, which is important to microfluidics, is the difference in the structures that can be created. Positive resist is used with a design that will be etched into the substrate and used as a microfluidic device. Negative resist is used when a negative of the intended microfluidic device should be etched so that it can be used as a casting mold for mass production of many equal microfluidic devices. An example of this use of negative resist is for the generation of master copies for micromolding.

Micromolding is a technique where soft polymers are introduced by pouring into a master mold created by etching negative features into a substrate. By curing the soft polymer against the small feature structures of the master mold substrate the polymer is left with the intended microfluidic design cured into its structure. The micromolding technique offers the opportunity for the mass production of devices from a single written master. This construction technique has resulted in substantial use of microfluidics by the biomedical community.[1]

The small structures generated through microfabrication have aspect ratios where the surface to volume ratio of the structure is significantly larger than in traditional systems. In lithography, a high aspect ratio describes how tall a feature can be made with the technique in comparison to the width of the feature. In the field of microfluidics, high aspect ratio components describe a channel where the surface area of the device is much greater than the volume of the liquid being controlled. This situation makes it possible for surface treatments to

manipulate the way liquid moves through the device. If surface treatments are not employed then the interaction between the sample and the material of the substrate will define the interaction and the way that the liquid moves through the device. In this thesis untreated polycarbonate substrates were used in the devices with aqueous samples. Therefore the interaction of the sample and the device was defined by the contact angle of water and polycarbonate. By employing surface treatments such as covalently bonding hydrocarbon chains to the substrate, the surface becomes greatly hydrophobic changing the contact angle and the way that the sample behaves in the channel. The effectiveness of surface treatments is increased when high aspect ratio devices are used because the surface-to-volume ratio is much higher. The more surface area, the more impactful the application of a surface treatment.

High aspect ratio devices introduce a very high surface-to-volume ratio, which makes surface tension a significant factor in the behavior of fluid flow within the device. Additionally, the properties of the interaction between the device surface and sample matrix will affect fluid flow through the device and from valves. The properties that define fluid flow behavior are essential considerations and are sometimes constraints to microfluidic system development. A focus of this thesis is the control of aqueous samples and their interactions with geometric restrictions to liquid flow. No surface treatments were used in the creation of the microfluidic devices produced in this thesis, which left the control of liquid movement to the geometric restrictions of the designs. By using geometric designs to control movement in centrifugal microfluidic devices, the deliberate design of the device is more important than manipulation with a chemical treatment enabling future researchers to use the design with any substrate appropriate for the sample of interest.

When discussing geometric restrictions to control liquid movement, it is important to first discuss the ideal situation in a high aspect ratio microfluidic device. The ideal situation is a straight and perfectly smooth channel where liquid flow is not interrupted by any resistive structures. In this theoretical scenario of a perfectly straight and smooth channel, the liquid would travel in a laminar flow pattern where parallel layers of liquid flow with no disruption between them. In application, the velocity of the layers of liquid would be different depending on their relative position to the surface of the channel. The liquid closest to the surface of the channel will interact with the substrate such that the flow will be slower than the liquid that is flowing through the center of the channel. When using microfluidics to control sample movement, it can also be advantageous to purposefully induce turbulent flow for applications such as mixing. Turbulence can be caused by liquid flow around obstructions or as a result of chemical treatment. The practical ability to control the level of laminar and turbulent liquid flow occurs on the length scale of most microfluidic devices. The amount of turbulence is also affected by the density, velocity and viscosity of the sample as indicated by Equation 1-1 where the Reynolds number is calculated. The Reynolds number is defined by the ratio of momentum forces (density and velocity) relative to viscosity. The dominant force will determine the type of flow condition. At a Reynolds number less than 2000, the flow of the liquid is determined to be generally laminar.

$$Re = \frac{\rho v d}{\mu}$$

**Equation 1-1. Reynolds number calculation for predicting laminar flow in a channel**
ρ = density of the sample (kg/m$^3$)
ν = mean velocity (m/s)
d = diameter of the channel (m)
μ = viscosity (kg/ms)

The following ranges are defined:
Laminar flow: Re $<2000$
Transitional flow: $2000<$ Re $< 4000$
Turbulent Flow: Re $> 4000$

The effect of laminar flow in traditional microfluidics is used for the prediction of the liquid behavior in small volumes and high aspect ratio channels. The control of volumes with laminar flow and large surface-to-volume ratios made measurements at the cellular level much easier to perform because the lack of turbulent flow enables accurate prediction and control of sample movement.[2] It also makes it possible to perform actions such as mixing just by having a channel deviate from a straight line. The layer of liquid that takes the "inside corner" will move ahead in the channel as compared to the layer of liquid that is traveling a longer path. A representation of this phenomenon is shown in Figure 1-1 to demonstrate one of the basic controls on sample handling affected by component design.

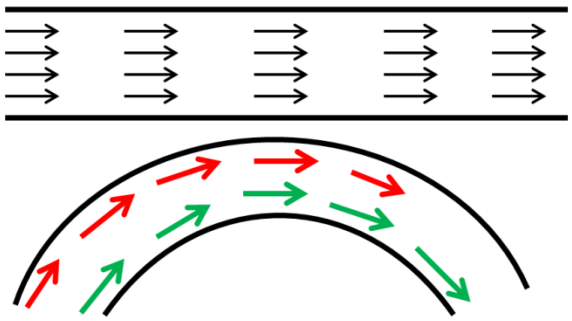

**Figure 1-1. Illustration of liquid flow in straight and curved microfluidic channels**
The description of laminar flow can be done through a quantitative calculation of the Reynolds number as seen in Equation 1-1. However, it can also be observed in the mixing that occurs in a curved channel. A liquid in laminar flow becomes turbulent in a curved channel due to the displacement that occurs when the liquid on the inside corner of a curved feature moves relatively forward by taking a shorter path. The result in the illustration is turbulence that would circulate counter clockwise in this image.

## Batch Microfluidics vs. Continuous Microfluidics

High-throughput setups and continuous sample introduction make it possible to effectively leverage the advantages of microfluidics.[3] The initial problem with high-throughput methods on microfluidic devices is the transfer of liquids onto the microfluidic device. This transition is termed the "world-to-chip" interface.[4] In continuous flow systems, the use of syringe pumps has been very effective in the consistent injection of a reagent into the device. However, batch processes and sample introduction in continuous systems required further work, in particular on solving the problem of the introduction of reagents and samples into the devices for analysis.

Many publications have presented designs focused on the connections between the macro scale and microfluidics. Some solutions, such as Atencia in 2010, were as simple as the introduction of magnets to hold tubing in place.[5] Liu et al. used a matrix design to solve the interface problem for performing 400 simultaneous polymerase chain reactions (PCR).[4] The matrix design used multiple parallel inlets for the addition of PCR substrates into the reaction chambers in order to simultaneously produce a multitude of experimental results and replicates. Mariella (2008) presented a review of designs that would allow sample preparation on the microfluidic device to perform biomedical assays which removed the need to interface bench

procedures with the device.[6] To address the interfacing issue, Ramos (2005) reviewed the status of miniaturization in sample treatments and provided a comprehensive insight into the ability to scale different preparation methods.[7] The logic of focusing on miniaturization was to accomplish multiple goals of microfluidics, including reductions of waste, cost and time. In the case of interfaces, doing preparation of samples on the device reduced the complexity of the instrumentation and infrastructure necessary to handle the transfer of liquid samples from a macro-scale to a microfluidic device. Ramos' review afforded a snapshot into the modern ability to reduce the scale of sample treatment for environmental analysis. The review identifies that miniaturization is limited by the constraints of the limit of detection and accuracy in the methodology and instrumentation.

# Micro Total Analysis Systems (μTAS)

## Lab on a Chip

In 2003, Felton wrote a paper entitled "Lab on a chip: poised on the brink" in which he discussed how Lab on a Chip (LOC) is an aspiration for microfluidic research.[8] LOC is the complete miniaturization of a benchtop macro-scale experiment so that it is constructed in the microfluidic domain. Miniaturization of an experiment reduces reagent volumes and impacts the analysis time and cost through reduced waste. The benefits of miniaturization make it an essential goal because they enable the design of high-throughput analysis. However, Felton argued that the label "LOC" is a misnomer. A number of publications had previously described microfluidic devices as LOC when the practice of continuing to perform benchtop sample preparation, delivery and detection was common. By performing integral analytical steps in traditional bulk laboratory preparations before using microfluidic devices, the benefits of reduced waste and time were limited.

Felton followed his critique of LOC with a discussion on microvalves.[9] In this letter he described the issues involved with full integration of experimental setups into LOC. Issues such as a lack of effective pumps and valves that could combine accurately and reproducibly to conduct analytical analysis. Additionally, the cost of installing effective microvalves was a prominent issue in Felton's letter. In 2005, Fiorini emphasized the impact of cost and reviewed the state of disposable microfluidic devices.[10] Fiorini's review correctly pointed out the effort to miniaturize and provided a presentation of construction methods for microfluidics. The cost of miniaturization is an important consideration because the goals of reduced waste material and analysis time are fiscal and environmental motivators.

Fiorini's review also highlighted the limitations in pumping and valving in LOC devices. Fiorini addressed the potential for complex procedures including separations by chromatography. However, separations required a large advance forward because chromatography requires precise control over liquid movement and pumping. In instances like chromatography, Felton's observation that LOC is a misnomer is demonstrated when gradients and small aliquots required for high quality separations are prepared in macro-scale methodologies off the device.

Batch separations, such as those in High Performance Liquid Chromatography (HPLC), have limitations that are amplified by application to the scale of microfluidics. In procedures requiring separations, the goal is often to purify a compound. Therefore, the processable volume is hindered by the capacity of the column. In microfluidics, a batch separation can be used for identification of a sample, however for purification in a synthetic setting the quantity is too small to be practical. In a batch separation one separation is performed at a time and can be the process and time limiting step in a procedure. Pamme conducted a review in 2007 of the ability to perform continuous flow separations as an alternative to batch separations.[11] Continuous flow

separations describe the ability of a system to handle the ongoing addition of a mixture that is to be separated. In the context of microfluidics, continuous flow is advantageous because very small aliquots of mixture do not have to be prepared or deposited so larger volumes can be separated continuously. However, Pamme's continuous flow approach is still limited by the ability to effectively overcome the "world-to-chip" issues of large connections and small volumes of sample, in addition to integration with sample preparation methods.

A review of sample analysis on μTAS was published by Crevillén in 2007, in which he discussed the application and limitations of microfluidics for clinical, environmental and food samples.[12] The focus on sample analysis provides an important shift in the application of microfluidic principles to create procedures that occur outside of an analytical lab. Clinical samples can be any bodily fluid or biopsy that must be processed on- or off-device before an analysis can occur. Clinical settings have the added difficulty of handling samples that can contain biohazardous materials or even virulent pathogens and thus the design of the device must be robust enough to ensure user safety. Environmental samples are typically less hazardous than clinical samples but these are sometimes in a matrix, such as rock or silicate deposits, that can be a considerable obstacle to analysis. Food samples are often extremely complex and require many analyses to demonstrate accuracy for regulatory bodies. Since all of these real samples have fully developed benchtop analytical procedures, microfluidic devices have replaced only small steps of the procedure while all the sample preparation must be done on a benchtop. Crevillén recognized that improvements were being made to the preparation and pre-treatment of samples so that the interface of the "world-to-chip" was simpler, but that it still needed significant development.

## Components > Operations > Functions

In 2007, Fair wrote a letter asking "Is a true lab-on-a-chip possible?"[13] The development of complex microfluidics was presented as being analogous to the development of processors and computers where individual components were designed and then combined to perform analytical tasks. Fair outlined the hierarchy that is observed when designing fully functional analytical devices. The levels of design are outlined with a selection of examples in Table 1-1.

| Hierarchy Level | Examples |
|---|---|
| Components | Valves, reaction chambers, spectroscopic chambers, channels, vents, metering, columns |
| Operations | Optical detection, small aliquots, Coriolis switch, separation |
| Functions | Full analysis of a sample by combining metering, separating, reacting and measuring |

**Table 1-1. Hierarchy of microfluidic building blocks**
The table lists the three tiers of microfluidic tools. The first, components, are the simplest and are used to build elemental operations. Operations are then combined in various methodologies to complete whole functions. The creation of new operations was the focus of this thesis. Individual components such as valves, channels and metering were assembled in novel configurations to produce new operations for future centrifugal microfluidic (CM) μTAS.

The most sophisticated level of microfluidic design is a complete function that executes all the steps of an analysis. This highest level would be composed of an elemental set of operations that were each responsible for a step in producing the whole device function. These elemental operations would be actions like transport, preparation, detection, etc. The most basic level is the set of structural components that make up the operations. This level of design is made up of channels, valves and different techniques to use varied substrates. The combinations of functions are then used to complete a full experiment from sample preparation to analytical output. The conclusion is that true lab-on-a-chip is possible as long as operations continue to be developed.

## Programmable Microfluidics

A new interpretation of the μTAS paradigm was Miro's 2007 publication of a "lab-on-a-valve" where microfluidic junctions would be responsible for the integration of increasingly complex functions into LOC designs.[14] The use of complex valving would be paired

with a downscale of continuous-flow systems to a programmable flow that would control both liquids and gases. Continuous-flow systems have been discussed as being ideal when compared to serial batches, especially for separations. However, Miro identified that the ability to program liquid movement by valves would allow logical steps to be included in the design of a LOC. The work of this thesis follows the programmable paradigm by using passive valves to restrict liquid movement until sufficient pressure is generated to burst the valve. As a single direction gate the valve allows the experimenter to determine when a step is complete and when it is appropriate to progress to the next operation.

Iverson evaluated the advances of microscale pumping in 2008.[15] The micropumps he considered did not rely on large syringes or gravity pumps to drive liquid flow, but instead used various designs to cause small volumes of liquid to move through the channels of the device. The pumps discussed fell under two major categories; 1) mechanical displacement and 2) electro- and magneto-kinetic. The more limited of the two categories is electro- and magneto-kinetic pumps which use an electromagnetic field to induce flow within the fluid in the device. This situation requires that the fluid be responsive to electromagnetic effects, which limits the practical application for widespread adaptation. Mechanical pumps are more varied and use physical interaction to drive liquid movement within the microfluidic device. These mechanical pumps include various designs such as diaphragms which are moved to create high and low pressure areas within the fluid located on the device. Diaphragms constitute the most common on-chip pumping methodology.

A review article by Ohno in 2008 focused on recent advancements and the rise in publications related to integrated microfluidic chips with applications in analytical chemistry and biochemistry.[16] This review included papers addressing all the components discussed in this

introduction and presented a future outlook on the importance of continued miniaturization. The goal of improvement in miniaturization involves the integration of multiple components into a single chip so that complete devices would be closer to fulfilling LOC status. The fields highlighted by Ohno included point-of-care (POC) clinical diagnostics where complete integration is a necessity in the function of such a device.

Mark et al. published a review of LOC platforms in 2010 which broadened the scope of expected capabilities to include automation and parallelization.[17] The programmable LOC designs that Miro discussed with respect to "Lab on a Valve" required that decisions be made during an experiment. These decisions can be logic based and use triggers within the device or they can be executed by the user. The goal of automation is to create LOC designs where the user can input samples and the output would be a usable result rather than an intermediate outcome. Programming the device through valving increases the system's ability to handle a sample through the entire experiment. Running multiple samples in parallel on the device is important for increasing confidence in a result through replicates. Additionally, parallelization permits multiple end results to be produced from a single sample input. This is an important component in POC diagnostics when the ideal goal is to use as small a specimen as possible from the patient while providing as much relevant information as possible. The discussion by Mark et al. included commercial applications, such as pregnancy and drug tests which could be used by the untrained public. The commercial applications described were seen as true LOC designs that did not require bench chemistry to prepare samples.

In 2012, Arora published a review of the latest μTAS developments which expanded upon the biomedical focus of Ohno's review and further included aspects of microfluidic operations; fabrication, assembly, optics, liquid control, sample preparation, separations and applications

amongst others.[18] Arora used the statement "Stand Operations" to present the most common functions that can be integrated into a μTAS to create a functioning LOC. This is another way of viewing the components and operations as described earlier by Fair. Both authors describe the compiling of individual microfluidic technologies to perform a complete analysis. The importance of flow control by using a combination of pumps, valves and switches to accomplish analytical goals is critical to the function of "Stand Operations". In order to effectively utilize these "Stand Operations", control through a programmable "Lab on a Valve" is necessary where "Lab on a Valve" is a device in which operations are controlled by restricting liquid flow with valves that are user-defined in order to execute an analysis. User-defined describes a system where the experimenter is able to modify the parameters of the experiment by making decisions regarding the next step in the process. Valving in a microfluidic device allows a pause in the experimentation as a sample moves from one part of the device to the next and an opportunity to manipulate the sample based on intermediate feedback from previous steps.

To overcome the need for external connections, Hoffman proposed the use of ampoules for pre-storage of liquid reagents in μTAS.[19] The long-term storage afforded by ampoules was beneficial as LOC development goals turned towards portability, standardization and ease of use by the general public. The storage of reagents on the device is an important consideration when designing analytical techniques, many of which have been standardized and packaged into kits for mass utilization by laboratories. Reagents such as indicators, catalysts and standardized solutions that are required to complete an experiment would all have to be provided by the user and added to the LOC if there is no storage methodology. By storing reagents on the device, the required benchtop preparation is reduced and more analytical functions can be included in the

LOC design to approach the ideal goal of μTAS. This also increases the ability of the general public to use the device since only the sample and the device are required to produce a result.

## Miniaturization

In 2012, Rios published a review that covered the future miniaturization of LOC designs.[20] In this review, he suggested that LOCs can be roughly categorized in two groups. The first group is in bioanalytical fields such as POC devices and molecular or organismal analysis while the second group is routine analysis in environmental and industrial fields, amongst others. Rios discussed designs that had application to routine analysis and expanded upon why there is limited application of these designs in analytical laboratories. These limitations included sample transfer, column variance in separations, production expenses and detection limits.

In 2013, Rios followed up his review of miniaturization with a review of sample preparation for μTAS.[21] This review expanded upon the limitations of sample transfer, discussing the misnomer of a total analysis system when sample preparation is widely executed outside a device. The discussion included identification of three major aspects of sample preparation; (1) pulling of analytes from a sample matrix, (2) sample pre-concentration and (3) handling of biological samples.

Both of Rios' reviews covered the current state of microfluidics and defined it as consolidation of increasingly complex functions into complete LOC devices. This consolidation occurred as the components were miniaturized, standardized and proven to be reliable and accurate for analytical use. The fidelity of these devices was considered an extremely high priority as the primary driving force behind their development was their application in biomedical and clinical work.[22]

# Centrifugal Microfluidics (CM)

Felton wrote a letter in 2003 entitled "CD Simplicity" focusing on a branch of μTAS called Centrifugal Microfluidics (CM).[23] CM encompasses devices where the operations use centrifugal force as the driver for liquid movement. In CM, the device is often assembled from layers and mounted on the spindle of a motor and rotated at frequencies that overcome the interactions of the liquid with the high surface area of the microfluidic device. An example of the layers for assembly and their placement on a spindle is shown in Figure 1-2, with images drawn from Chapter 4 of this thesis.

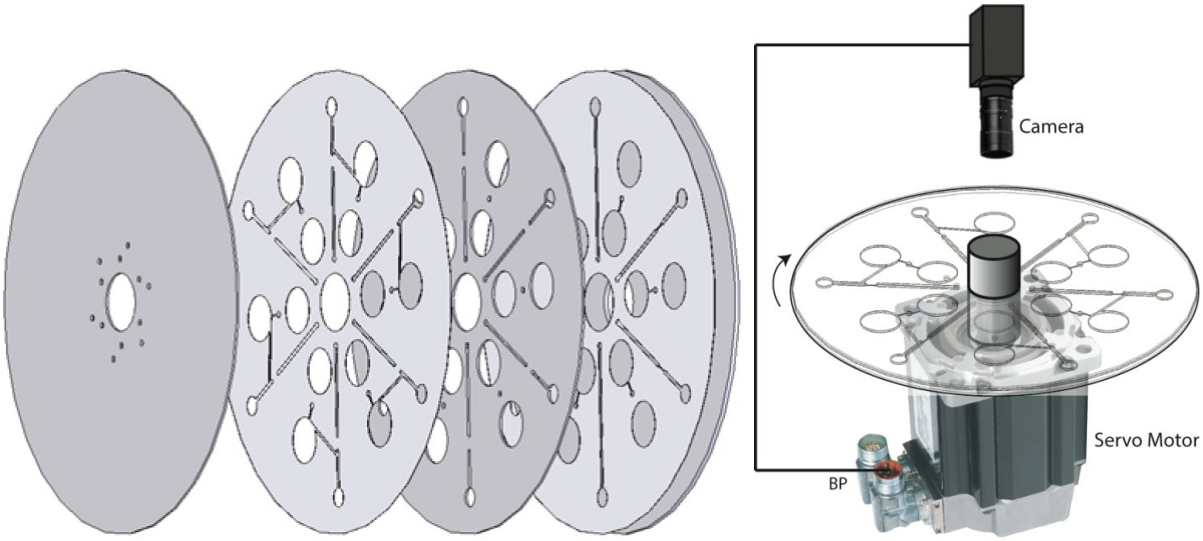


**Figure 1-2. A multilayered CM device is laminated together and mounted on a spindle for analysis**
The two images come from Chapter 4, Figure 4-6 (left) and Figure 4-8 (right), of this thesis showing the construction and analysis of enhanced passive valves on a CM device. The motorized spindle is wired to a camera to observe and record the experiments occurring when the device is rotating.

"CD Simplicity" discussed the current and potential advantages of CM as a form of LOC design. Discussion in this thesis addresses the many advantages to the use of CM over traditional microfluidics; however, at the time of Felton's review the potential advantages were larger samples, no electro-kinetics, no micropumps and parallel analysis. Additionally, the review

briefly discussed the commercial applications built by Tecan, Gyros and Burstein Technologies as examples of market driven designs.

The first centrifugal analyzers developed in the 1960s and 1970s were coarse and much larger than the current microfluidic volumes. Compact Disk (CD) manufacturing provided a standardized platform size and a medium that was inexpensive enough to develop single use CM μTAS. The construction of CM devices in this thesis was based on the versatility of the CD approach described by Felton.[23] The experiments were single use prototype designs that would be improved each iteration. The designs were milled from polycarbonate and layered using double-sided, cold-laminated adhesives. Milling is the act of removing material from a raw material substrate until the desired shape remains. Milling is a subtractive manufacturing process because a volume of material is removed from the original substrate. In the case of microfluidics, the milling creates the channels and chambers leaving behind empty volume for liquid movement and analysis. This method of manufacturing requires that the device have structures large enough that mechanical ripping of material with an end-mill can produce a precise and consistent product. Also, a milled microfluidic channel or chamber will require that the device be capped with an additional layer in order to enclose the volume that liquid will flow through.

Cold lamination is the process of using mechanical pressure to compress layers of material until they become a single unit by using double-sided adhesive. The benefits of polycarbonate made it an exceptional choice for building aqueous microfluidic components. The benefits include its use in CD and DVD manufacturing which provided standardized blanks, its easy milling and relatively unreactive properties to aqueous solutions.

In 1999, Duffy described CM devices that were constructed using two methods. The first method was casting polydimethylsiloxane (PDMS) with molds fabricated using

photolithography.[24] In a casting process, the structure of the device is created by developing a negative of the channel and chamber structure of the device using photolithography to remove material by wet or dry etching. The fluid material of the intended microfluidic substrate is then cast over the negative. Casting a structure is when a melted material is poured over the negative and cured to become solid, thus creating the required microfluidic structures. Curing can occur either by drying or by polymerization. This method can repeatedly use a single negative until the aspect ratio of the features is compromised by the act peeling the completed microfluidic device from its mold. In contrast, when hot-embossing the negative produced by lithography is used as a stamp to press the substrate and leave the desired microfluidic structures behind. Hot embossing requires that the substrate have a glass-transition temperature so that it can be molded without melting.

The second method of Duffy in 1999 involved milling the structure from poly(methyl methacrylate) (PMMA). Duffy characterized the fabrication of the devices, discussed the earlier methodologies of photolithography and micromolding, before describing the milling technique used. Duffy used a combination of milling and micromolding by milling the master microfluidic device out of PMMA, using it as a template for micromolding by casting a negative and then generating a copy of the master PMMA device in PDMS. In the devices constructed by Duffy the flow rates generated at different rotational frequencies were characterized empirically by stroboscopic video microscopy. The images generated timed the filling of a known volume chamber. In addition, the burst frequencies of passive valves ranging in diameter from 20 to 500 μm were determined empirically by the same stroboscopic technique by increasing the rotational frequency of the device by 10 RPM each second.

After characterization of CM principles, Duffy successfully performed 48 simultaneous enzymatic assays of bovine blood. This success was qualified by acknowledgement of the CM limitations, viz. (1) the rotating system required complex optical systems for capturing data related to the components in the CM device, (2) the direction of liquid movement cannot be reversed and (3) unlike electromagnetic pumping there is no in-line separation method built into the design. This thesis addresses complex optical systems in Chapter 2 (Synchronized Spectroscopy) and reversal of liquid flow in Chapter 3 (Small Aliquots).

In 2004, Zoval wrote a chapter in the Proceedings of the Institute of Electrical and Electronics Engineers (IEEE) entitled "Centrifuge-Based Fluidic Platforms"[25] in which he outlined the benefits of centrifugal force for driving liquid movement, including the lack of reliance on external pumps and the restrictions on the sample required by electrochemical pumping. The use of external pumps for traditional microfluidics created issues for the difference in volume that occurs in the world-to-chip interface. By using centrifugal force, the interface to drive liquid movement is not present and a larger range of microfluidic volumes can be used.

Zoval's chapter also introduced passive valves, metering and the highly parallel nature of CM. The devices of this thesis employed passive valves that restricted liquid movement into batches and sequential steps that were described as "Lab on a Valve" by Miro.[14] Passive valves were used for restricting liquid movement as a function of the rotational frequency of the device. An active valve would restrict liquid movement regardless of the rotational frequency and would only allow liquid movement if some other trigger occurred. In some cases active valves include diaphragms that must be moved from blocking a channel, melting wax blockages, or brittle material that must be broken to allow liquid to flow. In the case of this thesis, passive valves were used to restrict movement by having a geometric restriction to flow. Passive valves do not

require changing the structure of the device by removing or destroying a component actively blocking the flow of sample to the next operation. Passive valves can be a combination of geometric restrictions, venting manipulation or chemical treatment to modify the affinity of a material to the sample. Chemical treatment of the surface was not implemented in this thesis so that the versatility and cost of production was not hampered in future development. Additionally, by designing geometrically- and venting-restricted valves, the chemistry of future systems is not limited. The chemistry referred to is the interaction of the reagents and samples of interest with the substrate housing the microfluidic channels. The chemistry also refers to any interaction that can occur between surface treatments, additives or interfaces between the sample and other liquids or gases within the microfluidic device. Avoiding chemical treatments to change the hydrophobicity and additives such as wax to impede liquid movement meant that the designs of this thesis were more general and can be implemented in a wider array of future experiments.

Metering in CM is traditionally performed by having a chamber that is able to be over filled with reagent so that the excess volume can be drained off to waste. The volume of the aliquot from the metering chamber is determined by the volume of the chamber that is below a channel that leads to waste. This is a distinct advantage over traditional microfluidic devices where exact aliquots cannot be generated by overfilling a chamber of an exact volume. CM can do this while traditional microfluidics cannot because CM commonly has a gaseous headspace. Having a gaseous headspace means that there is venting which allows a portion of the sample to be removed without leaving a vacuum or having a liquid-liquid interface.

The highly parallel nature of CM is a key advantage over traditional microfluidic devices. Centrifugal force is equal on all segments of the CM device that are equidistant from the axis of rotation. This allows an exactly equal application of force to operations at the same radius

simultaneously on the same device. The calculation of the force applied and impact of the radius is shown in Equation 1-2.

$$F = m\omega^2 r$$

**Equation 1-2. Formula for Centrifugal Force**
The centrifugal force (F) is equal to the mass in kg (m), multiplied by the angular velocity in seconds$^{-1}$ (ω) squared, multiplied by the radius. The equation demonstrates that at equal radii on the same device and the same mass of sample, CM operations will experience the same force.

On a traditional chip-based microfluidic device multiple pumps would be required to drive experiments in parallel which introduces potential sources of error, while in CM the application of equal force at the same radius of the device greatly increases the potential for parallelism. Using Equation 1-2 to calculate the centrifugal force demonstrates that all passive valves in CM located at the same radius will burst at the same time. The implication is that the same passive valves cannot be used at all radii of the CM device and is shown in Figure 1-3.

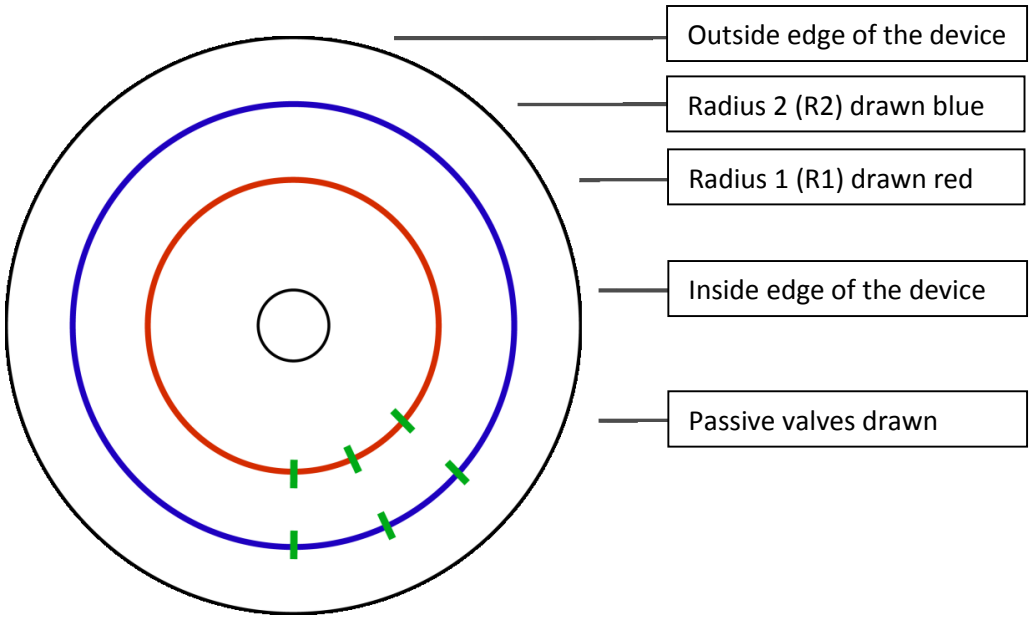


**Figure 1-3. Representation of equal application of centrifugal force at equal radii**
The inner radius R1 will have less centrifugal force at the same rotational frequency as R2. All of the components assembled at R2 will experience the same centrifugal force making the construction of parallel experimentation a matter of replicating the same functions in different segments of the device. The changing centrifugal force as the radius increases outlines why the same passive valves cannot be used at different radii. If the same restrictive valve were used at R1 and R2, when the rotational frequency is sufficient to burst at R1, it has already surpassed the burst frequency of the same valve at R2.

Madou made a direct comparison of the capabilities of CM versus traditional microfluidics in 2006 and expanded upon the work of Zoval by providing more discussion of the benefits CM afforded researchers.[26] It was noted that CM can handle a larger range of microfluidic volumes than other methods with the same operational design. The application of centrifugal force to drive liquid movement is not contingent on the limitations of a mechanical or electromagnetic force. In the case of POC devices where fully integrated operations are necessary, mechanical pumps are limited by stroke volume and the ability to generate enough force to move a larger volume of liquid. Electromagnetic pumps are limited by field strength and the ability to overcome attractive forces between the reagent and the substrate of the device. The use of on-chip pumping methods avoids the "world-to-chip" interface. CM does not require the integration of those limited and complex pumping methods or an interface between the pumping mechanism and the components of the device. As discussed earlier, the development of valving and micropumping to control small volumes was necessary to miniaturize traditional LOC designs to more completely meet the aspirations of μTAS. The advantage of CM in not requiring those pumping components is that the designs of valves and micropumps were so specific in their tuning that they had limited application from one experimental device to the next.

An important generalization of the strength of traditional microfluidics and that of CM is the difference between batch operations and continuous operations. In CM, the versatility of valving and liquid control lends itself to the design of batch operations where a sample is handled and analyzed in reaction chambers before passing through a valve to the next component. Traditional microfluidics excelled at continuous process analysis where the sample is pumped continuously through the device and is reacted and analyzed in real-time. This is a function of how liquid movement is most often driven by external pumps.

In order to restrict movement from one reaction chamber to the next, geometric restrictions such as passive capillary valves are used in CM. The passive valve restricts liquid flow until a critical burst frequency is met. At the burst frequency, the pressure of the liquid is high enough to overcome an opposing force in the form of a chemical treatment (e.g. hydrophobic surface) or geometric design feature (e.g. small channel). In 2007, Ducree published his work regarding a Bio-Disk Platform that included the theoretical derivation of the competing variables in a geometrically restricted passive valve.[27] Using Ducree's equations it was possible to calculate the predicted burst frequencies of passive valves used in this thesis. The equations and application are discussed in this Introduction-*Enhanced Passive Valves* page 34 and again in Chapter 4 of this thesis.

Manipulation of the burst frequency is possible through the design of chamber geometries and channels to change the head height of the liquid. If there are two chambers with the same radial location that are filled with two different volumes of liquid and have the same passive valve at the bottom, then the liquid with a smaller volume will have a smaller head height and have a higher burst frequency. The smaller volume of liquid does not fill as much of the chamber and the column of liquid above the passive valve is smaller. The head height of that column is measured by the difference between the outer radius of the liquid and the inner radius of the liquid sample. With less head height the pressure applied on the geometric restriction of the valve is reduced and the burst frequency of that valve is increased.

Furthermore, reagent selection and modification of a reagent through additives can greatly impact the burst frequency of a valve. The addition of a surfactant to a reagent will change both the surface tension ($\sigma$) and the contact angle with the substrate ($\Theta$). In Chapter 3 of this thesis a detergent surfactant was used to test preliminary designs for the delivery of small aliquots to a

reaction chamber. The surfactant reduced the surface tension and contact angle which made the valve burst at a markedly lower frequency.

Similarly, the choice of construction materials affects the predicted burst frequency. When an adhesive valve made of polycarbonate is used, the contact angle is slightly hydrophilic. Through the selection of device substrate the contact angle can be manipulated and the function of the device can be tuned. Additionally, the surface of the substrate can be modified with chemical treatments to change the hydrophobicity of the device. In this thesis only two substrates were used for the creation of valves. The majority of valves were cut into the adhesive layers with the same contact angle as polycarbonate. A second type of valve used in this thesis was the passive glass capillary valve. This valve type was used in the construction of the small aliquot device described in Chapter 3 and in the modules in Chapter 6. Glass capillaries have a much smaller radius than valves cut from adhesives.

With predicted burst frequencies an experimental design could be constructed where liquid flow from the center to the outside of the CM device is controlled by rotational frequency. Ducree's description of these passive valves as the junction between growing numbers of individual unit operations is the same programmable paradigm discussed by Miro in "Lab on a Valve" in 2007. The use of these valves to combine unit operations greatly increased the complexity of CM devices when assembled in series. This is a direct reference to the goal of combining stand operations into larger more complex total analysis systems.

Gorkin's 2010 review article on CM for biomedical applications emphasized the limitations of passive valves and channels for controlling the flow of liquid due to the exact requirements of balance between geometric shape, rotational frequency, viscosity, chemical treatments and location on the disk.[28] Gorkin viewed the same variables that have been described

as increasing the tunability of the burst frequency as a detriment, especially when discussing reagents that have different surface tensions, contact angles and viscosity. This thesis used only aqueous solutions which made the manipulation of passive capillary valves versatile in their application. It was highlighted by Gorkin that the benefits of passive valves are numerous for CM LOC in custom device designs because of the tunability afforded by the number of variables available to the experimenter. However, Gorkin noted that passive valves were limited in their ability to bring versatility to standardized components where changing reagents, volumes and rotational frequencies all affect the burst frequency.

## Construction of CM Devices

The construction of CM devices for this thesis was based on the use of standard size polycarbonate CDs and DVDs, 120 mm in diameter. Kido (2007) described the assembly of multilayered CM devices which employed polycarbonate disks with double-sided, cold-laminated adhesive.[29] Kido milled features into the polycarbonate layers and used xerography to cut the double-sided adhesive before treating the layers and cold laminating them together with a press. Lafleur (2009) published the construction method used for devices in this thesis based on the procedure shown by Kido.[30] The method described rapid prototyping through subtractive manufacturing of layers that can be assembled into a functioning Lab-on-a-CD. The method used by Lafleur was the same process used for the construction of devices in this thesis. The complete description and references for materials and tools used is provided in the first experimental section of this thesis in Chapter 2, page 8. Deviations from that construction process are outlined in the applicable experimental sections of following chapters.

A significant difference in the method of Kido and this thesis is in the preparation of the layers for lamination. Kido treated the surface of the polycarbonate using oxygen plasma. Kido's

experiment also involved the addition of a slurry to the experimental chambers during the assembly. The slurry required that the devices be dried under vacuum for a day before use. Both the oxygen plasma treatment and drying step were not used for the devices in this thesis, which made use of commercially available detergent and water to clean the polycarbonate followed by rinsing with 95% ethanol and drying with lint-free tissues before assembly.

CM devices constructed in this thesis had the layers of polycarbonate and adhesive assembled in a repeating pattern. The most basic design had a single experimental layer where there were three polycarbonate disks, including a top and a middle where the experiment would take place and a bottom. The three layers of polycarbonate were affixed using layers of adhesive for a total of five layers in the device. However, in more complex 3D designs, such as the modules of Chapter 6, the device was composed of up to 17 laminated layers.

The construction method of Lafleur was highly effective in its ease of design, cutting and assembly. The ability to prototype new components quickly is a great advantage afforded by a subtractive process that does not require the creation of master molds as is expected in micro-molding techniques. This methodology is not recommended for high throughput manufacturing or for the mass production of any components, but was effective in producing iterative improvements to the work presented in this thesis.

## Optical Detection in Microfluidics

Optical detection is broken down into two classifications when working with microfluidics. The first classification is “off-chip” and the second is “on-chip”. Off-chip involves using macro-scale external infrastructure to observe samples in a microfluidic component. This is an important classification as it allows the development of stationary multi-use equipment. With an aim of microfluidics to be affordable and consumable, the ability to keep optical

equipment off-chip while still effectively interfacing with the microfluidic operation is vital. However, off-chip infrastructure antagonizes the aspiration for microfluidics as a total analysis system. Additionally, portability becomes a concern as more off-chip infrastructure is added to a device for every operation. On-chip describes the integration of micro-scale sensors into the microfluidic device. As a solution to off-chip design, the integration of micro-scale components to support analytical operations also drives the cost of development and production higher while fulfilling the aspiration of μTAS.

In 2007, Kuswandi published a review on the status of these two classes of optical detection.[31] In the review options for measuring absorbance, fluorescence, chemiluminescence and refractive index were cataloged. Myers observed in 2008 that microfluidics had not produced POC devices for medical diagnostics in a volume expected based on the number of academic publications, especially given the volume of detection methodologies discussed by Kuswandi.[32] Myers stated that the major obstacle to development was the balance between cost, sensitivity and portability of a device. Moreover, the small geometries of microfluidic components are not advantageous to robust methods of detection such as absorbance and fluorescence. The reviews focused on the innovation of optical technologies for microfluidics and Myer's focused on the point that integration of optical techniques into microfluidics would greatly improve the ability of POC diagnostic devices. Furthermore, Myers recognized that the miniaturization of conventional optical methodologies discussed by Kuswandi would not be able to compete with the efficiency of macro-scale methods due to the geometric restrictions of path length. CM was discussed in this review, specifically, Steigert's work in 2006 which used a laser to detect alcohol in whole blood after a reaction with a colorimetric dye.[33] Steigert's work includes the real-time measurement of a CM cell while the device was in motion at 480 RPM. Steigert

overcame the issue of a short path length through the use of total internal reflection. Monolithic features were inserted into the device that had the correct index of refraction to guide light into the plane of the device. A limitation of this method was the necessity for constructing total internal reflection components and that the integration of light is defined by the time that the reflector is passing through the laser beam.

With the geometric considerations described by Myers in mind, the most likely conventional methodology to be used in microfluidics was fluorescence due to its low limits of detection and the fact that path length is not a major consideration. Focusing on fluorescence, DeMello (2009) developed components for the integration of polymer light-emitting diodes (pLEDs) and organic detectors into traditional microfluidic devices.[34] One experiment that DeMello performed with this setup was the observation of the fluorescence lifetime of rhodamine B in solution as a function of temperature. The pLEDs had the advantage of being smaller and more energy efficient for the incorporation into a μTAS. This example of an on-chip method is powerful for implementation in traditional microfluidics, though in CM devices, the space available is more limited and the motor must be able to handle the additional weight and balance issues introduced by affixing instrumentation to the device. The value added by an on-chip methodology must also be weighed against the added cost of integration of complex components like pLEDs and organic detectors into one time use microfluidic devices.

Mogensen published a review in 2009 that also made the observation that the development of on-chip optical detection is limited. The review discussed how the inclusion of optical components into microfluidic devices was ideal given the benefits of miniaturization but recognized the limitations of scale.[35] The review outlined the trend of exploring different polymers to solve the issue of cost and mass production of optical control on a microfluidic

device and concluded that optical techniques are still the strongest methodology for detection even when all its limitations have been considered.

Duford published a spinner and strobe setup in 2009 that was used for the collection of images while CM devices were in motion up to 50 Hz.[36] The setup was composed of a servo motor that triggered both a strobe light and a black and white digital camera. It was capable of saving one image approximately every second. The system built and presented by Duford was used in the development of this thesis. The servo motor provided the absolute position of the CM devices and made the synchronized spectroscopy presented in Chapter 2 possible. In addition, the images in this thesis were taken with the setup described by Duford with the replacement of the black and white camera with a color digital camera (GRAS-14S5C-C, Point Grey, BC, Canada.)

In this thesis, an off-disk instrumental setup for the synchronization of an LED light source and an Ocean Optics photo-diode array spectrometer[37] is described in Chapter 2. The demonstration was made successful by the triggering of electronics by the servo motor when the spectroscopic cell of interest was in the correct position. The setup was able to measure absorbance in real-time at a range of rotational frequencies and allowed the quantification of intermediate steps. In contrast to the work of Steigert, the method described in this thesis did not use a laser; instead, a white light source was utilized in order to collect spectral data over a range of wavelengths. The synchronized spectrometer used the trigger of the servo-motor to coordinate the rotation of the device with the pulse of the LED light source and the integration of the spectrometer to measure light passing through the spectroscopic cell rather than a reflector to divert light through the cell.

In either a continuous or batch microfluidic device, the ability to collect real-time data of any intermediate steps is an important consideration in the development of more complex analytical operations. It is envisioned that the development of real-time optical data collection for CM devices will provide the potential for accurate measurement of titrations, elutions for chromatography and sedimentations. This work is an improvement over the system developed by Steigert in that it is functional across the visible light spectrum, requires no manufacturing or insertion of total internal reflection components to guide light into the plane of the device, can occur at a range of rotational frequencies and has an integration time independent of rotational frequency.

## Repeatable Small Aliquots

The ability to generate accurate and reproducible small aliquots on CM devices has traditionally been done through the use of metering where liquid flows into a chamber of a known volume and excess is diverted to a waste chamber. An example of this type of metering was demonstrated in 2007 when Steigert published a design that was used for the analysis of whole blood.[38] The metering would occur when the matrix, whole blood, would enter a chamber with a volume smaller than that of the sample with a channel drained to waste. This channel for overflow of sample was placed at the top of the chamber so that centrifugal force filled the chamber from the bottom (located at a larger radius than the top) before overflowing. The result was an aliquot of whole blood with a known volume of 500 nL that remained in the chamber and could be used for analysis. After aliquoting by pouring excess sample to waste, the centrifugal force of the device separated plasma from whole blood at a high rotational frequency. A siphon then drew off the plasma from the hematocrit/cellular layer. This design concept was simple, robust and capable of being used repeatedly if there was a way to continuously fill and drain the

metering chamber. In Chapter 3 of this thesis, the metering chamber used to generate small aliquots of reagent had an exit valve that allowed the metered volume to flow into a receiving chamber without the use of a siphon. By not using a siphon it was possible to completely drain the metering chamber so that it could be refilled and reused.

In 2011, Mark described a design in which the reagent of interest filled multiple metering chambers.[39] This design had the sample of interest flow through a channel with openings to chambers of known volumes along its length. The sample would flow through the channel while filling each of the metering chambers with an exact aliquot. In Mark's design, the sample poured off to waste after flowing past all available individual metering chambers. This design was innovative in its transition from a single sample to multiple aliquots as sample preparation occurred before the filling of multiple metering chambers. It was also an example of a spiral design where the liquid flowed from the center of the device to the edge slowly because the channel did not follow the radius of the device. The channel feeding the metering chambers became progressively farther from the center of the device and allowed the multiple metering chambers filled by the process to be situated in different sections of the device so that larger and more complex functions could be installed. This spiral influenced the design of the spiral deposition of Chapter 5 in which the liquid of interest flows towards a single outlet as it is deposited on the device while in motion.

Missing in the literature were integrated small aliquot dispensing components that did not drain samples or reagents to waste. For example, Lafleur demonstrated a low waste methodology for the pre-concentration of trace metals on a CM device but required a micro-pipette to load small aliquots onto a stationary disk.[30] To overcome the need to stop the device to load a second aliquot, a design was created based on the idea that the metering chamber must be refilled and

used repeatedly. This concept was drawn from the work of Kazarine and Kong in 2014.[40] Their work used Kong's pneumatic pumping system[41] to recirculate reagent from the edge of the device to the center so that it could repeatedly pass through a metering chamber where the less dense liquid would drain to a collection chamber. This is the type of refilling that Steigert's metering chamber did not have. However, the volume of the metering chamber in Kazarine's device was 25 μL. This thesis aimed to produce a sub-microliter aliquot design which could repeatedly deliver to a single receiving chamber.

Dispensation of multiple small aliquots is demonstrated in this thesis with the expectation that it will be an integrated component of a CM device that cannot have the rotation stopped. Establishing the requirement that the component be able to work without the cessation of rotation is a constraint that drives the production of CM devices that are robust in their design and application. As stated earlier, some issues encountered with CM can be counteracted by ceasing rotation but that negates the benefits of constantly applying centrifugal force on the liquid in the device.

The design for small aliquots was drawn from this author's (Bouchard) earlier work. In a chamber that was not vented, trapped air on a CM device generated a pneumatic pressure that would serve to drive the liquid against the centrifugal force.[42] The design utilized a compression chamber that was not vented to atmosphere but was connected to a chamber with reagent to be driven to the center of the device from its edge. A driving liquid from an inner radius would be released at a high rotational frequency to compress air in the chamber that vented to the reagent to be driven. When the rotational frequency of the device was reduced the pressure overcame the centrifugal force on the liquid at the edge of the device to drive it radially inwards to a receiving chamber.

In the small aliquot design of this thesis, trapped air was responsible for moving liquid radially inward past a metering chamber when the disk was at a low rotational frequency. Unlike the earlier design of Kong and this author (Bouchard), which used a driving liquid to compress the air, the reagent of interest would compress the air in the compression chamber. The energy of the compressed air would be stored and move the reagent radially inward when the device was at a lower rotational frequency. When the liquid would move inward it would flow past the opening of a metering chamber and fill it.

At a high rotational frequency the air was compressed and the liquid moved away from the metering chamber. By raising the rotational frequency further, the valve at the base of the metering chamber drained into an experimental chamber. The design of this component drew on a concept presented in a paper published by Zehnle in 2012 which referenced this author's (Bouchard) earlier work.[43] Zehnle's design used the compression chamber as a way to store energy to drive liquid movement inward on the CM device in order to prime a siphon that draws the reagent to the center of the device at lower rotational frequencies. The operation presented in this thesis has a channel that is designed to not wick the liquid through capillary action so that the liquid can be easily transported past the opening of the metering chamber for multiple aliquots.

The ability to predict the functionality of these trapped air components in CM devices was described by Gorkin in a 2010 paper entitled "Pneumatic pumping in centrifugal microfluidic platforms".[44] Gorkin presented a full description of the equations that governed the compression of the trapped air at different frequencies. There was good agreement between the experimental and predicted location of liquid at different frequencies across a range of 0 to 7000 RPM. Gorkin used the equations to predict the height of the liquid as it compressed the air in the unvented

chamber. However, in this thesis the rotational frequencies were determined empirically for the generation of small aliquots since each aliquot of liquid removed a volume of reagent from the aliquoting liquid.

## Enhanced Passive Valves

Passive valves in CM Devices have been extensively used in designing multi-step analytical experiments that are not continuous flow. The use of passive valves ensures that liquid flow does not occur unless pressure is sufficient to overcome the restriction of the valve. In a CM device, this allows for serial components to be connected to construct an operation where analytical or preparative steps can occur before liquid flows to the subsequent chamber.

In 2003, Feng discussed the use of passive valves based on hydrophobic microfluidics.[45] He used a traditional microfluidic chip with a single channel to demonstrate back pressure in an aqueous reagent caused by the addition of a hydrophobic valve to the channel. The pressure of reagent required to overcome this particular construction was found to be 490 kPa. This meant that when there was less than 490 kPa of pressure driving the liquid, the liquid would not flow past the hydrophobic stop. Feng's valves were a combination of geometric restriction and a chemical surface treatment with hydrophobic organic chains covalently bonded to the silica substrate. By constricting the width of the channel the impact of the hydrophobic surface treatment was increased and the valve was better able to resist flow of the aqueous reagent.

It is also possible to restrict liquid movement by the use of only a geometric restriction without bonding hydrophobic chains to the substrate. The restriction relies on the contact angle of the solution with the substrate and the surface tension of the solution to resist flowing into a receiving chamber. The functionality of such geometric restrictions for use in valving was explored by Cho in 2007. Cho's paper presented a theoretical derivation of equations for the

bursting of these geometric passive capillary valves.[46] The basis of the derivation were observations made by Squire concerning the physics of fluids at the nanoliter scale.[47]

This thesis used the simplified equations of Ducree for the calculation of theoretical burst frequencies.[27] The calculation is shown in Equation 1-3 where the variables are used to tune the burst frequencies in the design of CM devices.

$$\nu\,(Hz) = \frac{1}{\pi}\sqrt{\frac{\sigma|cos\Theta|}{\rho r \Delta r d}}$$

**Equation 1-3. Calculation of burst frequency for cylindrical passive valves**
$\sigma$ = surface characterization of water = 0.07197 $Nm^{-1}$
$\Theta$ = contact angle of water with polycarbonate = $70^0$
$\rho$ = density of water = 1000 kg $m^{-3}$
r = average radius of the liquid plug
$\Delta$r = head height of the liquid plug
d = diameter of capillary opening

Surface characterization of water, $\sigma$ = 0.07197 N $m^{-1}$, is the measurement of the force exerted by the surface tension of water. Surface tension is an important characteristic of any reagent used in microfluidics that has passive valves in the form of geometric restrictions. The ability to restrict flow by a geometric shape is determined first by whether the liquid has a surface tension capable of spanning the opening of the passive valve.

Contact angle of water with polycarbonate, $\Theta = 70^o$, defines the angle at which the surface of the reagent will contact the substrate of the CM device. It is measured by observing a droplet of the reagent on the substrate and measuring the angle at which the surface of the reagent meets the surface of the substrate. $70^o$ is the contact angle of water on the polycarbonate substrate used in this thesis which indicates that polycarbonate is mildly hydrophilic. This affects the shape of the liquid surface at the opening of the passive valve.

Density of water, $\rho = 1000$ kg $m^{-3}$, is used since the experiments performed in this thesis were all aqueous. The density is a function of the mass of the liquid plug and is factored into calculating the force exerted when the liquid is rotated around the axis of the CM device.

The measurement of the average distance of a liquid sample from the axis of rotation on the CM device is defined as r. The farther the liquid is from the center of the device the greater the centrifugal force at the same rotational frequency. This is why the same restrictive valve cannot be used at multiple radii for the same volume of sample. This average distance is the mean of the inner and outer radius location of the liquid sample.

The head height of the liquid plug, $\Delta r$, is the radial length of the liquid sample in the CM device. When the head height of the liquid is larger the force exerted on the restrictive valve is larger. As the force increases the liquid can overcome the surface tension of the restrictive valve.

The diameter of capillary opening, d, is the distance that the liquid sample's surface tension is required to bridge and maintain under the force generated by the rotation of the CM device. Essentially, increasing the diameter of the geometric opening lowers the burst frequency of the valve.

The value of d in Equation 1-3 is the diameter of a circular capillary opening which is the value used for glass capillary valves of this thesis. In the case of rectangular adhesive valves, d is an approximation, Dh, shown in Equation 1-4.

$$Dh = \frac{2*H*W}{H+W}$$

**Equation 1-4. Approximation of *d* for rectangular passive valves in Equation 1-3**
H = height of the valve
W = Width of the valve

The calculation of predicted burst frequency in adhesive passive valves of this thesis using Equation 1-3 and the approximation for *d* in Equation 1-4 must be treated as an estimation of the

burst frequency due to the manner of construction. The calculation of burst frequency presented by Ducree requires that the opening of the valve be abrupt so that the liquid must transition from being in contact with the channel wall to being in an open chamber. In the case of the adhesive valves, this was true for three of the four sides of the channel. The topmost part of the channel was the top layer of polycarbonate which acted as the ceiling for chambers and channels and therefore was not an abrupt opening, but a continuing surface. By convention, adhesive valves in this thesis were constructed in the topmost adhesive layer of the device so that gravity would distort the surface of the liquid traversing the opening so that the liquid was not impacted by the presence of the chamber ceiling. There was good agreeability between observed burst frequencies and the estimation predicted by Ducree's equation; therefore, this equation was used for predicting burst frequency ranges for adhesive valves.

In 2011, Moore explored other construction methods for passive valves and experimentally demonstrated the use of capillary valves in CM devices manufactured by 3D printing.[48] The most important conclusion to be drawn from Moore's work is the impact of geometric shape on the effects of channels in predicting the function of microfluidic devices. The 3D printers used by Moore would not produce perfect rectangular or circular channels as are seen in the theoretical derivations of Cho or the empirical studies of Ducree. Often there would be striations between the layers of printed material that made the surfaces of the channel uneven. Therefore, while the production of microfluidics by 3D printers can reduce cost and make the generation of prototypes easier, it increases the opportunity for such small features to fail due to the variability in the printing.

In 2009, Lacroix-Frailish published a comparison between calculated and experimental burst frequencies using small diameter glass capillary valves.[49] She used the same construction

techniques employed in this thesis when glass capillary valves were implemented in the generation of small aliquots in Chapter 3 and in the demonstration of modular microfluidics in Chapter 6. The glass capillary was selected for its inner diameter and then rinsed with 95% ethanol. The segment of glass capillary was then scored with a ceramic edge to break the piece into the desired length for the valve. Usually, these valves were cut between 5 and 10 mm in length and then mounted into the device during construction of the layers. The valves were sealed into the device using a fast drying epoxy, which would leave only the inner diameter of the valve available for liquid flow. All calculations of burst frequency were based on the geometric shape of the valve end. By using different construction methods, various geometric restrictions can be generated, each with significant impact on the burst frequency. This thesis used two construction methods. The first method is the glass capillary valve as described by Laxroix-Frailish, the other is a passive capillary valve cut into the 100 μm thick adhesive layer that laminates the polycarbonate disks together into a single device. The adhesive valve would be rectangular in shape and feed into a receiving chamber. Owing to the xerography of cutting the adhesive it would always have a height of 100 μm and width that varied between 200 and 400 μm. The glass capillary valves were used in higher rotational frequency applications because the cross-sectional area of the valve was much smaller than could be produced using an adhesive valve.

A restrictive geometric shape in a microfluidic device can control the flow of liquid through the operations of a CM device. A second method for constriction of liquid movement is controlling the air when it vents out of the system as the liquid moves from one chamber to the next. Recognizing that the air in a receiving chamber must vent, Mark described a pneumatic restricted valve in which there was no venting of air from the receiving chamber, thus the burst

frequency was greatly increased.[50] If the air cannot be vented, then the air will resist compression and provide pressure at the interface between the gas and the liquid. In the case of a receiving chamber just after a passive valve, the pressure at the interface increases the burst frequency of the valve as the column of liquid must generate a higher pressure to overcome the restriction. This increased the burst frequency of the valve by pneumatically restricting the receiving chamber. Mark's design prompted a derivation of liquid-air interface calculations for the breaking of surface tension in order to let the valve flow.

A third method for restricting liquid movement was performed by Gorkin who inserted a dissolvable film into the CM device to restrict flow from a passive valve.[51] This was a modification of the trapped air methodology of Mark. A thin film in a channel would trap a volume of air against the liquid in the channel. This pocket of trapped air would resist compression and create a barrier between the reagent and the dissolvable film. At low rotational frequencies, the surface tension of the reagent would maintain the gas-liquid interface and the reagent would not be in contact with the dissolvable film. At a higher rotational frequency the surface of the reagent would become unstable and break through the trapped air dissolving the film. This methodology was effective at increasing the burst frequency up to ten times that of a traditional passive capillary valve.

A key performance indicator of valving is the ability of the valve to resist greater rotational frequencies and is the goal of continuing to develop new methods of restricting liquid movement, such as the dissolvable film. This continued through to the methodology of Al-Faqheri in 2013 with a modification of the passive valve which involved restricting the flow of air creating a Vacuum/Compression Valve (VCV).[52] In Al-Faqheri's design, the rotational frequency would not increase thereby destabilizing the liquid-gas interface as it did in Mark's design. Instead, Al-

Faqheri's design removed the restriction of gas flow from the receiving chamber. The gas was stopped from venting by a wax stop in the vent channel which was melted when the valve was intended to burst. Al-Faqheri also explored sealing the vent of the draining chamber before the passive valve. This approach also increased the burst frequency of the valve by having a low-pressure area develop so that the liquid could not flow from the draining chamber through the valve without creating a vacuum. This vent restriction would also be removed to open the valve rather than drive the rotational frequency high enough to overcome the additional resistance to flow.

Increasing the burst frequency for passive valves is explored in Chapter 4 of this thesis. First, a passive valve configuration that increased the accuracy of the burst frequency of a passive adhesive valve was examined. This was accomplished with a 3D design similar to Gorkin[51] and Templeton.[53] This design would have liquid flow in one layer from an inner radius to an outer radius and then travel perpendicular to the plane of the device (axial) before continuing to a further radius in a second layer. The second increase in burst frequency was demonstrated when the 3D valve was enhanced with a compression valve without requiring dissolving or melting stops.[54] A volume of water was used as a valving liquid which would flow out of the vent at a high RPM to open the vent and cause the primary liquid of interest to flow. The valve that acted as a vent was opened by increasing the rotational frequency of the device, thereby removing the venting restriction.

## Deposition and Coriolis Switch

There are two goals that must be addressed involving the addition of reagents and samples to CM devices in motion; (1) the ability to construct devices that can be assembled and stored for a very long time without having any reagents present on the device, (2) to allow the

incorporation of methodologies, such as chromatography, that require the constant addition of a reagent or a mobile phase. In the case of chromatography, further improving the functionality of the device is accomplished when it is possible to add analyte while the device is in motion.

The first attempt at liquid deposition in motion was by Andersson in 2003 who described, in a patent, how droplets of reagent could be flicked into openings in a spinning CM device.[55] This was accomplished by deriving empirical parameters for different rotational frequencies and the viscosity of reagents and samples. The need for intensive empirical evidence to program the deposition of reagents to the device limited the practical usage of the deposition system. In order to develop a system that was more robust, creative constraints in design were necessary.

In work by this author (Bouchard) in 2010 three requirements were considered in the design; (1) the deposition method must be a continuous stream of liquid so that control of the flow rate would be more consistent, (2) the deposition allows for accurate aliquot volumes and equal distribution to sample inlets on the device and (3) the system must work at a wide range of rotational frequencies. This published design was the Centrifugal Liquid Addition Distributor (CLAD), which took a stream of liquid and deposited it into different inlet holes on a rotating CM device by dividing the surface with 3D printed walls.[56]

In contrast to this author's (Bouchard) previous work, this thesis describes a spiral shape for the deposition of a stream of liquid into a single inlet on a CM device. The use of a single inlet is a divergence from a field that is heralded for its ability to function in parallel. There are applications in which a single inlet is preferable. For instance, a design in which (1) prototyping a single experiment is necessary, (2) where the addition of a sample, or reagent is in such a small volume that a single deposition point is necessary to allow the liquid to be aliquoted to multiple

replicates once inside the device, or (3) where different segments of the device require the addition of different samples or reagents.

The spiral deposition was paired with a Coriolis switch to select whether the deposited liquid was going into a metering chamber or to waste for rinsing the spiral. Being able to select the direction of flow at a junction is an important functionality for the design of more complex microfluidic methodologies. The junction is a passive valve that is responsible for the programmability of the device as described by Miro.[14] By further adding the ability for a valve to direct liquid flow into a specific receiving chamber the number of logical gates that the liquid must flow through in the programming increases dramatically. If-then statements can determine which channel the liquid will flow to from a junction making it possible for a single device to handle a much greater range of samples. Methods for preferentially selecting flow direction at a junction have included controlling flow with rotational direction, valves that can be manipulated such as diaphragms or wax stops that are melted,[51] or using trapped or compressed air to restrict liquid movement.[57]

A switch design was demonstrated by Steigert in 2005 which depended on a combination of geometry and Coriolis force to ensure that liquid flowed in a desired direction.[58] A Coriolis switch with a median divider in a wide channel located after a passive valve was included in Steigerts design. Above a critical frequency defined by the design, the Coriolis force selected the direction of flow past the divider in the channel. When the device was rotating at a rate lower than the critical frequency the liquid was split between the two available paths around the divider. The passive valve above the divider was designed to burst at a frequency higher than the critical frequency for the Coriolis switch. With this constraint, other functions of the device could be performed and the direction of rotation changed before the path of liquid movement

was selected. This is in contrast to the design in this thesis where the valve above the Coriolis switch would open below the critical frequency. A higher burst frequency was not required because the design of this thesis was used for the deposition of liquid into the device, therefore at lower frequencies no liquid would be added to the device and the direction of rotation could be changed at that time. In 2008 Kim used a Coriolis switch that had the same basic principle of a passive valve followed by a median divider to two receiving chambers in order to produce a predictive equation and demonstrate the application of driving liquid movement by Coriolis force and constricted air.[59] The same equations can be applied to the work of Kim and to this thesis, though both were developed empirically.

Kim's work was followed by En Lin in 2010 who designed channels that evenly split liquid into multiple chambers regardless the magnitude of Coriolis force generated by the CM device.[60] En Lin's work focused on the distribution of junctions along different radii of a CM device where the objective was to evenly distribute liquid reagent to multiple receiving chambers by taking into account the effect that the Coriolis force had on liquid movement through junctions in a rotating device. En Lin used geometric designs in combination with surface treatments to split a single liquid stream into four equal parts by using three T-Junctions. The application of this work was to generate even splitting of liquid for enzyme-linked immunosorbent assay experimentation.

While En Lin sought to evenly split liquid at a T-Junction, Kong used a method of pneumatic pressure applied to a T-Junction in a CM device which discouraged liquid flow to one side of the junction and forced liquid flow entirely into the opposing channel.[57] In comparison to the work of Steigert and that in this thesis, the demonstration by Kong did not use a passive valve to restrict movement of the liquid into a T-junction where the direction of liquid flow

would be selected. With no external forces applied, the T-junction would cause liquid from the reservoir above to flow equally in both directions perpendicular to the radius of the device. It was observed that at the range of frequencies between 400 to 1200 RPM, the Coriolis force did not have a discernible effect on the even split of liquid to the two receiving chambers after the T-junction. Kong applied pneumatic pressure to the liquid forcing it to flow in the desired direction of the junction. The compressed air does not require the stopping of the device to change rotational directions like a Coriolis switch. By not stopping the device greater control over the liquid in the device can be maintained.

In a novel approach this thesis explored the notion of 'Open CM' whereby the Coriolis drift in a Coriolis switch is increased. In 2013, Casavant presented an introduction to Open Microfluidics (OM).[61] In the paper, OM is described as the control of small volumes of fluid with a geometric structure that has no covering. This type of design lends itself to development of high throughput and reusable components. Open microfluidics (OM) has the ability to be a high throughput methodology due to its ability to be constructed using photolithography which can create highly repetitive structures. The use of OM also allows the construction of parts that are more reusable since the surface can be cleaned with greater ease than a closed microfluidic channel. Casavant also discussed suspended microfluidics where the liquid does not sit upon a surface nor is enclosed by three sides with an open top, but is instead suspended between two or more interfaces. This thesis does not demonstrate suspended microfluidics where the liquid is maintained in the plane of the device by attractive forces with the substrate material. Here the base of the device is responsible for maintaining the sample in the plane of the experiment by preventing the sample from falling due to gravity.

In 2013, Huang discussed why OM with no contact from outside forces is ideal and presented pneumatic, magnetic and hydrophilic/phobic possibilities.[62] His device was built by laser micromachining of a super hydrophobic PDMS surface. The surface characteristic gave the opportunity to control liquid droplets through the use of applied suction in order to move and mix samples on the device. The normal parameters of open microfluidic liquid manipulation that Huang sought to avoid were the applied electrical, optical and thermal energies. These modes of manipulation have the tendency to interfere with sensitive bio-molecules, therefore Huang used pneumatics.

Contact with liquid movement requires an interface so that force can be applied to manipulate the liquid of interest. This was discussed in 2010 by this author (Bouchard) and Kong in the paper on radially pumping liquid toward the center of the device.[42] Both a liquid-liquid interface and a gas-liquid interface were explored for application of force to the liquid of interest. Both methods have similar concerns as traditional microfluidics. Liquid-liquid interfaces are common in traditional microfluidics through the use of immiscible liquids, often aqueous solutions formed as droplets suspended in oil. This approach allows for small volume reactions to be carried out in aqueous solutions and be processed by the microfluidic device without any interaction between the droplets. The use of suspended droplets as reaction vessels combines the ability of continuous flow microfluidics with the benefits of batch processing and analytics. However, it is regularly required that the sample of interest not come in contact with another liquid even if immiscible.

In 2009, Khare avoided the gas-liquid and liquid-liquid interfaces demonstrated by Kong and this author (Bouchard) by using wrinkled PDMS surfaces to determine flow in OM devices.[63] Khare explored groove wetting in the PDMS as a model for use in microfluidic

devices. By studying groove channels in a planar substrate Khare provided methods for the creation of more efficient and predictable open microfluidic devices. Neither Huang nor Khare used CM principles in their OM devices.

## Modular Microfluidics

In the development of experiments that involve multiple steps it is necessary that the device be custom designed in order to accommodate functionality requirements of the individual components. For example, in centrifugal microfluidics the placement and selection of valving to control liquid flow must be done specifically for each design to ensure that control of the liquid is accurate and precise. In traditional microfluidics the method of construction often dictated that the design of the device be custom made to integrate multiple functions. Custom designs were required because the construction did not allow the addition of connections between different small scale components in designs that were etched or molded. The custom design would include both the experimental components in addition to the channels and valves to connect them. The design would then be able to only perform the intended experiment without the ability to be modified based on the observations of the experimenter.

In 2003, Grodizinski developed a modular microfluidic setup for cell pre-concentration for use in genetic sample preparation.[64] Grodizinski was able to replace the connecting channels with tubes and o-rings in order to transport the reagents and samples between modular layers. Grodizinski had overcome the limitation of adding connections to the substrate of a traditional microfluidic device. This made replacing a single component that is ineffective or defective possible and did not require re-design and re-construction of the device to attempt another prototype. Modular microfluidics enables prototyping of procedures so that a custom design can be implemented more effectively. Early development of new experiments in microfluidics should

be performed on modular prototypes to prove concepts and establish the parameters for later custom design and mass production.

The desire for prototyping and a reduction in production cost has led researchers to continue developing modular components. The goals of modular microfluidics include the mass production of components and overcoming the requirement for custom designs. Having standardized connections and components enables researchers to more easily modify experiments based on observation which is an advantage over custom design and construction. Additionally, the mass production reduces cost by allowing single use components to be replaced while others are re-used. It can be imagined that there are components in a microfluidic experiment that are robust enough to be re-used, while there are others that must be replaced. In an ideal system the one-time use components would be inexpensive, modular and replaced every experiment, while the remainder of the device would be used in the next experiment. For instance, any reaction chambers with specialized surface chemistry would be one time use while the pumping and liquid metering components would remain for continuous use.

Shaikh described, in 2005, a modular microfluidic infrastructure for building biochemical analysis methodologies.[65] The infrastructure design used an oxidized silicon wafer as a substrate for the attachment of functional components. In 2008, Rhee used PDMS microfluidic assembly blocks designed to be constructed on a glass slide to assemble more complex analytical tasks.[66] The PDMS and glass slide design were made more robust by Langelier (2011) with the introduction of dovetails to the modules for better joining.[67]

Yeun has published two papers on modular microfluidic systems. The first design, published in 2008, was termed SmartBuild and is similar to an electronic breadboard where components are designed to be ‘plug and play’.[68] The second, in 2009, was an expansion in

which multi-dimensional flow was added to the functionality of the modular system.[69] In 2011, Liou described modular components for portable microfluidic devices. The functionalities included pumping, valving, reaction chambers and mixing.[70]

This thesis demonstrates a design concept with a wedge-based module construction for CM. The experimental wedges were connected with Kong's method of pneumatic pumping that move liquid from the edge of a device to the center.[41] The pneumatic pumping was used to move liquid radially inward after each experimental step. This was achieved by using a solenoid-controlled canister of compressed dry air directed through a small nozzle. The nozzle was affixed at the radial position of an inlet port on the CM devices. As the device rotated the inlet would be exposed to the stream of air once every rotation; at a high enough volume of air and a low enough rotational frequency the pneumatic pressure would overcome the centrifugal force and drive liquid movement inward on the device.

The use of a dedicated pumping layer for the handling of reagents and samples allowed experimental components to occupy more space on the device.[71] In a traditional CM device, all the experimental components, reagent storage and liquid transfer mechanisms are contained in a single experimental layer. This limits the space available on the device for additional components or replicates of the same analytical operation. Both wedge-based modules and layer-based modules use dedicated pumping layers to house liquid handling apparatus in a different layer than the experimental layers thereby effectively creating more space for functional components. The wedge-based modules have a layer for experimentation and a dedicated pumping layer making them ideal for prototyping complex experiments. The wedge nomenclature comes from the manner in which the analytical components were separated in angular space and rotated around the center of the CM device. This provided more radial space

for increased size or complexity in the analytical components. However, by separating the components by wedges the length of sequential steps would be limited by the number of wedges that fit around the center of the device. The use of wedge located components is ideal for prototyping an experimental methodology since the components exist independently separated by a pneumatic pumping mechanism. It also means that clear imaging of the entire operation can be done without being obstructed by layers of components above. It was envisioned that as a prototyping design this method would contain a single experimental replicate per device.

For more established methodologies that require multiple replicates in parallel a second layered module construction was developed. Layered modules have a dedicated layer for each experimental step paired with a pumping layer. Therefore, the disk would be constructed by stacking an experimental layer, pumping layer, experimental layer, pumping layer, etc., until the experiment is complete. In the layered modules, the first set of components representing all the replicates to be completed in parallel is located as the top experimental layer. After the first step is complete pneumatic pumping is used to move the reagent to the next experimental layer. Each experimental layer has liquid movement from an inner radius to an external radius, at the end of which the sample moves to the next pumping layer. The pumping layer then moves the sample to the inner radius and the beginning of the next experimental layer in the device.

The major advantage of layered modules over wedges is that the length of the experiment is not dictated by "real-estate" as described by Madou.[26] The real-estate in CM devices is a combination of the amount of radial space available to fit serial components in an analytical operation and the amount of angular space used by the operation determining how many experiments can be performed in parallel. The layered design of experiments does not rely on the radius to add additional components as shown in Figure 1-4. The layered design also does not

use additional wedges of real-estate for the addition of more functions. Each layer functions independently and the continued addition of layers increases the amount of functions.

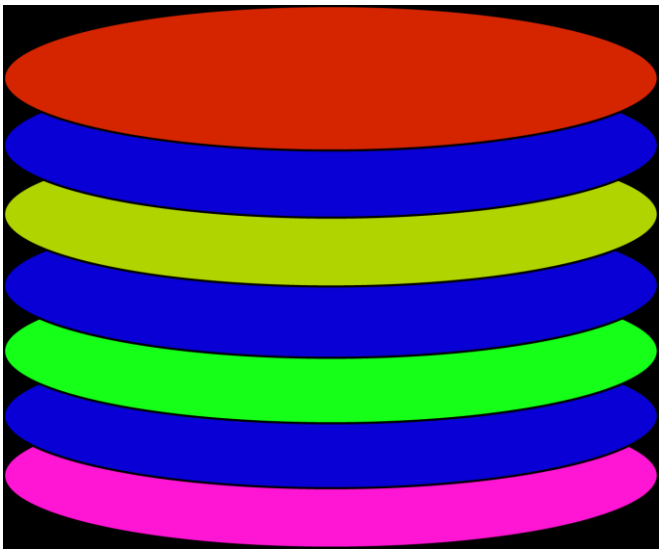

**Figure 1-4. Representation of layers in a modular microfluidic device**
The blue layers are pumping layers that are standardized and repeated. The other colored layers represent unique experimental layers that are serially connected by the blue pumping layers. Each experimental layer contains replicates of the analytical function and additional functions can be added to the whole device by the stacking of an additional pumping and experimental layer.

## Thesis Objectives

The purpose of this thesis is to demonstrate new design concepts that can fundamentally change the way that CM devices are considered for experimental procedures. The work of this thesis focuses on components and operations that ease design and assembly while enhancing CM μTAS by providing functions that can expand the complexity of experiments without stopping the disk. There are very few limitations in CM that cannot be solved by stopping the disk and treating it like a traditional microfluidic device, but at that point the advantages of CM are lost. By overcoming these limitations those who use these devices will have the ability to construct more complex experiments.

The chapters of this thesis are organized into three parts; Chapter 2 is the development of instrumentation to collect optical data from CM Devices, Chapters 3, 4 and 5 are CM components that can stand alone or be utilized as a step in a larger procedure, Chapter 6 is a design and demonstration of how components can be assembled and used to make increasingly more complex experiments in either single run prototypes or a highly parallel configuration.

## Thesis Outline

**Chapter 2** demonstrates a synchronized spectrometer that takes full visible light spectra from spectroscopic cells on a CM device in motion. The accuracy and reliability of the system is shown through the creation of calibration curves and an analysis of its sources of noise. The instrumentation was used to measure the precision of the light source, the accuracy of the measurements against a serial dilution and to calculate the extinction coefficient of bromothymol blue. Additionally, this device was used to determine the volume of aliquots generated in Chapter 3.

**Chapter 3** outlines the design of a CM configuration that allows the addition of small aliquots of reagent to an experimental chamber by adjusting the rotational frequency of the device. By cycling through a pattern of higher and lower frequencies multiple aliquots can be generated. The accuracy of the volume is verified by spectroscopic measurements taken with the synchronized spectrometer of Chapter 2.

**Chapter 4** presents a new configuration for passive adhesive valves in CM devices. The change in design significantly increased the accuracy of the burst frequency calculation. The valve was also paired with a compression valve which greatly increased the burst frequency.

**Chapter 5** illustrates the use of open microfluidics to reduce the rotational frequency that is required to take advantage of Coriolis drift. A Coriolis switch was paired with a novel liquid

addition design that takes liquid being added to the device and channels it to only one experimental cell. The Coriolis switch was used to direct sequential additions of reagent and wash solutions through the liquid addition design.

**Chapter 6** demonstrates two designs for the construction of modular CM devices. The first is a single experimental layer that can be used to make fast prototypes for the optimization of complex experiments. The second is an expansion into multiple experimental layers with each layer only containing one operation of the CM device. The layered setup maximized real-estate for parallel operations.

**Chapter 7** is a discussion of the conclusions drawn from the chapters of this thesis. The results are summarized and continuation of this work is imagined.

**Appendix 1** presents an introduction to the MATLAB graphical user interface (GUI) used in Chapters 2 and 3 to calculate absorbance from data collected during synchronized spectroscopy in Chapters 2 and 3.

# References


1. Manz, A.; Eijkel, J. C. T., Miniaturization and chip technology. What can we expect? *Pure and Applied Chemistry* **2001,** *73* (10), 1555-1561.
2. Beebe, D.; Wheeler, M.; Zeringue, H.; Walters, E.; Raty, S., Microfluidic technology for assisted reproduction. *Theriogenology* **2002,** *57* (1), 125-35.
3. Fang, Q.; Xu, G. M.; Fang, Z. L., A high-throughput continuous sample introduction interface for microfluidic chip-based capillary electrophoresis systems. *Analytical Chemistry* **2002,** *74* (6), 1223-1231.
4. Liu, J.; Hansen, C.; Quake, S. R., Solving the "world-to-chip" interface problem with a microfluidic matrix. *Analytical Chemistry* **2003,** *75* (18), 4718-4723.
5. Atencia, J.; Cooksey, G. A.; Jahn, A.; Zook, J. M.; Vreeland, W. N.; Locascio, L. E., Magnetic connectors for microfluidic applications. *Lab on a Chip - Miniaturisation for Chemistry and Biology* **2010,** *10* (2), 246-249.
6. Mariella Jr, R., Sample preparation: The weak link in microfluidics-based biodetection. *Biomedical Microdevices* **2008,** *10* (6), 777-784.
7. Ramos, L.; Ramos, J. J.; Brinkman, U. A. T., Miniaturization in sample treatment for environmental analysis. *Analytical and Bioanalytical Chemistry* **2005,** *381* (1), 119-140.
8. Felton, M. J., Product Review: Lab on a chip: Poised on the brink. *Analytical Chemistry* **2003,** *75* (23), 505 A-508 A.
9. Felton, M. J., The new generation of microvalves. *Analytical Chemistry* **2003,** *75* (19), 429A-432A.
10. Fiorini, G. S.; Chiu, D. T., Disposable microfluidic devices: Fabrication, function, and application. *BioTechniques* **2005,** *38* (3), 429-446.
11. Pamme, N., Continuous flow separations in microfluidic devices. *Lab on a Chip - Miniaturisation for Chemistry and Biology* **2007,** *7* (12), 1644-1659.
12. Crevillén, A. G.; Hervás, M.; López, M. A.; González, M. C.; Escarpa, A., Real sample analysis on microfluidic devices. *Talanta* **2007,** *74* (3), 342-357.
13. Fair, R. B., Digital microfluidics: Is a true lab-on-a-chip possible? *Microfluidics and Nanofluidics* **2007,** *3* (3), 245-281.
14. Miró, M.; Hansen, E. H., Miniaturization of environmental chemical assays in flowing systems: The lab-on-a-valve approach vis-à-vis lab-on-a-chip microfluidic devices. *Analytica Chimica Acta* **2007,** *600* (1-2 SPEC. ISS.), 46-57.
15. Iverson, B. D.; Garimella, S. V., Recent advances in microscale pumping technologies: A review and evaluation. *Microfluidics and Nanofluidics* **2008,** *5* (2), 145-174.
16. Ohno, K. I.; Tachikawa, K.; Manz, A., Microfluidics: Applications for analytical purposes in chemistry and biochemistry. *Electrophoresis* **2008,** *29* (22), 4443-4453.

17. Mark, D.; Haeberle, S.; Roth, G.; Von Stetten, F.; Zengerle, R., Microfluidic lab-on-a-chip platforms: Requirements, characteristics and applications. *Chemical Society Reviews* **2010,** *39* (3), 1153-1182.

18. Arora, A.; Simone, G.; Salieb-Beugelaar, G. B.; Kim, J. T.; Manz, A., Latest developments in micro total analysis systems. *Analytical Chemistry* **2010,** *82* (12), 4830-4847.

19. Hoffmann, J.; Mark, D.; Lutz, S.; Zengerle, R.; Von Stetten, F., Pre-storage of liquid reagents in glass ampoules for DNA extraction on a fully integrated lab-on-a-chip cartridge. *Lab on a Chip - Miniaturisation for Chemistry and Biology* **2010,** *10* (11), 1480-1484.

20. Ríos, Á.; Zougagh, M.; Avila, M., Miniaturization through lab-on-a-chip: Utopia or reality for routine laboratories? A review. *Analytica Chimica Acta* **2012,** *740*, 1-11.

21. Ríos, Á.; Zougagh, M., Sample preparation for micro total analytical systems (μ-TASs). *TrAC - Trends in Analytical Chemistry* **2013,** *43*, 174-188.

22. Webster, A.; Greenman, J.; Haswell, S. J., Development of microfluidic devices for biomedical and clinical application. *Journal of Chemical Technology and Biotechnology* **2011,** *86* (1), 10-17.

23. Felton, M. J., CD simplicity. *Analytical Chemistry* **2003,** *75* (13), 302A-306A.

24. Duffy, D. C.; Gillis, H. L.; Lin, J.; Sheppard Jr, N. F.; Kellogg, G. J., Microfabricated centrifugal microfluidic systems: Characterization and multiple enzymatic assays. *Analytical Chemistry* **1999,** *71* (20), 4669-4678.

25. Zoval, J. V.; Madou, M. J., Centrifuge-based fluidic platforms. *Proceedings of the IEEE* **2004,** *92* (1), 140-153.

26. Madou, M.; Zoval, J.; Jia, G.; Kido, H.; Kim, J.; Kim, N., Lab on a CD. Yarmush, M. L., Ed. 2006; Vol. 8, pp 601-628.

27. Ducrée, J.; Haeberle, S.; Lutz, S.; Pausch, S.; Von Stetten, F.; Zengerle, R., The centrifugal microfluidic Bio-Disk platform. *Journal of Micromechanics and Microengineering* **2007,** *17* (7), S103-S115.

28. Gorkin, R.; Park, J.; Siegrist, J.; Amasia, M.; Lee, B. S.; Park, J. M.; Kim, J.; Kim, H.; Madou, M.; Cho, Y. K., Centrifugal microfluidics for biomedical applications. *Lab on a Chip - Miniaturisation for Chemistry and Biology* **2010,** *10* (14), 1758-1773.

29. Kido, H.; Micic, M.; Smith, D.; Zoval, J.; Norton, J.; Madou, M., A novel, compact disk-like centrifugal microfluidics system for cell lysis and sample homogenization. *Colloids and Surfaces B: Biointerfaces* **2007,** *58* (1), 44-51.

30. Lafleur, J. P.; Salin, E. D., Pre-concentration of trace metals on centrifugal microfluidic discs with direct determination by laser ablation inductively coupled plasma mass spectrometry. *Journal of Analytical Atomic Spectrometry* **2009,** *24* (11), 1511-1516.

31. Kuswandi, B.; Nuriman; Huskens, J.; Verboom, W., Optical sensing systems for microfluidic devices: A review. *Analytica Chimica Acta* **2007,** *601* (2), 141-155.

32. Myers, F. B.; Lee, L. P., Innovations in optical microfluidic technologies for point-of-care diagnostics. *Lab on a Chip - Miniaturisation for Chemistry and Biology* **2008,** *8* (12), 2015-2031.

33. Steigert, J.; Grumann, M.; Brenner, T.; Riegger, L.; Harter, J.; Zengerle, R.; Ducrée, J., Fully integrated whole blood testing by real-time absorption measurement on a centrifugal platform. *Lab on a Chip - Miniaturisation for Chemistry and Biology* **2006,** *6* (8), 1040-1044.

34. DeMello, A. J.; French, P. M. W.; Neil, M. A. A.; Edel, J. B.; Benninger, R. K. P.; Bradley, D. D. C.; Robinson, T.; Srisa-art, M.; Hofmann, O.; DeMello, J. C. In *Optical detection in microfluidics: From the small to the large*, 2009; pp 712-717.

35. Mogensen, K. B.; Kutter, J. P., Optical detection in microfluidic systems. *Electrophoresis* **2009,** *30* (SUPPL. 1), S92-S100.

36. Duford, D. A.; Peng, D. D.; Salin, E. D., Magnetically driven solid sample preparation for centrifugal microfluidic devices. *Analytical Chemistry* **2009,** *81* (11), 4581-4584.

37. Ocean Optics, USB 4000 Data Sheet. 830 Douglas Ave. Dunedin. FL 34698.

38. Steigert, J.; Brenner, T.; Grumann, M.; Riegger, L.; Lutz, S.; Zengerle, R.; Ducrée, J., Integrated siphon-based metering and sedimentation of whole blood on a hydrophilic lab-on-a-disk. *Biomedical Microdevices* **2007,** *9* (5), 675-679.

39. Mark, D.; Weber, P.; Lutz, S.; Focke, M.; Zengerle, R.; Von Stetten, F., Aliquoting on the centrifugal microfluidic platform based on centrifugo-pneumatic valves. *Microfluidics and Nanofluidics* **2011,** *10* (6), 1279-1288.

40. Kazarine, A.; Kong, M. C. R.; Templeton, E. J.; Salin, E. D., Automated liquid-liquid extraction by pneumatic recirculation on a centrifugal microfluidic platform. *Analytical Chemistry* **2012,** *84* (16), 6939-6943.

41. Kong, M. C. R.; Salin, E. D., Pneumatically pumping fluids radially inward on centrifugal microfluidic platforms in motion. *Analytical Chemistry* **2010,** *82* (19), 8039-8041.

42. Kong, M. C. R.; Bouchard, A. P.; Salin, E. D., Displacement pumping of liquids radially inward on centrifugal microfluidic platforms in motion. *Micromachines* **2012,** *3* (1), 1-9.

43. Zehnle, S.; Schwemmer, F.; Roth, G.; Von Stetten, F.; Zengerle, R.; Paust, N., Centrifugo-dynamic inward pumping of liquids on a centrifugal microfluidic platform. *Lab on a Chip - Miniaturisation for Chemistry and Biology* **2012,** *12* (24), 5142-5145.

44. Gorkin Iii, R.; Clime, L.; Madou, M.; Kido, H., Pneumatic pumping in centrifugal microfluidic platforms. *Microfluidics and Nanofluidics* **2010,** *9* (2-3), 541-549.

45. Feng, Y.; Zhou, Z.; Ye, X.; Xiong, J., Passive valves based on hydrophobic microfluidics. *Sensors and Actuators, A: Physical* **2003,** *108* (1-3), 138-143.

46. Cho, H.; Kim, H. Y.; Kang, J. Y.; Kim, T. S., How the capillary burst microvalve works. *Journal of Colloid and Interface Science* **2007,** *306* (2), 379-385.

47. Squires, T. M.; Quake, S. R., Microfluidics: Fluid physics at the nanoliter scale. *Reviews of Modern Physics* **2005,** *77* (3), 977-1026.

48. Moore, J. L.; McCuiston, A.; Mittendorf, I.; Ottway, R.; Johnson, R. D., Behavior of capillary valves in centrifugal microfluidic devices prepared by three-dimensional printing. *Microfluidics and Nanofluidics* **2011,** *10* (4), 877-888.

49. Lacroix-Fralish, A.; Templeton, E. J.; Salin, E. D.; Skinner, C. D., A rapid prototyping technique for valves and filters in centrifugal microfluidic devices. *Lab on a Chip - Miniaturisation for Chemistry and Biology* **2009,** *9* (21), 3151-3154.

50. Mark, D.; Metz, T.; Haeberle, S.; Lutz, S.; Ducrée, J.; Zengerle, R.; Von Stetten, F., Centrifugo-pneumatic valve for metering of highly wetting liquids on centrifugal microfluidic platforms. *Lab on a Chip - Miniaturisation for Chemistry and Biology* **2009,** *9* (24), 3599-3603.

51. Gorkin, R.; Nwankire, C. E.; Gaughran, J.; Zhang, X.; Donohoe, G. G.; Rook, M.; O'Kennedy, R.; Ducrée, J., Centrifugo-pneumatic valving utilizing dissolvable films. *Lab on a Chip - Miniaturisation for Chemistry and Biology* **2012,** *12* (16), 2894-2902.

52. Al-Faqheri, W.; Ibrahim, F.; Thio, T. H. G.; Moebius, J.; Joseph, K.; Arof, H.; Madou, M., Vacuum/Compression Valving (VCV) Using Parrafin-Wax on a Centrifugal Microfluidic CD Platform. *PLoS ONE* **2013,** *8* (3).

53. Templeton, E. J.; Salin, E. D., A novel filtration method integrated on centrifugal microfluidic devices. *Microfluidics and Nanofluidics* **2013**, 1-7.

54. Park, J. M.; Cho, Y. K.; Lee, B. S.; Lee, J. G.; Ko, C., Multifunctional microvalves control by optical illumination on nanoheaters and its application in centrifugal microfluidic devices. *Lab on a Chip - Miniaturisation for Chemistry and Biology* **2007,** *7* (5), 557-564.

55. Andersson, P.; Jesson, G.; Soderman, T.; Sjoberg, J., **2003**.

56. Bouchard, A. P.; Duford, D. A.; Salin, E. D., Non-contact addition, metering, and distribution of liquids into centrifugal microfluidic devices in motion. *Analytical Chemistry* **2010,** *82* (20), 8386-8389.

57. Kong, M. C. R.; Salin, E. D., Pneumatic flow switching on centrifugal microfluidic platforms in motion. *Analytical Chemistry* **2011,** *83* (3), 1148-1151.

58. Steigert, J.; Grumann, M.; Brenner, T.; Mittenbühler, K.; Nann, T.; Rühe, J.; Moser, I.; Haerberle, S.; Riegger, L.; Riegler, J.; Bessler, W.; Zengerle, R.; Ducrée, J., Integrated sample preparation, reaction, and detection on a high-frequency centrifugal microfluidic platform. *JALA - Journal of the Association for Laboratory Automation* **2005,** *10* (5), 331-341.

59. Kim, J.; Kido, H.; Rangel, R. H.; Madou, M. J., Passive flow switching valves on a centrifugal microfluidic platform. *Sensors and Actuators, B: Chemical* **2008,** *128* (2), 613-621.

60. En Lin, S. I., A novel splitter design for microfluidic biochips using centrifugal driving forces. *Microfluidics and Nanofluidics* **2010,** *9* (2-3), 523-532.

61. Casavant, B. P.; Berthier, E.; Theberge, A. B.; Berthier, J.; Montanez-Sauri, S. I.; Bischel, L. L.; Brakke, K.; Hedman, C. J.; Bushman, W.; Keller, N. P.; Beebe, D. J., Suspended microfluidics. *Proceedings of the National Academy of Sciences of the United States of America* **2013,** *110* (25), 10111-10116.

62. Huang, C. J.; Ke, M. S.; Yang, J. T. In *A pneumatic open-surface microfluidic platform for droplet manipulation*, 2013; pp 313-316.

63. Khare, K.; Zhou, J.; Yang, S., Tunable open-channel microfluidics on soft poly(dimethylsiloxane) (PDMS) substrates with sinusoidal grooves. *Langmuir* **2009,** *25* (21), 12794-12799.

64. Grodzinski, P.; Yang, J.; Liu, R. H.; Ward, M. D., A modular microfluidic system for cell pre-concentration and genetic sample preparation. *Biomedical Microdevices* **2003,** *5* (4), 303-310.

65. Shaikh, K. A.; Ryu, K. S.; Goluch, E. D.; Nam, J. M.; Liu, J.; Thaxton, C. S.; Chiesl, T. N.; Barron, A. E.; Lu, Y.; Mirkin, C. A.; Liu, C., A modular microfluidic architecture for integrated biochemical analysis. *Proceedings of the National Academy of Sciences of the United States of America* **2005,** *102* (28), 9745-9750.

66. Rhee, M.; Burns, M. A., Microfluidic assembly blocks. *Lab on a Chip - Miniaturisation for Chemistry and Biology* **2008,** *8* (8), 1365-1373.

67. Langelier, S. M.; Livak-Dahl, E.; Manzo, A. J.; Johnson, B. N.; Walter, N. G.; Burns, M. A., Flexible casting of modular self-aligning microfluidic assembly blocks. *Lab on a Chip* **2011,** *11* (9), 1679-1687.

68. Yuen, P. K., SmartBuild - A truly plug-n-play modular microfluidic system. *Lab on a Chip - Miniaturisation for Chemistry and Biology* **2008,** *8* (8), 1374-1378.

69. Yuen, P. K.; Bliss, J. T.; Thompson, C. C.; Peterson, R. C., Multidimensional modular microfluidic system. *Lab on a Chip - Miniaturisation for Chemistry and Biology* **2009,** *9* (22), 3303-3305.

70. Liou, D. S.; Hsieh, Y. F.; Kuo, L. S.; Yang, C. T.; Chen, P. H., Modular component design for portable microfluidic devices. *Microfluidics and Nanofluidics* **2011,** *10* (2), 465-474.

71. Thio, T. H. G.; Ibrahim, F.; Al-Faqheri, W.; Moebius, J.; Khalid, N. S.; Soin, N.; Kahar, M. K. B. A.; Madou, M., Push pull microfluidics on a multi-level 3D CD. *Lab on a Chip - Miniaturisation for Chemistry and Biology* **2013,** *13* (16), 3199-3209.

# CHAPTER 2: Synchronized visible light spectroscopy on a centrifugal microfluidic device in motion

Early in the development of centrifugal microfluidics (CM), an inability to take real-time spectroscopic data while a CM device was in motion severely limited design opportunities. Methodologies comprised of multiple experimental steps that could not be stopped had to be designed with the final step as the only measurement opportunity. If the experiment could be stopped and started again then measurements could occur at intermediate steps. In response, techniques for data collection while a device was in motion were developed and included methods for taking images of the device or taking single wavelength measurements of absorbance. No designs existed for an apparatus that could collect full spectrum data while a CM device was rotating. In the previous work of CM experimentation, the device would be stopped and the full spectrum absorbance measurements taken, breaking the control that had been maintained by constantly applying centrifugal force to the liquid. This limitation was highlighted in a 2014 review by King where the methodologies discussed did not include a setup for full visible light spectrum data collection as described in this chapter.[1]

As the first experimental chapter of this thesis, the development of synchronized spectroscopy sets up the ability to measure volumes of small aliquots as described in Chapter 3.

## Contribution to Original Knowledge

An assembly of electrical components was designed to facilitate synchronized spectroscopy, which is the collection of spectroscopic data from a CM device while it is in motion. The equipment allowed experiments requiring measurements to continue without having

to stop the rotation of the device. Discussed in this present chapter are the validation of this novel system and its application in volume determination of small aliquot volumes and the measurement of sedimentation.

## Abstract

The focus of this chapter is the development of instrumentation that permits the recording of multiple wavelength optical data from cells on a CM device in motion. This chapter demonstrates the use of the instrumentation during the determination of signal noise sources and in practical use. The instrumentation was used to; (1) observe empirical extinction coefficients and limits of detection, (2) track the volume of liquid added in sequential aliquots and (3) monitor sedimentation in real time on a CM device. As an off-chip addition to a servo-motor CM testing platform, this instrumentation can supplement a great number of future research endeavors such as tracking reaction progress in intermediate chemical steps or observing bands of analyte while eluting from chromatographic columns.

Visible light spectra were collected from samples on CM devices in motion. The CM devices were synchronized with a visible light absorbance apparatus by a servo motor that provided absolute location. The design and implementation is described and evaluated here. The relative standard deviations of raw intensities of light were calculated to be ~0.5%. The stability of the light source is an important component of a new optical analytical instrument. The stability of the light source and confidence in the precision of the source is paramount to confidence in the results from an analytical experiment. By examining the standard deviation of raw intensities it was determined that a single spectra was precise enough that single measurements could be taken in the generation of data for a time point study such as the flow of analyte from a chromatographic column.

The accuracy of the instrumentation designed and built for this chapter was observed using a ratiometric calculation[2] of absorbance to create a six point (n = 4) linear calibration curve ($R^2$ greater than 0.999) for a serially diluted solution of yellow dye. Taking spectroscopic measurements while the centrifugal device rotates provides greater control over sample manipulation and collection of real-time full spectrum data over the course of an experiment. This demonstration of the expected linear response from serial dilution proved that the instrumentation was synchronized and could collect data at any rotational frequency. Through the study of the results from blank measurements and the serial dilution of the yellow dye it was determined that the instrumentation was predictable and that there was a consistent 11% of data that must be discarded as a result of the failure of the servo-motor to trigger properly and not as a result of the instrumentation circuitry presented here.

After the development, testing and validation of this synchronized spectrometer three different experiments utilized the instrumentation. The first is described in this chapter where standard solutions of bromothymol blue in a solution of ethanol, water and acetic acid were prepared through serial dilution in order to calculate and present the absorbance of the solution. The absorbance is shown in a full spectrum plot and then used to produce an empirically derived extinction coefficient at the maximum intensity of the white light source, 466 nm. The data was also used to calculate the limit of detection (LOD) of the instrumentation for the bromothymol blue standard. At 466 nm the extinction coefficient was found to be $1.78 \times 10^4$ $mol^{-1}cm^{-1}$ and the LOD was calculated as $2.71 \times 10^{-7}$ molar bromothymol blue.

The second experiment is described in Chapter 3 of this thesis. This involved using small aliquots where a high concentration of yellow dye in aqueous solution was put through a design component that generated a series of sub-microliter aliquots to a receiving chamber. Owing to

the success of the instrumentation of the current chapter, it was possible to determine the volume of the sub-microliter aliquots transferred into a receiving chamber. The receiving chamber acted as a spectroscopic cell without ceasing rotation of the device.

The third experiment, where sand particulates were filtered on a CM device, has been described by Erin Templeton.[3] This study used real-time transmittance measurements without ceasing rotation to demonstrate the inefficiency of sedimentation by centrifuging and the effectiveness of an in-line filter. The present author's (Bouchard) contribution to the experiment was the development of the instrumentation as described here, as well as the additional MATLAB code to plot a wavelength in time for a cell on a CM device. This was done to observe scattering of light by reduced transmittance when the sample was a slurry of sand and water. In the future, this module of code can be used for observing eluting bands from chromatographic columns or to observe intermediate reactions in time.

# Introduction

High throughput analytical devices on the microfluidic scale generate less waste and decrease the cost and time required for analysis when compared to similar chemistries applied on a benchtop scale. Microfluidic principles have been used to develop micro total analysis systems (μTAS).[4] One classification of μTAS is the centrifugal microfluidic (CM) device, sometimes called Lab on a CD.[5] The benefits of CM are numerous with the most important to this demonstration being the consistent and easily controlled force that allows parallel operations on a single platform.[6] Optical detection was needed for analytical measurements while the device was in motion to fully take advantage of the controlling force.

Optical detection is broken into two classifications when working with microfluidics. The first is "off-chip" and the second is "on-chip." Off-chip describes using macro-scale

infrastructure to measure samples in a microfluidic component while on-chip describes the integration of micro-scale sensors into the microfluidic device. In 2007, Kuswandi published a review of the status of these two classes of optical detection.[7] In the review, absorbance, fluorescence, chemiluminescence and refractive index were explored. However, an application for centrifugal microfluidics was missing since even the integrated on-chip components were still wired to other instrumentation. One design of an on-chip methodology that might be applied to CM was discussed by Rodrigues in 2009 with the development of micro-flow devices by milling into a substrate of poly (methyl methacrylate).[8] Rodrigues used bromothymol blue as one of the standards for proving the design. This chapter describes an off-chip setup for CM devices to have optical detection while the device is in motion using two standard solutions; a commercial yellow dye and bromothymol blue.

The collection of spectroscopic data from CM devices in real time has been discussed by Steigert, in 2006, who used a laser to detect alcohol in whole blood after a reaction with a colorimetric dye.[9] Steigart collected single wavelength absorbance data by using refraction to take a laser beam from traveling perpendicular (axial) to the device to moving in the plane through the spectroscopic cell and then a second refractive surface to direct the laser beam out of the device and towards a detector.

Also collecting data in real-time, Duford published a servo-motor and strobe setup in 2009 for the collection of images while CM devices were in motion at speeds of up to 50 Hz.[10] The setup was comprised of a servo-motor that triggered both a strobe light and a black and white digital camera. It was capable of saving one image approximately every second.

The ability to perform full spectrum spectroscopy for qualitative and quantitative determination has been used in CM in the past. In an experiment to perform thin layer

chromatography on a CM device, Penrose et al. separated three coloured dyes and calculated plate height by measuring image intensity.[11] Xi et al. succeeded in determining the concentration of nitrate and nitrite by full spectrum absorbance with CM using the disk as a spectroscopic cell.[12] Kong et al. used a CM device in experiments to accurately measure aqueous sulfide in a sample by full spectrum absorbance. [13] Xi and Kong used the same setup for collection of spectroscopic data. The cells on the devices were filled with reagent and measured using a white light source and spectrometer. The devices were securely mounted on a stationary spindle separate from the instrumentation where the CM steps occurred. Both required that the CM device be stopped, removed from the servo-motor, transported to a spectrometer station where it was affixed and each cell measured individually.

The single wavelength methodology of Steigart was elegant in its ability to only collect light when the spectroscopic cell was located in a position where the laser beam would be directed by the refractive components into the device. Otherwise, the laser beam would pass through the device and not reach the detector. The ability to only collect data when the cell is correctly oriented was the determining factor in the development and success of the research described in this chapter. As indicated in the experimental section of this chapter, multiple iterations of methods to control when light from the LED source would reach the spectrometer were tested until selecting delay circuitry to time the generation of light so that it only occurred when a cell was present. A limitation of Steigert's approach was the use of a laser for collection of the spectroscopic data. A single wavelength for collecting data meant that the ratiometric method of this chapter could not be applied. By not compensating for differences in spectroscopic cells, the Steigert setup is less robust than the full spectrum methodology of this chapter. Additionally, the amount of light collected by Steigert was dependent on the rotational

frequency of the device. When the device was rotating faster, the cell passed by the laser beam faster and the amount of light collected by the detector was less at each revolution. In the method of this chapter, the integration time was independent of the rotation of the device since the pulse of the LED was controlled by delay circuitry.

All previous full spectrum experiments required stopping the motor so the disk could be used as a stationary spectroscopy cell. Synchronization of the spectrometer and the light source with the motor is necessary for real-time spectroscopic acquisition. Using the servo-motor configuration described by Duford et al.[10] an LED white light source and spectrometer were synchronized to measure absorbance in real-time at a range of rotational frequencies. Synchronized spectroscopy will allow the quantification of intermediate steps in CM and provide the opportunity to perform full spectrum data collection in real-time.

An LED provides the pulse of white light such that the length of the pulse can be controlled and be less dependent on a stabilization period. Also, the spectrum of light produced by the source can be selected by installing a different LED. The LED used for this thesis was a white light source with the greatest intensity of light produced around peaks at 466 and 550 nm. For use in this thesis, the application of the ratiometric method meant that absorbance measurements at 466 nm with reference measurements between 540 to 640 nm ensured an abundance of light was available for the calculation and use of higher concentrations of dyes. Bromothymol blue had a yellow appearance and absorbed around the highest intensity of the white light source when prepared with a 10% acetic acid aqueous solution; there was no absorbance at 600 or 640 nm, which were used as reference wavelengths.

# Experimental

## Fabrication of centrifugal device

A seven-layered test disk was constructed using materials and techniques previously described by Lafleur and Salin in 2009.[14] The chambers and channels of the design elements were created by Computerized Numerically Controlled (CNC) milling of polycarbonate layers with a QuickCircuit 5000 (T-Tech, Inc., Norcross, GA). The polycarbonate layers were blank DVDs 0.6 mm in thickness and CDs 1.2 mm in thickness (UTech Media Corp., Taiwan). Adhesive layers were produced using xerography and had chambers and channels cut from the layer in addition to passive adhesive valves. The adhesive, FLEXmount DFM-200-Clear V-95 150 poly V-95 400 poly, (FLEXcon, Spencer, MA, USA) was 0.102 mm in thickness. The adhesive was cut by xerography using a cutting plotter, CE3000MK2-60, (Graphtec America, Inc., Santa Ana, CA, USA). Chambers and channels were cut from the polycarbonate, 0.6 or 1.2 mm in depth.

The test disk shown in Figure 2-1 was designed to have 24 spectroscopic chambers. This design was used for the collection of data to demonstrate the setup accuracy and precision using serially diluted yellow dye.

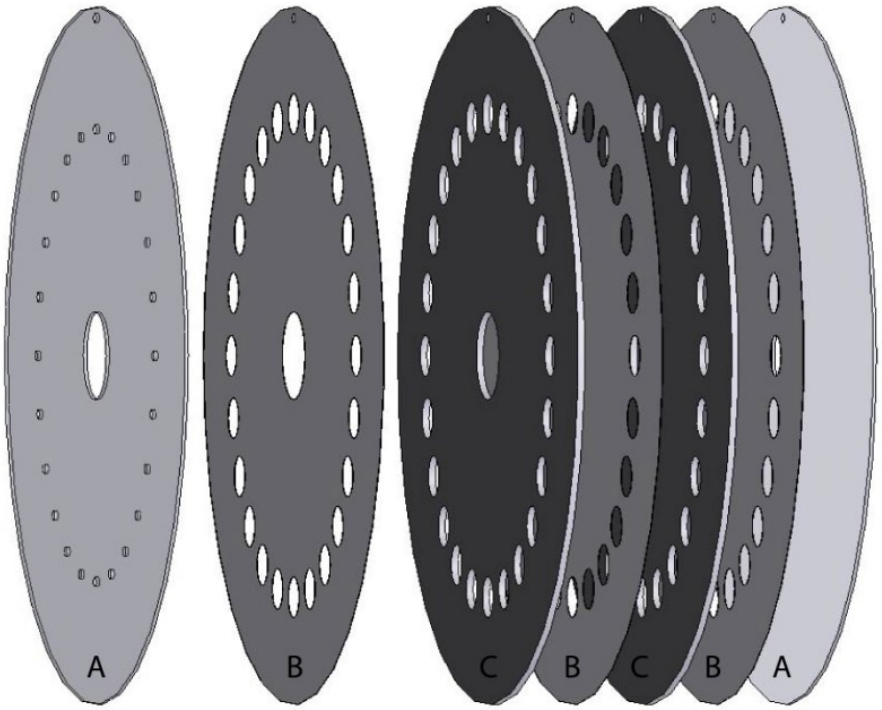


**Figure 2-1. Layers for construction of test disk**
Test disk of seven layers with 24 optical cells at a disk radius of 41.5 mm with a path length of 2.7 mm and a diameter of 6 mm. The construction includes (A) polycarbonate DVDs 0.6 mm thick, (B) double sided pressure sensitive adhesives 0.102 mm thick and (C) polycarbonate CDs 1.2 mm thick. This test disk was used for the measurement of the yellow dye.

A second test disk was fabricated using the same methodology for use with bromothymol blue. The disk had 20 spectroscopic cells, 10 mm in diameter. The centers of the cells were positioned equally around the center of the device at a radius of 50 mm. The cells were 5.3 mm in path length which was created by having four internal polycarbonate layers of 1.2 mm and 5 layers of double sided adhesives of 0.102 mm in thickness. The selection of polycarbonate as the substrate for the CM device, and therefore the spectroscopic cells, limited the range of wavelengths that could be measured due to polycarbonate not transmitting wavelengths less than 380 nm with severly reducing transmittance from 400 to 380 nm.

The design of CM devices in this thesis was performed using SolidWorks (2005 Dassault Systèmes, SolidWorks Corp.), a 3D Computer Aided Design (CAD) program that allowed the drawing of scale measured components. The files produced by the CAD can be milled with a

(CNC) from polycarbonate or cut from an adhesive using a cutting plotter xerography machine. The advantage of design in a CAD environment was the ability to adjust the specifications of design elements while maintaining desired relationships between components. In an iterative design process, the need to modify the location of chambers and valves while still maintaining the functional structure of the operation was critical for success.

Milling and cutting of layers for the construction of the device was achieved with a CNC mill and a cutting plotter. The designs generated in SolidWorks were saved in a format that could be implemented by the subtractive device. The CNC mill was a T-Tech milling machine that could read a.dxf file that would be translated by its software (ISO Pro). The cutting plotter would read a .dxf file that was processed through Adobe Illustrator. The plotter would then trace the design with a sharp cutting edge. The major difference in the interface between the design and production of different layers was the offset of the tool being used. The T-Tech used endmills, cutting tools which spin at a high speed (15,000 RPM) to rip material by cutting from the substrate. The tools used in this thesis had diameters ranging from 1 mm to 3.175 mm, which affected the design of the tooling path. The designed path is an infinitely small line, but the cutting path is the width of the endmill. Therefore, every design needed an offset from the path to the cutting edge of the tool to ensure the outcome matched the intended specification. The cutting plotter was treated as a perfect cut with no offset performed. Some attempts at an offset of 0.05 mm were made, however it was determined that the effect was negligible in the construction method.

The polycarbonate disks of the experimental layers were CD and DVD blanks that had been milled with microfluidic structures using a T-Tech milling machine. The lowest layer was a 1.2 mm thick CD blank to provide more stiffness to the finished device. The thicker CDs were

used in the building of the spectroscopic cells employed in this chapter where a longer path length was desirable. The adhesives were cut from a roll of FLEXmount and were 0.102 mm thick. The layers were aligned on a construction stage consisting of an aluminum base and a central spindle. Adhesive layers were affixed to the base of the construction stage using transfer tape and the polycarbonate disks were aligned by hand and lowered on the spindle onto the adhesive. The two pieces were pulled from the stage and cold laminated on a two roller press. After being rolled through the cold laminating press the next layer was added.

## Setup

The spinner and strobe setup described in 2009 by Duford[10] was supplemented with three additional self-contained modules in order to accomplish synchronized full spectrum visible light spectroscopy (Figure 2-2, Chapter 2 page 13). The Duford system included a Parker MPJ0922D3ENPSN servo motor with a Parker AR-08AE servo drive. Both the motor and drive were purchased from Cadence Automation, Quebec, Canada. The system was synchronized with a high-speed digital camera (Sony XCD-V50) and a strobe light (Shmpo DT-311A, Primo Instruments, Quebec, Canada). The system was controlled using "LabVIEW 8.6" (Developer Version, National Instruments, Quebec, Canada). In this chapter the camera and strobe light were not used for collecting images while the spectrometer was collecting data.

The first module added to the Duford system was a USB4000 (Ocean Optics Inc. Dunedin, FL, USA) spectrometer[15] controlled by SpectraSuite software (V 5.1, Ocean Optics, Inc.). The second module was a light-handling apparatus to collimate the light from a white light source before it was passed through the spectroscopic cell and focused into a collecting fiber optic attached to the USB4000. The third module was circuitry that (1) coordinated the collection

of light and the location of the spectroscopic cell, (2) delayed the pulse of the LED until the spectrometer was collecting light and (3) determined the length of the LED pulse.

The first and second design iterations of real-time spectroscopy on a rotating CM device used only the USB 4000 spectrometer and the light-handling apparatus. The light-handling apparatus was an optical arrangement of fiber optics that directed the light, lenses that collimated the light and an iris that reduced the intensity of light before it reached the spectroscopic cell. In the first design, the spectrometer would collect light from a single spectroscopic cell on a blacked out disk by having the light source continuously on. The second design attempted to coordinate the frequency of spectra collection with the rotational frequency of the device. The second design still used a single spectroscopic cell on a blacked out disk. The attempt was made so that data could be collected for shorter integration times. Such coordination proved unsuccessful.

The third design iteration used direct connections with the servo-motor in an attempt to synchronize the spectroscopic cell, the light source and the spectrometer. It was hoped that using the absolute position of the servo-motor to trigger the spectrometer to collect data and trigger the light source to pulse would give accurate and reproducible results on multiple spectroscopic cells without having to black out the disk. It was found that the noise of this third design was so great that it was not possible to determine which spectra were correct and which were incorrect. The noise was a result of direct electrical connections with no voltage handling circuitry between the servo-motor, the spectrometer and the light source.

The fourth iteration had a third module in addition to the spectrometer and light-handling apparatus. Its layout and usage is presented in detail in the remainder of this chapter as the successful design that enabled the performance of synchronized spectroscopy. The third module

consisted of delay circuitry that converted the falling edge output, or break point (BP), of the servo-motor into a rising edge for the USB4000 and a controlled pulse for a white light LED (Table 2-1, Figure 2-3). The collection of light by the spectrometer was triggered by the rising edge voltage generated by the delay circuitry.[15] The setup and circuitry are described in detail in the following; Figure 2-2, Figure 2-3, Table 2-1, Equation 2-1 and Table 2-2. Application of the setup is then described in the text following.

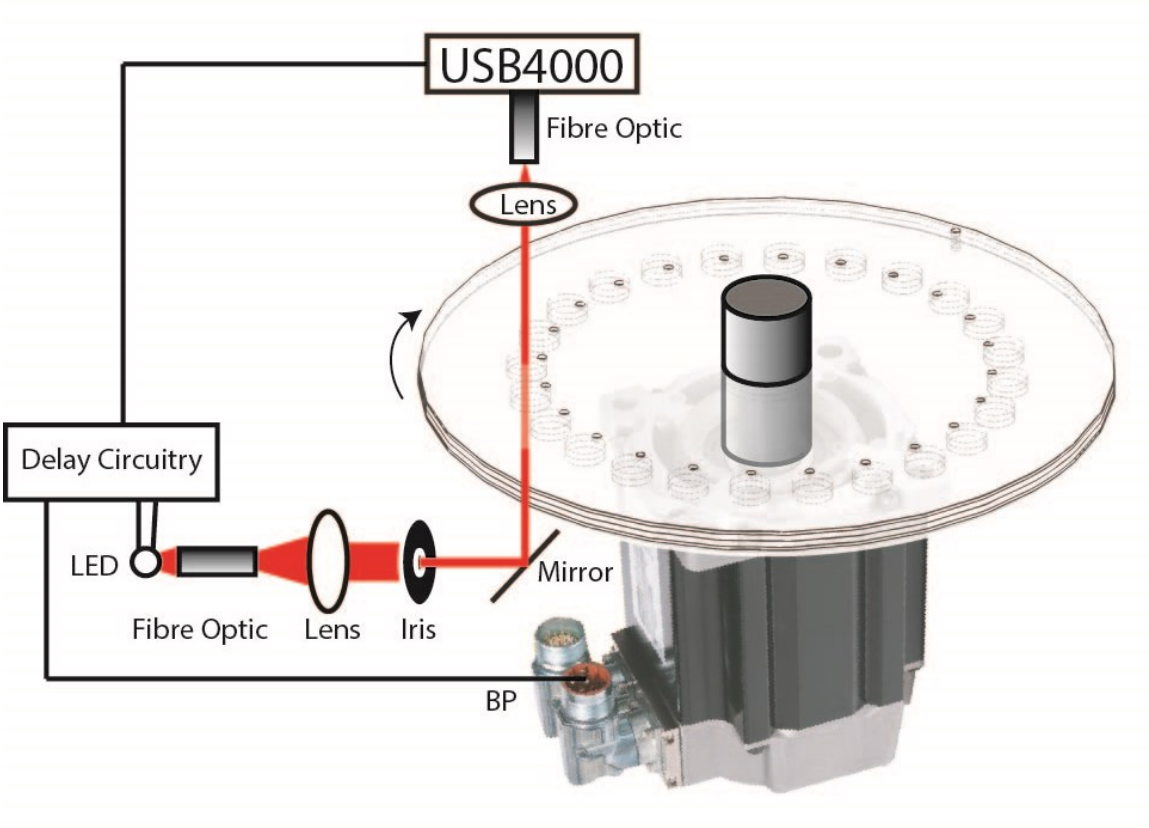


**Figure 2-2. Global schematic of experimental setup for synchronized spectroscopy**
The LED of Figure 2-2 has a cone of light that is collected by a fiber optic and then collimated by a lens and truncated by an iris. The iris reduced the area of the light on the disk so that smaller optical cells could be used on the CM device. A mirror directed the light through the disk and then a second lens focused the light into a fiber optic fed into the USB4000. Not shown is a plexiglass container surrounding the spinning device as an important safety feature if a reagent was to leak from the device.

The representation of Figure 2-2 references the delay circuitry and its connection to the servo-motor, spectrometer and LED. The delay circuitry layout is provided in Figure 2-3 where

the order of operations starts at the BP from the servo-motor. The delay circuitry reduced the noise of the servo-motor BP and coordinated signals to the USB4000 and LED. The signal first passed through a low pass filter to reduce the amount of high frequency noise from the servo-motor. (Figure 2-3a) Then the falling edge was simultaneously presented to a NAND gate (Figure 2-3b) and to the input of the first mono-stable vibrator. (Figure 2-3d1). The NAND gate was used as an inverter to generate a rising edge to be read by the USB4000 (Figure 2-3c), thus initializing the acquisition process on the USB4000 at the same time as the BP. The first monostable vibrator determined the delay until the LED pulse began. The first monostable vibrator generated a logic high signal pulse for 0.100 ms. The falling edge of the first mono-stable pulse triggered the second mono-stable vibrator (Figure 2-3d2), whose high signal pulse opened a Darlington pair (Figure 2-3e) which remained open for 0.175 ms, set by the resistor-capacitor (RC) circuit. The open Darlington pair allowed current to flow through the LED (Figure 2-3f) which acted as the white light source for the synchronized spectrometer.

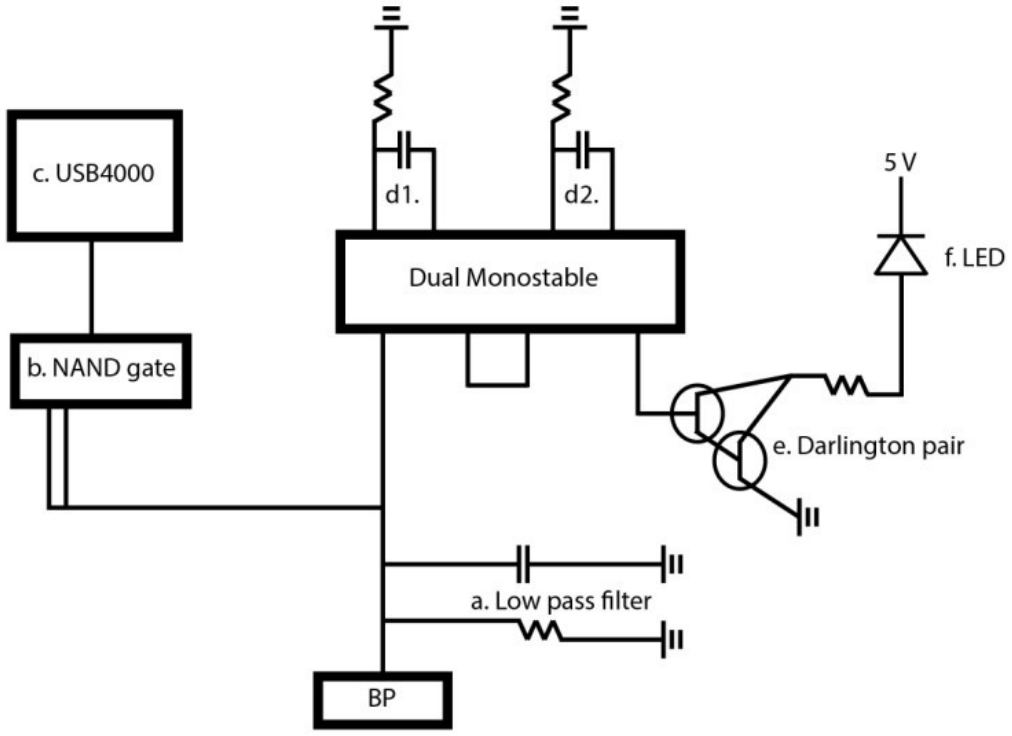


**Figure 2-3. Delay circuitry schematic for synchronized spectroscopy**
The BP (break point) from the servo motor passed through a low pass filter to remove high frequency noise. A NAND gate inverted the signal of the BP to trigger the USB4000. The BP also triggered Monostable 1 (d1), which in turn triggered Monostable 2 (d2) with delays of 0.100 ms and 0.175 ms respectively. Monstable 2 then triggered a Darlington pair that allowed current to flow to the LED when open. The determination of the pulse widths by the values of the RC circuit is explained in Equation 2-1.The resistor and capacitor values are outlined in Table 2-2.

The components and suppliers of the electronics described by Figure 2-3 are outlined in Table 2-1.

| Section | Component | Supplier |
|---|---|---|
| NAND Gate | 7404 | NEC Corporation, Minato, Tokyo, Japan |
| Monostable Vibrators | 74123 | Texas Instruments, Dallas, Texas, USA |
| Power Supply | 7805 | Motorola, Schaumburg, Illinois, USA |
| LED | #L1-1-W5TH15-1 | LED Supply, Randolph VT, USA |

**Table 2-1. Delay circuitry components**

The delays of 0.100 ms and 0.175 ms described in Figure 2-3 were generated by the dual monostable vibrator 74123 chip from Texas Instruments. The pulse width was determined by the

RC circuit and can be calculated by using Equation 2-1 provided by the manufacturer of the 74123 chip.

$$t_w = KR_xC_x$$

**Equation 2-1. Delay circuitry pulse width calculation based on resistor-capacitor values[16]**
This equation calculates the pulse width generated by the dual monostable vibrator chip 74123. An oscilloscope was used to tune the pulse widths using the two trimpots listed in Table 2-2. This equation was used to calculate the approximate resistance of those trimpots. $t_w$ is in ns, $R_x$ is in kΩ, $C_x$ is in pF, K is 0.37

The formula of Equation 2-1 references the resistance and capacitance of the RC circuits wired with the 74123 chip. The pulse widths were measured empirically with an oscilloscope and tuned by using trimmer potentiometers (trimpots) as the resistors. This was done to facilitate testing of the system by changing the pulse widths and to afford future users the flexibility to change the parameters of the light source. Knowing the pulse width and capacitance of the capacitors let the resistance values of the trimpots be calculated and are provided in Table 2-2. Table 2-2 also includes the magnitude of other resistors and capacitors shown in Figure 2-3.

| Location | Resistance and Capacitance Values |
|---|---|
| a. Low Pass Filter | 10 M Ω resistor<br>0.1 µF capacitor |
| d1. Monostable 1 | 50 k Ω trimpot (~2.7 K ohm setting)<br>0.1 µF capacitor |
| d2. Monostable 2 | 10 K Ω trimpot (~4.7 K ohm setting)<br>0.1 µF capacitor |
| f. Resistor to LED | 100 Ω resistor |

**Table 2-2. Resistance and capacitance values of Figure 2-3 (location labels match Figure 2-3)**

The second mono-stable pulse, and therefore the start of the LED, was delayed by 100 µs so that the LED did not turn on while the USB4000 was initializing which took 75 +/- 6 µs after it received the rising edge. The second mono-stable pulse of 175 µs after the initial delay determined the length of time the LED was on. This sequence of timed events starting with the BP at T=0 is outlined in Figure 2-4.

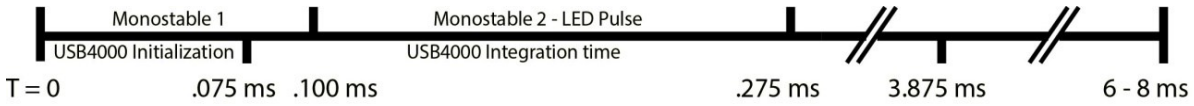


**Figure 2-4. Sequence of timed events for synchronized spectroscopy**

## Reagents

A yellow dye was used to establish the precision of the instrumentation and verify that the system was robust enough to generate accurate data from spectroscopic cells cut from a CM device. The yellow dye was a commercially available yellow food colouring (Club House, McCormick Canada, London Ontario) and was diluted in distilled deionized water (DDW). This specific yellow dye absorbed strongly at 466 nm and did not absorb at 542 nm. With both an absorbing and non-absorbing wavelength, a ratiometric method was used to overcome construction variance in the path length of the spectroscopic cells. A solution of three drops of yellow dye diluted in 100 mL of DDW was normalized at a concentration of 1.00 (unit less). Quantitative concentrations of 0.500, 0.250, 0.125 and 0.0625 were prepared by serial dilution. The absorbances of the coloured dye concentrations were measured using the synchronized spectrometer system to characterize the system. The reference spectrum for a blank of water is shown in Figure 2-5.

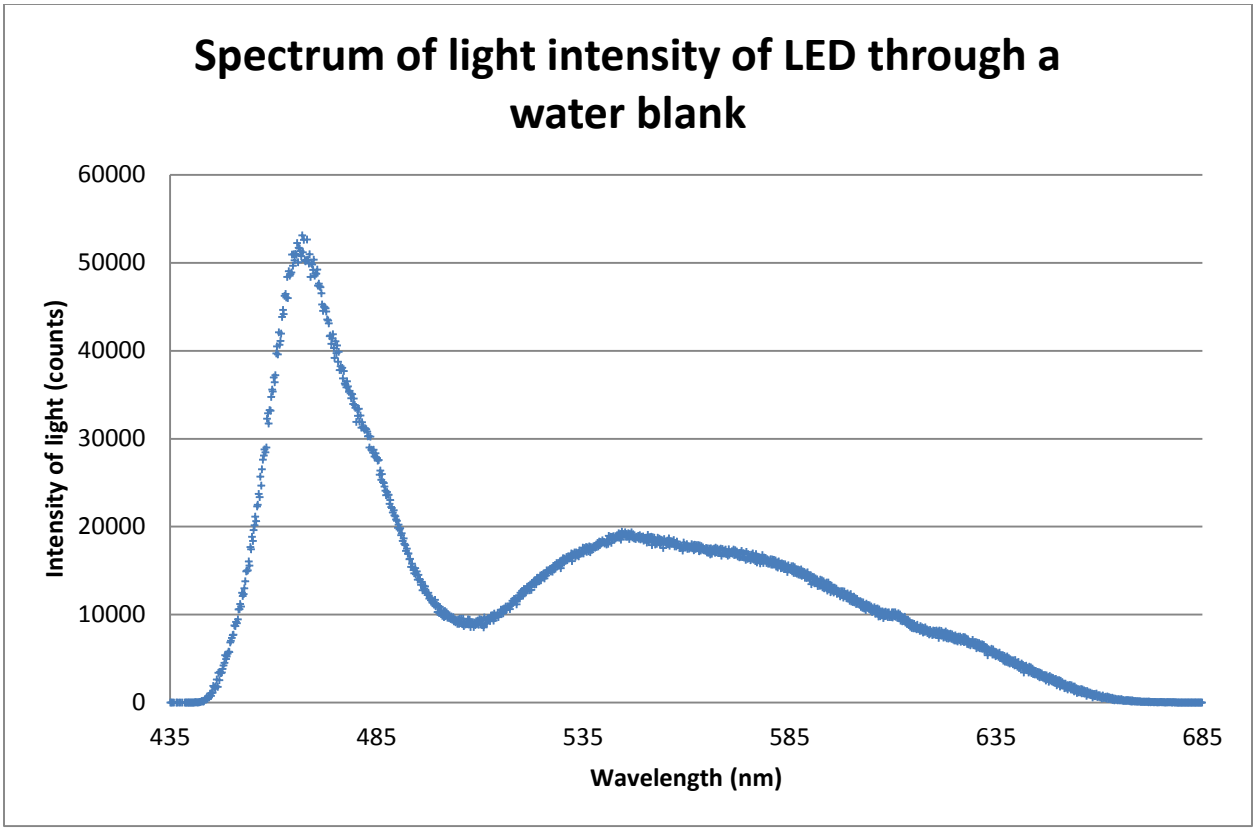


**Figure 2-5. Reference spectrum of the blank light intensity**
The commercial yellow dye and bromothymol blue were selected as standards for this chapter because of the highest intensity wavelengths produced by the LED. Yellow solutions absorb strongly at the wavelengths of highest intensity of the LED around 466 nm and do not absorb at the secondary peak between 540 and 640 nm.

To use the instrumentation to determine the extinction coefficient of a known substance, quantitative solutions of bromothymol blue were prepared. The bromothymol blue sodium salt crystals (Sigma-Aldrich, A.C.S. reagent: 114413-56, 12517AB, CAS# 76-59-5, FW 624.4, MW03271) were weighed by difference into two 100 mL volumetric flasks. The first was $5.54 \times 10^{-5}$ moles (0.0346 g) diluted to 100 mL in a 50% v/v ethanol solution. The solution was then serially diluted into four concentrations which each had 10 mL of glacial acetic acid (ACP A-0300 UN-2789 CAS# 64-19-7 Glacial Acetic Acid – 99.7%) added before dilution to 100 mL with DDW water. The second set of dilutions of bromothymol blue was made by starting with $6.01 \times 10^{-5}$ moles (0.0375 g) diluted in a 50% v/v ethanol solution. This was serially diluted into four solutions which each had 10 mL of glacial acetic acid added before dilution to

100 mL with DDW water. Combining the data from the two serial dilutions produced the calibration curve presented in the Results and Discussion section of this chapter (Figure 2-9, Chapter 2 page 31) and was used in the determinations of the bromothymol blue extinction coefficient and LOD. The blanks used for calculating absorbance of bromothymol blue were generated as 10 mL glacial acetic acid diluted to 100 mL with DDW. The solutions produced are outlined in Table 2-3 where the weight measured by difference was then serially diluted into the molar concentrations calculated.

| **Initial Weight (g): ->** | 0.03750 | **Initial Weight (g): ->** | 0.03460 | **Molar Concentration:** |
|---|---|---|---|---|
| ---- | ---- | Dilute by 1/8: | 0.00433 | 6.9266E-06 |
| ---- | ---- | Dilute by 1/2: | 0.00216 | 3.4633E-06 |
| Dilute by 1/32: | 0.00117 | ---- | ---- | 1.8768E-06 |
| Dilute by 1/2: | 0.00059 | ---- | ---- | 9.3840E-07 |
| Dilute by 1/2: | 0.00029 | ---- | ---- | 4.6920E-07 |
| Blank: | 0.00000 | ---- | ---- | 0.0000 |

**Table 2-3. Molar concentrations of bromothymol blue by serial dilution**
Two starting weights of bromothymol blue were used to serially dilute the molar concentrations used in the calibration curve of Figure 2-9. The five concentrations used are shown in the *Molar Concentration* column. These were generated by serially diluting by the ratios listed in the other columns into 100 mL volumes.

## Methods

The instrumentation was examined for precision of the light source through testing both without a CM device and with a single polycarbonate disk with no spectroscopic cells. The observations made during these tests were used to create methodologies for removing outlying data in a consistent way that produced valid data sets post-processing. The data collected by the USB4000 was stored by SpectraSuite's *High-Speed Acquisition Mode* in single text files that were parsed and analyzed using a custom MATLAB (VR2012a, MathWorks Inc., Natick, MA, USA) program (Appendix 1).

After confirming the precision of the light source, a 24 cell test disk was spun at 180 RPM with four replicates each of the blank (DDW) and five concentrations of serially diluted yellow

dye. Data collection was coordinated using LabVIEW (LabVIEW 8.6, Developer 17 version, National Instruments, Vaudreuil-Dorion, QC, Canada) to synchronize the LED pulse length and the integration time of the USB4000 spectrometer with the spectroscopic cell of interest as specified by the user. The servo-motor provided the absolute location of the spectroscopic cell by triggering the BP, while the generation of the BP was determined by settings in LabDAQ programmed by the user. The calibration curve prepared with the results of the commercially available yellow dye was used to prove the accuracy of the system by showing that the change in absorbance for each serial dilution was linear.

After establishing the accuracy of the system by generating expected absorbances for a series of serially diluted dye, the instrumentation was used to determine the extinction coefficient and LOD at 466 nm for bromothymol blue. A calibration curve of serially diluted concentrations of bromothymol blue dissolved in ethanol, DDW and glacial acetic acid was prepared. The spectroscopic cells of the device were 5.3 mm in path length. Using the calculated absorbance from the experimental data and the concentration from the quantitative dilutions it was possible to calculate the wavelength dependent extinction coefficient and LOD for bromothymol blue.

Additionally, this instrumentation was used to determine aliquot volumes generated by the design described in detail in Chapter 3 of this thesis. Moreover, this instrumentation was used in the publication reported by Erin Templeton for observing sedimentation of sand and fine particles in real time on a CM device.[3]

## Results and Discussion

The collection of multiple sets of spectra allowed the characterization and evaluation of the system described here. The precision of spectra taken from a single cell was compared with that from a set of spectra collected with no disk present. The intensities in both cases exhibited a

0.5% relative standard deviation (RSD) for a 0.66 nm bandpass and 1.050 ms integration time. The data of the 1.050 ms integration time was calculated by summing six spectra taken by the setup. Each spectrum had an integration time determined by the number of LED pulses with a pulse width of 175 μs, which rendered calculating longer integration times impractical. For example, a one second integration time would require 6000 spectra per cell.

Effective integration times of 0.175, 1.05 and 4.20 ms were calculated by summing the intensity of one, six and twenty-four spectra, respectively. Averages of 1, 3 and 5 pixels, corresponding to bandpasses 0.66, 1.98 and 3.30 nm respectively, were calculated at both the absorbing and non-absorbing wavelengths for each effective integration time. The RSDs of the raw intensities of blank spectra were calculated using different integration parameters and are displayed in Table 2-4.

| | **Integration Time (ms)** | | |
|---|---|---|---|
| Pixels Used | 0.175 | 1.050 | 4.200 |
| 1 | .65 | .42 | .28 |
| 3 | .49 | .36 | .30 |
| 5 | .47 | .35 | .28 |

**Table 2-4. Average RSD of light intensity of four blank cells at 466 nm and path length of 2.7 mm**
The average RSD of light intensity through blank spectroscopic cells were calculated using various parameters. The number of pixels was adjusted to 1, 3 or 5 giving bandpasses of .66, 1.98 or 3.30 nm respectively. These different bandpasses were each paired with integration times of 0.175, 1.050 or 4.200 ms.

The use of raw intensity for the calculation of RSD in Table 2-4 is important since confidence in the system is contingent on a stable and reproducible light source. The data suggests that even at one pixel and one pulse of the LED the error in light intensity is sufficiently small to be used in quantitative experiments. The statistic shown by Table 2-4 is the effect that averaging a greater number of pixels and summing a greater number of light pulses has on the RSD of the intensity of light coming through a spectroscopic cell filled with DDW. The setting used throughout this thesis was a bandpass of five pixels and a single pulse of light. The data of all the spectra would then be used to generate averages and standard deviations for that particular

cell. Only one pulse of light was ever used in these demonstrations because the objective was use in monitoring chemical reactions or elution chromatography in real time. In those proposed uses, the shorter integration time provides more data points and affords the researcher better insight into the intermediate steps of the experiment.

The intensity of light produced by the LED each pulse, along with its measured precision, indicates that it is sensitive enough for real-world samples when properly paired with devices with sufficient path length, rotational speed and delay of monostable 2 for the pulse width of the LED. After determining that each pulse of the LED maintained a consistent RSD unaffected by the presence of a device an external calibration curve was created to test the accuracy of the system.

Data was generated for calculation when an experiment was complete and the spectrometer output a .txt file that contained the spectra collected with each trigger by the servo-motor BP. A custom program, designed and coded by this author (Bouchard), controlled the loading of the .txt file from the spectrometer into the workspace of MATLAB where the first function was the exclusion of three types of spoiled spectra. These spoiled spectra made up ~ 11% of every set of raw data saved by the USB4000. At the rate data was collected (3 Hz), this amounted to only one spoiled time point every 3 seconds. The demonstration of the program and the code used is available in Appendix 1 and 2 of this thesis respectively.

The spoiled spectra were removed by the program by binning the intensities at a non-absorbing wavelength for each spectrum in increments of 1% of the highest intensity (i.e., the intensities were sorted into 100 bins). The bin with the highest occurrence was selected, and searching in both increasing and decreasing intensity, adjacent bins with non-zero values were included in the final set. Eventually, a zero value bin was encountered at a lower and higher

intensity than the highest value bin. These marked the extremes of the usable dataset and all others outside that range were excluded as spoiled spectra.

To trace the cause of the spoiled spectra three sets of data were collected. The first was to run the LED continuously with no disk and to run the USB4000 in the *High-Speed Acquisition Mode,* which measured the RSD of the USB4000 to be ~0.3% at 466 nm with a 0.66 nm bandpass. A second and third experiment were run collecting spectra from the pulsed LED with no disk present and with a disk present, where the RSDs were measured as ~0.5%. The only difference observed was a spectrum wide reduction in light intensity by ~10%, matching the refractive index of two air-polycarbonate interfaces, once when the light entered the disk and once when the light left the disk. Therefore, it was shown that there was a slight increase in RSD when the light source went from being continuously on to pulsing, but that there was no difference in the RSD when there was no disk present and when there was a disk present.

It was determined that there were two sources of spoiled spectra and increased noise. The first cause of spoiled spectra was the noise of the servo-motor break point (BP). If the noise triggered the spectrometer but not the LED, then the result was a dark spectrum. The second cause of error occurred when the servo-motor failed to trigger a BP. When running multiple optical cells on a single disk, failed BPs caused cells to be skipped in the set. The skipped cells then needed to be corrected for in the parsing of the file. As a result of the failed BP triggers, a small percentage of spectra registered a light intensity statistically higher than the rest of the dataset. The intensity of light from the LED was determined by the pulse width of the LED set by an RC circuit configured in a mono-stable vibrator. A longer light pulse resulted when the RC circuit was allowed to charge for more time and produced a statistically higher light intensity.

Therefore, when a BP trigger failed a cell spectrum was missed and a second spectrum needed to be removed.

The timestamp on each spectrum taken by the system was used in order to identify spectra that needed to be deleted or be filled with a placeholder. As described before, if the noise of the trigger from the servo-motor overcomes the threshold required to initiate the collection of light by the spectrometer, then there would be an erroneous spectrum in the dataset. This spectrum can be identified because it would be a dark spectrum with no intensity of light. Additionally, it was possible for a breakpoint to not trigger the spectrometer. In this case, there would be no spectrum at the expected timestamp. Not having the required spectrum in the set has implications for the sorting of a multi-cell experiment.

When running a multi-cell experiment the data is taken in a repetitive set such as cell 1, 2, 3, 4, 1, 2, 3, 4 … etc. Therefore, the set can be sorted by binning every $n^{th}$ spectrum as having been taken from the same cell. This only works after post-processing the dataset to ensure that each spectrum is located in the correct position in the dataset by both removing additional spectra and adding placeholders where spectra are not present. Examples of the corrections made when parsing the spectrometer file for multiple cells is provided in Table 2-5.

| Description | Set of Cells | Correction |
|---|---|---|
| Ideal | 1, 2, 3, 4, 1, 2, 3, 4 | N/A |
| Additional spectra taken | 1, 0, 2, 3, 0, 4, 1, 2, 0, 3, 4 | Remove additional spectra |
| Spectra are missing | 1, 3, 4, 2, 3, 4 | Add place holders:<br>1, , 3, 4, , 2, 3, 4 |

**Table 2-5. Outline of the two dataset error corrections made for parsing a spectrometer file**
To ensure that the dataset accurately reflected the state of the sample in the spectroscopic cell, the dataset of spectra had to be cleaned by removing spoiled spectra and by adding placeholders for missing spectra.

The program calculated absorbance as described previously[2] with a ratiometric calculation using the ratio of intensities at an absorbing wavelength ($\lambda 1$) and a non-absorbing wavelength ($\lambda 2$) from an average of all blank spectra from all blank cells. The formula used to calculate the

ratio is presented in Equation 2-2. This ratio is a measurement of the relative difference between the intensity of light at the absorbing wavelength and the non-absorbing wavelength. This ratio can then be used in Equation 2-3 to account for difference in path length, spectroscopic cell construction and light source noise by measuring intensity relative to a non-absorbing wavelength.

$$Ratio = \frac{I_{\lambda_{1blank}} - I_{\lambda_{1dark}}}{I_{\lambda_{2blank}} - I_{\lambda_{2dark}}}$$

**Equation 2-2. Calculation of ratio for the determination of transmittance for synchronized spectroscopy**
I is the intensity of light in counts as recorded by the USB4000 spectrometer. λ is the wavelength of either the blank or the dark spectrum.

The ratio generated by Equation 2-2 was then used to calculate transmittance from each spectra of every sample cell according to Equation 2-3.

$$Transmittance = \frac{I_{\lambda_{1sample}} - I_{\lambda_{1dark}}}{Ratio(I_{\lambda_{2sample}} - I_{\lambda_{2dark}})}$$

**Equation 2-3. Ratiometric calculation of transmittance for synchronized spectroscopy**
I is the intensity of light in counts as recorded by the USB4000 spectrometer. λ is the wavelength of either the sample or the dark spectrum.

Using the methods described, the serially diluted yellow dye proved the accuracy and precision of the instrumentation. The demonstration was executed by building an external calibration curve which was created by collecting data from 24 successive cells at 2.625 Hz from a disk spun at 180 RPM (3 Hz) for 23 minutes which generated a total of 147 spectra per cell. The reduction in collection frequency compared to the rotational frequency of the device was a result of collecting spectra from multiple spectroscopic cells during the same use of the device. In the case of a ten cell device, a spectrum would be taken every eleven-tenths of a rotation. This additional one-tenth of a rotation was calculated by LabVIEW and meant that it would take eleven rotations of the device to collect one spectrum from each of the ten cells. In this particular

experiment, the 24 cell device had spectra collected in three sets of eight cells each. The collection time of 23 minutes is a total time of collection over all 24 cells on the device. This collected 147 spectra per cell used to demonstrate further confidence in the precision of the light source and instrumentation since multiple cells were used for each concentration of the dye. The same observations of the RSD of the light intensity through a blank cell presented in Table 2-4 (Chapter 2, page 21) showed that a single non-spoiled spectrum reproducibly provides the intensity of light passing through a spectroscopic cell.

The instrumentation was recording data at a rate just less than 3 Hz. In practical terms, after the removal of spoiled spectra the instrument was producing 10 spectra every 4 seconds from a single cell and less if the time of the spectrometer was split amongst multiple cells i.e. 5 spectra every 4 seconds if there are two cells or 1 spectrum every 4 seconds if there are 10 cells. For the application of tracking absorbance in a single reaction chamber or the channel at the end of a chromatographic separation, the system is producing multiple full spectrum data sets every second. As demonstrated in Table 2-4 (Chapter 2, page 21) the relative standard deviation of the blank using single spectra is ~.5% which is precise enough for many applications.

A non-absorbing wavelength of 542 nm was used to account for variability in the light source and construction of the device.[2] It was observed that there was a consistent 10% reduction in intensity when observing light that passed through a single layer of polycarbonate vs. light that did not have any polycarbonate device in its path. When measuring intensity of light through an unmodified polycarbonate disk the variability in the surface of the polycarbonate is not observable with the combined noise of the light source and spectrometer. However, the spectroscopic cells of the devices used in this thesis were comprised of a cell filled with reagent that had a polycarbonate bottom and top. The two layers were assembled as described and have

variation in parallelism and in path length. Additionally, the light source had variation in the intensity of each light pulse. The combination of inter-cell variation and light source variation prompted the use of a non-absorbing wavelength to calculate the absorbance ratiometrically. If the path lengths were longer or shorter, and/or the intensity of light was greater or less, then the ratiometric method would compensate by using the non-absorbing wavelength as a standard against which to process the wavelength of interest.

The yellow dye solution absorbed strongly at 466 nm overlapping the highest intensity peak of the LED and was used to build the linear external calibration curve for the serially diluted concentrations. The absorbance was calculated with 542 nm as the non-absorbing wavelength with the previously described ratiometric method and removal of spoiled spectra. The curve built from the six concentrations was calculated to have an $R^2$ equal to 0.9996. The dataset was comprised of six samples including the blank, with four replicates of each. The concentrations were serially diluted from the normalized 1.00 stock solution. The concentrations, absorbance and standard deviation are presented in Table 2-6.

| Concentration | Average Absorbance | Standard Deviation |
|---|---|---|
| 0.00 | 0.0000 | 0.0016 |
| 0.0625 | 0.0093 | 0.0011 |
| 0.125 | 0.0217 | 0.0026 |
| 0.250 | 0.0383 | 0.0009 |
| 0.500 | 0.0763 | 0.0026 |
| 1.00 | 0.1499 | 0.0034 |

**Table 2-6. Concentration, average absorbance and standard deviation for serially diluted yellow dye**
The measurements were taken on a single device with four replicate cells of each concentration.

The plot of data in Table 2-6 is shown in Figure 2-6 with the linear equation and $R^2$ value.

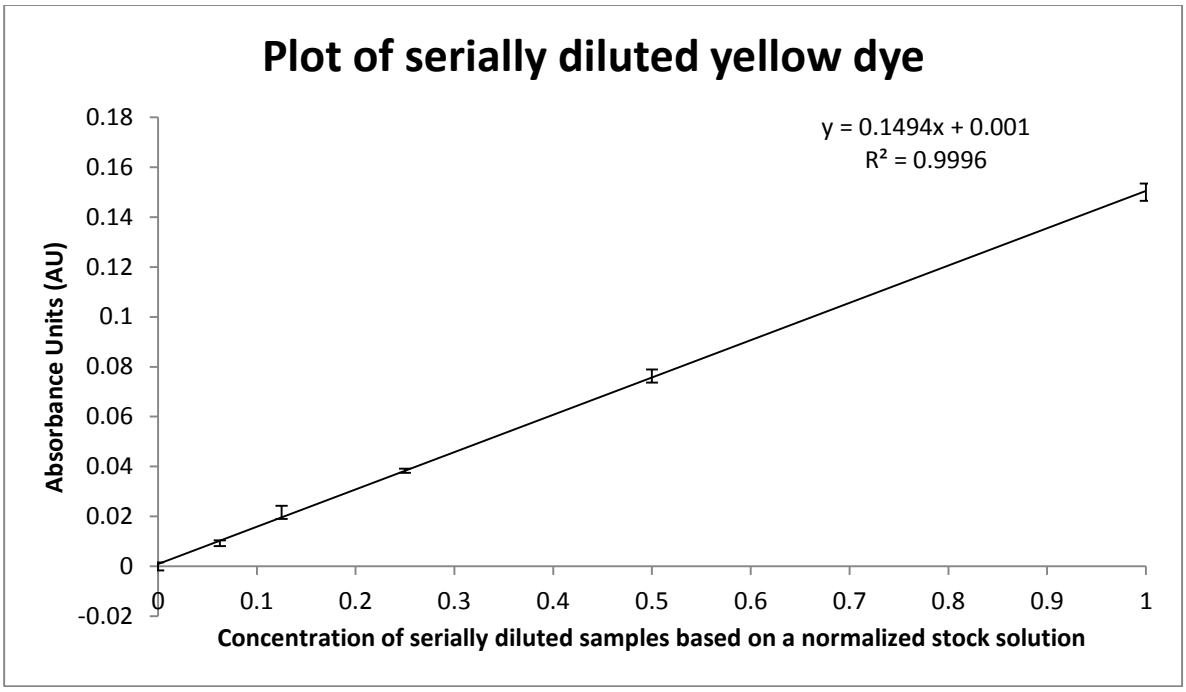


**Figure 2-6. Plot of serially diluted yellow dye**
The concentrations of the commercially available yellow dye were normalized on a stock solution and then serially diluted to produce the set of concentrations seen here. The absorbance was calculated for each individual spectroscopic cell with 147 spectra making up the calculated absorbance for each. The absorbances of the four cells at each concentration were then averaged and the standard deviation calculated to create the curve with the error bars presented in this figure.

The LOD and dynamic range were not calculated for the commercial yellow dye because a non-quantitative, normalized starting concentration was used for the creation of the solutions. Additionally, both LOD and dynamic range are dependent on the path length of the cell which is tunable for real-world samples. The system produces enough torque and light for much larger devices and longer path lengths and would not be taxed to produce accurate and precise results. Initial tests with serial dilutions of dye succeeded in the objective of this chapter: to construct and validate a method for synchronized visible light spectroscopy on a CM device in motion. Both precision and accuracy were proven by studying the noise of the light intensity and the accurate demonstration of linear response to dilution.

At the conclusion of demonstrating the instrumentation, showing that it performed as designed and was robust enough to generate accurate results for a serial dilution, further

experimentation was executed with the system. One of those experiments was the determination of the extinction coefficient of bromothymol blue at a wavelength of 466 nm. The CM device used had twenty evenly spaced spectroscopic cells, each with a 5.3 mm path length. The device was constructed from polycarbonate as described earlier. The cells were filled with varying concentrations of bromothymol blue prepared through serial dilution as outlined in Table 2-3 of the *Reagent* section of this chapter. (Chapter 2, page 19) The concentrations are also provided in Table 2-7 along with the measured absorbance and standard deviation at 466 nm.

| **Molar concentration x $10^7$** | **Molar concentration** | **Absorbance** | **Standard deviation** | **Number of values** |
|---|---|---|---|---|
| 0.0 | 0.00 | 0.000 | 0.0085 | 163 |
| 4.7 | 4.69E-07 | 0.034 | 0.0026 | 170 |
| 9.4 | 9.38E-07 | 0.060 | 0.0028 | 156 |
| 18.8 | 1.88E-06 | 0.133 | 0.0028 | 158 |
| 34.6 | 3.46E-06 | 0.282 | 0.0091 | 104 |
| 69.3 | 6.93E-06 | 0.650 | 0.0062 | 114 |

**Table 2-7. Data of calibration curve in Figure 2-9, concentration vs. absorbance.**
The values of Table 2-7 were used to plot the calibration curve for bromothymol blue in Figure 2-9. The calculation of absorbance was done using the ratiometric method with an absorbing wavelength of 466 nm. The linear regression of this data determined the extinction coefficient and LOD for bromothymol blue. The data was collected using two devices. Both devices contained four replicates each of a blank and four serially diluted concentrations of bromothymol blue.

A plot of the light intensity spectrum for the high concentration of bromothymol blue has been superimposed with the light intensity spectrum of a blank comprised of DDW and acetic acid in Figure 2-7. It can be seen that the range of non-absorbing wavelengths begins at approximately 590 nm and continues beyond the range of light produced by the white light LED of the synchronized spectrometer setup. This range was used in the removal of spoiled spectra and in the calculation of absorbance by ratiometric method.

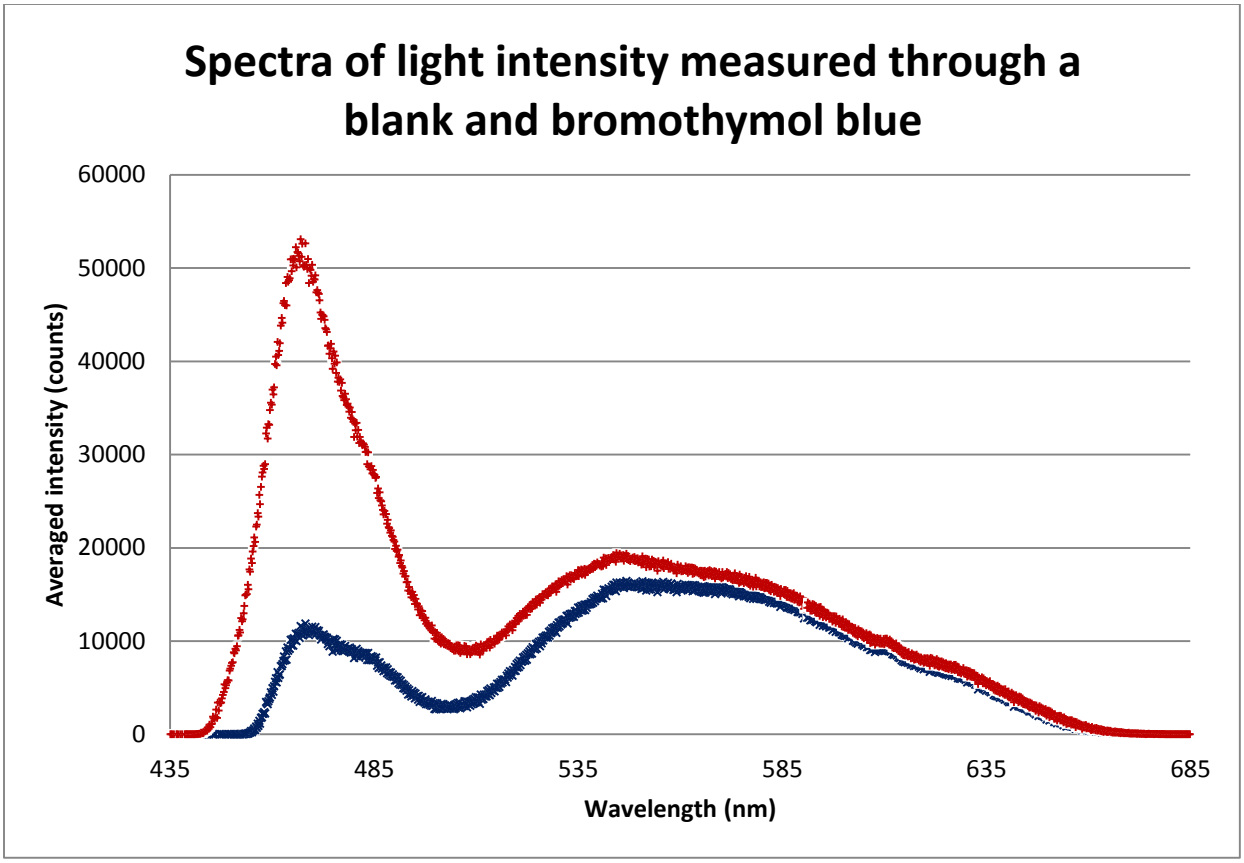


**Figure 2-7. Spectra of light intensity measured through a blank (red) and bromothymol blue (blue)**
These curves are comprised of 20 averaged 175 µs integration time spectra collected 5.3 mm path length spectroscopic cells. The molar concentration of the bromothymol blue was $6.93 \times 10^{-7}$. The red curve with an averaged intensity above 50,000 at 466 nm is the spectra of light intensity of the blank. At the same wavelength of 466 nm the concentration of bromothymol blue, the blue curve, has an intensity of approximately 10,000 counts.

In the calculation of absorbance by wavelength in Figure 2-8 no ratiometric method was implemented. Each pixel had its absorbance calculated using Equation 2-4.

$$A = -log(\frac{I_0}{I_T})$$

**Equation 2-4. Calculating the absorbance by wavelength**
The equation used for calculating the absorbance at each pixel for Figure 2-9. $I_0$ is the intensity of the light input, i.e. the blank intensity. $I_T$ is the intensity of the light transmitted, i.e. the sample intensity.

In Equation 2-4 the ratio of input intensity to blank intensity is the transmittance of the sample. This transmittance was replaced with the transmittance calculated in Equation 2-3 (Chapter 2, page 25) for the ratiometric method to calculate the absorbances in Table 2-7. When

calculating the absorbance at each wavelength as in Figure 2-8, the ratio was not implemented. When calculating the absorbance at a single wavelength across multiple samples and spectroscopic cells, the ratiometric method was implemented.

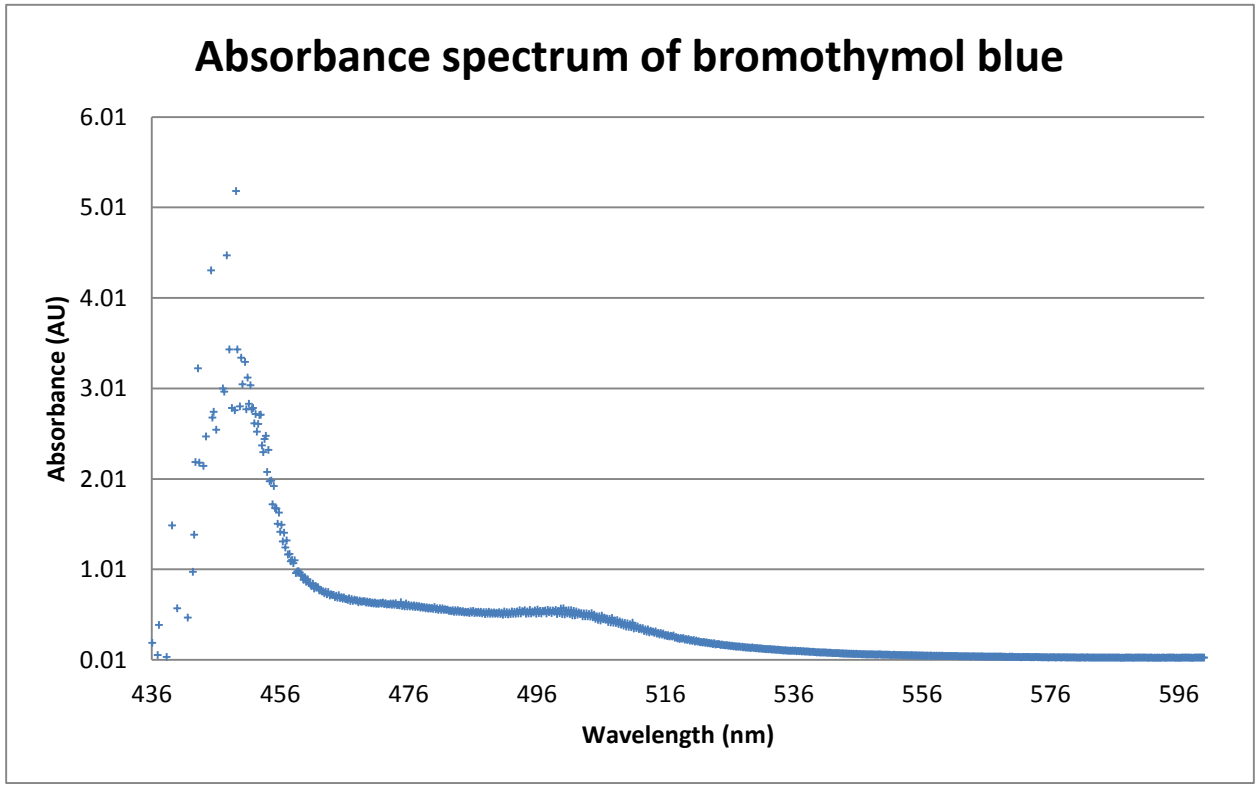


**Figure 2-8. Absorbance spectrum of bromothymol blue**
The absorbance spectrum of a 6.93 x $10^{-7}$ molar bromothymol blue solution in a 5.3 mm path length cell and a 175 µs integration time is shown here. The blank and standard measurements are comprised of 20 averaged spectra and the absorbance was calculated for each pixel using Equation 2-4. No ratiometric method was used.

The increase in noise observed in Figure 2-8 at wavelengths less than 466 nm is a result of the decreased intensity of light produced by the LED at those wavelengths. In Figure 2-7 the blank spectrum of the white light source can be seen where, at the maximum absorbance of bromothymol blue (436 nm), the white light source produced fewer photons which decreased the signal-to-noise ratio.

The plot of Figure 2-9 was built using the results from five serially diluted concentrations of bromothymol blue presented in Table 2-7. (Chapter 2, page 29)

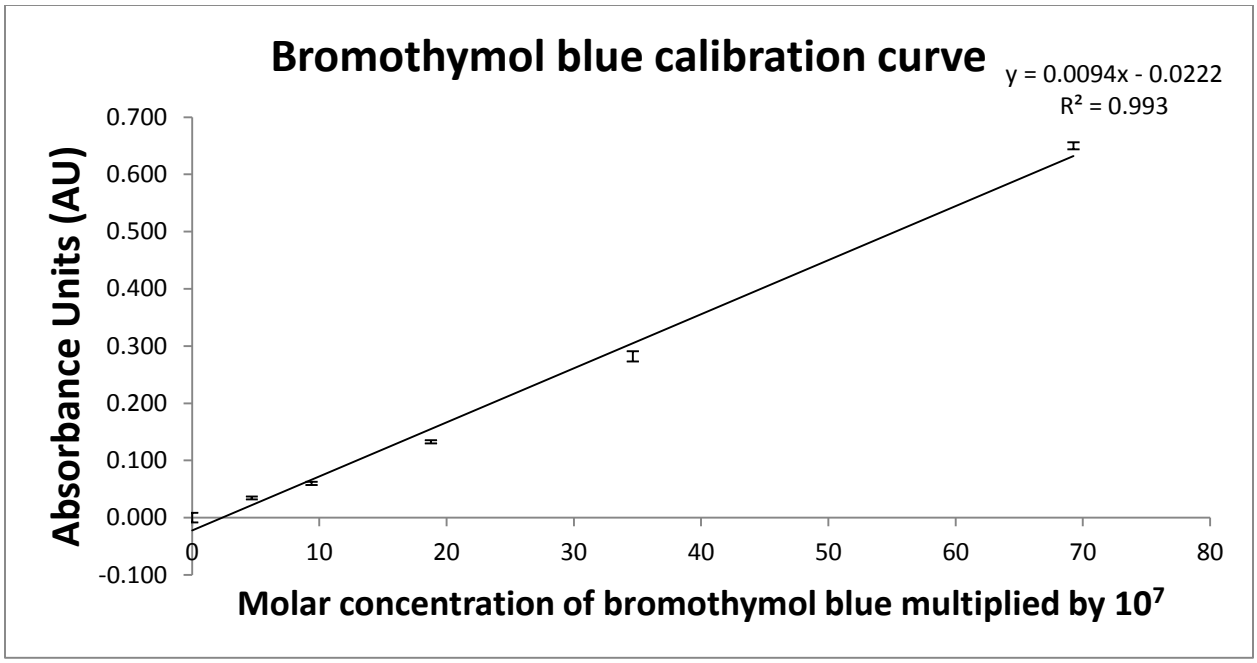


**Figure 2-9. Bromothymol blue calibration curve**
The methodology described produced the linear curve used to determine the extinction coefficient of bromothymol blue at 466 nm.

The data of Table 2-7 (Chapter 2, page 29) produced the plot of Figure 2-9 and is statistically described by the linear regression provided in Table 2-8.

| | | | |
|---|---|---|---|
| Slope | 94000 | -0.022 | Intercept |
| Error Slope | 3900 | 0.013 | Error Intercept |
| $R^2$ | 0.993 | 0.0225 | Error on Y |
| F | 590 | 4 | Degrees of Freedom |
| Regression SS | 0.30 | 0.0020 | Residual SS |

**Table 2-8. Statistics of the bromothymol blue calibration curve in Figure 2-9 and the values of Table 2-7**

Using the data of Table 2-8 the extinction coefficient of bromothymol blue at 466 nm was found to be $1.78 \times 10^4$ $mol^{-1}cm^{-1}$. The extinction coefficient was calculated by dividing the slope of the calibration curve in Figure 2-9 by the path length of the spectroscopic cells in centimeters. The LOD was calculated using Equation 2-5 to be $2.71 \times 10^{-7}$ molar bromothymol blue at a wavelength of 466 nm.

$$LOD = \frac{3S_{bk}}{m}$$

**Equation 2-5. Calculating the Limit of Detection (LOD)**
The equation used for calculating the LOD of bromothymol blue at 466 nm using the spectroscopic cells and apparatus described in this chapter where the LOD is the molar concentration, $S_{bk}$ is the standard deviation of the blank, m is the slope of the calibration curve. The standard deviation of the blank was measured using 163 measurements from the blank cells of the device.

The error observed in the calibration curve can be attributed to variation in cell construction and sample preparation. The small standard deviations for multiple measurements taken in the same cell are indicative of the precision of the instrumentation. This is contrasted with the results presented in Chapter 3 and included in this chapter for comparison. The error inherent in producing 750 nL aliquots generated large noise in comparison to the volumetrically prepared dilutions of bromothymol blue. The absorbance was used to calculate the volume added with each aliquot and is shown in detail in Chapter 3, Figures 3-10 and 3-11.
(Chapter 3, pages 19 and 20)

## Experiments using Synchronized Spectroscopy

The setup was used in two further experiments after its accuracy and precision were established as detailed above. The first was small aliquots outlined in Chapter 3 of this thesis. A design was developed to repeatedly deliver 750 nL aliquots of aqueous solution to a receiving chamber. The accuracy and precision of the design was determined using the spectrometer and equations outlined in this chapter. The absorbance of a receiving chamber at specified time increments that aligned with an aliquot addition was able to determine that the volume added was 750 nL with a standard deviation of 170 nL over the course of eight sequential aliquots. The methodology of the small aliquot design and the measurement of the aliquot volume are discussed in Chapter 3 of this thesis. For comparison to the curves built for the serially diluted

commercial yellow dye and bromothymol blue, the averaged absorbances for small aliquots is plotted here in Figure 2-10. The absorbance is converted into volume added per aliquot in the calculation of Chapter 3.

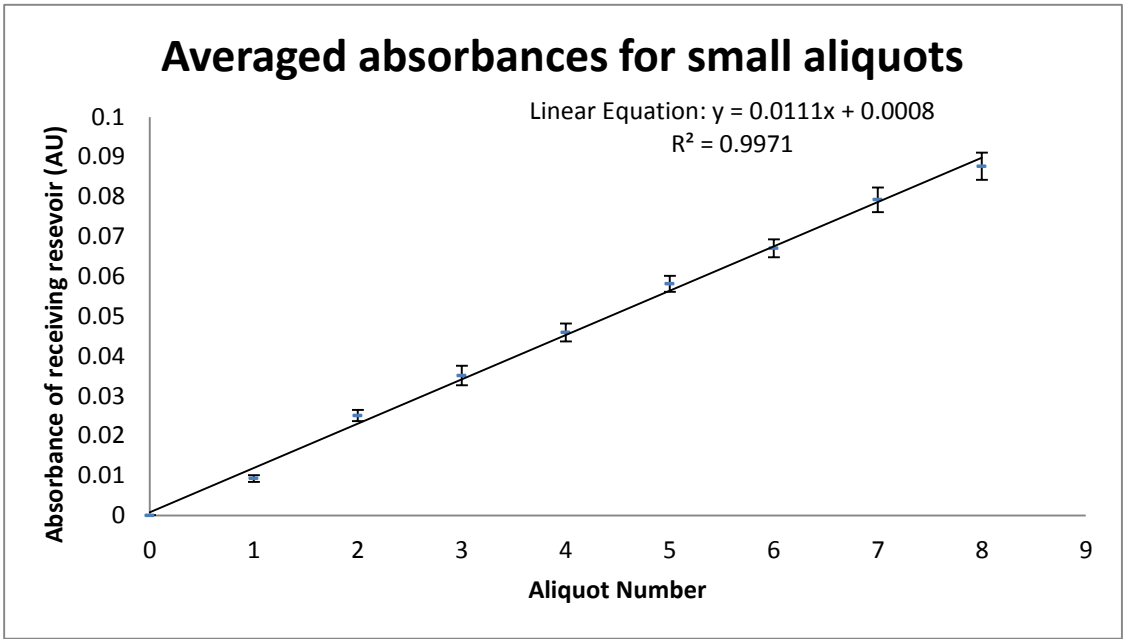


**Figure 2-10. Use of the spectrometer to measure absorbance for calculating aliquot volume**
This plot is a demonstration of the use of the synchronized spectrometer to take real time absorbance measurements of a receiving reservoir while small aliquots of yellow dye were dispensed. The design and testing of that CM function is discussed in detail in Chapter 3 of this thesis. The calculated absorbance was used to determine the volume added each aliquot.

The spectrometer running in real-time is critical to the structure of the small aliquot design. If rotation were stopped then control of the aliquoted liquid would be lost rendering the metering chamber useless. The application of spectroscopy instrumentation to the analytical tools of the CM laboratory directly influenced the decision to pursue the generation of small aliquots. Prior, it was not possible to observe volumes in the sub-microliter range given the limitation of milling the devices and the limited pixels for the observation of the volume via imaging. In the paper by Kazarine et al., the limitation of image processing for determination of volume in a chamber was limited to volumes of 10 μL with an RSD of 1%.[17]

The second experiment that utilized synchronized spectroscopy for the collection of real time data was the measurement of sand sedimentation in water on a CM device.[3] Sedimentation was defined by the amount of light that was scattered by particles that did not settle due to the application of centrifugal force on the microfluidic cell filled with sand suspended in an aqueous solution. The intensity of light was used to demonstrate the scattering of the sample. This experiment was done to show that a novel filtration design successfully kept fine particles of sand from entering the receiving reservoir/spectroscopic cell. The plot of light intensity over time while the sample is sedimenting is shown in Figure 2-11. If it were required that the disk is stopped to take each measurement then the demonstration of sedimentation over time would not be possible.

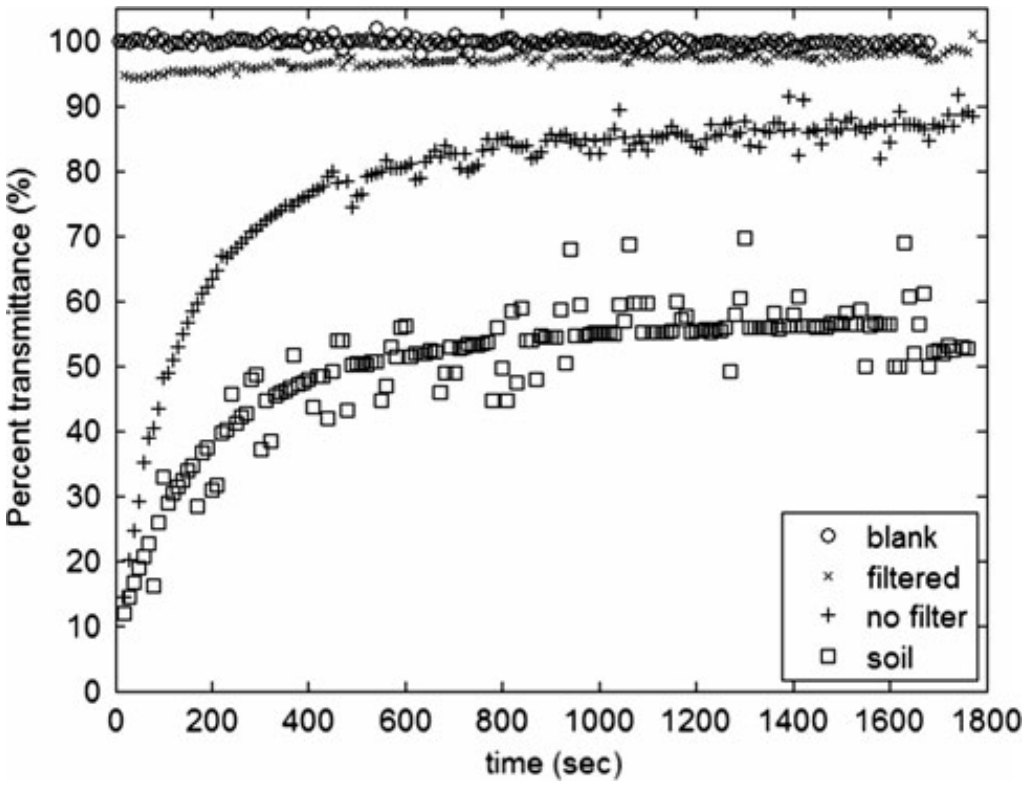


**Figure 2-11. Demonstration of Filtration by Erin Templeton[3] (Figure and caption taken from paper)**
Light loss caused by particles at 467 nm measured in per cent transmittance over 30 min in blank (DDW) samples (N = 3), filtered samples (N = 4), samples run both through the 3D path with no filter (no filter, N = 4), and simply injected into the detection chamber (soil, N = 3)

# Conclusions

A highly reproducible and accurate setup to perform synchronized full spectrum visible light spectroscopy on a CM Device in motion has been demonstrated. The problem of liquid control while the CM device is not in motion is alleviated by using synchronized spectroscopy. Using the instrumentation built for this Chapter; (1) the light intensity of a single cell was calculated as ~.5% RSD, (2) $R^2$ values greater than 0.999 were demonstrated for an external calibration curve of five concentrations of dilute yellow dye, (3) the extinction coefficient and LOD for bromothymol blue was calculated, (4) sub-microliter volumes of reagent aliquots were measured and (5) sedimentation was observed on a preparative CM device.

The modular components enable quantitative full spectrum measurements to be taken at intermediate steps of experiments while continuously applying centrifugal force and could be applied to the measurement of titrations and elutions in the future. While stopping a disk to take spectra will always be available as an option in CM experiments, the use in small aliquots and sedimentation show the importance of the ability to collect real time data.

# Acknowledgements

The work of this chapter was aided by the early contributions from Ling Yi Tam, who would assemble CM devices to test the synchronized spectrometer setup and then troubleshoot electrical issues. The data analysis was completed using a MATLAB GUI program designed and written by the author (Bouchard). The program was optimized and made more robust in collaboration with Alexei Kazarine. Additionally, Erin Templeton used the setup and MATLAB GUI to produce a figure of her results which is included and referenced in Chapter 2 with her permission.

The author (Bouchard) would like to also thank Rick Rossi and Weihua Wang for electronics support. They constructed the final housing and soldered the delay circuitry from the design drawn and prototyped by the author (Bouchard).

# References


1. King, D.; Osullivan, M.; Ducrée, J., Optical detection strategies for centrifugal microfluidic platforms. Journal of Modern Optics 2014, 61 (2), 85-101.
2. LaCroix-Fralish, A.; Clare, J.; Skinner, C. D.; Salin, E. D., A centrifugal microanalysis system for the determination of nitrite and hexavalent chromium. Talanta 2009, 80 (2), 670-675.
3. Templeton, E. J.; Salin, E. D., A novel filtration method integrated on centrifugal microfluidic devices. Microfluidics and Nanofluidics 2013, 1-7.
4. Arora, A.; Simone, G.; Salieb-Beugelaar, G. B.; Kim, J. T.; Manz, A., Latest developments in micro total analysis systems. Analytical Chemistry 2010, 82 (12), 4830-4847.
5. Madou, M.; Zoval, J.; Jia, G.; Kido, H.; Kim, J.; Kim, N., Lab on a CD. Yarmush, M. L., Ed. 2006; Vol. 8, pp 601-628.
6. (a) Gorkin, R.; Park, J.; Siegrist, J.; Amasia, M.; Lee, B. S.; Park, J. M.; Kim, J.; Kim, H.; Madou, M.; Cho, Y. K., Centrifugal microfluidics for biomedical applications. Lab on a Chip - Miniaturisation for Chemistry and Biology 2010, 10 (14), 1758-1773; (b) Mark, D.; Haeberle, S.; Roth, G.; Von Stetten, F.; Zengerle, R., Microfluidic lab-on-a-chip platforms: Requirements, characteristics and applications. Chemical Society Reviews 2010, 39 (3), 1153-1182; (c) Zoval, J.; Jia, G.; Kido, H.; Kim, J.; Kim, N.; Madou, M. J., Springer Handbook of Nanotechnology 2007, 549-570.
7. Kuswandi, B.; Nuriman; Huskens, J.; Verboom, W., Optical sensing systems for microfluidic devices: A review. Analytica Chimica Acta 2007, 601 (2), 141-155.
8. Rodrigues, E. R. G. O.; Lapa, R. A. S., Development of micro-flow devices by direct-milling on poly(methyl methacrylate) substrates with integrated optical detection. Microchimica Acta 2009, 166 (3-4), 189-195.
9. Steigert, J.; Grumann, M.; Brenner, T.; Riegger, L.; Harter, J.; Zengerle, R.; Ducrée, J., Fully integrated whole blood testing by real-time absorption measurement on a centrifugal platform. Lab on a Chip - Miniaturisation for Chemistry and Biology 2006, 6 (8), 1040-1044.
10. Duford, D. A.; Peng, D. D.; Salin, E. D., Magnetically driven solid sample preparation for centrifugal microfluidic devices. Analytical Chemistry 2009, 81 (11), 4581-4584.
11. Penrose, A.; Myers, P.; Bartle, K.; McCrossen, S., Development and assessment of a miniaturised centrifugal chromatograph for reversed-phase separations in micro-channels. Analyst 2004, 129 (8), 704-709.
12. Xi, Y.; Templeton, E. J.; Salin, E. D., Rapid simultaneous determination of nitrate and nitrite on a centrifugal microfluidic device. Talanta 2010, 82 (4), 1612-1615.
13. Kong, M. C. R.; Salin, E. D., Spectrophotometric determination of aqueous sulfide on a pneumatically enhanced centrifugal microfluidic platform. Analytical Chemistry 2012, 84 (22), 10038-10043.

14. Lafleur, J. P.; Salin, E. D., Pre-concentration of trace metals on centrifugal microfluidic discs with direct determination by laser ablation inductively coupled plasma mass spectrometry. Journal of Analytical Atomic Spectrometry 2009, 24 (11), 1511-1516.
15. Ocean Optics, USB 4000 Data Sheet. 830 Douglas Ave. Dunedin. FL 34698.
16. Semiconductor, F., DM74LS123: Dual Retriggerable One-Shot with Clear and Complementary Outputs. 1986 - Revised 2000.
17. Kazarine, A.; Salin, E. D., Volumetric measurements by image segmentation on centrifugal microfluidic platforms in motion. Lab on a Chip - Miniaturisation for Chemistry and Biology 2014, 14 (18), 3572-3581.

# CHAPTER 3: Small Aliquots

In Centrifugal Microfluidics, a limitation that has been repeatedly identified is the inability to perform a series of sequential steps on one device.[1] This is especially true with repetitive steps like the addition of aliquots to a reaction chamber. Therefore, opportunity existed for the development of a methodology for continuous addition of small aliquots. This chapter presents repetitive metered aliquots, of sub-microliter volumes, that could be used for titrations or the slow addition of reactive reagents.

## Contribution to Original Knowledge

A novel method for reproducibly and repeatedly adding sub-microliter volumes of reagent to an experimental chamber was developed and demonstrated. The applications envisioned when selecting this function for development included titrations, slow addition of reactive reagents and accurate small aliquots to use for quantitative separations. The function also allowed the continued demonstration of the synchronized spectrometer of Chapter 2.

# Abstract

A centrifugal microfluidic (CM) device was designed to repeatedly deliver sub-microliter aliquots of aqueous solution to a reaction chamber. The accuracy and precision of the design was determined using visible light spectroscopy collected in real-time as the device was in motion. The volume delivered was found to be tunable and the device was capable of producing measured volumes of 750 nL with a standard deviation of 170 nL over the course of eight sequential aliquots. The design utilized the compression of air in a valveless, ventless chamber. The compressed air generated the force used to move reagent to the center of the device every time the rotational frequency of the CM device was lowered. The reagent would then fill a small metering chamber located at an inner radius of the disk. After the metering chamber was filled the rotational frequency of the CM device would be increased to re-compress the air and drain the metering chamber into the receiving reservoir.

# Introduction

A branch of micro total analysis systems (μTAS) called Centrifugal Microfluidics (CM) was described in a letter by Felton in 2003 titled "CD Simplicity."[2] Felton discussed the current and potential advantages of this form of lab-on-a-chip design and reviewed the commercial applications built by Tecan, Gyros and Burstein Technologies. However, one disadvantage of CM that has been repeatedly identified is the inability to perform a series of sequential steps.[1] This is a disadvantage when compared to the high-throughput methodologies of traditional μTAS.

The most common design feature to control experimental steps in a CM device is the passive capillary valve. A capillary valve is a small opening that restricts liquid flow by surface tension at an opening. In this thesis, surface tension restricts flow from capillary valves. High

pressure generated by centrifugal force can overcome the surface tension. At a high rotational frequency the liquid will "burst" or rapidly clear from the capillary valve. In 2007, Ducree published work on a Bio-Disk Platform that included the theoretical derivation of the competing variables in passive valves that use the described geometric restrictions.[3] Using the equations of Ducree it was possible to calculate rotational frequencies that can be used to "burst" passive valves. The design presented in this chapter used a single passive valve to restrict liquid flow at the base of a metering chamber.

The accurate measurement of reagent volumes during experimentation is essential to the quantification of an analysis. In microfluidics, volumes of liquid are used on the microliter or sub-microliter scale. As a result, the ability to generate accurate, reproducible aliquots in the single microliter range is important. On CM devices, aliquots have traditionally been produced with a metering chamber where excess solution is diverted to a waste chamber and the volume that had been metered is drained into an experimental cell.[4] In 2007, Steigert published a siphon-based metering design that was used for the analysis of whole blood.[5] This design concept is simple, robust and capable of being used repeatedly if there is a way to continuously fill and drain the metering chamber. Mark described a design in 2011 that has the reagent of interest fill multiple metering chambers as the excess reagent pours off to waste.[6] These multiple metering chambers would drain into different reaction chambers. This made the device highly parallel but it was not able to repeatedly add to the same reaction chamber.

Missing in the literature were integrated small aliquot designs that do not drain reagents to waste and can be reused for multiple aliquots in a single receiving reservoir. For example, in a paper that demonstrated a low waste methodology, Lafleur described pre-concentration of trace metals on a CM device but needed to use a micro-pipette on a stationary disk to load sequential

small aliquots.[7] This chapter will demonstrate the generation of small aliquots as an integrated component of a CM device. The generation of these sub-microliter aliquots is different from previous literature because stopping the device is not required to inject to the same port. The design succeeds in placing a precise volume of reagent to the same receiving chamber repeatedly as compared to methods that can only provide a single aliquot. One method similar to this design is recirculation that Kazarine performed in the liquid-liquid extraction of iodine from a solution.[8] The design used a 25 μL metering chamber in addition to Kong's externally produced pneumatic pumping[1] to move the liquid of interest to the metering chamber after each addition. The work of this chapter succeeded in generating sub-microliter aliquots without using external pneumatic pressure.

The concept of the compression chamber for this version of small aliquot generation was drawn from work this author (Bouchard) did with Kong in which compressed trapped air on a CM device generated pneumatic pressure that drove liquid against centrifugal force.[9] This can be seen in Figure 3-1 and shows the filling of a trapped air chamber with red liquid that will compress air that drives blue liquid movement inward on the device.

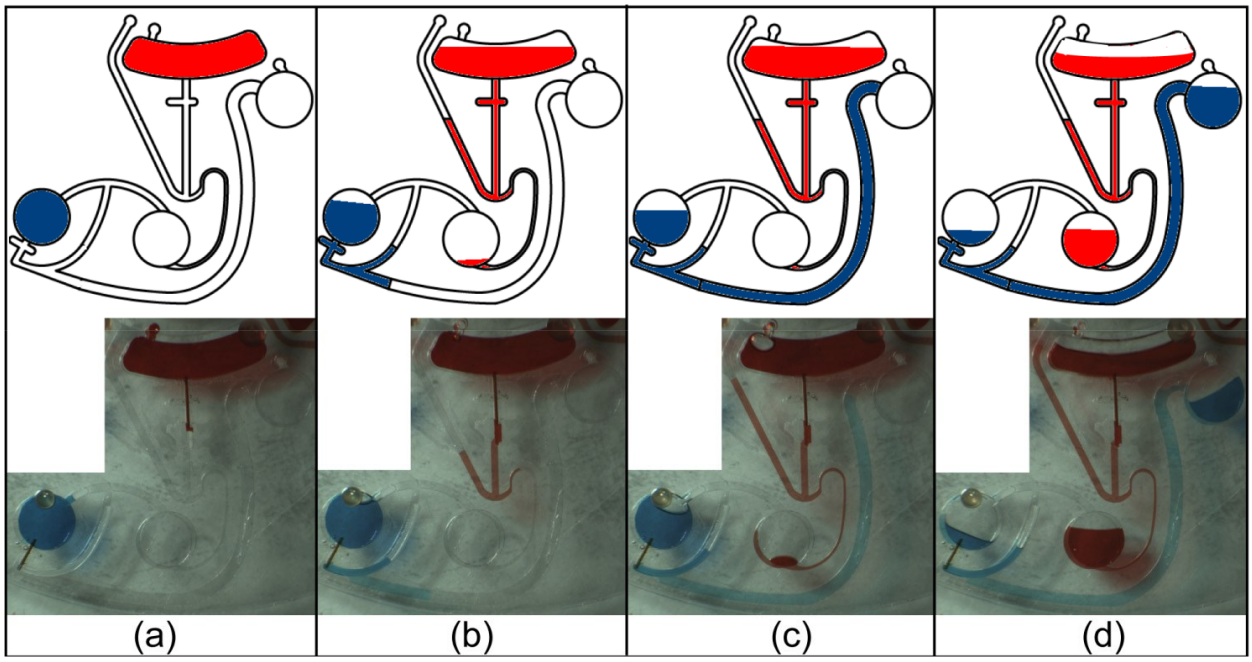


**Figure 3-1. Schematics and strobed images of the gas-liquid pump in operation**
t indicates the time elapsed. (a) Sample Chamber is filled with [simulated processed analytical sample] PAS (blue); 0 RPM, t = 0 s; (b) Pumping fluid (red) has begun to empty and displacing the PAS from the Sample Chamber; 300 RPM, t = 12 s; (c) PAS has been displaced up the Transfer Channel towards the Final Chamber, with an air gap between the two liquids; 300 RPM, t = 41 s; (d) PAS has been displaced into the Final Chamber by the pumping liquid; 700 RPM, t = 420 s.

The final design presented in this chapter used the unvented chamber shape presented by Zehnle et al. whose paper referenced the author's (Bouchard) work with trapped air shown in Figure 3-1.[10] In all three cases, energy stored in compressed air on the device drove liquid movement toward the center of the device against centrifugal force. Zehnle used a valveless chamber with a channel entrance at the bottom so that the compressed air could be used to pump the liquid towards the center through a high aspect ratio channel to induce a siphon. The shape is seen in the compression chamber of Figure 3-7C. (Chapter 3, page 13)

In the small aliquot design of this thesis, trapped air was compressed when the device was at a high rotational frequency. At a low rotational frequency, this compressed air moved liquid past a metering chamber. When a high rotational frequency was applied again, the liquid drained from the metering chamber into the receiving chamber and the remaining liquid compressed the

trapped air. The ability to predict the functionality of these trapped air components in CM devices was described by Gorkin et al. in a 2010 paper titled "Pneumatic pumping in centrifugal microfluidic platforms." [11] Trapped air was modified in this design as the key feature in the functionality of small aliquots.

# Experimental

## Early Design Concepts

Several design concepts were attempted in order to develop the final configuration. In the first iteration a small aliquot configuration for CM devices was built based the observation of reagents wicking into passive valves cut from adhesive layers. The first iteration is shown in Figure 3-2. The design shown was spun for a time of 3 seconds each at 950 RPM, 0 RPM, 450 RPM and 3000 RPM. Completion of the sequence resulted in deposition of ~ 830 nL aliquot into the large receiving chamber and cycle repetition resulted in further aliquot delivery. The design concept of Figure 3-2 was also used with a metering valve volume of ~120 nL.

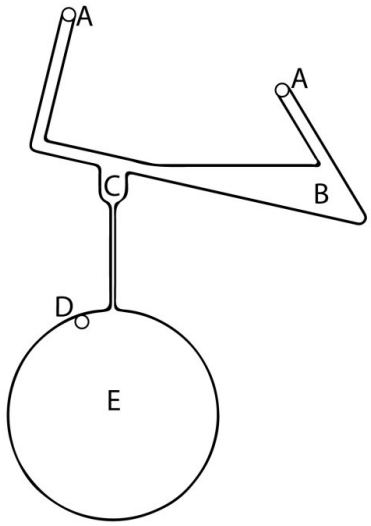


**Figure 3-2. Structure labels of Design Concept 1 for small aliquots**
(A) Air vent and loading hole for aliquoting liquid, (B) triangular reservoir for aliquoting liquid, (C) adhesive metering valve, (D) air vent and loading hole for receiving liquid, (E) receiving chamber

The application of design concept 1 in Figure 3-2 is shown in the illustration and experimental images of Figure 3-3.

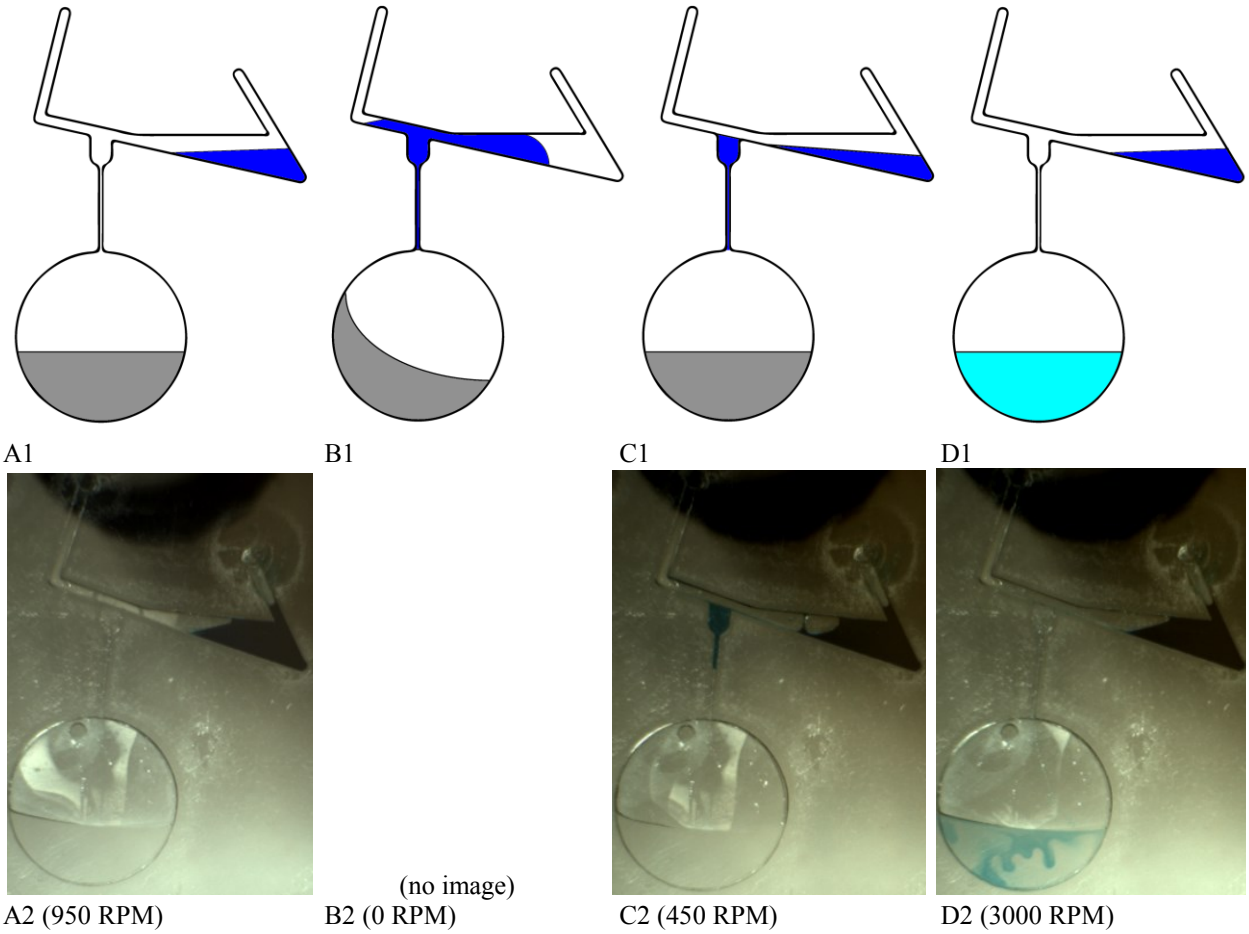


**Figure 3-3. Ideal and experimental images for small aliquot design concept 1**
(A) Dark blue liquid to aliquot was stored in the triangle reservoir and controlled by centrifugal force. (B) When the rotation was ceased, liquid to aliquot flowed past the opening of the metering valve. (C) At a low rotational frequency the liquid to aliquot returned to the triangle reservoir leaving the metering valve primed. (D) At a high rotational frequency the the metered volume was aliquoted.

In Figure 3-3A1 and 3-3A2, at 950 RPM water is in the receiving reservoir and blue dyed water is in the triangular reservoir. In Figure 3-3B1 the rotation of the device was abruptly stopped and the liquid would flow above the valve which also functioned as the metering chamber. The metering valve shown in Figure 3-2 was designed to aliquot 830 nL of blue dyed water. In Figure 3-3C1 and 3-3C2 the device was spun at 450 RPM so that the excess liquid

would flow back to the triangular reservoir leaving the 830 nL aliquot in the valve. In the final step, Figure 3-3D1 and 3-3D2, the device was spun at 3000 RPM which drained the aliquot from the valve into the receiving chamber.

The design shown in Figures 3-2 and 3-3 was eventually rejected for three reasons; (1) it required a surfactant (a solution of 0.1% TritonX 100) to wick the reagent into the valve/metering chamber and to allow for complete drainage of the valve, (2) the metering valve would not always fill entirely which yielded imprecise aliquot volumes and (3) the design required stopping the rotation of the device. By stopping the device, the integration of other CM functions that require constant rotation was not possible thus reducing the functionality of combining this design with other CM operations.

In the second iteration, a design concept was developed to overcome the requirement of stopping rotation. The configuration is shown in Figure 3-4. The liquid to be aliquoted would be metered by the volume of the adhesive metering valve labeled E. The liquid would repeatedly fill the valve by cycling the rotational frequency of the device from high to low. At low frequencies, the valve would be filled and at high frequencies the valve would be drained into the receiving chamber.

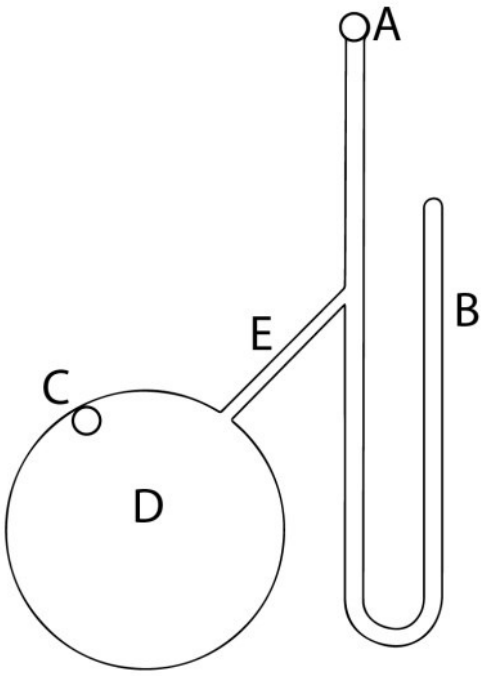


**Figure 3-4. Structure labels of Design Concept 2 for small aliquots**
(A) Air vent and loading hole for reagent (B) compression channel (C) air vent and loading hole for the receiving liquid (D) receiving chamber (E) adhesive metering valve

The upper illustration of Figure 3-5 represents the operational principles based on design concept 2 in Figure 3-4. The second design concept still required the use of a surfactant and would also not reliably fill the metering valve as seen in Figure 3-5D and no geometric designs allowed for replicating accurate droplets. Additionally, the metering valve was oriented in such a way that when the reagent to be aliquoted was added to the adhesive metering valve some would drain to the receiving chamber as seen in Figure 3-5A. This design also lacked the ability to be easily tuned for different volumes. The size of the valve could not be easily adjusted to accommodate larger volumes and the channel for compressed air was too small to handle larger volumes required for longer experiments.

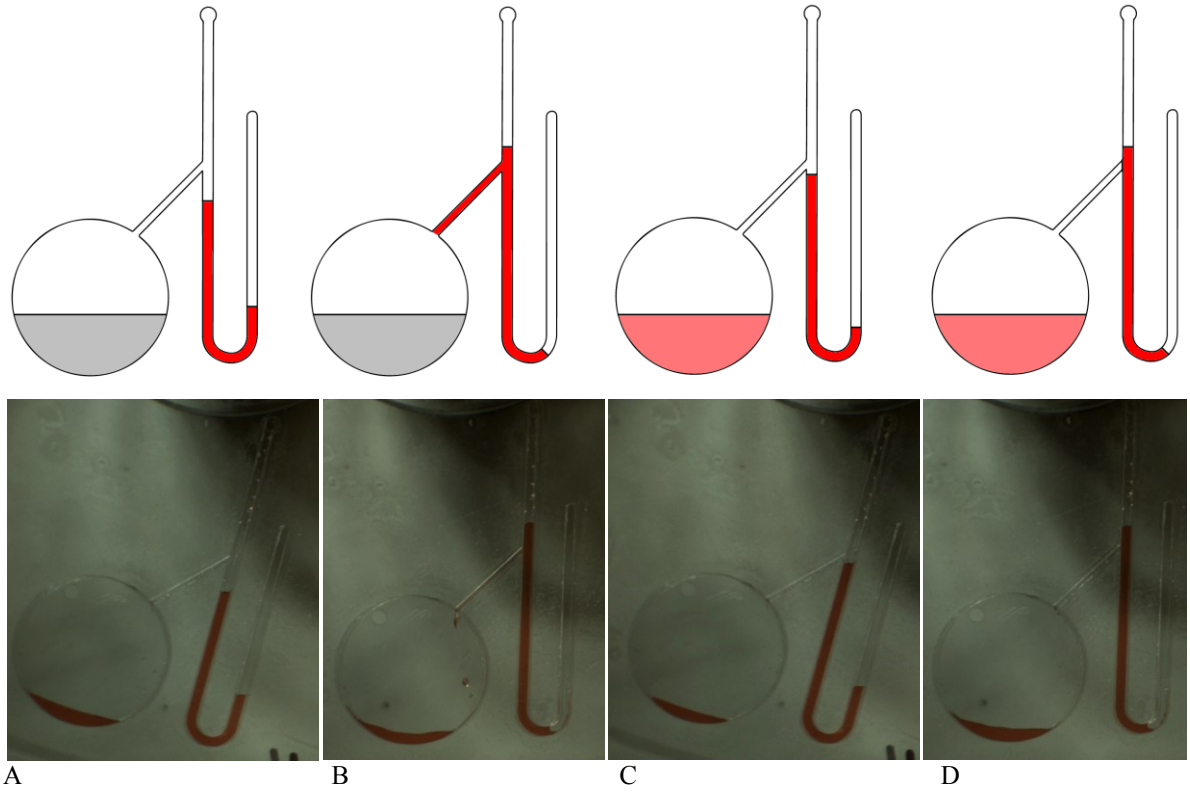

A B C D

**Figure 3-5. Illustrations and experimental images for small aliquot Design Concept 2**
(A) The disk was spun at 2400 RPM, priming the system and compressing the air, (B) 300 RPM allowed for loading of the metering valve, (C) 950 RPM was used to empty the valve into the receiving chamber, (D) 300 RPM, attempt to load the metering valve which failed. The color in the receiving chamber changes in the cartoon from gray to red because of the addition of a small aliquot of red dye. The experimental images did not have liquid in the receiving chamber.

The final design for the CM small aliquot delivery system that adequately addressed all the issues outlined is described in the remainder of this Chapter.

## Fabrication of Centrifugal Device

The final configuration was a five-layered test disk fabricated using materials and techniques previously described by Lafleur and Salin in 2009.[7] The methodology was discussed in detail in the *Experimental: Fabrication of Centrifugal Device* section of Chapter 2 in this thesis (Chapter 2, page 8). Modification to that construction included the passive valves cut from the adhesive layer (0.102 mm in height) or inserted in the form of a glass capillary (50 to 322 μm inner diameter).

When aligning the layers on the aluminum spindle assembly stage for cold lamination it was important that the alignment be accurate. An adhesive that was not aligned with the chamber or channel could cause two issues; (1) on one side of the chamber the adhesive would be in the chamber where the reagent flowed which exposed the reagent to the adhesive glue of that layer and (2) on the opposite side of the feature, the misalignment with the chamber would leave a 0.102 mm high channel that wicked liquid along the edge of the chamber, which was especially an issue when constructing adhesive valves. The adhesive valve should act as a geometric restriction to liquid flow, but when wicking from misalignment was introduced the valve was rendered ineffective.

As previously discussed, passive valves afford one method of restricting liquid flow from one chamber to the next in a CM device. This thesis uses a combination of both adhesive passive valves and capillary passive valves. Capillary valves are made from gas chromatography tubing with no solid phase on its inner diameter (Polymicro Technologies, Phoenix, AZ, USA). These glass valves were cleaned with ethanol and cut to length using a 90 degree ceramic edge to score the glass. The glass capillary valves were assembled into the device as the layers were stacked and cold laminated. The capillary itself was affixed using a commercially available five minute epoxy. This specific method for glass capillary valves was demonstrated by Laxroix-Frailish in 2009.[12]

The disk, as seen in Figure 3-6, had six replicates of the experimental design situated around the axis of rotation.

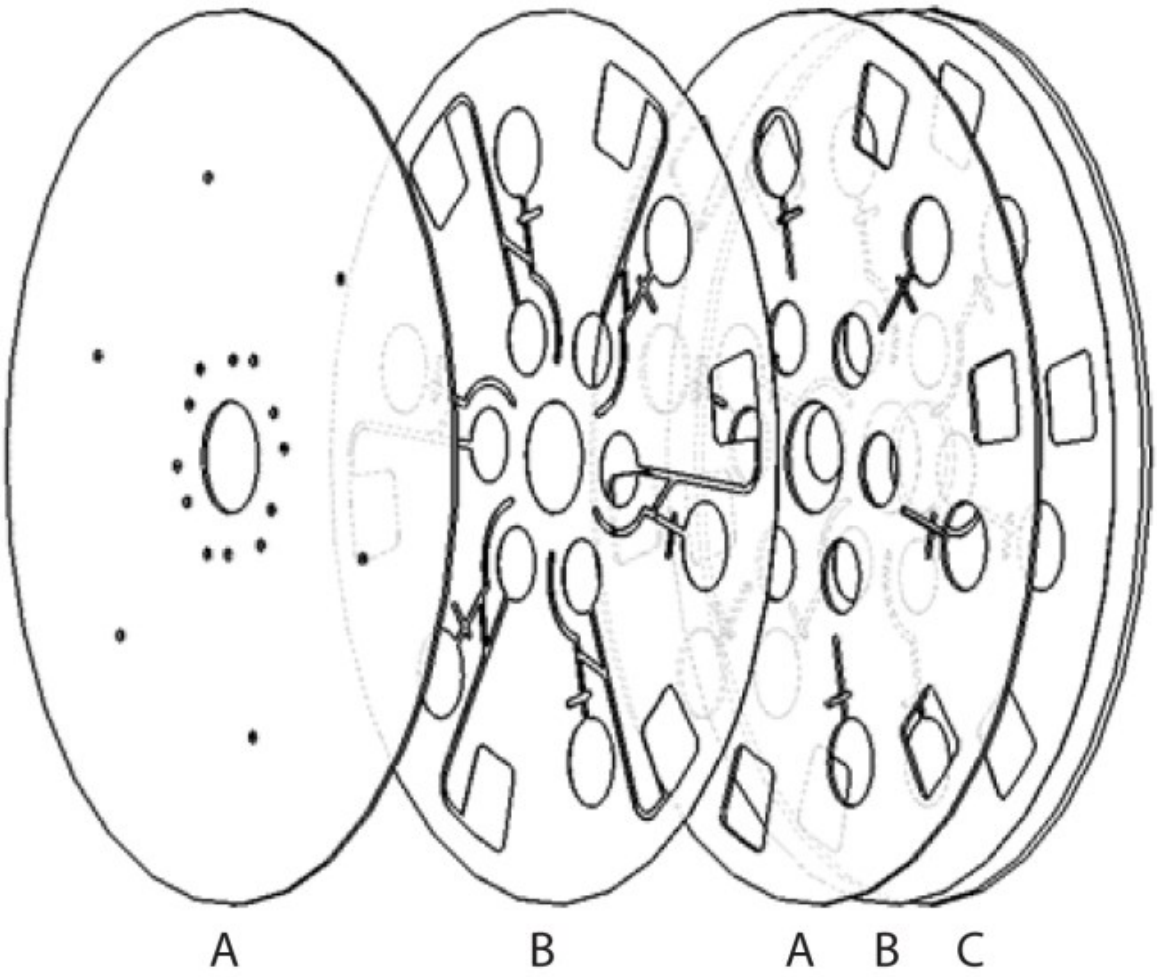


**Figure 3-6. Layers for construction of small aliquots**
Three disks of five layers with six experimental replicates each were constructed. The construction includes (A) polycarbonate DVDs 0.6 mm thick, (B) double sided pressure sensitive adhesives 0.102 mm thick and (C) polycarbonate CD 1.2 mm thick.

The features, along with the inclusion of a glass capillary valve and important dimensions of the design are highlighted in Figure 3-7.

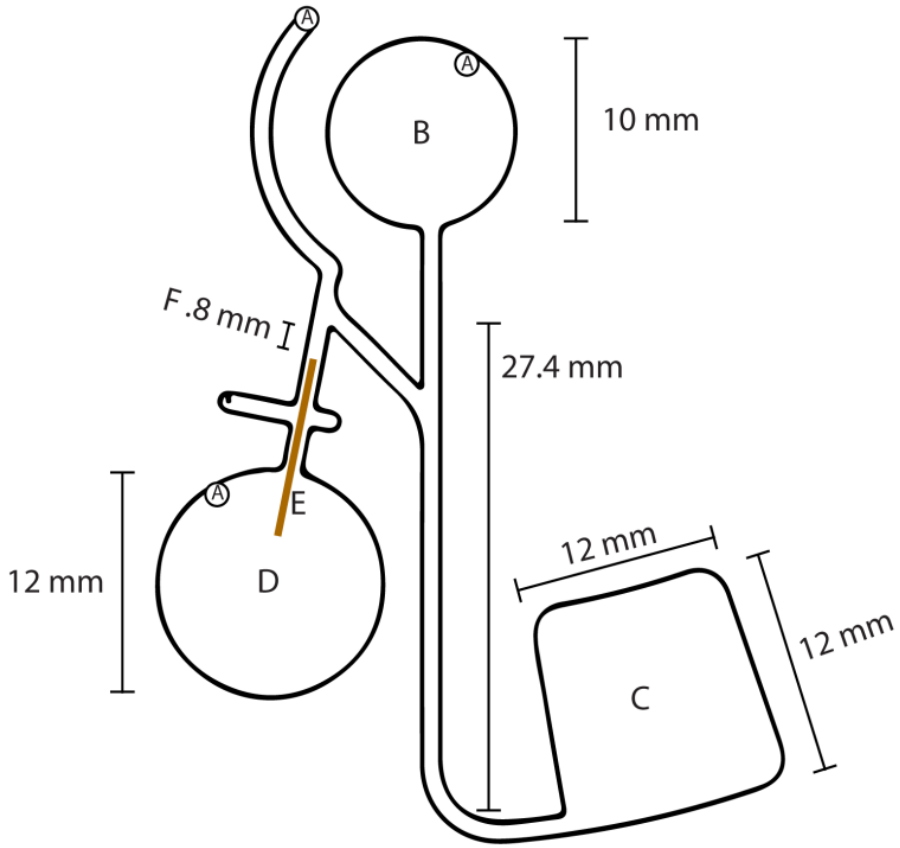


**Figure 3-7. Structure labels and dimensions of small aliquots experimental design**
Each replicate of the experiment on the devices had the same construction and features. (A) vent holes/loading ports (B) loading chamber (C) compression chamber that is not vented (D) receiving chamber (E) 10 mm long capillary valve with 50 µm inner diameter, it is sealed in place by resin epoxy (F) metering chamber with height of 0.800 mm, total calculated volume, including valve is 750 nL.

## Setup and Data Acquisition

The spinner and strobe setup described by Duford and Peng[13] was supplemented with a color digital camera (GRAS-14S5C-C, Point Gray, BC, Canada), with the entire system synchronized from a single computer through LabVIEW software (LabVIEW 8.6, Developer Version, National instruments, QC, Canada). The system was also updated with a synchronized spectrometer as outlined in Chapter 2 of this thesis. The entire servo-motor and spectroscopic module setup, including the CM device, is shown in Figure 3-8.

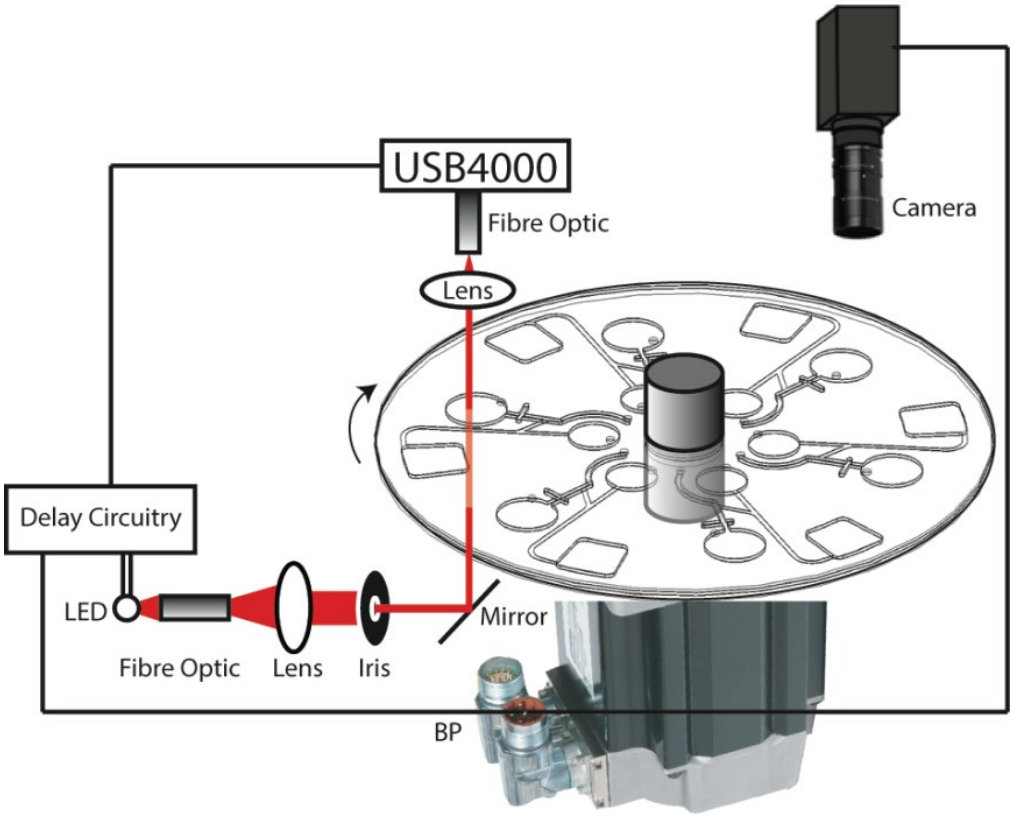


**Figure 3-8. Global schematic of experimental setup for small aliquots**
The Break Point (BP) of the servo motor used to trigger the synchronized spectrometer and the camera would trigger once every 10 rotations to take a spectra or a picture.

When images were to be taken using the camera, blue food colouring was used. This increased contrast and facilitated easier analysis. When spectra were to be taken for quantification, yellow dye was used. Due to the sources of noise discussed in Chapter 2 the use of the ratiometric method as described by LaCroix was required to calculate accurate results.[14] The ratio of light intensity at an absorbing and non-absorbing wavelength was used to calculate the absorbance as described in Equations 2-2 and 2-3. (Chapter 2, page 25)The absorbing wavelength selected was 466 nm which the yellow dye absorbed strongly at and was the highest intensity wavelength of the LED used in the setup. The non-absorbing wavelength was 545 nm. The spectra collected were processed using Microsoft Excel and taken at a rate of one spectrum per 10 rotations of the device.

Using the described system three experiments were conducted for presentation in this chapter. The rotational frequencies selected were calculated using equations published by Ducree in 2007.[3] Using a 10 mm valve with an inner diameter of 50 μm there was a calculated burst frequency of 1050 RPM. Therefore, the generation of aliquots had two frequency ranges: lower than 1050 RPM would load the metering chamber and higher than 1050 RPM would drain the metering chamber. Drainage was run at 2900 RPM, a speed that guaranteed the metering chamber is emptied completely. An ideal small aliquot experiment is demonstrated in Figure 3-9.

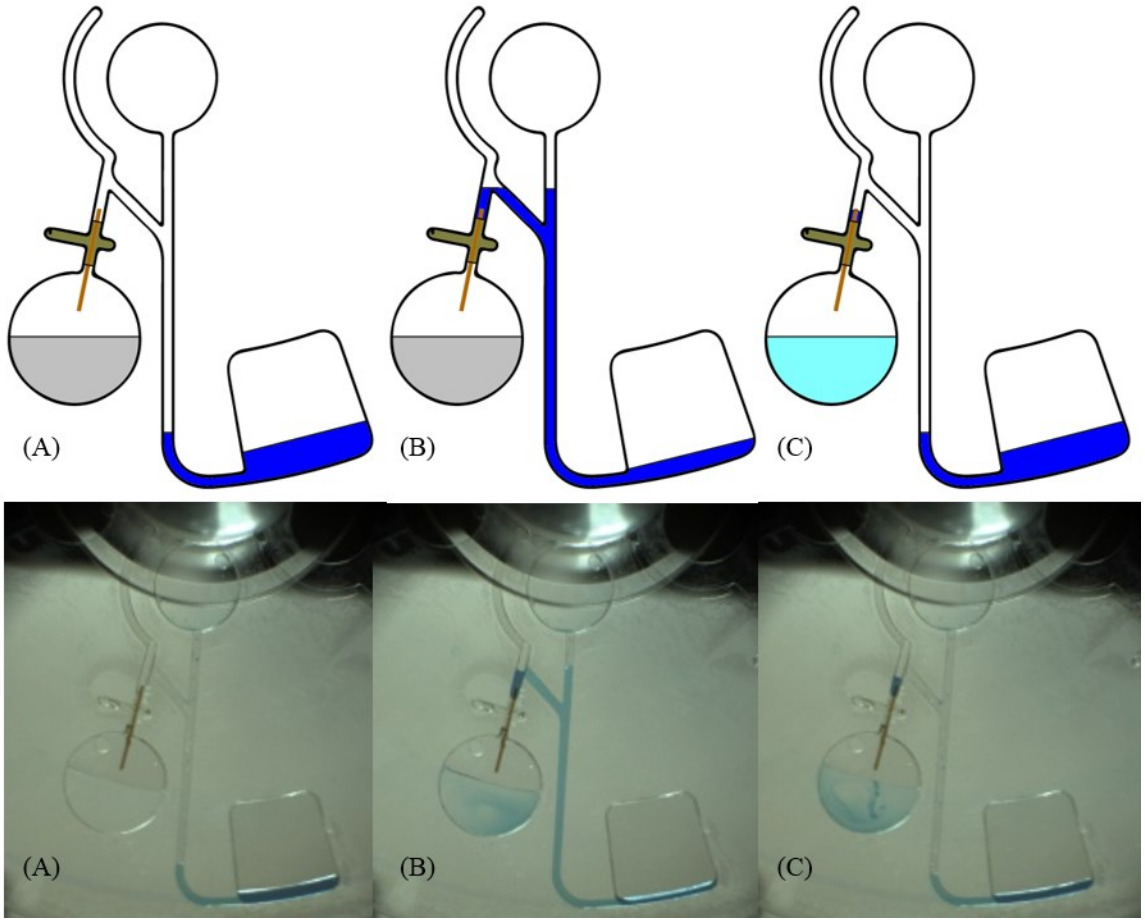


**Figure 3-9. Ideal small aliquot illustrations and experimental images**
(A) At 2900 RPM the dark blue liquid to be aliquoted compressed the air in the compression chamber. (B) At 900 RPM the centrifugal force did not overcome the pressure from the compression chamber and the liquid to be aliquoted was deposited in the metering chamber. (C) At 2900 RPM the liquid from the metering chamber was drained to the receiving chamber; the remainder of the liquid returned to the compression chamber.

The process of oscillating the rotational frequency from higher than 1050 RPM to lower than 1050 RPM (i.e. the 2500 to 900 RPM shown in Figure 3-9), allowed the repeated metering of the same volume of reagent. Three different experiments were conducted with different rotational frequencies and times to prove the function of the design. The information presented in Table 3-1 outlines the rotational frequencies that were used in the three experiments of this chapter. The goals and results of these experiments are given in detail in the results and discussion section of this chapter.

| Experiment and Applicable Figure | Description of experimental settings |
|---|---|
| Experiment 1<br>Data in Figure 3-9: Pictures | (2900 RPM for 5 seconds, 900 RPM for 2 seconds) x 11 replicates |
| Experiment 2<br>Data in Figure 3-10:<br>Spectra converted to volume aliquoted | (2500 RPM for 13 seconds, 900 RPM for 2 seconds) x 8 replicates. |
| Experiment 3<br>Data in Figure 3-11:<br>Spectra converted to volume aliquoted | 2500 RPM for 13 seconds, 900 RPM for 2 seconds.<br>The speed was then oscillated between 2500 RPM and:<br>850/800/750/690/620/540/450/350/240/120 RPM.<br>*i.e.* the experiment ran at:<br>2500 RPM, 900 RPM, 2500 RPM, 850 RPM,<br>2500 RPM, 800 RPM … |

**Table 3-1. Three experimental collection parameters for small aliquots**

All of the experiments used distilled deionized water (DDW) and food colouring. In Experiment 1, 50 µL of DDW was deposited in the receiving chamber; 14 µL of blue food colouring in DDW was used as the aliquoted liquid. The experimental images of Experiment 1 are outlined in Figure 3-10. (Chapter 3, page 19)

In Experiment 2, 50 µL of DDW was deposited in the receiving chamber; 14 µL of yellow dye in DDW was used as the aliquoted liquid. Five replicates of equal dimensions were built. The dimensions of the design are shown in Figure 3-7. (Chapter 3, page 13) The head height in the metering chamber gives a theoretical aliquot volume of 750 nL. Experiment 2 further included the creation of an external calibration curve to quantify the volume of each aliquot

using the absorbance. This calibration curve was built from six samples: a blank made of DDW, then 3, 6, 9, 12 and 15 µL of the same yellow dye in 50 µL of DDW. This calibration curve allowed the quantification of the volume added by each aliquot. The results of Experiment 2 are outlined in Figure 3-11. (Chapter 3, page 21) The calculation compensated for the change in volume after each aliquot as discussed below.

In Experiment 3, 50 µL of water was deposited in the receiving chamber; 14 µL of yellow dye and DDW was used as the aliquoted liquid. Experiment 3 was built with four replicates with different head heights on the metering chamber. The head heights were set to produce a volume of 1200 nL, 750 nL, 560 nL and 560 nL. These volumes were determined by the dimensions of the metering chamber. The results of Experiment 3 are outlined in Figure 3-11.

## Results and Discussion

The three experiments outlined in Table 3-1 of the experimental section were performed as described. Experiment 1 used images to demonstrate that at 750 nL the metering chamber would drain completely into the receiving chamber at the high RPM. Experiment 2 used five replicates of a 750 nL metering chamber and the spectrometer presented in Chapter 2 of this thesis to quantify the volume added in each aliquot. It was found that over eight aliquots an average of 750 nL with a standard deviation of 170 nL was generated. Experiment 3 used different metering chamber volumes, 1200 nL, 750 nL and 560 nL and a changing rotational frequency to attempt extending the number of aliquots that could be accurately generated from eight to eleven. The accuracy was verified with the spectrometer presented in Chapter 2 of this thesis.

Experiment 1 collected images of the device producing aliquots. The images of Figure 3-10 show the first three aliquots of a set completed by oscillating the RPM of the disk from 2900 RPM for five seconds to 900 RPM for two seconds. The images from Figure 3-10

were used to determine that the design was functioning as intended, that the aliquoting liquid in the metering chamber drained and that the liquid to aliquot transferred to fill the metering chamber at the lower RPM. Blue food colouring was used for the images in Figure 3-10 in order to improve the contrast and see the 750 nL aliquots.

Figure 3-10A demonstrates the draining of blue solution from the injection chamber to the compression chamber. Figure 3-10B shows the blue solution compressed the air in the compression chamber at 2900 RPM. The compression of the air is a function of how much liquid remains to aliquot. After each aliquot the volume decreases and the pressure exerted by the reagent on the compression chamber reduces. Figure 3-10C shows the metering chamber about to be filled at 900 RPM. Figure 3-10D represents the metering chamber filled and about to be drained at 2900 RPM and Figure 3-10E shows the metering chamber being drained into the receiving chamber. Figure 3-10F through I show the same cycle of rotational frequencies to deposit the second and third small aliquot to the receiving chamber.

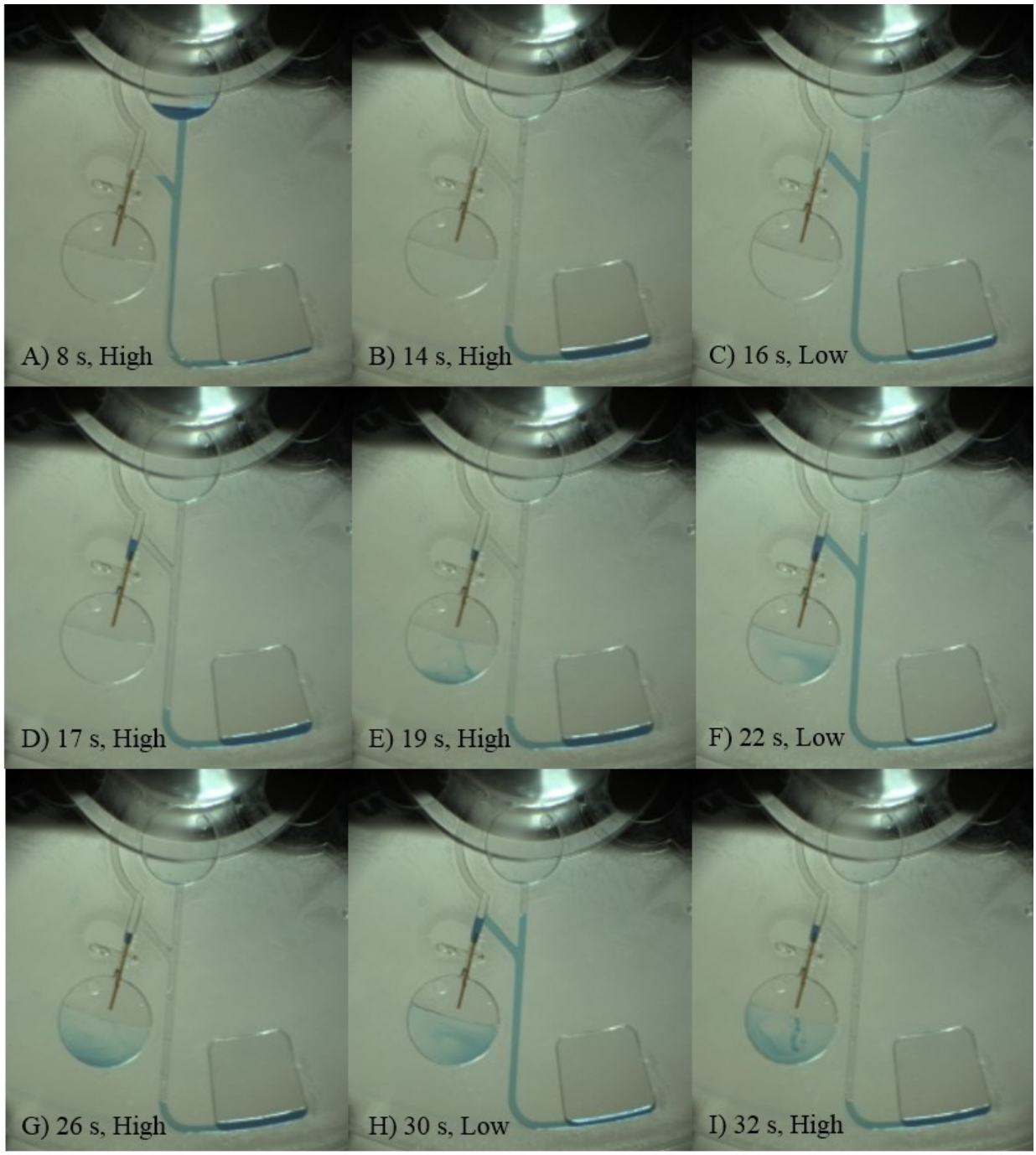


**Figure 3-10. Experimental images of the small aliquot device**
The timestamps on images A through I of Figure 3-10 indicate the time that the image was taken during the demonstration of small aliquot generation. “High” denotes 2900 RPM when the liquid to aliquot would most compress the trapped air in the unvented compression chamber. “Low” denotes 900 RPM when the centrifugual force was not sufficient to compress the trapped air and the liquid to aliquot would be driven towards the center of the device and past the opening of the metering chamber. Image A shows the initial compression of the trapped air when the liquid first moved from the loading chamber through the channel to the compression chamber.

The mixing of the aliquot in the receiving chamber was done through diffusion during the high RPM portion of the cycle. For the purposes of taking spectra, Experiment 2 cycled from 2500 RPM for 13 seconds to 900 RPM for two seconds. The spectra used to plot the absorption were taken from the last 3 seconds every time the device was rotating at 2500 RPM. The average absorptions of five runs of equally built devices were used to calculate the total volume deposited after each aliquot. The result of Experiment 2 is shown in Figure 3-11.

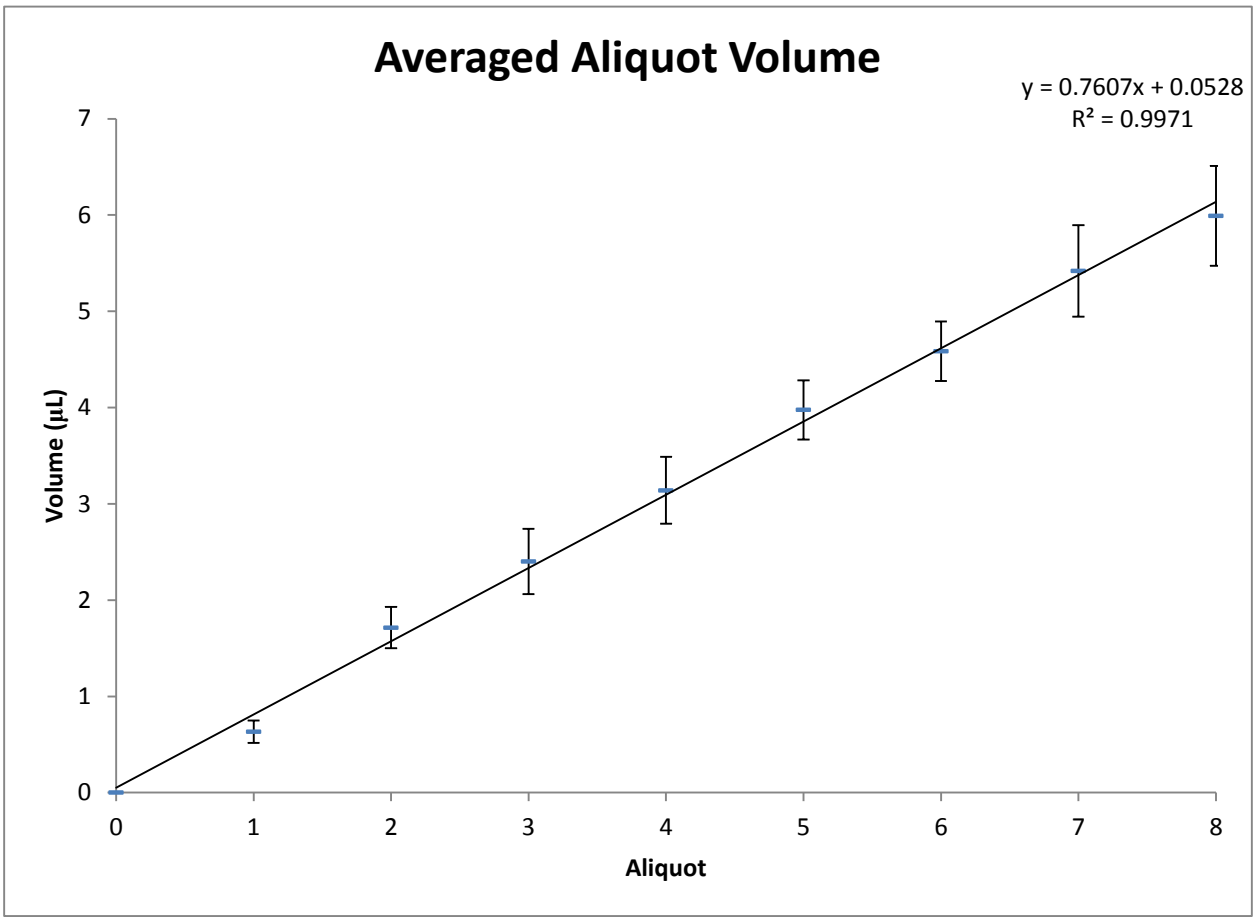


**Figure 3-11. Average of five replicates of eight small aliquots**
The volume calculated from absorbance after each aliquot is presented. A calibration curve and the change in absorbance were used to determine the volume aliquoted. It was found that the average volume of each aliquot was 750 nL with a standard deviation of 170 nL. (Error bars are the standard error for the averaged results of multiple cells.)

The data that populated the plot of Figure 3-11 is provided in Table 3-2.

| Aliquot Number | Volume Added (µL) | Change in Volume (µL) | Standard Error (µL) |
|---|---|---|---|
| 0 | 0 | ----- | ----- |
| 1 | 0.633 | 0.633 | 0.116 |
| 2 | 1.714 | 1.081 | 0.214 |
| 3 | 2.401 | 0.687 | 0.339 |
| 4 | 3.140 | 0.739 | 0.347 |
| 5 | 3.976 | 0.835 | 0.307 |
| 6 | 4.586 | 0.610 | 0.309 |
| 7 | 5.418 | 0.832 | 0.476 |
| 8 | 5.992 | 0.574 | 0.519 |
| ***Average of Change in Volume:*** | | 0.749 | |
| ***Standard Deviation of Change in Volume:*** | | 0.166 | |

**Table 3-2. Showing the change in volume and standard error for the cells used in Figure 3-11**
The average change in volume was reported as 750 nL and the standard deviation as 170 nL. The five averaged replicates used to calculate the volume added were generated using two devices.

Eight aliquots were generated accurately using the design presented in Figure 3-7. (Chapter 3, page 13) More than eight aliquots could not be accurately generated because the volume of liquid to be aliquoted was too small to properly fill the metering chamber. When the metering chamber was not completely filled then the volume aliquoted was less than 750 nL.

It was determined that the oscillation between 2500 and 900 RPM as described for Experiment 2 limited the ability of the design to produce more than eight accurate replicates as determined by linear regression. The reservoir volume of liquid to be aliquoted decreased by 750 nL after each aliquot. For the first aliquot, there was 14 µL of liquid available to fill the metering chamber. For the eighth aliquot, there was approximately 8 µL of liquid. This smaller volume was not large enough for the compressed air to move inward and fill the metering chamber completely. The change of rotational frequency from 2500 to 900 RPM in Experiment 2 was not calibrated for the change in volume of the liquid to be aliquoted. Therefore, in order to extend the number of aliquots, Experiment 3 was designed and four runs were completed successfully. In Experiment 3, the rotational frequency to fill the metering chamber would slow after each aliquot. The frequencies are listed in Table 3-1. (Chapter 3, page 16)

The four runs of Experiment 3 were designed with varying volumes of the metering chamber. This was accomplished by changing the radial position of the capillary valve at the base of the metering chamber. The first position lowered the valve location of Experiment 2 by 200 nm. The second position was at the same radial location as in Experiment 2. The third and fourth positions were raised by 200 nm. This provided metering chamber volumes of 1200, 750, 560 and 560 nL as represented in Figure 3-12 by runs 1, 2, 3 and 4 respectively.

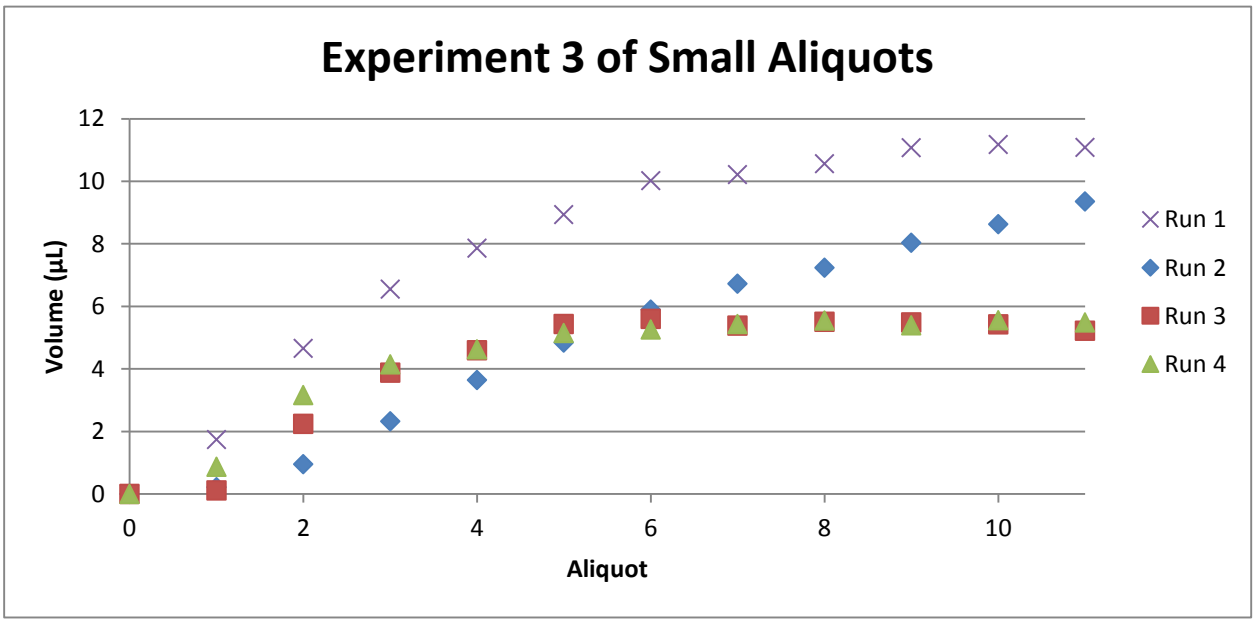


**Figure 3-12. Change in rotational frequency each cycle for small aliquots**
Two modifications to the design were made to collect the data of this figure. (1) The rotational frequency of the loading phase was reduced after each aliquot. The change in rotational frequency after each aliquot is outlined as *Experiment 3* in Table 3-1 (Chapter 3, page 16). (2) The construction was modified so that three different volumes of aliquot were generated. The total volume added after each aliquot is presented. A calibration curve and the change in absorbance were used to determine the volume aliquoted. All four runs are single replicates from the same device.

The runs shown in Figure 3-12 were taken with the rotational frequency reduction after each aliquot shown in Table 3-1. (Chapter 3, page 16) The gradual reduction in rotational frequency when loading the metering chamber was done because the volume of liquid available to aliquot decreased after each cycle. With lower volumes of aliquoting liquid, there was not as much liquid to move towards the center of the device. This required that the rotational frequency

at the low RPM portion of each cycle be decreased to move the head height of the aliquoting liquid above the opening of the metering chamber.

The metering chamber volumes were modified to demonstrate the different variables that can be adapted for different experiments. Run 1 had the largest theoretical aliquot volume, followed by Run 2 and then the smallest aliquot volumes were produced by Runs 3 and 4, which were equal. As the volume of the aliquot became smaller the tendency for failure increased because the decreased head height reduced the pressure on the valve when the rotational frequency was set to drain the chamber. It was empirically found that a volume of 750 nL worked consistently well over a large number of aliquots. The volume delivered was large enough to be measured through spectroscopy; it was also not so large that it would run out of aliquoting liquid. This was the volume used in the runs averaged in Figure 3-11 (Chapter 3, page 21) and in Run 2 of Figure 3-12. However, if paired with the correct rotational frequencies a wide range of metering volumes could be obtained for different experimental purposes.

The cause of a smaller volume in the first aliquot in the experiments was the priming of the glass capillary valve. Before each run was performed the valve would be loaded with water that had been deposited in the receiving chamber before the start of the experiment. Therefore, the first addition would have a smaller aliquot of dyed reagent.

The result of Experiment 3 was the determination that the basic configuration can be further tuned to allow for more than eight aliquots. The change in the rotational frequency in Experiment 3 extended the number of potentially accurate aliquots to eleven in Run 2 when the aliquot volume was 750 nL. However, the system is quite robust and does not need any extensive tuning for experiments requiring fewer aliquots.

# Conclusions

A reproducible and accurate design for the generation of sub micro-liter aliquots in a CM device has been demonstrated. Without ceasing rotation, eight aliquots of 750 nL were generated and sequentially added to a receiving chamber. Variability in design and the precision of the system was quantified using synchronized spectroscopy that took accurate measurements of absorption in real-time. The addition of small aliquots to the toolbox of potential functions in CM designs will allow for the creation of more complex quantitative measurements while continuously applying centrifugal force. Additionally, the continued integration of compressed air chambers in CM will greatly impact the design of experiments, as control over the movement of reagent towards the center of the device is more common and tunable.

# Acknowledgements

The author (Bouchard) would like to thank Brittany Rocque for contributing to the early designs of this project. Specifically, the consultation on different geometric shapes and application of surfactants for the preliminary work done on adhesive metering valves described in Figures 3-2 and 3-4.

# References


1. Kong, M. C. R.; Salin, E. D., Pneumatically pumping fluids radially inward on centrifugal microfluidic platforms in motion. Analytical Chemistry 2010, 82 (19), 8039-8041.
2. Felton, M. J., CD simplicity. Analytical Chemistry 2003, 75 (13), 302A-306A.
3. Ducrée, J.; Haeberle, S.; Lutz, S.; Pausch, S.; Von Stetten, F.; Zengerle, R., The centrifugal microfluidic Bio-Disk platform. Journal of Micromechanics and Microengineering 2007, 17 (7), S103-S115.
4. Mark, D.; Haeberle, S.; Roth, G.; Von Stetten, F.; Zengerle, R., Microfluidic lab-on-a-chip platforms: Requirements, characteristics and applications. Chemical Society Reviews 2010, 39 (3), 1153-1182.
5. Steigert, J.; Brenner, T.; Grumann, M.; Riegger, L.; Lutz, S.; Zengerle, R.; Ducrée, J., Integrated siphon-based metering and sedimentation of whole blood on a hydrophilic lab-on-a-disk. Biomedical Microdevices 2007, 9 (5), 675-679.
6. Mark, D.; Weber, P.; Lutz, S.; Focke, M.; Zengerle, R.; Von Stetten, F., Aliquoting on the centrifugal microfluidic platform based on centrifugo-pneumatic valves. Microfluidics and Nanofluidics 2011, 10 (6), 1279-1288.
7. Lafleur, J. P.; Salin, E. D., Pre-concentration of trace metals on centrifugal microfluidic discs with direct determination by laser ablation inductively coupled plasma mass spectrometry. Journal of Analytical Atomic Spectrometry 2009, 24 (11), 1511-1516.
8. Kazarine, A.; Kong, M. C. R.; Templeton, E. J.; Salin, E. D., Automated liquid-liquid extraction by pneumatic recirculation on a centrifugal microfluidic platform. Analytical Chemistry 2012, 84 (16), 6939-6943.
9. Kong, M. C. R.; Bouchard, A. P.; Salin, E. D., Displacement pumping of liquids radially inward on centrifugal microfluidic platforms in motion. Micromachines 2012, 3 (1), 1-9.
10. Zehnle, S.; Schwemmer, F.; Roth, G.; Von Stetten, F.; Zengerle, R.; Paust, N., Centrifugo-dynamic inward pumping of liquids on a centrifugal microfluidic platform. Lab on a Chip - Miniaturisation for Chemistry and Biology 2012, 12 (24), 5142-5145.
11. Gorkin Iii, R.; Clime, L.; Madou, M.; Kido, H., Pneumatic pumping in centrifugal microfluidic platforms. Microfluidics and Nanofluidics 2010, 9 (2-3), 541-549.
12. Lacroix-Fralish, A.; Templeton, E. J.; Salin, E. D.; Skinner, C. D., A rapid prototyping technique for valves and filters in centrifugal microfluidic devices. Lab on a Chip - Miniaturisation for Chemistry and Biology 2009, 9 (21), 3151-3154.
13. Duford, D. A.; Peng, D. D.; Salin, E. D., Magnetically driven solid sample preparation for centrifugal microfluidic devices. Analytical Chemistry 2009, 81 (11), 4581-4584.
14. LaCroix-Fralish, A.; Clare, J.; Skinner, C. D.; Salin, E. D., A centrifugal microanalysis system for the determination of nitrite and hexavalent chromium. Talanta 2009, 80 (2), 670-675.

# CHAPTER 4: A passive valve configuration for centrifugal microfluidics

Variation in the construction of passive adhesive valves led to innacuracy in the predicted burst frequency and impacted the development of more complex CM functions. The passive adhesive valves would often, yet inconsistently, burst at rotational frequencies much lower than predicted thus ruining experiments where the reagent or sample must be handled in specific reaction chambers for set amouts of time. Therefore, the development of more robust valves was necessary.

## Contribution to Original Knowledge

An improvement in the construction of CM devices was made by modifying the design of passive adhesive valves to include movement perpendicular (axial) to the plane of the device. These three dimensional (3D) valves were then paired with a compression valve that restricted air from venting and increased the burst frequency.

## Abstract

A centrifugal microfluidic (CM) device was constructed to demonstrate a passive valve configuration. A valve was cut from the adhesive layer in a CM device that had three main parts; (1) an adhesive channel in one layer, (2) a hole axial to the device and (3) an adhesive channel in a second layer. The addition of the hole in the third dimension to separate two adhesive channels to form a valve is a novel design and is referred to here as a 3D valve. The design increased both the calculated burst frequency and accuracy as compared to standard passive adhesive valves of

similar cross sectional area and radius. The 3D valve was then supplemented with a compression valve (CV) to further increase the burst frequency.

This chapter demonstrates passive capillary valves cut from the 0.102 mm thick adhesive that bonds polycarbonate CD's and DVD's in CM devices. The constructed CM valves were evaluated using a servo motor and camera setup. The images of the reagents moving from one cell to the next were used to determine the burst frequencies. Unmodified adhesive passive capillary valves were built with a calculated burst frequency of 630 RPM that would experimentally burst at 290 ± 10 RPM. By implementing the 3D valve demonstrated in this chapter there was a calculated burst frequency of 660 RPM that burst experimentally at 650 ± 40 RPM. The improvement in accuracy allowed the design and construction of modules with multiple valves in Chapter 6. The addition of a CV increased the burst frequency of the same 3D valve to 1540 ± 170 RPM.

# Introduction

In order to create high throughput analytical devices with less waste, microfluidic principles have been used to develop micro total analysis systems (μTAS).[1] One classification of μTAS is the centrifugal microfluidic (CM) device, sometimes called a Lab on a CD.[2] The benefits of CM are numerous, including consistent and easily controlled force allowing parallel operations on a single device.[3] [4] [5] On these CM devices, passive valves are a standard method of controlling liquid flow from inner chambers located close to the center to outer chambers located at farther radii. Passive valves are small cross sectional channels that are governed by capillary forces that restrict liquid flow from one chamber to another. The small channel opening allows surface tension of the liquid to resist flow at low RPM thus retaining the liquid located in inner chambers.

The use of passive valves in CM devices has been a staple of the field when designing multi-step analytical experiments. In 2003, Feng discussed the use of passive capillary valves based on hydrophobic microfluidics.[6] A capillary valve is a small opening that constrains liquid flow by surface tension across an opening. In this thesis, capillary valves restricted liquid movement between chambers in order to control the transition from one analytical step in the procedure to the next. High pressure generated by centrifugal force can overcome the surface tension. At a sufficient rotational frequency, the liquid will "burst" through the capillary valve. The threshold is called the burst frequency and can be calculated. Cho presented a derivation of equations in 2007 for the bursting of geometric passive capillary valves[7] which was based on observations made by Squire in 2005 concerning the physics of fluids at the nanoliter scale.[8]

This thesis used the simplified equations of Ducree published in 2007 for the calculation of theoretical burst frequencies.[9] As a follow-up to Ducree, in 2008 Chen described an experimental treatment on capillary valves for CM.[10] Additionally, Lacroix-Frailish demonstrated in 2009 burst frequencies of passive valves using the equations of Ducree and small diameter glass capillary valves[11] with the same construction techniques used in this thesis. With all calculations of burst frequency based on the geometric shape of the valve terminus, modifications to the geometry caused by different construction methods have a significant impact on functionality.

Two methods of creating passive valves in CM devices were used in this thesis;
(1) short 4 to 10+ mm long glass capillaries as described by Lacroix-Frailish were inserted to transport liquid between chambers at differing radii.[11] Capillary cross sectional area is determined by the inner diameter of the glass capillary and can range from 25 μm to 450 μm,
(2) xerography cut 0.102 mm tall and 0.200 to 0.400 mm wide channels out of the adhesive layer

that bonded DVD and CD layers of the CM device.[12] The adhesive valves were used in the demonstration of 3D valves in this chapter.

The variables that determine the burst frequency include the size of the valve opening and the distance from the center of rotation, as well as constants associated with the liquid and the material of CM device. In this thesis, two different types of passive valves are constructed, one built from glass capillary tubing and the other by cutting a thin channel in the adhesive of the device. The adhesive valves were easier to construct but the calculated prediction of burst frequency was extremely unreliable. The addition of a 3D design made the adhesive valve burst at the predicted rotational frequency and is the focus of this chapter.

Even when made more accurate by the 3D component, adhesive valves have a low burst frequency compared to glass capillary valves; however, an enhancement of the passive valve can be obtained by restricting the flow of air by creating a compression valve as described by Al-Faqheri in 2013.[13] The concept had been explored earlier in 2012 by Gorkin who inserted a dissolvable film into the CM device and trapped air to restrict flow from a passive valve.[14] Additionally, Mark published a pneumatic restricted valve in 2008 where there was no venting of air from the receiving chamber, thus greatly increasing the burst frequency.[15] Mark's design prompted the derivation of liquid-air interface calculations for the breaking of surface tension in order to permit valve flow.

This chapter presents a passive valve cut from adhesive layers in a CM device with a 3D design similar to Gorkin[14] and Templeton.[16] Also shown is the addition of a compression valve configuration that increased the burst frequency of the 3D valve. The system presented here represents a significant enhancement of the compression valve technique as it eliminates the need for dissolving and melting stops.[17]

# Experimental

## 3D Valve

The design of a 3D adhesive valve that was tested for burst frequency accuracy is shown in Figure 4-1. It was experimentally determined that the 3D valve had a much more accurate burst frequency.

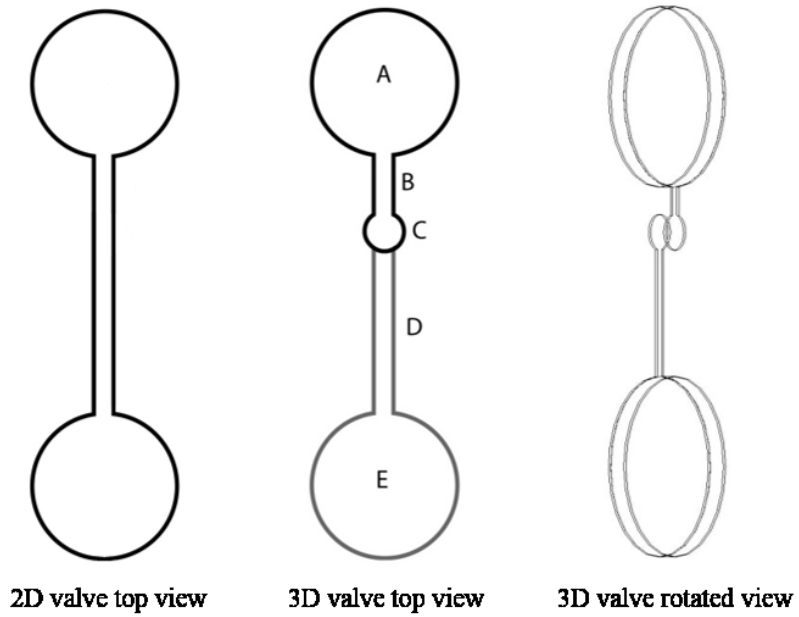


**Figure 4-1. Structure labels for design of a 3D valve**
In the 3D valve top view: (A) starting reservoir 0.804 mm in height (B) adhesive valve 0.400 mm wide 0.102 mm high cut from bottom adhesive (C) hole axial to the device 1.5875 mm in diameter (D) adhesive channel 0.400 mm wide, 0.102 mm high cut from the top adhesive (E) receiving reservoir 0.804 mm in height. For comparison a traditional 2D valve is shown from a top view. Its adhesive valve would also be 0.400 mm wide and 0.102 mm high cut from the adhesive layer. However, its opening of the valve is located at a larger radius than the 3D valve because there is no hole between the starting reservoir and the receiving reservoir.

## Early Compression Valve Design Concepts

The early design concepts of the CV enhancement were not successful, but did lead to the development of the final design presented in this chapter. Design concept 1 is presented in Figure 4-2 and used a double U-channel configuration to trap air in the large reservoir. The main

valve being affected by the CV is 3D so that the burst frequency can be accurately predicted when the receiving chamber is vented. This concept was based on the design of the author (Bouchard) in 2012.[18] In that paper, the author (Bouchard) used this type of U-Channel to block the air vent of a chamber in order to use compressed air to push reagent radially inward on a CM device. Using a similar concept, the compression valve stopped the venting of the receiving chamber by obstruction with a plug of liquid. An illustration of design concept 1 is shown in Figure 4-2.

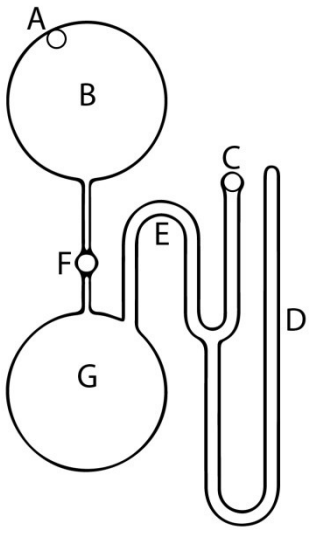


**Figure 4-2. Structure labels for design concept 1 of compression enhanced 3D valve**
(A) Air vent and loading hole for reagent (B) Reagent Chamber (C) Air vent and loading hole for valving liquid (D) Air compression channel (E) Adhesive channel (F) 3D valve (G) Receiving Chamber

The application of design concept 1 in Figure 4-2 is illustrated and demonstrated in Figure 4-3.

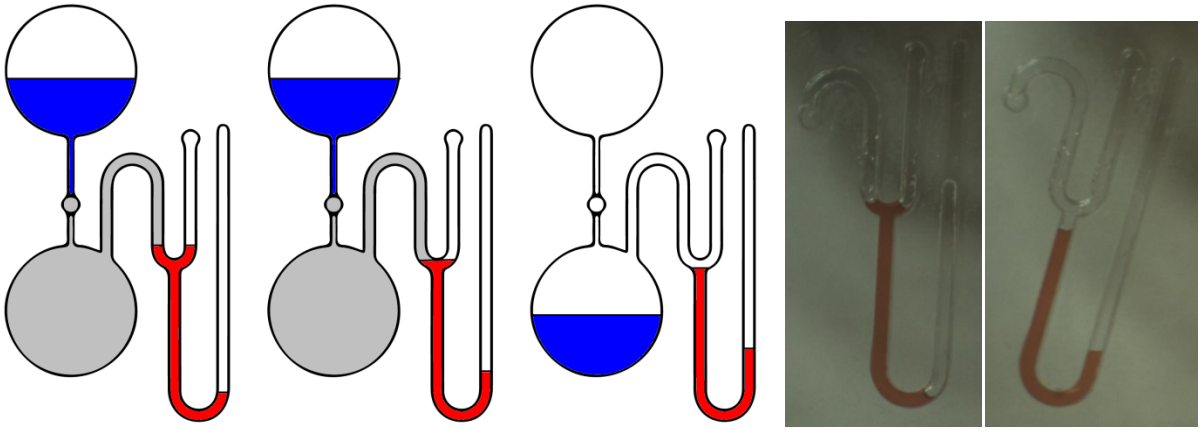

Low RPM Middle RPM High RPM 400 RPM 1800 RPM

**Figure 4-3. Ideal and experimental images of design concept 1 of compression enhanced 3D valve**
As shown by grey shading in the ideal cartoon, at low RPM air would be trapped in the Receiving Chamber by the valving liquid. At High RPM, the Receiving Chamber would be vented and the 3D valve would burst. This can be seen when the trapped air in the Receiving Chamber, marked by grey, disappears in the High RPM cartoon. In the experimental images, 15 µL of liquid was spun at 400 and 1800 RPM respectively.

The design of Figure 4-2 was discarded because the plug of valving liquid separated leaving air bubbles in the channel when the volume of valving liquid in the air compression channel was smaller than 15 µL. In addition, the high frequency required to open the venting channel meant that the design was not suitable for additional experimentation.

Design concept 2, presented in Figure 4-4, was based on the compressed air chamber of small aliquots in Chapter 3 of this thesis. The goal was to develop a tunable design where changing the volume of valving liquid would change the burst frequency of the 3D valve.

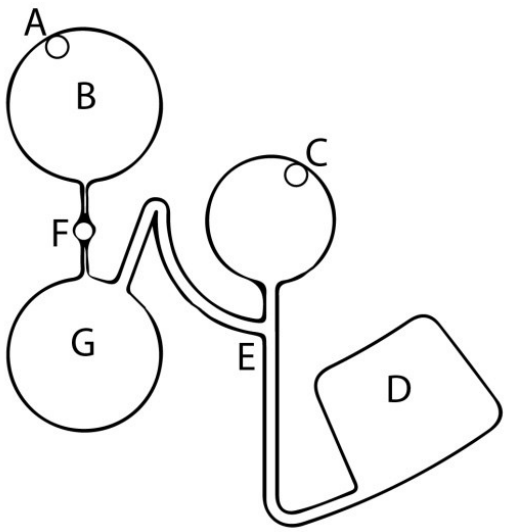


**Figure 4-4. Structure labels for design concept 2 of compression enhanced 3D valve**
(A) air vent and loading hole for reagent, (B) reagent chamber, (C) air vent and loading hole for valving liquid, (D) compression chamber, (E) adhesive channel, (F) 3D valve, (G) receiving chamber.

The ideal use of the design in Figure 4-4 is illustrated in Figure 4-5 as the rotational frequency of the device is increased from low to high. Also shown in Figure 4-5 is the experimental reality that the obstructing liquid in the vent allowed bubbles of air to escape. The escaping bubbles are included as an illustration of the experimental reality along with experimental images taken that show the valve slowly leaking at a constant rotational frequency.

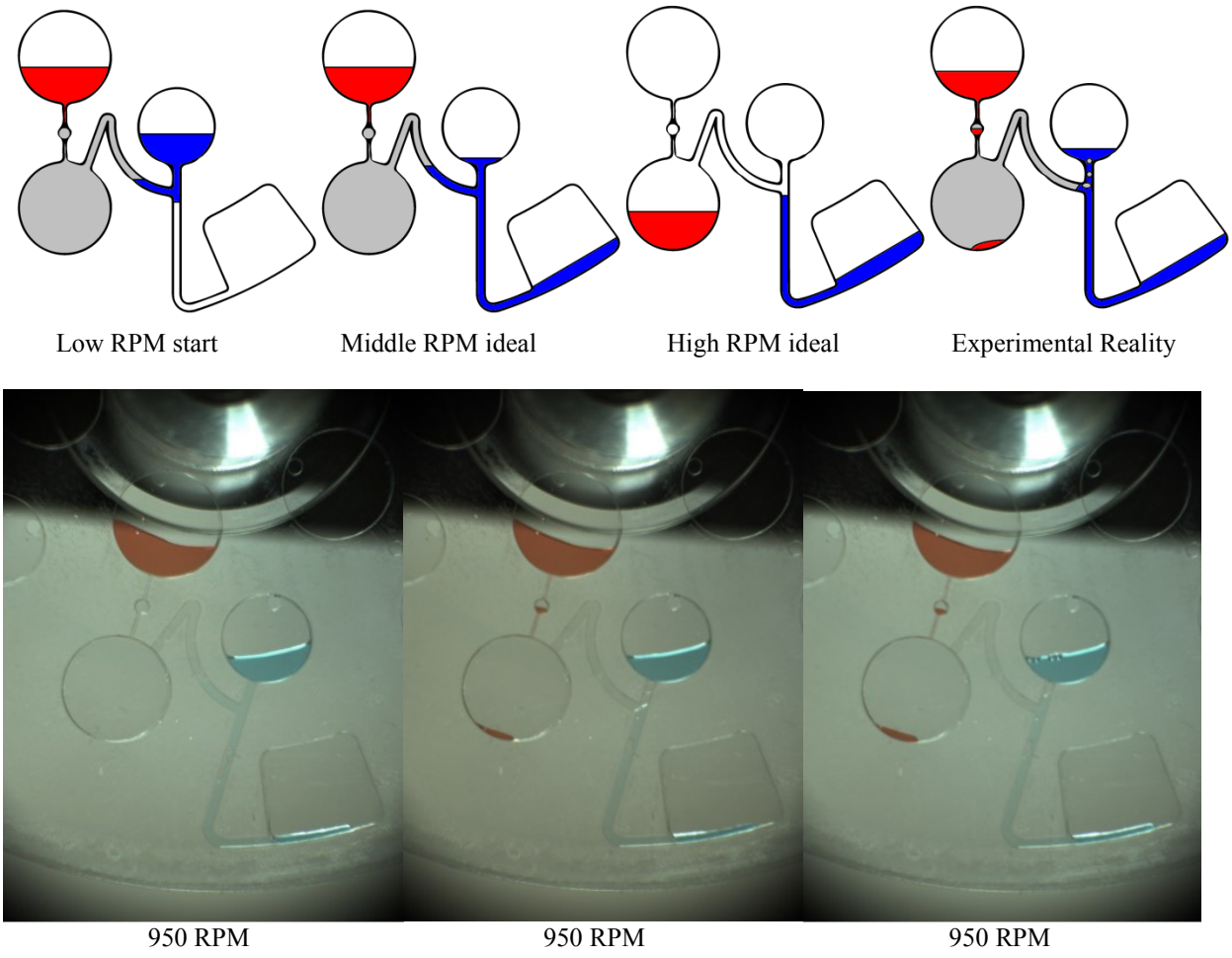


**Figure 4-5. Ideal and experimental images for design concept 2 of compression enhanced 3D valve**
The receiving chamber is vented through the adhesive channel marked in Figure 4-4E. When valving liquid is loaded through the air vent in Figure 4-4C air is trapped in the receiving chamber. Ideally, at high RPM, the valving liquid would drain into the compression chamber shown in Figure 4-4D, venting the receiving chamber. In reality, the high pressure in the receiving chamber caused bubbles to escape through the valving liquid. The images of the bubbles escaping through the valving liquid are presented. All three images were taken at 950 RPM.

It was found that the rotational frequency required to open the channel in design concept 2 was much more precise as compared to the design in Figure 4-2. However, the design concept failed. As the reagent volume applied pressure on the receiving chamber the air pressure pushed bubbles out through the adhesive channel through the valving liquid. Failure would occur at low rotational frequencies. No modifications to this design were attempted.

The remainder of this chapter will focus on the final design that overcame the previously described issues in developing a CV enhanced 3D valve.

## Fabrication of the CM Device

A five-layered test disk was fabricated using materials and techniques previously described by Lafleur and Salin in 2009.[19] The methodology was discussed in detail in the *Experimental: Fabrication of Centrifugal Device* section of Chapter 2 in this thesis (Chapter 2, page 8). The disk, as seen in Figure 4-6, has six replicates of the experimental design.

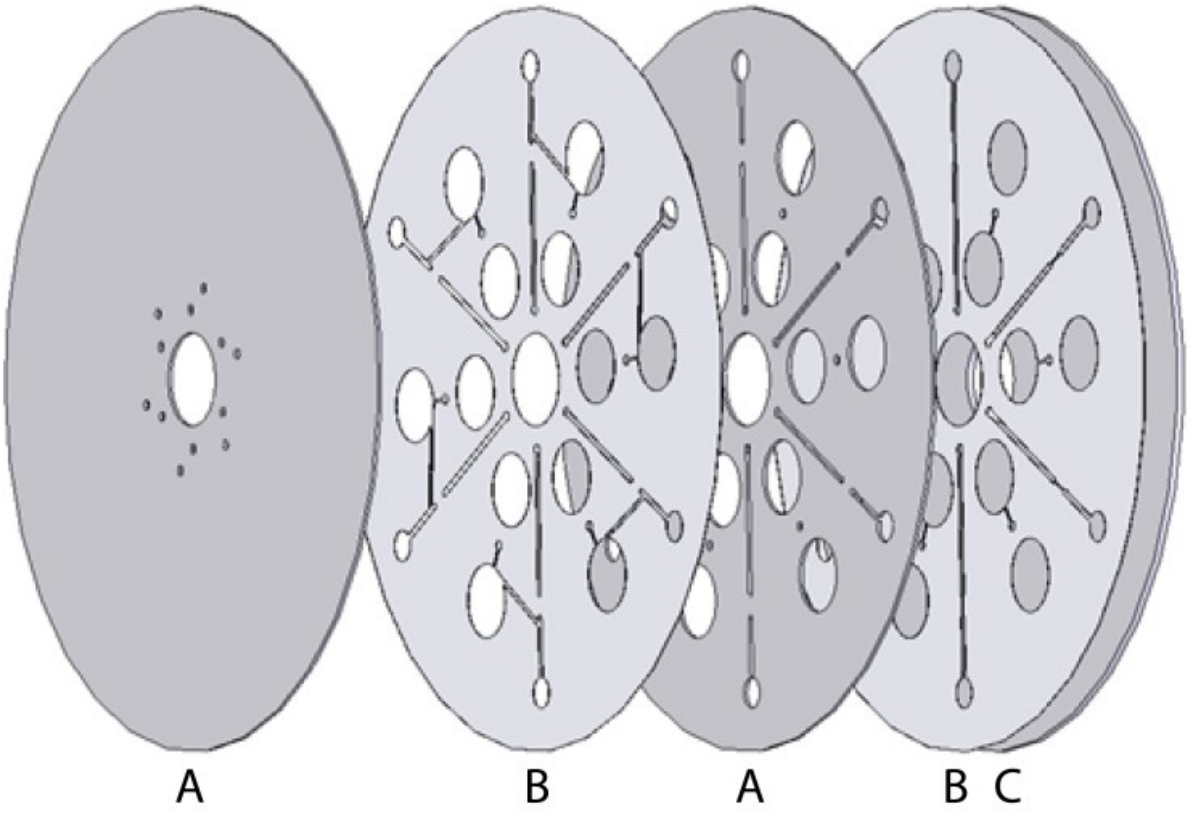


**Figure 4-6. Layers for construction of compression enhanced 3D valve device**
Three disks of five layers with six experimental replicates were constructed. The construction includes (A) polycarbonate DVDs 0.6 mm thick, (B) double sided pressure sensitive adhesives 0.102 mm thick and (C) polycarbonate CD 1.2 mm thick.

The features and important dimensions of the design are highlighted in Figure 4-7.

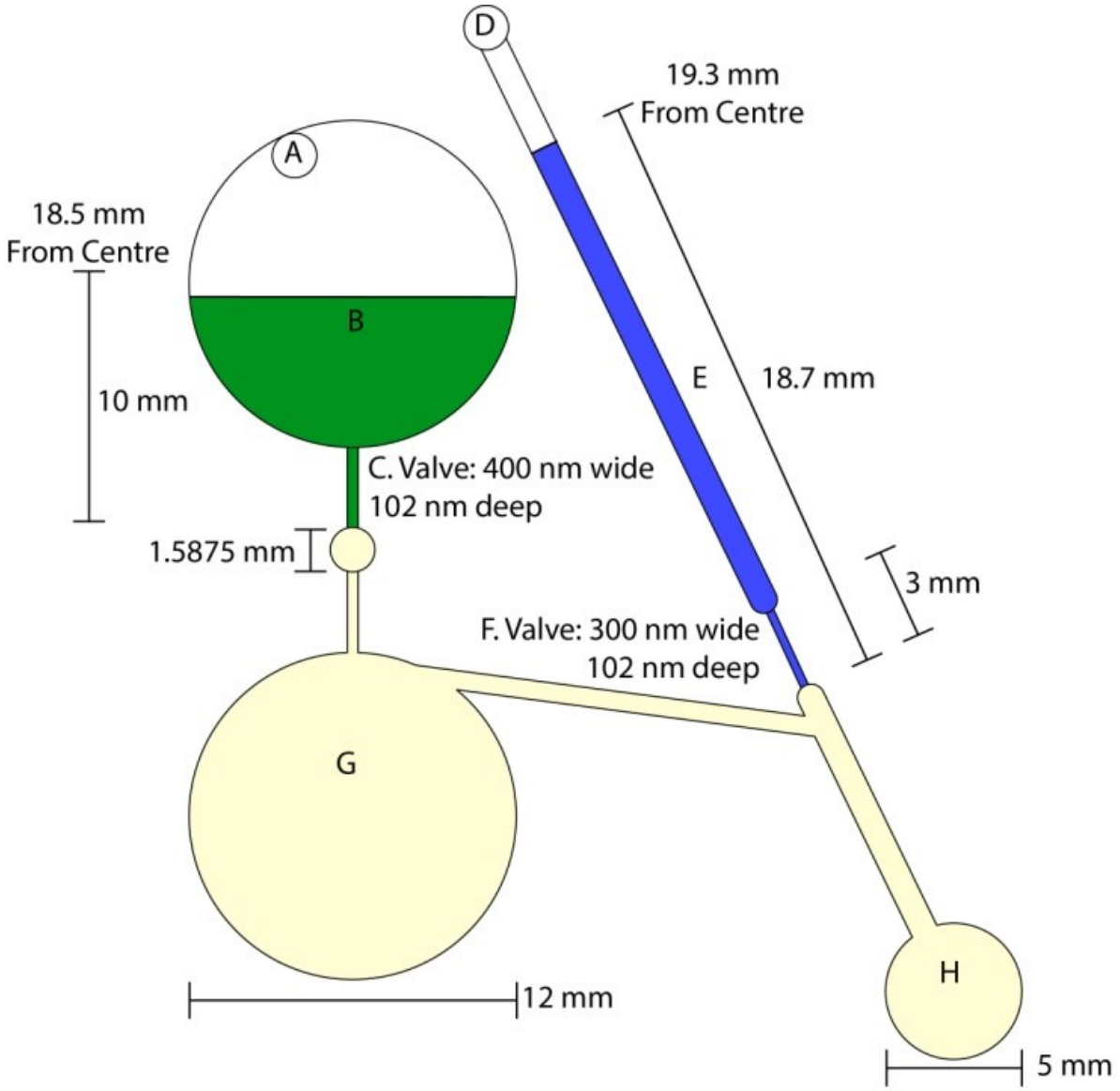


**Figure 4-7. Structure labels and dimensions for compression enhanced 3D valve design**
(A) air vent and loading hole for reagent, (B) reagent in the reagent chamber, (C) 3D valve of reagent chamber, (D) air vent and loading hole for valving liquid, (E) valving liquid in above the compression valve, (F) compression valve, (G) receiving chamber, (H) valve chamber.

Each replicate of experiments with the final design in Figure 4-7 had the same construction and features. On the left are a reagent chamber and a large receiving chamber separated by a 3D valve cut out of the adhesive layers. On the right is a CV filled with valving liquid and a valve chamber. The two sides are connected by an adhesive channel. If the two valves were vented, the

3D valve on the left was designed to burst at 660 RPM, while the compression valve on the right was designed to burst at 450 RPM.

The final design concept presented in this chapter was first tested using a glass capillary valve of 50 μm inner diameter as the compression valve marked by Figure 4-7F. It failed because air did not traverse the capillary valve sufficiently to drain the reagent into the receiving chamber. Due to the airflow restriction, reagent slowly poured through the 3D valve over the course of minutes. This may be useful in future applications but did not achieve the objective of producing a rapidly draining valve. By replacing the glass capillary valve with a passive adhesive valve, the design concept addressed the goals of this chapter. The use of adhesive valves here and in subsequent chapters is possible because of the improvement made by adding the 3D component and the implementation of the CV. Futhermore, the ability to use adhesive valves improves the assembly process of CM devices because they are simpler to construct than glass capillary valves since they do not require additional components or epoxy for assembly

The key component in the 3D valve is the 1.5875 mm diameter hole of Figure 4-7 at the base of the adhesive valve marked as Figure 4-7C. By adding the 3D component, the opening of the valve moved from the top of the receiving reservoir to the smaller hole through the device. This moved the radius closer to the center increasing the calculated burst frequency from 630 RPM to 660 RPM. (Table 4-1, Chapter 4, page 17)

## Setup and Data Acquisition

The spinner and strobe setup described by Duford in 2009[20] was supplemented with a color digital camera (GRAS-14S5C-C, Point Gray, BC, Canada). The entire system was synchronized from a single computer through LabVIEW software (LabVIEW 8.6, Developer Version,

National instruments, QC, Canada). The servo-motor and camera is illustrated with the CM device in Figure 4-8.

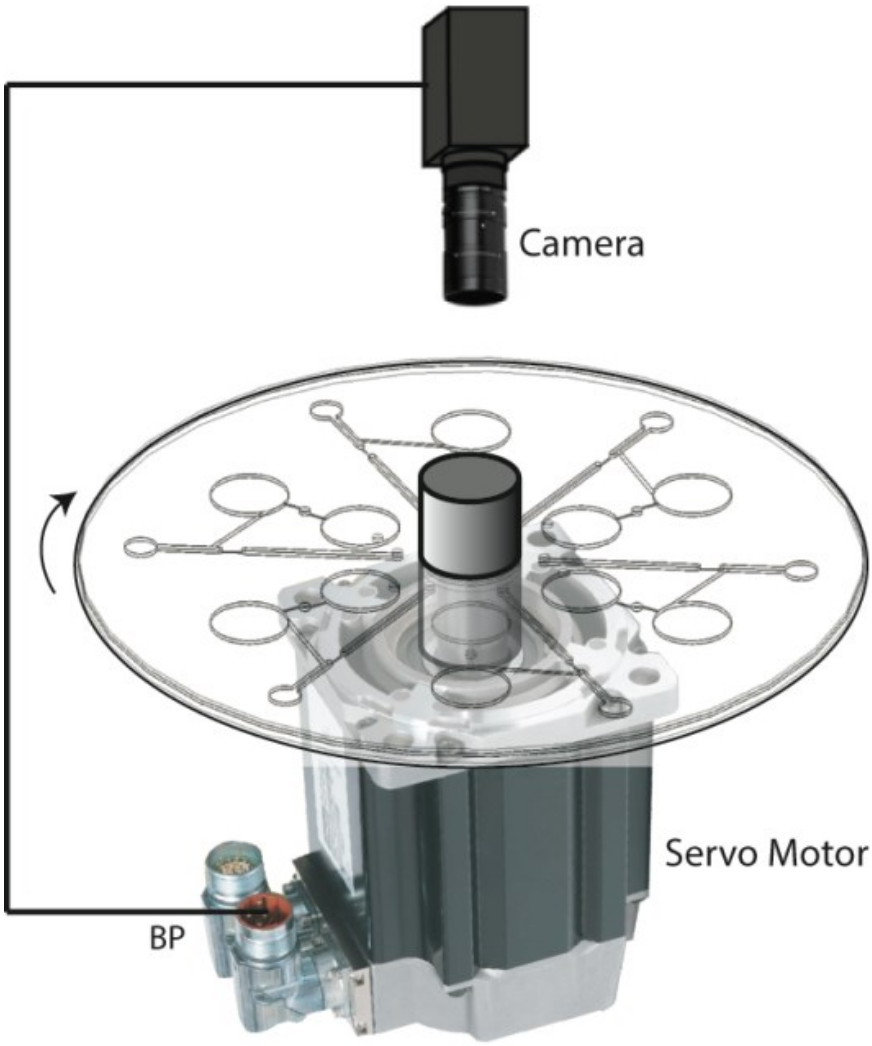


**Figure 4-8. Global schematic of experimental setup for compression enhanced 3D valves**
The Break Point (BP) of the servo motor was used to trigger a synchronized camera and strobe every 10 rotations of the device. The images were used to determine the frequency at which valves burst.

Using the described system, multiple replicate experiments were conducted for presentation in this chapter. The starting rotational frequency was calculated with equations published by Ducree in 2007.[9] The disk was loaded with 30 µL of reagent in the main chamber

and 15 µL of valving liquid in the CV column. The device was then spun at 600 RPM increasing the rotational frequency by 10 RPM every five seconds until the device reached a frequency of 2100 RPM. A sequence of an ideally controlled experiment and experimental images are presented in Figure 4-9.

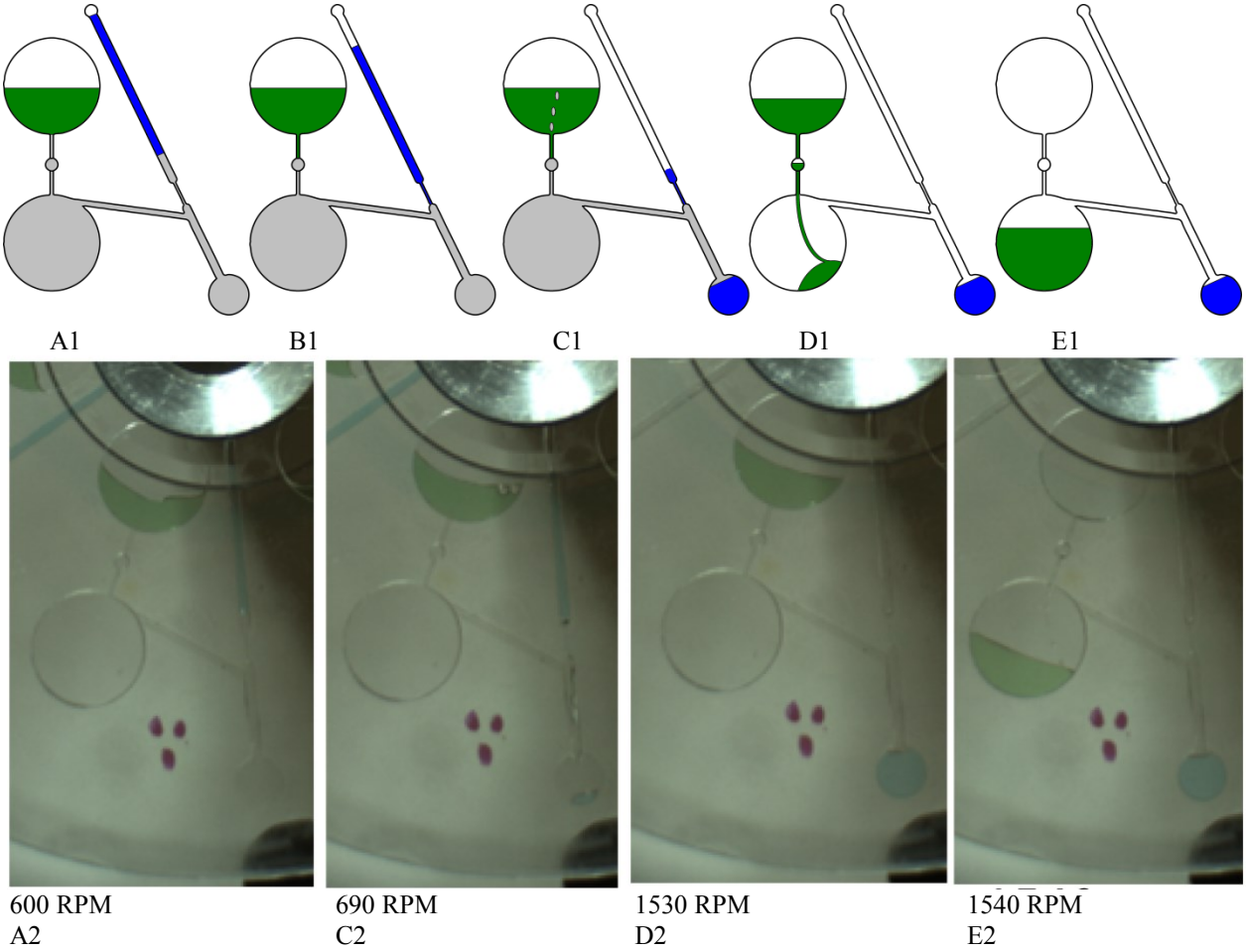


**Figure 4-9. Ideal and experimental images of compression enhanced 3D valve**
An illustration of an ideal experiment is paired with the experimental images. The experiment was performed by rotating the device at 600 RPM for five seconds and then increasing by 10 RPM every five seconds until 2100 RPM to determine the burst frequency of the compression enhanced 3D valve. In A, B and C in both the illustration and experimental images the air in the receiving chamber and valve chamber is not vented and is trapped and denoted with the gray shading in the illustration. In D and E the receiving reservoir is vented through the compression valve.

In Figure 4-9A1 and 4-9A2, 30 µL of green reagent and 15 µL of blue valving liquid were loaded into the device trapping the air in the receiving chamber marked by the grey colour there was no change in the location of the liquid up to 600 RPM. At 690 RPM in Figure 4-9B1 (note

that the camera did not capture an experimental image of 4-9B2), the blue valving liquid compressed the air in the valve chamber but did not burst through the compression valve. At higher RPM, the blue valving liquid drained into the valve chamber as shown in Figure 4-9C1 and 4-9C2. This generated air pressure that caused a bubble in the reagent. This bubble occurred when the trapped air pressure was higher than the pressure of the reagent. In the experiment, bubbling began at 690 RPM. At the enhanced 3D valve burst frequency in Figure 4-9D1 and 4-9D2 the last blue valving liquid drained into the valve chamber releasing the compressed air. With the receiving chamber vented to air (atmospheric pressure through the vent hole) the reagent drained into it. In the experimental image, Figure 4-9D2, the 3D valve had not started to drain but the valving liquid had left the compression valve. Finally, in Figure 4-9E1 and 4-9E2, at a rotational frequency higher than the 3D valve burst frequency the valving liquid was in the valve chamber and the reagent was in the receiving chamber.

Note that by design, the compression valve was at a greater radius (farther from the center of the device) and had a larger head height than the 3D valve. These differences in location and head height meant that, with all other things being equal, the compression valve would burst into the compression chamber before the 3D valve burst. This was consistent with the calculations performed to calculate the burst frequency of passive valves with Equation 4-1 and 4-2 presented in the *Results and Discussion* section of this chapter. The distinction between Equations 4-1 and 4-2 and this CV implementation is that the back pressure from the trapped air in the receiving chamber is not accounted for. Therefore, the burst frequency was much higher for these two valves than is calculated. The difference in the theoretical and experimental burst frequencies of the two valves is outlined in Table 4-1.

The process of increasing the rotational frequency by 10 RPM every five seconds allowed for accurate assessment of burst frequencies. The calculation of multiple frequencies was important for this demonstration. The first is the burst frequency of the 3D valve with a vented receiving reservoir. The second is the burst frequency of the compression valve with a vented valve chamber. The third is the burst frequency of the configuration shown in Figure 4-6 where the 3D valve and the compression valve have no venting for their receiving chambers. This configuration in Figure 4-6 is called a Compression-Enhanced 3D valve.

# Results and Discussion

The burst frequencies of the design presented in the experimental section of this chapter were calculated using Equation 4-1 taken from Ducree's 2007 paper.[9]

$$\nu\,(Hz) = \frac{1}{\pi}\sqrt{\frac{\sigma|cos\Theta|}{\rho r \Delta r d}}$$

**Equation 4-1. Calculation of burst frequency for cylindrical passive valves**
$\sigma$ = surface characterization of water = 0.07197 $Nm^{-1}$
$\Theta$ = contact angle of water with polycarbonate = $70^0$
$\rho$ = density of water = 1000 kg $m^{-3}$
r = average radius of the liquid plug
$\Delta$r = head height of the liquid plug
d = diameter of capillary opening

The value of d in Equation 4-1 is the diameter of a circular capillary opening. In this case, d is an approximation, Dh, because the opening of the adhesive valve is rectangular. The approximation is shown in Equation 4-2.

$$D_h = \frac{2*H*W}{H+W}$$

**Equation 4-2. Approximation of *d* for rectangular passive valves in Equation 4-1**
H = height of the valve
W = Width of the valve

The results of the calculations and the experimental results for the burst frequencies of the different configurations are presented in Table 4-1. The calculation of the CV burst frequency showed that the CV would burst before the 3D adhesive valve if they were both vented. Therefore, the CV was expected to burst first in the experiment.

| Valve Type | Calculated Burst Frequency(RPM) | Experimental Burst Frequency (RPM) | Replicates |
|---|---|---|---|
| Passive Adhesive Valve | 630 | 290 +/- 10 | 8 |
| 3D Adhesive Valve | 660 | 650 +/- 40 | 4 |
| Compression Valve | 450 | N/A | N/A |
| Compression Enhanced 3D Valve | N/A | 1540 +/- 180 | 14 |

**Table 4-1. Calculated and experimental burst frequencies for the passive valves of Chapter 4**
The passive adhesive valves were measured on two devices. The 3D adhesive valves were measured on one device. The compression enhanced 3D valves were measured on two devices.

The most striking improvement gained from the implementation of 3D valves was the accuracy of the experimental burst frequency when compared to the calculated burst frequency. The passive adhesive valve with no 3D modification consistently burst at a rotational frequency lower than the calculated value. The reduction in burst frequency occurred due to the imperfect nature of the geometric opening at the terminus of the adhesive valve. Specifically, there was a tendency to have wicking away from the opening of the adhesive valve into the receiving chamber. Due to wicking, regular passive capillary valves cut from adhesives do not maintain surface tension at the opening of the valve. Without surface tension at the valve opening the liquid can flow almost without restriction. The wicking results from misalignment between milled channels and the adhesive. The small gap that forms between two disks when adhesive is misaligned creates a channel that wicks reagent through capillary force thus breaking the surface tension at the opening of the valve. Therefore, at a lower rotational frequency than the theoretical burst frequency the valve allows liquid to flow. This change in burst frequency based on the imperfection of the valve opening was discussed by Moore in 2011 when observing the burst

frequency in 3D printed microfluidic devices.[21] The 3D printed channels were not perfectly circular or rectangular and changed the surface tension's ability to bridge the valve opening. The change in the liquid interface affected the burst frequency just as seen here with imperfect alignment of the adhesive valve with the receiving chamber.

The 3D design feature presented here substantially reduces the wicking phenomenon caused by imperfections in adhesive alignment and thus makes the valve a more reliable CM component. The change in design makes a misalignment much less likely due to the method of construction. When aligning multiple layers of a device for lamination the most important components to ensure a successful programmable experiment are the valves. With a very small transfer opening axial to the disk the alignment by hand is much easier than when aligning large chambers.

The easy implementation of the 3D valve into CM devices improved accuracy, but still had a very low burst frequency, <700 RPM at the radii tested with the design of Figure 4-1. The low burst frequency of the 3D valve on its own prompted the successful development of the compression enhanced valve design presented in Figure 4-7.

Several experiments were conducted with the compression enhanced 3D valve in order to determine if changing the volume of the valving liquid would change the burst frequency of the 3D valve. Valving liquid volumes of 5, 10 and 15 µL were used in an attempt to tune the burst frequency of the 3D valve. It was determined that it is not possible to tune the burst frequency of the 3D valve using different volumes of valving liquid. Five µL of valving liquid did not generate more pressure than the reagent. Therefore, the 3D valve would burst at approximately 650 RPM as if it were vented. Above a certain volume, there is no significant difference in the burst frequency using different volumes of valving liquid. Both 10 and 15 µL of valving liquid

would cause the 3D valve to burst at ~1540 RPM. When the valving liquid was 10 or 15 µL the valve acted the same due to the bubbling that is shown in Figure 4-9C. Both 10 and 15 µL of valving liquid would drain into the valve chamber and generate enough pressure in the trapped air that bubbles would escape through the 3D valve. Therefore, the air pressure generated by both the 10 and 15 µL of valving liquid would reach the same equilibrium and produce the same burst frequency for the 3D valve.

The variability of bubbling by the trapped air through the 3D valve caused the high standard deviation on the burst frequency seen in Table 4-1. The pressure of the trapped air would reach equilibrium with the pressure of the reagent through bubbling. However, the air pressure would not always fully release through bubbling causing the variability in the burst frequency.

# Conclusions

Modifications to passive capillary valves cut in the adhesive layers of CM devices have been demonstrated. Addition of a multi-layered 3D design and compression valve made burst frequencies more accurate and allowed the frequency to be much higher for the same radial position. The precision of the design was quantified through multiple replicates. The addition of these designs to the CM toolkit will greatly improve the application of passive adhesive valves in experimental setups. The increase in burst frequency allows the use of simple adhesive valves at higher RPMs and at greater radii in CM designs.

# References:


1. Arora, A.; Simone, G.; Salieb-Beugelaar, G. B.; Kim, J. T.; Manz, A., Latest developments in micro total analysis systems. Analytical Chemistry 2010, 82 (12), 4830-4847.
2. Madou, M.; Zoval, J.; Jia, G.; Kido, H.; Kim, J.; Kim, N., Lab on a CD. Yarmush, M. L., Ed. 2006; Vol. 8, pp 601-628.
3. Gorkin, R.; Park, J.; Siegrist, J.; Amasia, M.; Lee, B. S.; Park, J. M.; Kim, J.; Kim, H.; Madou, M.; Cho, Y. K., Centrifugal microfluidics for biomedical applications. Lab on a Chip - Miniaturisation for Chemistry and Biology 2010, 10 (14), 1758-1773.
4. Mark, D.; Haeberle, S.; Roth, G.; Von Stetten, F.; Zengerle, R., Microfluidic lab-on-a-chip platforms: Requirements, characteristics and applications. Chemical Society Reviews 2010, 39 (3), 1153-1182.
5. Zoval, J.; Jia, G.; Kido, H.; Kim, J.; Kim, N.; Madou, M. J., Springer Handbook of Nanotechnology 2007, 549-570.
6. Feng, Y.; Zhou, Z.; Ye, X.; Xiong, J., Passive valves based on hydrophobic microfluidics. Sensors and Actuators, A: Physical 2003, 108 (1-3), 138-143.
7. Cho, H.; Kim, H. Y.; Kang, J. Y.; Kim, T. S., How the capillary burst microvalve works. Journal of Colloid and Interface Science 2007, 306 (2), 379-385.
8. Squires, T. M.; Quake, S. R., Microfluidics: Fluid physics at the nanoliter scale. Reviews of Modern Physics 2005, 77 (3), 977-1026.
9. Ducrée, J.; Haeberle, S.; Lutz, S.; Pausch, S.; Von Stetten, F.; Zengerle, R., The centrifugal microfluidic Bio-Disk platform. Journal of Micromechanics and Microengineering 2007, 17 (7), S103-S115.
10. Chen, J. M.; Huang, P. C.; Lin, M. G., Analysis and experiment of capillary valves for microfluidics on a rotating disk. Microfluidics and Nanofluidics 2008, 4 (5), 427-437.
11. Lacroix-Fralish, A.; Templeton, E. J.; Salin, E. D.; Skinner, C. D., A rapid prototyping technique for valves and filters in centrifugal microfluidic devices. Lab on a Chip - Miniaturisation for Chemistry and Biology 2009, 9 (21), 3151-3154.
12. Xi, Y.; Templeton, E. J.; Salin, E. D., Rapid simultaneous determination of nitrate and nitrite on a centrifugal microfluidic device. Talanta 2010, 82 (4), 1612-1615.
13. Al-Faqheri, W.; Ibrahim, F.; Thio, T. H. G.; Moebius, J.; Joseph, K.; Arof, H.; Madou, M., Vacuum/Compression Valving (VCV) Using Parrafin-Wax on a Centrifugal Microfluidic CD Platform. PLoS ONE 2013, 8 (3).
14. Gorkin, R.; Nwankire, C. E.; Gaughran, J.; Zhang, X.; Donohoe, G. G.; Rook, M.; O'Kennedy, R.; Ducrée, J., Centrifugo-pneumatic valving utilizing dissolvable films. Lab on a Chip - Miniaturisation for Chemistry and Biology 2012, 12 (16), 2894-2902.

15. Mark, D.; Metz, T.; Haeberle, S.; Lutz, S.; Ducrée, J.; Zengerle, R.; Von Stetten, F., Centrifugo-pneumatic valve for metering of highly wetting liquids on centrifugal microfluidic platforms. Lab on a Chip - Miniaturisation for Chemistry and Biology 2009, 9 (24), 3599-3603.
16. Templeton, E. J.; Salin, E. D., A novel filtration method integrated on centrifugal microfluidic devices. Microfluidics and Nanofluidics 2013, 1-7.
17. Park, J. M.; Cho, Y. K.; Lee, B. S.; Lee, J. G.; Ko, C., Multifunctional microvalves control by optical illumination on nanoheaters and its application in centrifugal microfluidic devices. Lab on a Chip - Miniaturisation for Chemistry and Biology 2007, 7 (5), 557-564.
18. Kong, M. C. R.; Bouchard, A. P.; Salin, E. D., Displacement pumping of liquids radially inward on centrifugal microfluidic platforms in motion. Micromachines 2012, 3 (1), 1-9.
19. Lafleur, J. P.; Salin, E. D., Pre-concentration of trace metals on centrifugal microfluidic discs with direct determination by laser ablation inductively coupled plasma mass spectrometry. Journal of Analytical Atomic Spectrometry 2009, 24 (11), 1511-1516.
20. Duford, D. A.; Peng, D. D.; Salin, E. D., Magnetically driven solid sample preparation for centrifugal microfluidic devices. Analytical Chemistry 2009, 81 (11), 4581-4584.
21. Moore, J. L.; McCuiston, A.; Mittendorf, I.; Ottway, R.; Johnson, R. D., Behavior of capillary valves in centrifugal microfluidic devices prepared by three-dimensional printing. Microfluidics and Nanofluidics 2011, 10 (4), 877-888.

# CHAPTER 5: A centrifugal open microfluidic reagent deposition system with Coriolis switching

In overcoming limitations native to CM, one topic that has been previously discussed by this author (Bouchard) was the continuous addition of liquid to a CM device in motion. The objective of liquid deposition was to avoid requiring reagents to be stored on the device. Liquid deposition made more device space available for operations and made it so that fresh reagents could be introduced to the device at the time of analysis. Additionally, the ability to generate gradients and elution mixtures off-disk expanded the cabability of a CM device to perform chromatography. Early work of this author (Bouchard) focused on the parallel nature of CM and deposited liquid to multiple device outlets. The design presented in this chapter shifted the focus towards the deposition of liquid to a single outlet so that greater control over gradients and volume could be maintained.

In this author's (Bouchard) earlier development of deposition methods, the concept of open microfluidics became a point of interest as a new way to manipulate samples. Therefore, this chapter also includes an examination of applying the open microfluidic concept to CM devices.

## Contribution to Original Knowledge

Liquid addition to CM devices in motion can be used for the addition of different reagents in more complex experiments. A novel design for liquid distribution was demonstrated that allowed the addition of liquid to a single CM experiment on a device. Open microfluidics (OM) were explored for the enhancement of a Coriolis switch. The switch allowed for the addition of reagents and the subsequent wash solutions to an experiment.

# Abstract

In order to create a low RPM Coriolis switch, the potential of using open microfluidics (OM) on a centrifugal microfluidic device was explored. A device for testing the effect of OM on Coriolis drift of a reagent stream was constructed. It was determined that if the height of the chamber was less than 0.300 mm than Coriolis drift was less than in OM. When the height was greater than 0.300 mm the addition of a top to the chamber did not affect Coriolis drift as compared to OM. The reagent stream would not contact the top of the chamber due to gravity and would not be affected by having a chamber ceiling. Therefore, a chamber with a height of 0.800 mm was used for a Coriolis switch when running liquid deposition rather than an open chamber.

Next, a liquid deposition CM device was designed and constructed with a novel configuration for the deposition of reagent while the device was in motion. The design presented in this chapter is a non-contact, in-motion reagent addition module for the deposition of reagents, rinses or diluents to a CM device in motion. A spiral away from the center of the device allowed deposited liquid to flow radially outwards to a single opening. This opening led to a Coriolis switch to select whether the liquid being deposited would be collected or sent to waste. The configuration allowed for the deposition of reagent followed by a wash solution to waste and then a second reagent.

# Introduction

In 2013, Casavant presented an introduction to OM.[1] In that paper OM was described as the control of small volumes of fluid with a geometric structure that has no covering. This type of design lends itself to the development of high throughput and reusable components. In 2013, Huang discussed why OM with no contact from outside forces is ideal and presented pneumatic,

magnetic and hydrophilic/phobic treatments for that purpose.[2] In an earlier paper from 2009, Khare used wrinkled PDMS surfaces to control flow in OM devices.[3] Neither Huang nor Khare used CM principles in their OM devices. This Chapter describes a test of the effect OM has on Coriolis drift on a CM device.

The addition of reagents and samples to CM devices in motion has been published in several forms. Andersson patented a concept where droplets of water were flicked into openings in a spinning CM device in 2003.[4] This was accomplished by empirically derived parameters for different rotational frequencies and viscosity of reagents and samples. In 2010, this author (Bouchard) published the Centrifugal Liquid Addition Distributor (CLAD) which took a stream of liquid and deposited it into different inlet holes on a CM device by dividing the surface with 3D printed walls.[5] This Chapter describes a spiral shape for the deposition of a stream of liquid into a single inlet on a CM device. This has been paired with a Coriolis switch to select whether the reagent is going into the inlet or to waste for rinsing the spiral.

The spiral of this chapter was influenced by Mark's 2011 design in which the reagent of interest filled multiple metering chambers.[6] Mark's design had the sample of interest flow through a channel with openings to chambers of known volumes along its length. The sample would flow through the channel while filling each of the metering chambers with an exact volume to aliquot. In the design, the sample poured off to waste after flowing past all available individual metering chambers. The operation was innovative in its transition from a single sample to multiple aliquots as sample preparation occurred before the filling of multiple metering chambers. It was also an example of a spiral design where the liquid flowed from the center of the device to the edge slowly because the channel did not follow the radius of the device. The channel feeding the metering chambers became progressively farther from the center

of the device and allowed the multiple metering chambers filled by the process to be situated in different sections of the device so that larger and more complex functions could be installed. This spiral influenced the design of the spiral deposition of this chapter in which the liquid of interest flows towards a single outlet as it is deposited on the device while in motion.

Being able to select the direction of flow at a junction is an important functionality for the design of more complex microfluidic methodologies. Methods involved controlling flow with valves, or to use trapped air or, in the case of Kong in 2011, compressed air to restrict liquid movement.[7] Haeberle published the use of Coriolis force for the mixing of two liquids in a Y-junction in 2005.[8] Steigert demonstrated a switch that depended on a combination of geometry and Coriolis force to ensure liquid flowed in a desired direction in 2005.[9] Kim later used a Coriolis switch in 2008 that required no geometric shape but used a higher RPM to select the direction of flow.[10] This was followed in 2010 by En Lin who used a combination of Coriolis force and geometric shapes to distribute reagent into one of four receiving chambers without the use of valves.[11]

Described here is the use of a spiral shape for the deposition of reagent into a Coriolis switch to select either the input to a CM experiment or waste for the rinsing of the spiral deposition structure. The CLAD paper described the many potential benefits for the use of reagent addition while the disk is spinning.[5] These include gradient addition, elimination of storage reservoirs or reagent degradation and the availability of "unlimited" volumes of reagent.

# Experimental

## Fabrication of CM Devices

Test disks were fabricated using materials and techniques previously described by Lafleur and Salin in 2009.[12] The methodology was discussed in detail in the *Experimental: Fabrication*

*of Centrifugal Device* section of Chapter 2 in this thesis (Chapter 2, page 8). An example of an assembly is shown in Figure 5-1 using the liquid deposition design.

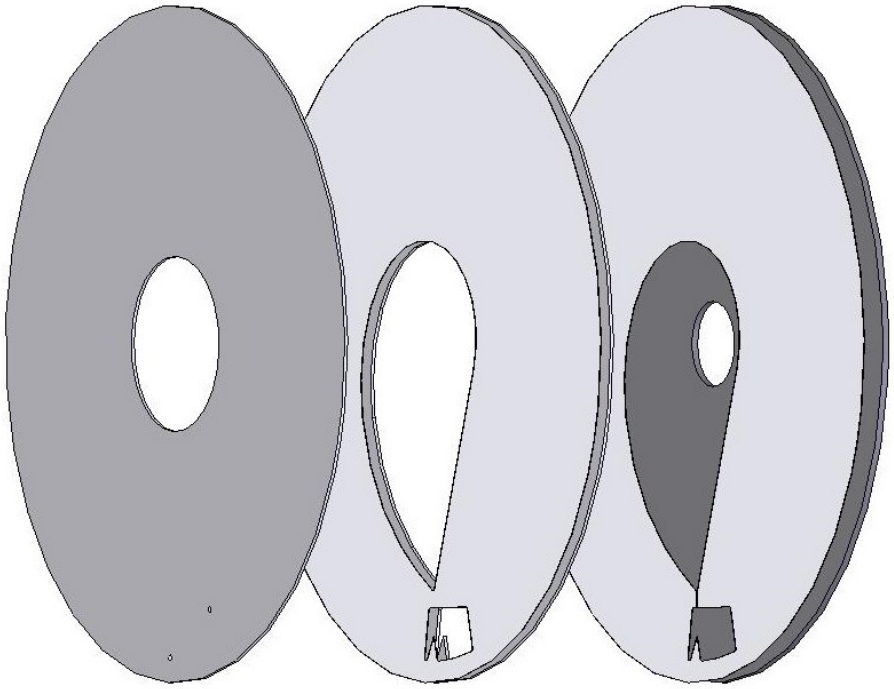


**Figure 5-1. Layers for construction of spiral deposition and Coriolis switch device**
A disk of five layers was constructed. The construction includes (A) polycarbonate DVDs 0.6 mm thick, (B) double sided pressure sensitive adhesives 0.102 mm thick and (C) polycarbonate CD 1.2 mm thick.

The designs of the two experiments are shown in Figures 5-2 and 5-3 respectively.

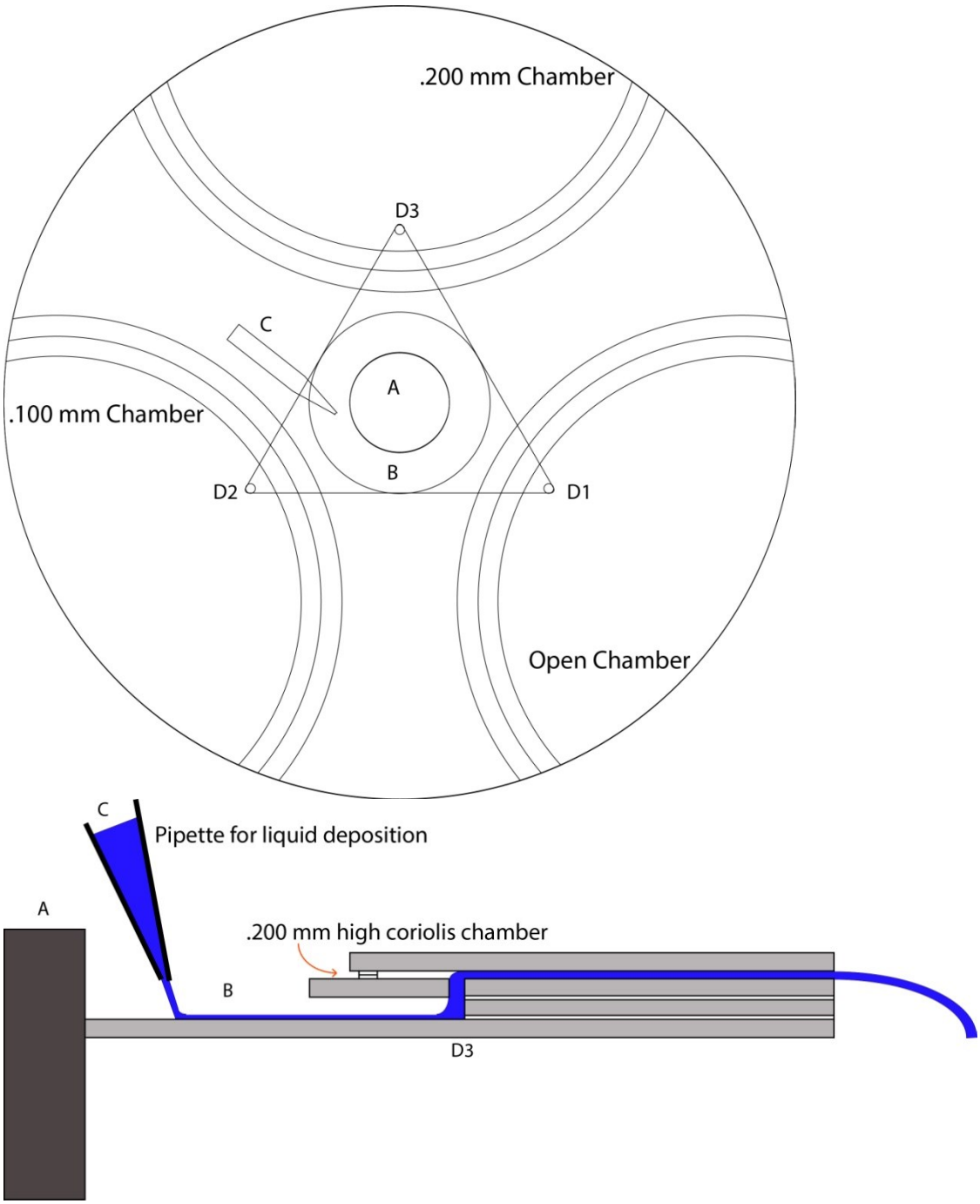


**Figure 5-2. Structure labels and dimensions of experimental design for the open microfluidic device**
(A) center hole for motor shaft, (B) deposition opening, (C) pipette, (D) hole opening from deposition layer to Coriolis chambers. Liquid deposited by a pipette is spun by centrifugal force into three openings which drain out of a Coriolis chamber. Three chamber heights were used in the figures of this chapter; Open, 0.100 mm and 0.200 mm. The side view shows the 0.200 mm chamber.

The different chamber heights for the OM test were created by stacking 0.102 mm thick layers of adhesive. In the device presented here, there were three chamber heights; Open,

0.100 mm and 0.200 mm. In other devices not shown, heights of 0.300 mm and 0.600 mm were tested as well.

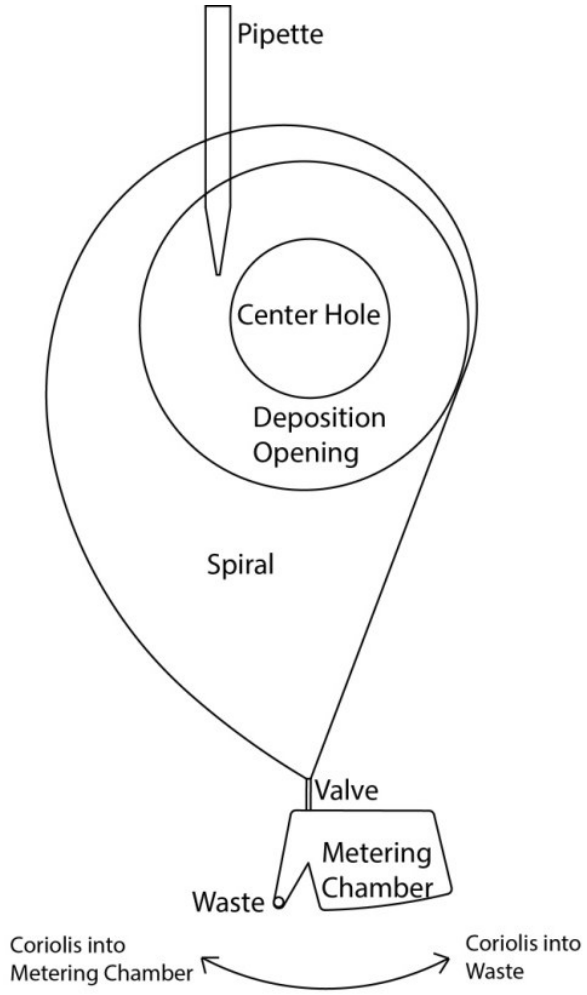


**Figure 5-3. Structure labels for the spiral deposition and Coriolis switch device**
A pipette was used to deposit liquid onto the device while it is in motion. Centrifugal force drove the liquid from the Deposition Opening to the edge of the Spiral Chamber. The spiral drained into a single adhesive valve 0.400 mm in width and 0.102 mm in height. The valve opened to a Coriolis switch that drained to waste or to a metering chamber depending on the direction of rotation.

## Setup and Data Acquisition

The spinner and strobe setup described by Duford in 2009[13] was supplemented with a color digital camera (GRAS-14S5C-C, Point Gray, BC, Canada), with the entire system synchronized from a single computer through LabVIEW software (LabVIEW 8.6, Developer

Version, National instruments, QC, Canada). The full setup can be seen with a different device in Chapter 4, Figure 4-8.

# Results and Discussion

## Examination of Open Microfluidics

The first experiment compared the use of open and closed microfluidics on Coriolis drift on CM devices. First, it was determined that a high flow rate of liquid (17 mL/min) was required to overcome the imperfections, such as dust and scratches, on the polycarbonate. This was observed by varying the flowrate of liquid deposition and observing the consistency of the liquid stream. The comparison of low and high flowrate is shown in Figure 5-4. From that point, higher flow rates of liquid were used. Next, the range of rotational frequencies generated by the servo motor were tested (Figure 5-4). The images of Figure 5-5 were put together by overlapping the images of the same microfluidic device at different RPM in order to compare the Coriolis drift. It was found that across the range of 1200 to 2800 RPM there was no significant difference in Coriolis drift.

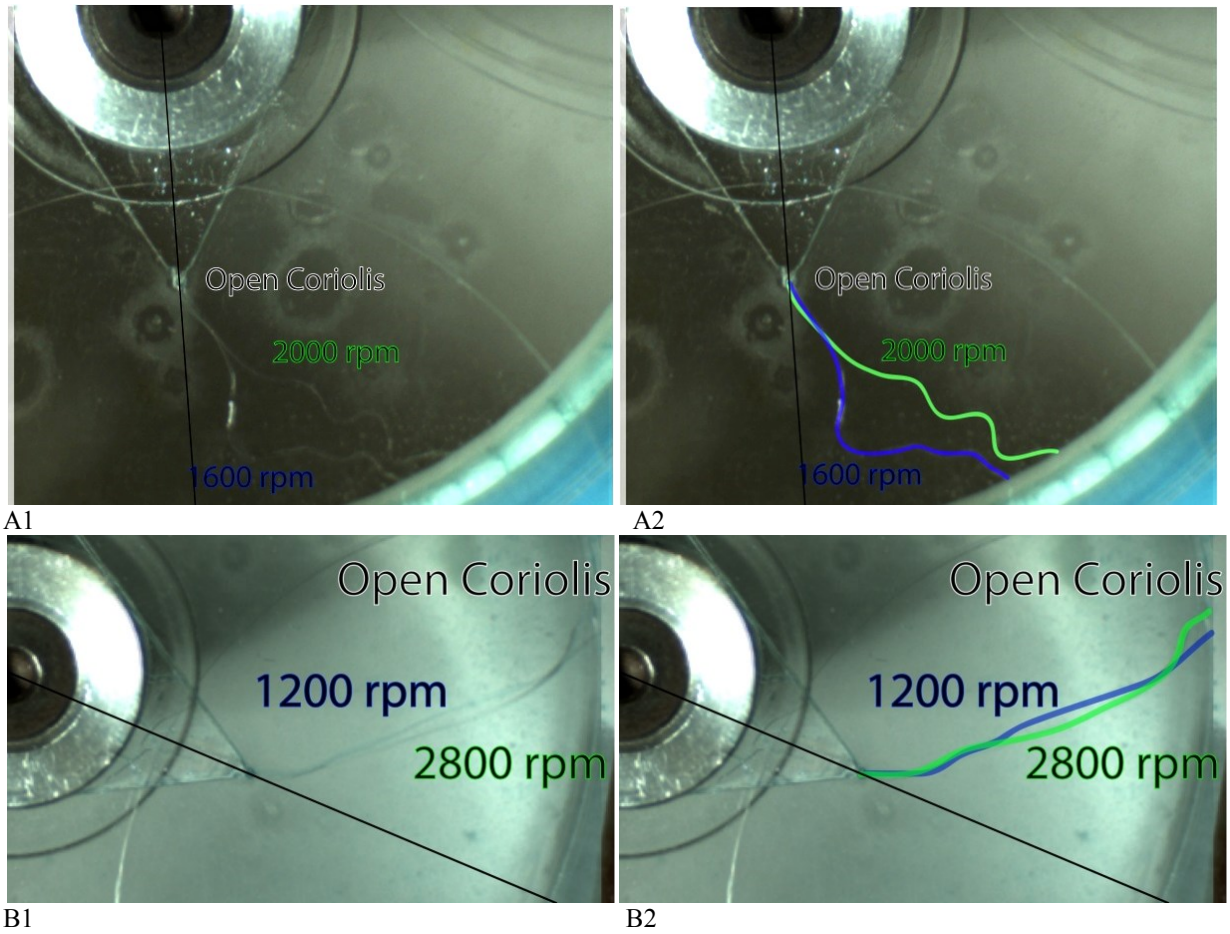


**Figure 5-4. Comparison of mid and high RPM on Coriolis drift on the open microfluidic device**
(A) The demonstration of a low flow rate (6.2 mL/min) at 1600 RPM (blue stream) and 2000 RPM (green stream) on an open microfluidic device with no structures. A1 is the unaltered image, A2 has the liquid streams highlighted in green and blue (B) is the demonstration of a high flow rate (17.0 mL/min) at 1200 RPM (blue stream) and 2800 RPM (green stream) on an open microfluidic device with no structures. B1 is the unaltered image; B2 has the liquid streams highlighted. The consistent flow path illustrated in B1 and B2 is more desirable and illustrates the need for higher flow rates.

All four images of Figure 5-4 have a black line drawn from the center of the device through the hole labeled in Figure 5-2D where the liquid enters the chamber and begins to follow a curve caused by Coriolis force. The liquid would follow the path of this black radial line if there was no Coriolis drift. In addition to determining that the flow rate of liquid deposition needed to be at least 17.0 mL/min, the observations of Figure 5-4 determined that there was no difference in the Coriolis drift when rotating between 1200 and 2800 RPM. Therefore, a comparative analysis between open and closed CM devices was conducted at a single rotational

frequency. It was found that in devices with a height at 0.300 mm high and higher the CM device acted as if it were open with no ceiling. This is due to gravity keeping the liquid stream on the floor of the chamber. In Figure 5-5 open and closed chambers were overlapped. It can be seen that there was consistently more Coriolis drift in the open CM configuration.

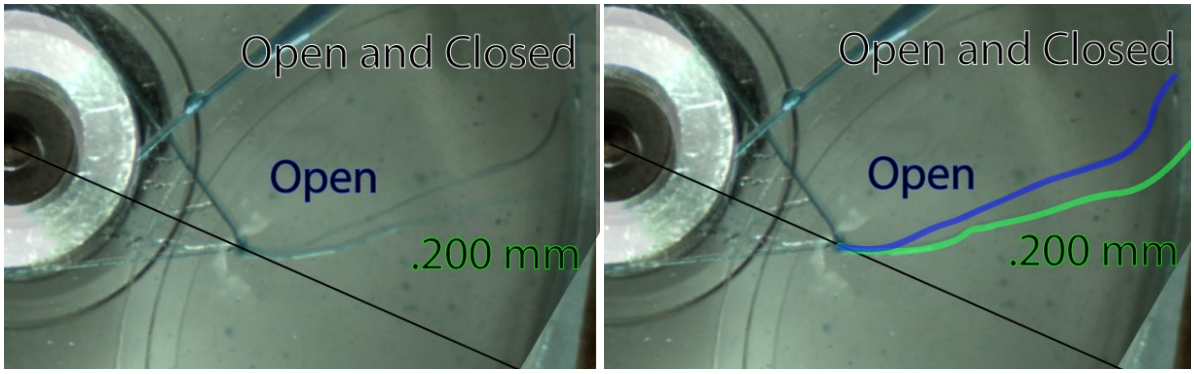


A1 A2

**Figure 5-5. Comparison of open and closed microfluidics on Coriolis drifts on the open microfluidic device**
A high flow rate comparison of Coriolis drift on an open and closed CM device are shown at1200 RPM. In A1 the image is unaltered; in A2 the reagent streams are highlighted. It can be seen that there is a significant difference in the Coriolis drift.

At 0.200 mm height, the liquid stream contacted the floor and ceiling of the chamber. Two contact points with the polycarbonate of the CM device made the liquid stream resist Coriolis drift. Polycarbonate is mildly hydrophilic and the liquid stream in the closed configuration resisted Coriolis force due to that attraction. A chamber height of 0.800 mm was created when assembling a CM device with a DVD and two layers of adhesive. At that height the chamber acted as an open system for streams of liquid and had the benefit of not being exposed to external contaminates. It was also found that at 0.100 mm in height a liquid stream does not form and wicking overcomes Coriolis force.

Figure 5-6 shows the full device rotating at 1200 RPM with three chamber configurations; open, 0.100 mm in height and 0.200 mm in height. As liquid was introduced into the device, the open chamber and 0.200 mm height chamber allowed liquid streams to form which were

influence by the Coriolis force. In contrast, the 0.100 mm height chamber did not exhibit the effects Coriolis force due to wicking of the sample.

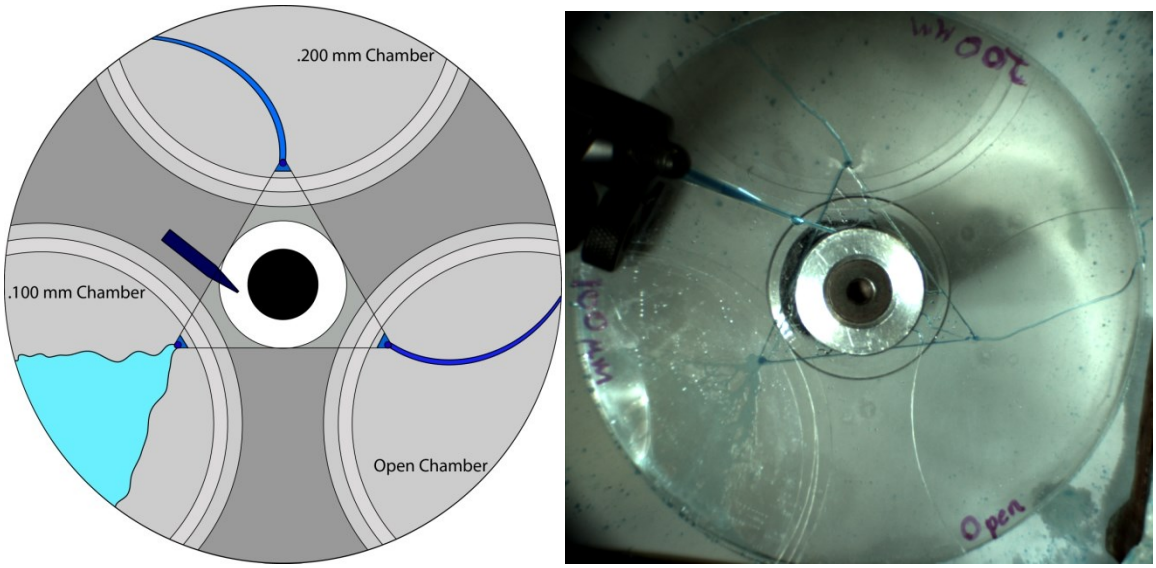


**Figure 5-6. Illustration and experimental image of the open microfluidic device at 1200 RPM**
The experimental image was duplicated so that the open and 0.200 mm height chambers could be overlayed and presented in Figure 5-5.

## Spiral Deposition

The design for deposition in motion as presented in Figures 5-2, 5-5 and 5-6 worked by having chamber edges that became progressively farther from the center of the CM device. The design for a three chamber distribution is very efficient at equally distributing a single reagent addition to three parallel experiments. However, when an experiment called for a single iteration a single deposition design was required. The application of the design in Figure 5-3 is shown in Figure 5-7.

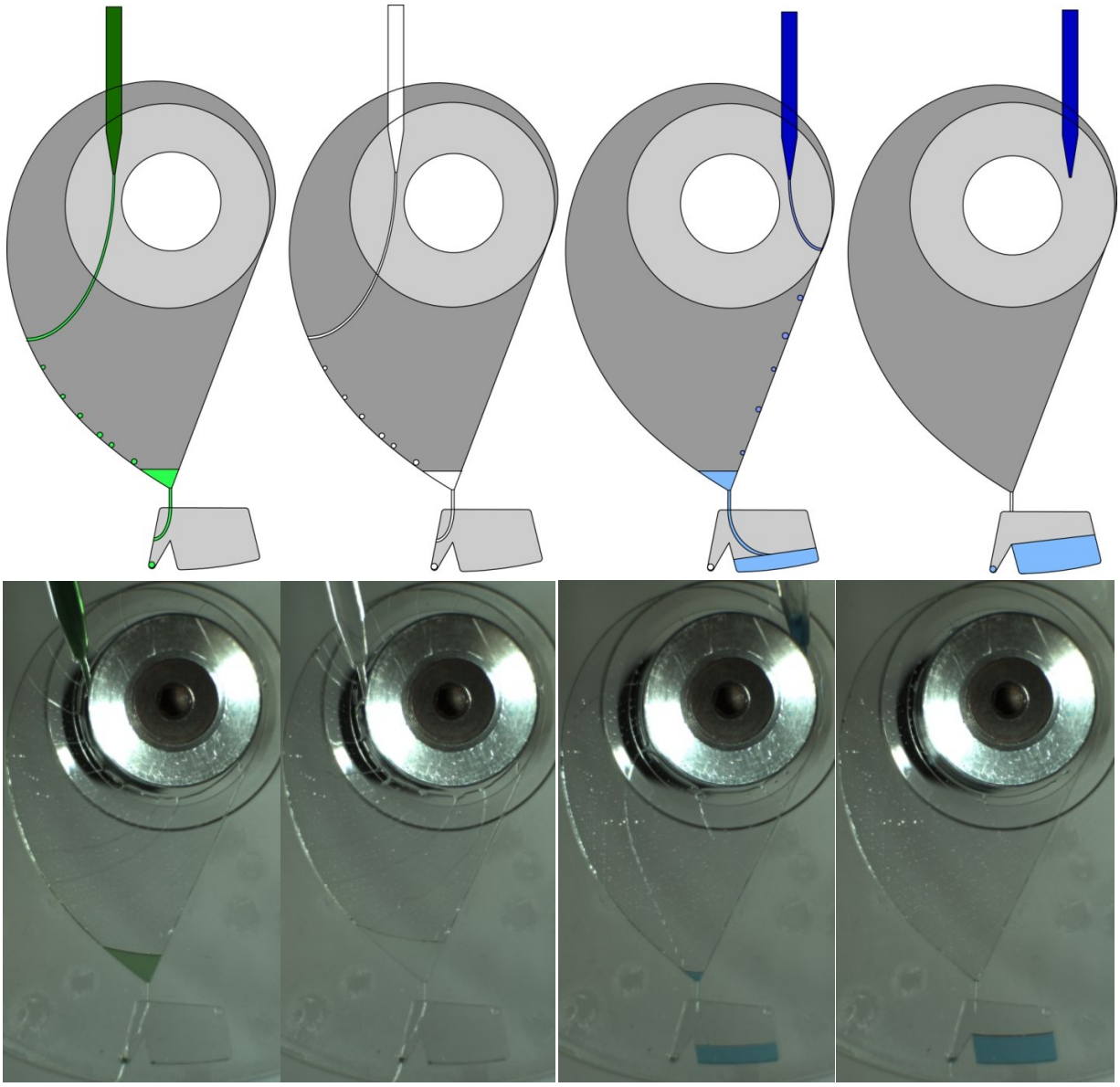

| A | B | C | D |
|---|---|---|---|
| -1800 RPM Counter Clockwise (CCW) | -1800 RPM Counter Clockwise | 1800 RPM Clockwise (CW) | 1800 RPM Clockwise |

**Figure 5-7. Ideal and experimental images of the spiral deposition device**
(A) At -1800 (CCW) RPM green liquid was deposited. (B) The spiral was washed with DDW. (C) At 1800 RPM (CW) blue reagent was deposited. More volume than the volume of receiving chamber was deposited (D) The excess flowed into waste metering the volume of blue reagent.

A spiral design was utilized in order to have the edge of the spiral deposition chamber constantly increasing in distance from the center of the CM device. The spiral moved all deposited liquid to a single valve outlet with a Coriolis switch so that wash solutions could be

used between reagent depositions. The reagent of interest was deposited at 1800 RPM (CW) and wash solutions were deposited at -1800 RPM (CCW) and drained to waste off the device.

When designing the device, polar coordinates were used to describe the properties of the spiral. A spiral geometry of greater than one millimeter increase in radius per 45 degree change in angle was required to enable draining of the spiral at moderately low RPM. Earlier designs attempted to compress the spiral (i.e., to reduce the increase in radius about the spiral) in order to increase the available radial space after the valve. It was found that the rotational frequency required to drain the spiral was too high for the additional radial space to be usable.

# Conclusions

A novel spiral configuration for liquid deposition to a single outlet on a CM device has been demonstrated. The design included an addition of Coriolis switch to select in which direction the liquid was directed. The effectiveness of OM on a CM device was also explored for creating a low RPM Coriolis switch. It was found that when the chamber had a height higher than 0.300 mm, the stream of liquid acted as if there was no ceiling. While at 0.200 mm in height, Coriolis drift was reduced due to the hydrophilic attraction of water to polycarbonate.

The easy integration of liquid deposition into single and multi-experiment disks may be useful in the design of complex experiments where storage of liquid reagents and wash solutions is not possible. Additionally, the use of open CM should be explored further as it greatly improves the ability to clean and reuse the device.

# References


1. Casavant, B. P.; Berthier, E.; Theberge, A. B.; Berthier, J.; Montanez-Sauri, S. I.; Bischel, L. L.; Brakke, K.; Hedman, C. J.; Bushman, W.; Keller, N. P.; Beebe, D. J., Suspended microfluidics. *Proceedings of the National Academy of Sciences of the United States of America* **2013,** *110* (25), 10111-10116.
2. Huang, C. J.; Ke, M. S.; Yang, J. T. In *A pneumatic open-surface microfluidic platform for droplet manipulation*, 2013; pp 313-316.
3. Khare, K.; Zhou, J.; Yang, S., Tunable open-channel microfluidics on soft poly(dimethylsiloxane) (PDMS) substrates with sinusoidal grooves. *Langmuir* **2009,** *25* (21), 12794-12799.
4. Andersson, P.; Jesson, G.; Soderman, T.; Sjoberg, J., **2003**.
5. Bouchard, A. P.; Duford, D. A.; Salin, E. D., Non-contact addition, metering, and distribution of liquids into centrifugal microfluidic devices in motion. *Analytical Chemistry* **2010,** *82* (20), 8386-8389.
6. Mark, D.; Weber, P.; Lutz, S.; Focke, M.; Zengerle, R.; Von Stetten, F., Aliquoting on the centrifugal microfluidic platform based on centrifugo-pneumatic valves. *Microfluidics and Nanofluidics* **2011,** *10* (6), 1279-1288.
7. Kong, M. C. R.; Salin, E. D., Pneumatic flow switching on centrifugal microfluidic platforms in motion. *Analytical Chemistry* **2011,** *83* (3), 1148-1151.
8. Haeberle, S.; Brenner, T.; Schlosser, H. P.; Zengerle, R.; Ducrée, J., Centrifugal micromixer. *Chemical Engineering and Technology* **2005,** *28* (5), 613-616.
9. Steigert, J.; Grumann, M.; Brenner, T.; Mittenbühler, K.; Nann, T.; Rühe, J.; Moser, I.; Haerberle, S.; Riegger, L.; Riegler, J.; Bessler, W.; Zengerle, R.; Ducrée, J., Integrated sample preparation, reaction, and detection on a high-frequency centrifugal microfluidic platform. *JALA - Journal of the Association for Laboratory Automation* **2005,** *10* (5), 331-341.
10. Kim, J.; Kido, H.; Rangel, R. H.; Madou, M. J., Passive flow switching valves on a centrifugal microfluidic platform. *Sensors and Actuators, B: Chemical* **2008,** *128* (2), 613-621.
11. En Lin, S. I., A novel splitter design for microfluidic biochips using centrifugal driving forces. *Microfluidics and Nanofluidics* **2010,** *9* (2-3), 523-532.
12. Lafleur, J. P.; Salin, E. D., Pre-concentration of trace metals on centrifugal microfluidic discs with direct determination by laser ablation inductively coupled plasma mass spectrometry. *Journal of Analytical Atomic Spectrometry* **2009,** *24* (11), 1511-1516.
13. Duford, D. A.; Peng, D. D.; Salin, E. D., Magnetically driven solid sample preparation for centrifugal microfluidic devices. *Analytical Chemistry* **2009,** *81* (11), 4581-4584.

# CHAPTER 6: Modular Microfluidics

The development of commercial applications in CM is complicated by the necessity of custom designed functions and operations to execute an analysis. The work of this chapter aimed to make the future implementation of the operations demonstrated in this thesis more simple and robust by demonstrating a method for designing and constructing modular CM devices.

## Contribution to Original Knowledge

Two methods of designing modular CM devices were developed. The first used a single experimental layer segmented into wedges for quick prototyping of multi-step experiments. The second used multiple layers where each was responsible for a single experimental step and could perform several iterations in parallel.

## Abstract

In order to develop increasingly complex Centrifugal Microfluidic (CM) experiments, two distinct methods for the construction of modular CM devices are demonstrated. The first of the modular methods consists of a single experimental layer that can be used for rapid prototyping and optimization. The single experimental layer is divided into wedges that each contains an experimental function. The wedges are connected by a pneumatic pumping step that reduces the normal centrifugal microfluidic constraints of a limited radius on the disk and the need for increasingly higher rotational frequencies to burst passive valves. The use of a single experimental layer is ideal for prototype work and demonstration of concepts. The experimental wedges are set upon a pumping layer dedicated to the pneumatic pumping of the reagent back to

the center of the device. The advantage of such a pumping layer is that the space in the experimental layer is not used for transferring reagent and is available for more sequential steps.

The second modular method uses the same pairing of experimental layers with pumping layers on a single CM device. However, rather than separate experimental steps into wedges in a single experimental layer, each experimental step is its own layer with a dedicated pumping layer below. Layered modules have alternating experimental and pumping layers that are stacked in order to link the sequential functions. The dedication of only one experimental step to each experimental layer allows multi-step experiments to be constructed without using more space on the disk. By extending the sequential steps into another layer many replicates of the same experiment could be conducted simultaneously.

By demonstrating the use of multiple functional layers in a CM device, this chapter provides the ability to increase the complexity of CM devices and show that designs should not be limited by the radius of the device, rotational frequency or the ability to have higher burst frequency valves.

# Introduction

In 2007, Fair described the development of microfluidics as the combination of individual components and design themes that can be combined into operations which act in series or in parallel to accomplish complex functions and tasks.[1] These multi-step experiments required custom design and construction to integrate multiple components. This has led to interest in the development of connection methods to assemble multiple modules into a single experimental setup. Modular components have been shown to be effective in microfluidics, but have had limited application due to the amount of connections required and a lack of standardization.

In 2003, Grodizinski developed a modular microfluidic setup for cell pre-concentration to use for genetic sample preparation.[2] Grodizinski used layers of microfluidic components connected by tubes and o-rings in order to transport the reagents and sample. The use of tubing and o-ring connections was a hindrance in the ability to design more complex systems.

Shaikh developed a modular microfluidic infrastructure in 2005 for the building of biochemical analysis methodologies.[3] This design used an oxidized silicon wafer as a substrate for the attachment of functional components. Later, in 2008, Rhee constructed PDMS microfluidic assembly blocks which were designed to be fixed on a glass slide to design more complex analytical tasks.[4] The design was made more robust by Langelier in 2011 with the introduction of dovetails to the modules for better construction.[5]

In a different method, Yeun published two papers on modular microfluidic systems. The first was in 2008 where the design was termed SmartBuild and is similar to an electronic breadboard where components are designed to be 'plug and play.'[6] The next year, Yeun published an expansion to SmartBuild where multi-dimensional flow was added to the functionality of the modular system.[7] In 2011, Liou published a paper describing modular components for portable microfluidic devices which included pumping, valving, reaction chambers and mixing.[8]

The concept of constructing CM devices with modules was improved by the implementation of three dimensional design and construction of the device. The use of multiple layers of the device took advantage of the ability to segregate operations of the device in order to organize and accomplish the analytical process. An example of layered implementation was produced by Thio in 2013, who used a dedicated layer in the CM device to house a pumping operation.[9] The pump was themo-pneumatic that generated air pressure by convection heating of

trapped air. The trapped air then moved liquid against centrifugal force towards the center of the device. Thio's design did not have liquid traveling in the additional layer of the device, but instead used the layers to separate the heating elements and heated CM operation from the experimental layer with reagent.

This chapter demonstrates the two modular construction designs for CM devices. The modular experimental components were separated by either (1) rotation around the axis of the device into wedges or (2) layers that were each dedicated to a single experimental operation. The designs relied on a pneumatic pump to move liquid from the edge of a device to the center using a technique that was published by Kong in 2010.[10] The pneumatic pumping method made it possible to transport liquid to the next module without complex designs inside of the disk.[11] Both designs utilized dedicated pumping layers for the handling and transport of samples from one operation to the next. Segregating the liquid transport components gave experimental components access to more real-estate on the device.[12]

# Experimental

## Fabrication of CM Device

Two test disks were fabricated using materials and techniques previously described by Lafleur and Salin in 2009.[13] The methodology was discussed in detail in the *Experimental: Fabrication of Centrifugal Device* section of Chapter 2 in this thesis (Chapter 2, page 8). The features and important dimensions of the design are highlighted in Figure 6-1. The features of the wedge and layered disks are the same; however, the layers in which the features were cut differ.

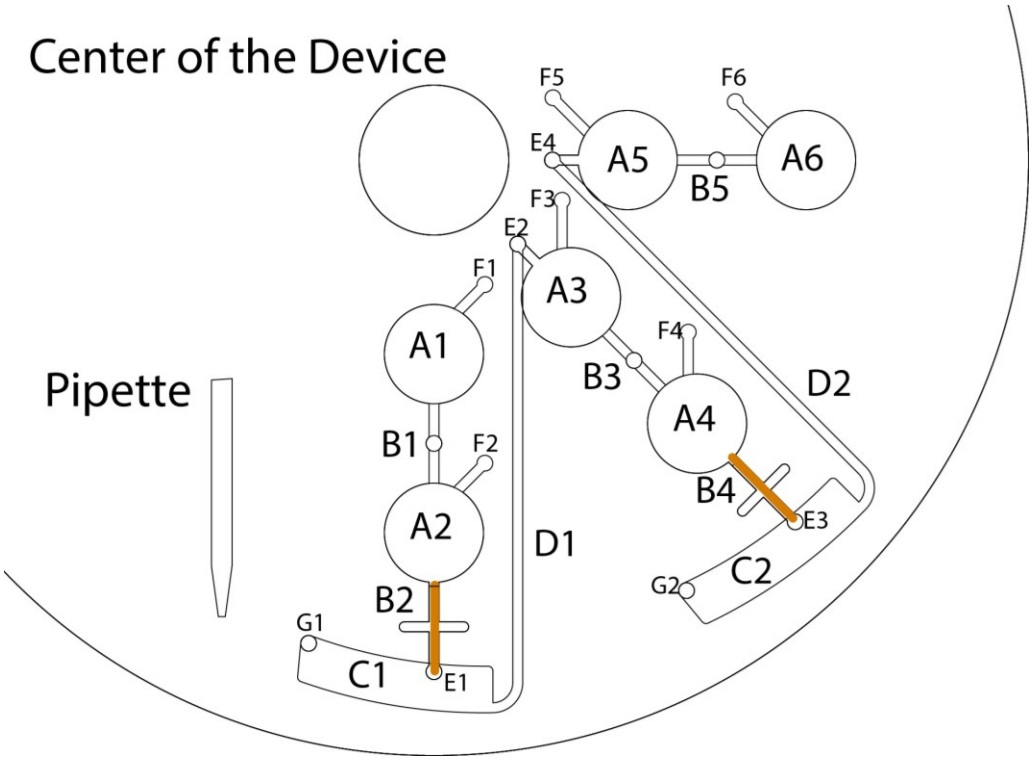


**Figure 6-1. Structure labels for demonstrative design of a modular CM device**
The demonstrations used six reaction chambers where the liquid of interest would flow through each chamber in series. These reaction chambers are placeholders for any CM operations used in a CM μTAS. The components are labeled: (A) experimental chambers, (B) passive valve, (C) pumping chamber, (D) pumping channel, (E) transfer hole, (F) vent hole, (G) pneumatic pumping vent hole.

The difference in construction is shown in Figure 6-2 where it can be seen how each of the functions are present in different layers depending on whether the device is wedged or layered. Figure 6-2A and Figure 6-2B are the experimental and pumping layer of the wedge based modular CM device. All of the operations to modify the sample occur in a single experimental layer that sits upon a pumping layer. The remaining drawings of Figure 6-2 show how each operation in sequence, including pumping of the sample, is maintained in a separate layer of the CM device.

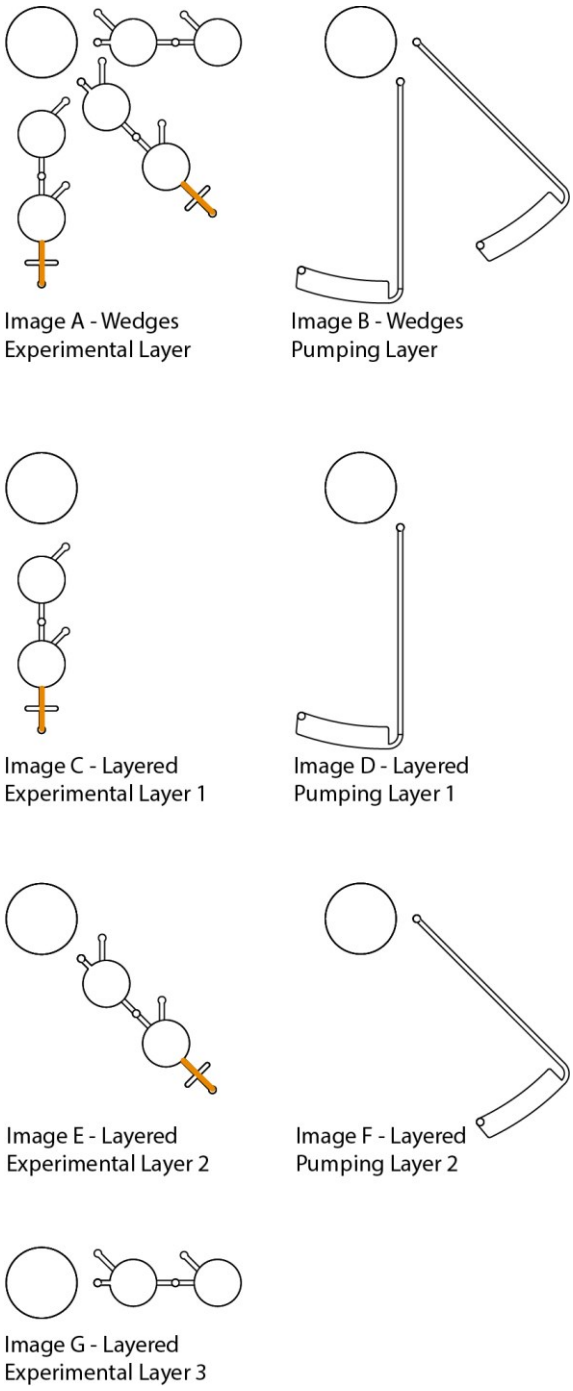


**Figure 6-2. Layout of experiment and pumping layers in the two modular devices**
Two devices were constructed by aligning and assembling previously cut layers in the same manner as previously described. (Chapter 2, page 8) Layers of polycarbonate DVDs 0.6 mm thick were cold laminated with double sided pressure sensitive adhesives 0.102 mm thick to construct the devices. The lowest layer of the device was a polycarbonate CD 1.2 mm thick. In Images A and B, the Wedge Module design is shown. Image A is the Experimental Layer with three wedges. Image B is the Pumping Layer with two pneumatic pumps. These were stacked vertically and made a single device. In Images C through G, the experimental layers and pumping layers were alternately stacked to create a single device.

### Setup and Data Acquisition

The spinner and strobe setup described by Duford in 2009[14] was supplemented with a color digital camera (GRAS-14S5C-C, Point Gray, BC, Canada). The system was synchronized from a single computer through LabVIEW software (LabVIEW 8.6, Developer Version, National instruments, QC, Canada). The full setup, including an example of a CM device on the motor spindle, can be seen in Chapter 4, Figure 4-8. (Chapter 4, page 13)

## Results and Discussion

By using reagent movement to demonstrate a novel layered construction, the functionality of two modular designs has been shown. The first was a wedge design comprised of an experimental layer and a pumping layer to move reagent to the center of a device. The second used multiple alternating layers of experimental and pumping layers.

The experimental images of the wedge modules and layered modules show the same design for demonstrative purposes. The design consists of multiple reaction chambers separated by passive valves and pneumatic pumping. The outcome of the design is the demonstration of controlling a reagent's movement through six reaction chambers.

The power of the modules is the ability to continuously add more experimental components thereby allowing more complex and multi-step experiments. The ability to prototype CM devices is traditionally hampered by a lack of radial space in order to fit additional experimental steps and the need to increase rotational frequency after each step to burst the next passive valve controlling the liquid flow. By separating sets of experimental chambers by a pneumatic pumping step the radial space does not limit the design of the experiment. The secondary effect of pneumatic pumping is the reduction in required rotational frequency.

In the experiments demonstrated in this chapter, each experimental wedge or layer was comprised of two experimental chambers. The reagent would flow through each chamber before it was pumped back to the center of the device. An illustration of the experiments is shown in Figure 6-3 with the description and rotational frequencies in Table 6-1. The images of the wedge and layered versions of the design appear the same when imaged from above for demonstrative purposes and can be seen in Figures 6-4 and Figure 6-5 respectively.

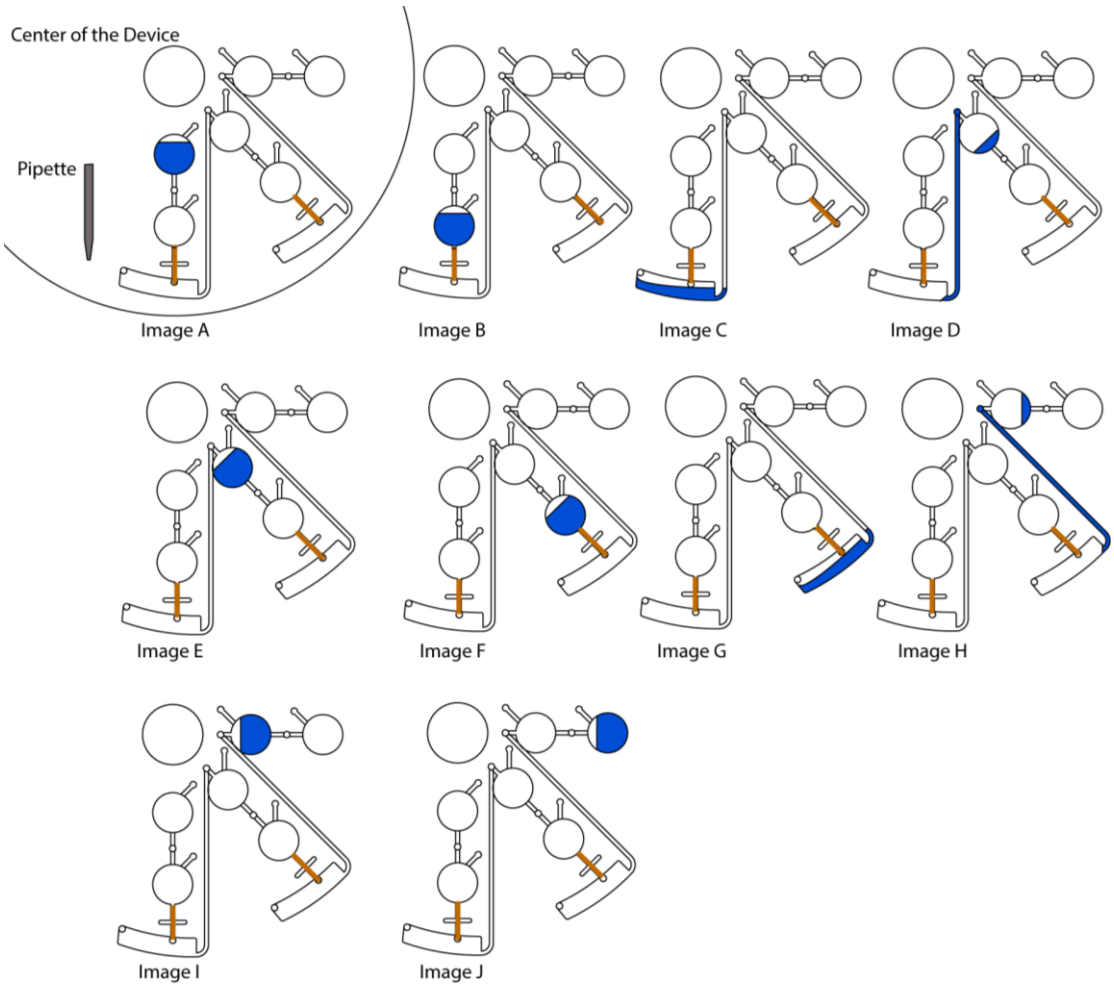


**Figure 6-3. Ideal images of the modular demonstrations**
The labeling of the chambers, valves and channels are provided in Figure 6-1. The descriptions of the rotation frequencies and location of the reagents are found in Table 6-1. The labeling of images in this figure and in subsequent experimental figures is consistent with each other and with the labels of Figure 6-1. The liquid of interest is shown passing through the six reaction chambers and the two pumping operations to demonstrate a flow path where CM operations can be installed.

The ideal illustration of the liquid movement in Figure 6-3 does not account for the volume of liquid that does not successfully transfer from the pumping chamber into the experimental layer and the next reaction chamber. The small volume that the pneumatic pumping does not move can be seen in Image J of Figures 6-4 and 6-5.

| | | | Liquid Location | |
|---|---|---|---|---|
| **Step** | **RPM** | **Image** | **Wedge Modules (Fig 4)** | **Layered Modules (Fig 5)** |
| Loaded reagent | **400** | **A** | Experimental layer<br>First Reaction Chamber | First Experimental layer<br>First Reaction Chamber |
| Burst first valve | **750** | **B** | Experimental layer<br>Second Reaction Chamber | First Experimental layer<br>Second Reaction Chamber |
| Burst second valve | **2800** | **C** | Pumping Layer<br>First Pumping Chamber | First Pumping Layer<br>First Pumping Chamber |
| First pumping | **300** | **D** | Pumping Layer<br>First Pumping Chamber and Channel | First Pumping Layer<br>First Pumping Chamber and Channel |
| Post first pumping | **300** | **E** | Experimental Layer<br>Third Reaction Chamber | Second Experimental Layer<br>Third Reaction Chamber |
| Burst third valve | **750** | **F** | Experimental Layer<br>Fourth Reaction Chamber | Second Experimental Layer<br>Fourth Reaction Chamber |
| Burst fourth valve | **2800** | **G** | Pumping Layer<br>Second Pumping Chamber | Second Pumping Layer<br>Second Pumping Chamber |
| Second pumping | **300** | **H** | Pumping Layer<br>Second Pumping Chamber and Channel | Second Pumping Layer<br>Second Pumping Chamber and Channel |
| Post second pumping | **300** | **I** | Experimental Layer<br>Fifth Reaction Chamber<br>(no image) | Third Experimental Layer<br>Fifth Reaction Chamber |
| Burst fifth valve | **750** | **J** | Experimental Layer<br>Sixth Reaction Chamber | Third Experimental Layer<br>Sixth Reaction Chamber |

**Table 6-1. Description of modular images shown in cartoon Figure 6-3 and Experimental images Figures 6-4 and 6-5**

The same design was utilized to demonstrate the application of wedges and layers to an experiment. The top-down view of the liquid movement looks the same as observed in the illustration of Figure 6-3 and the experimental images of Figures 6-4 and 6-5. This table outlines the rotational frequencies applied to the CM device in each image with the labeling consistent across all three figures. One note is that the frequency does not change between images D-E and H-I. In images D and H the liquid was being pneumatically pumped at a low rotational frequency into the third and fifth reaction chambers respectively. The valve from the third reaction chamber burst at a higher rotational frequency, therefore the frequency was not immediately increased when the liquid reached the third reaction chamber.

The application of the rotation frequencies outlined in Table 6-1 can be seen in the experimental images of the wedge module device in Figure 6-4.

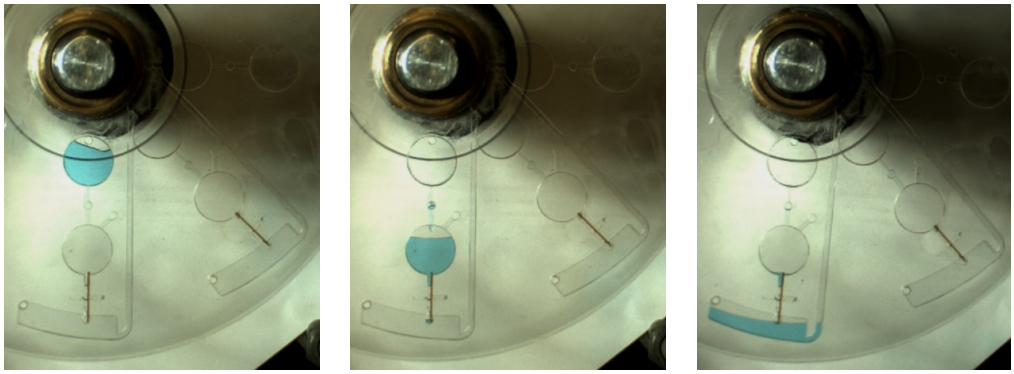

A B C

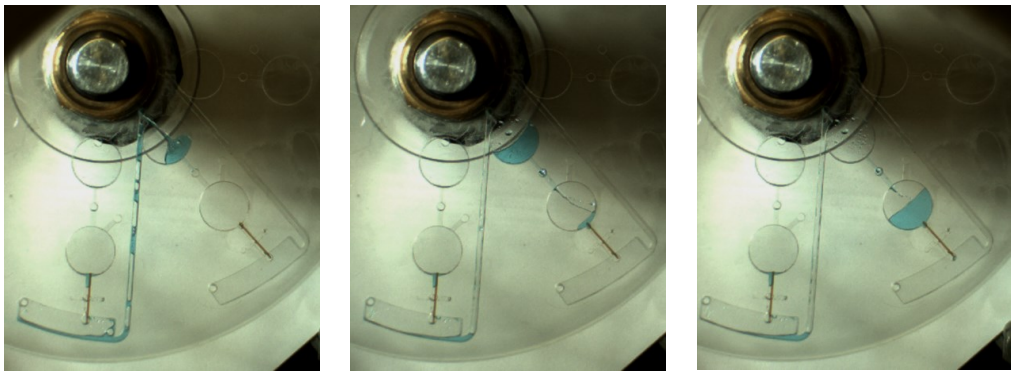

D E F

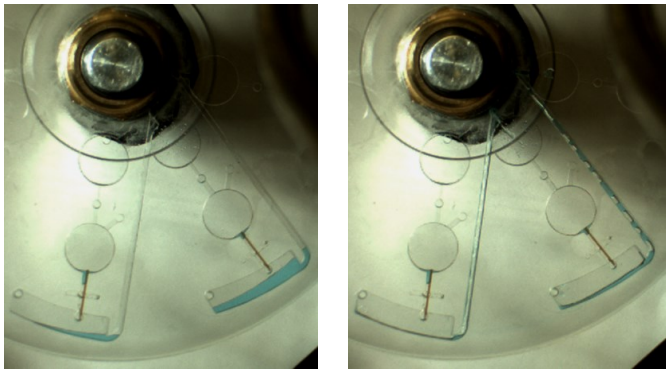

G H (no image) I

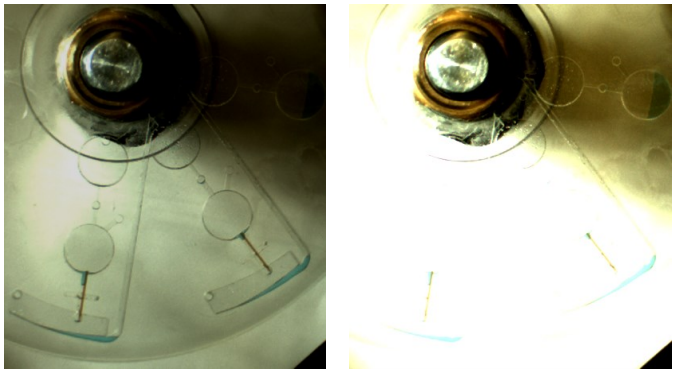

J1 (Same image as J2) J2 (same image as J1)

**Figure 6-4. Experimental images of wedge based modular device**
The details of liquid location and rotational frequencies can be found described in Table 6-1 and in the text immediately following this caption. Image J is provided twice as J1 and J2 with different brightness and contrast settings to make the liquid in the sixth reaction chamber more visible.

Figure 6-4 presented the wedge based modular experiment. In the experiment 55 μL of DDW with blue dye was loaded into the first chamber in the experimental layer. The device was spun at 400 RPM to obtain Image A of the reagent in the first reaction chamber. The first valve was burst at 750 RPM to move the reagent into the second reaction chamber (Image B).

The second valve was burst and drained at 2800 RPM to move the reagent out of the experimental layer and into the pumping layer and the first pumping chamber (Image C).

The device was spun at 300 RPM for pneumatic pumping to the third reaction chamber. Pneumatic flow of 0.5 SCFM of dry compressed air was used to move the liquid through the first pumping channel and back to the experimental layer (Images D and E).

The third valve was burst at 750 RPM to move the reagent to the fourth reaction chamber (Image F). The fourth valve was burst at 2800 RPM to move the reagent out of the experimental layer into the pumping layer and the second pumping chamber (Image G).

The device was spun at 300 RPM for pneumatic pumping to the fifth reaction chamber. Pneumatic flow of 0.5 SCFM of dry compressed air was used to move the liquid through the second pumping channel and back to the experimental layer for the second time (Image H).

The fifth valve was burst at 750 RPM to move the reagent to the sixth and final reaction chamber (Image J).

The same experimental steps are demonstrated in Figure 6-5. The description that follows is specific to the layered module device and differs from the Figure 6-4 because of the additional experimental and pumping layers.

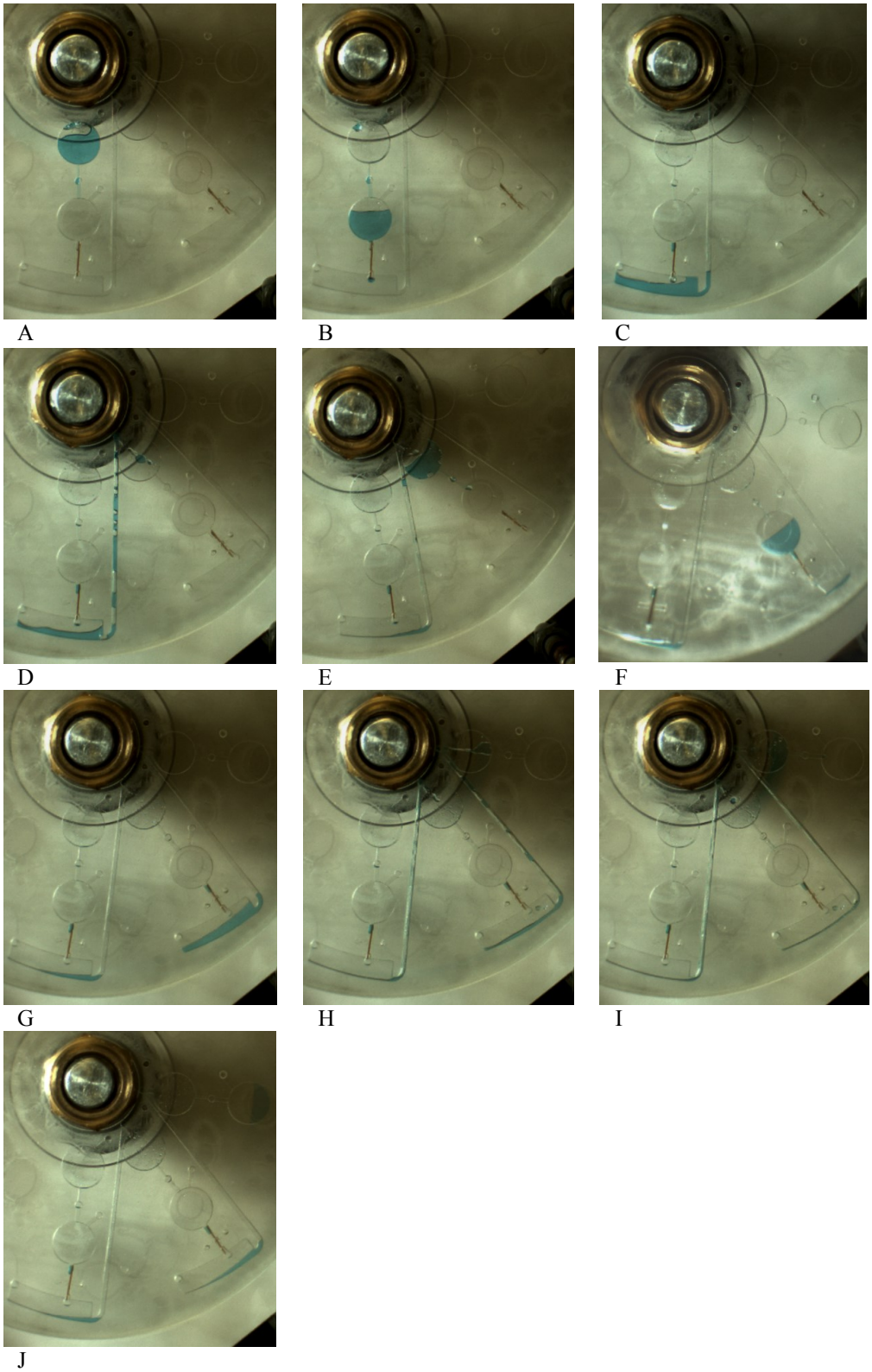


**Figure 6-5. Experimental images of layer based modular device**
The details of liquid location and rotational frequencies can be found described in Table 6-1 and the in text immediately following this caption. While the images presented seem very similar to the images of Figure 6-4, they are the demonstration of the same modular experiment constructed in two different manners.

Figure 6-5 presented the layer based modular device. In the experiment 55 μL of DDW with blue dye was loaded into the first chamber in the first experimental layer. The device was spun at 400 RPM to get images of the reagent in the first reaction chamber in the first experimental layer (Image A). The first valve of the first experimental layer was burst at 750 RPM to move the reagent into the second reaction chamber of the first experimental layer (Image B). Subsequently, the second valve of the first experimental layer was burst and drained at 2800 RPM to move the reagent out of the first experimental layer and into the first pumping layer and the first pumping chamber (Image C).

The device was spun at 300 RPM for pneumatic pumping of reagent from the first pumping chamber through the first pumping channel to the third reaction chamber of the second experimental layer. Pneumatic flow of 0.5 SCFM of dry compressed air was used to move the liquid through the first pumping channel and into the second experimental layer (Images D and E). The third valve of the second experimental layer was burst at 750 RPM to move the reagent to the fourth reaction chamber of the second experimental layer (Image F). Next, the fourth valve of the experimental layer was burst at 2800 RPM to move the reagent out of the second experimental layer and into the second pumping layer and the second pumping chamber (Image G).

The device was spun at 300 RPM for pneumatic pumping from the second pumping layer to the fifth reaction chamber of the third experimental layer. Pneumatic flow of 0.5 SCFM of dry compressed air was used to move the liquid through the second pumping channel and into the third experimental layer (Images H and I). The fifth valve of the third experimental layer was burst at 750 RPM to move the reagent to the sixth and final reaction chamber in the third experimental layer (Image J).

Two important discussions of the success of this demonstrative design have to be addressed. The first discussion is the application of flow into different experimental layers. In Chapter 4, a 3D valve was discussed but it was composed of adhesives surrounding the experimental layer. In the design of modular experiments, the transfer of liquid between experimental layers and pumping layers was demonstrated. This approach is a deviation from the standard design and construction of microfluidic devices. The ability to add more layers will greatly expand the possibilities of microfluidic development. The second discussion is the extension of experimental steps without requiring increasing rotational frequencies. When the reagent is pneumatically pumped to the center of the device and to a new set of experimental chambers the rotational frequency of the device is lowered and then passive valves can again restrict the flow. In a traditional CM device, the addition of more experimental chambers requires higher RPM in order to burst the next passive valve in the series. Separating experimental steps with pneumatic pumping made it possible for the three adhesive valves to be of the same construction and utilize the same burst frequency. The same is true for the construction of the two glass capillary valves which increases the potential for standardization in CM design.

# Conclusions

Two methods for the construction of modular CM devices have been demonstrated. The first was a single experimental layer that can be used to make prototypes for the optimization of complex experiments. The single experimental layer is ideal for prototype work and demonstration of concepts especially if paired with a mass production technique to generate standardized functions designed to be mounted onto an unchanging pumping layer.

The second method involved an expansion of the first concept into multiple experimental layers with each layer only containing one operation of the CM device. Layered modules have alternating experimental and pumping layers than can be stacked to link the sequential functions. By extending the sequential steps into another layer, many replicates of the same experiment could be conducted simultaneously.

By demonstrating a design concept where experimental steps can be compartmentalized into modules, it is possible to move CM in the direction of mass manufacturing of standard functions. The production of standard functions will reduce the cost of production and increase the ability of researchers to develop new methodologies. Greater access with increased development of enhanced CM designs will increase the ability to apply CM to industrial and academic needs.

# References:


1. Fair, R. B., Digital microfluidics: Is a true lab-on-a-chip possible? Microfluidics and Nanofluidics 2007, 3 (3), 245-281.
2. Grodzinski, P.; Yang, J.; Liu, R. H.; Ward, M. D., A modular microfluidic system for cell pre-concentration and genetic sample preparation. Biomedical Microdevices 2003, 5 (4), 303-310.
3. Shaikh, K. A.; Ryu, K. S.; Goluch, E. D.; Nam, J. M.; Liu, J.; Thaxton, C. S.; Chiesl, T. N.; Barron, A. E.; Lu, Y.; Mirkin, C. A.; Liu, C., A modular microfluidic architecture for integrated biochemical analysis. Proceedings of the National Academy of Sciences of the United States of America 2005, 102 (28), 9745-9750.
4. Rhee, M.; Burns, M. A., Microfluidic assembly blocks. Lab on a Chip - Miniaturisation for Chemistry and Biology 2008, 8 (8), 1365-1373.
5. Langelier, S. M.; Livak-Dahl, E.; Manzo, A. J.; Johnson, B. N.; Walter, N. G.; Burns, M. A., Flexible casting of modular self-aligning microfluidic assembly blocks. Lab on a Chip 2011, 11 (9), 1679-1687.
6. Yuen, P. K., SmartBuild - A truly plug-n-play modular microfluidic system. Lab on a Chip - Miniaturisation for Chemistry and Biology 2008, 8 (8), 1374-1378.
7. Yuen, P. K.; Bliss, J. T.; Thompson, C. C.; Peterson, R. C., Multidimensional modular microfluidic system. Lab on a Chip - Miniaturisation for Chemistry and Biology 2009, 9 (22), 3303-3305.
8. Liou, D. S.; Hsieh, Y. F.; Kuo, L. S.; Yang, C. T.; Chen, P. H., Modular component design for portable microfluidic devices. Microfluidics and Nanofluidics 2011, 10 (2), 465-474.
9. Thio, T. H.; Ibrahim, F.; Al-Faqheri, W.; Soin, N.; Abdul Kahar, M. K.; Madou, M., Multi-level 3D implementation of thermo-pneumatic pumping on centrifugal microfluidic CD platforms. Conference proceedings : ... Annual International Conference of the IEEE Engineering in Medicine and Biology Society. IEEE Engineering in Medicine and Biology Society. Annual Conference 2013, 2013, 5513-5516.
10. Kong, M. C. R.; Salin, E. D., Pneumatically pumping fluids radially inward on centrifugal microfluidic platforms in motion. Analytical Chemistry 2010, 82 (19), 8039-8041.
11. Kong, M. C. R.; Bouchard, A. P.; Salin, E. D., Displacement pumping of liquids radially inward on centrifugal microfluidic platforms in motion. Micromachines 2012, 3 (1), 1-9.
12. Thio, T. H. G.; Ibrahim, F.; Al-Faqheri, W.; Moebius, J.; Khalid, N. S.; Soin, N.; Kahar, M. K. B. A.; Madou, M., Push pull microfluidics on a multi-level 3D CD. Lab on a Chip - Miniaturisation for Chemistry and Biology 2013, 13 (16), 3199-3209.
13. Lafleur, J. P.; Salin, E. D., Pre-concentration of trace metals on centrifugal microfluidic discs with direct determination by laser ablation inductively coupled plasma mass spectrometry. Journal of Analytical Atomic Spectrometry 2009, 24 (11), 1511-1516.
14. Duford, D. A.; Peng, D. D.; Salin, E. D., Magnetically driven solid sample preparation for centrifugal microfluidic devices. Analytical Chemistry 2009, 81 (11), 4581-4584.

# CHAPTER 7: Conclusions

This thesis developed new centrifugal microfluidic (CM) functions. Novel designs for spectroscopy, aliquots, valves, deposition and modules have been designed, tested and presented here. The new contributions to the field of CM will allow further development of increasingly complex and robust analytical instrumentation in the future.

## Summary of Thesis Work

### Thesis Objectives

This thesis demonstrated new design concepts that expanded the potential for CM in experimental procedures and overcame limitations native to small volumes in CM. The work presented extended the range of capabilities for microfluidic analysis and focused primarily on components that enhance CM and that did not require stopping the disk. The results contribute to the creation of CM functions by providing new components and operations and demonstrating new design and construction techniques.

There are very few limitations in CM that cannot be solved by stopping the disk and treating it like a traditional microfluidic device, but at that point many advantages of CM are lost. By overcoming these limitations CM devices have the ability to accurately perform complex experiments with all the advantages of CM intact.

## Thesis Conclusions

**Chapter 2** demonstrated a synchronized spectrometer that took full visible light spectra from cells on a CM device in motion. The system's relative standard deviation for raw intensities was calculated to be ~ 0.5%. Accuracy was demonstrated using a ratiometric calculation of

absorbance to create a six point (n = 4) linear calibration curve ($R^2$ greater than 0.999) for a serially diluted solution of yellow dye. Additionally, the system was used for the determination of the extinction coefficient and limit of detection of bromothymol blue at 466 nm. The device was used again in Chapter 3 for the quantification of small aliquot additions.

The modular components of the setup are capable of supplementing servo motor CM platforms to perform real-time data collection. This enables quantitative full spectrum measurements to be taken at intermediate steps while continuously applying centrifugal force. The application can be used for the measurement of titrations, elutions and sedimentations. While stopping a disk to take spectra will always be available as an option in CM experiments, the use in small aliquots and sedimentation highlighted the importance of the ability to collect real time data with the constant application of centrifugal force.

**Chapter 3** demonstrated the design of a CM configuration that performed the addition of small aliquots to an experimental chamber by adjusting the rotational frequency of the device. Multiple aliquots were generated by cycling through a pattern of higher and lower rotational frequencies. The accuracy of the volume was verified by spectroscopic measurements taken with the synchronized spectrometer of Chapter 2. It was found that the configuration produced aliquots of 750 nL +/- 170 nL without ceasing rotation. The addition of small aliquots to the toolbox of potential functions in CM designs will allow for the creation of more complex quantitative measurements while continuously applying centrifugal force. Additionally, the integration of compressed air chambers in CM will greatly impact the design of experiments as control over the movement of reagent towards the center of the device is made without external additions to the setup.

**Chapter 4** presented a new configuration of passive adhesive valves in CM devices that had the liquid traveling in a third dimension perpendicular (axial) to the plane of the disk. The change in design significantly affected the magnitude and accuracy of burst frequency predictions. Without the 3D component, valves calculated to burst at 630 RPM would burst at 290 RPM; while, with the 3D component valves calculated to burst at 660 would burst at 650 RPM. The improvement in accuracy allowed the design and construction of modules with multiple valves in Chapter 6.

When paired with a compression valve, the burst frequency of the same 3D valve at the same radius was raised to 1540 RPM.

**Chapter 5** considered the use of open microfluidics (OM) and Coriolis drift to implement a Coriolis switch. It was found that OM did have larger Coriolis drift than low height chambers. It also found that in chambers with a height larger than 0.300 mm the CM device behave as if it is an OM chamber.

The Coriolis switch was paired with a novel spiral liquid addition design that took liquid being added to the device and channeled it to only one outlet. The Coriolis switch was used to drain wash fluid to waste and the design facilitated metering the reagent of interest.

The easy integration of liquid deposition into single and multi-experiment devices will be essential in the design of complex experiments where storage of liquid reagents and wash solutions is not possible.

**Chapter 6** demonstrated two designs for the construction of modular CM devices. The first was a single experimental layer that can be used for the optimization of complex experiments. This is ideal for prototype work and demonstration of concepts.

The second design was an expansion of the first concept into multiple experimental layers with each layer only containing one operation of the CM device. Layered modules have alternating experimental and pumping layers than can be stacked to link the sequential functions. This allowed multi-step experiments to be constructed without competing for real-estate with parallel replicates. By extending the sequential steps into another layer many replicates of the same experiment could be conducted simultaneously.

## Future Directions

Three segments of CM should be pursued following the work of this thesis. Open Microfluidics, reusable devices and real-time feedback. The complete integration of these three segments into common CM designs would greatly improve the opportunities for application to high throughput and commercial endeavors.

Open Microfluidics was discussed in Chapter 5. OM was explored to be used as one function in a series of three. First, there would be liquid deposition, then an open Coriolis switch and then a metering chamber. The device would be closed-open-closed. It is proposed that a true OM device would have no closed segments. This OM device would have many benefits. It is envisioned that CM devices that use geometric restrictions rather than chemical treatments to control the liquid flow would create a chemically inert substrate for a wide range of experiments. The configurations would be tuned for the surface properties of the samples and not require the addition of more materials. By having the device be OM the requirement of sealing the device is no longer needed. It can be pressed, milled or lithographed and then used immediately. After use it can be easily cleaned and reused.

Reusable devices would drive the cost of development down. In many instances, the early experiments presented in this thesis were used on devices that were reused. After drying a

component it would be reset and tested again. In the early stages when volumes, rotational frequencies and duration of the experiment were still being empirically determined, the need to build dozens of the same device became unwieldy and impractical. Components that can be reused will positively affect the ability to develop new concepts and test the limitations of the design. The ability to clean and reuse devices will be easy when implementing OM as there will be no closed channels and chambers for used reagent to become stuck. Furthermore, the ability to reuse individual components is a possibility through the application of modular CM devices as described in Chapter 6. Expensive experimental wedges or layers that contain difficult to manufacture designs or integrated on-chip components can be reused while mass produced wedges and layers can be replaced.

The development of real-time feedback will also greatly improve the functionality of CM devices. Currently, a complete experiment is conceived and then designed, cut, assembled and tested without the ability to adjust parameters as circumstances dictate. The strongest example is the small aliquots of Chapter 3. The rotational frequencies were empirically derived over multiple devices with many replicates. The servo motor was controlled by a program that needed to have the full experiment outlined. As soon as the experiment begins the process must continue to completion. By not having the ability to receive real-time feedback that could then be used to change the parameters, many replicates were wasted. Feedback could be used automatically by programming for expected outcomes or manually by the experimenter. Programmable outcomes could include balancing pH before the next step in an experiment, or determining if a wash solution has completely removed the previous reagent.

It is imagined that future CM devices would be open, reusable and tunable in real-time. The functions described in this thesis will hopefully aid in the development of those devices and provide some design concepts on which to base future work.

# Appendix 1 – Presentation of MATLAB processing for data from synchronized spectroscopy

The MATLAB graphical user interface (GUI) presented here was used to process the data generated when using the synchronized spectrometer of Chapter 2. Appendix 1 demonstrates the program GUI. Appendix 2 is the code of the GUI and the functions that it called. The code was written by the author (Bouchard), with help in optimization by Alexei Kazarine.

The USB4000 of the synchronized spectrometer saved data from an experiment as a single .txt file. The text file structure is shown in Table A1-1.

| Wavelength | Time Stamp 1 | Time Stamp 2 | … | Time Stamp 11 |
|---|---|---|---|---|
| 178.01 | Intensity | Intensity | … | Intensity |
| 178.23 | Intensity | Intensity | … | Intensity |
| 178.45 | Intensity | Intensity | … | Intensity |
| 178.67 | Intensity | Intensity | … | Intensity |

**Table A1-1. Structure of a .txt file saved by the synchronized spectrometer.**

The GUI is run using MATLAB and the interface is shown in Figure A1-1.

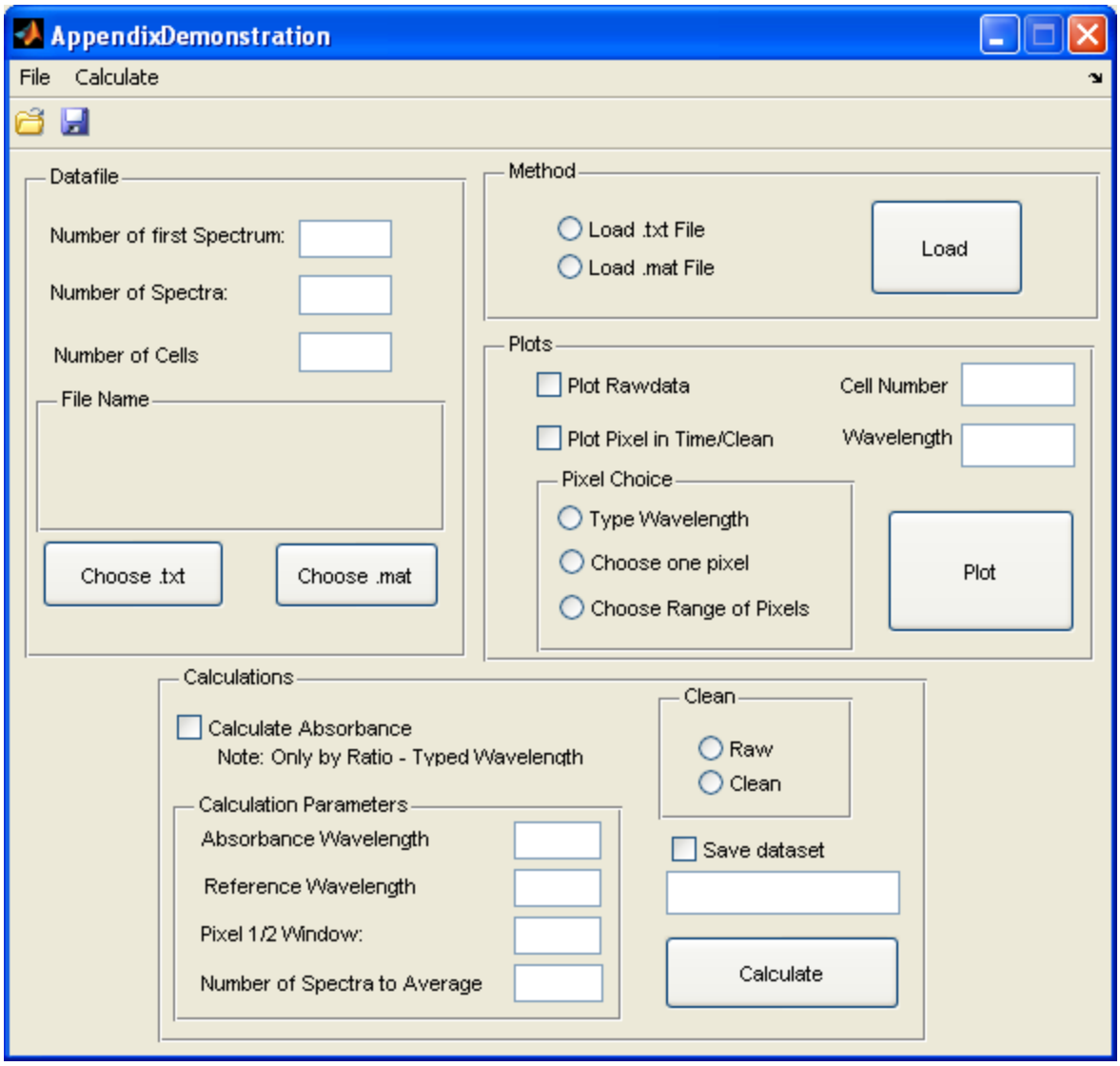


**Figure A1-1. GUI Interface**

The box labeled "Data file" is where the details outlining the .txt file were input and the file selected. "Number of first Spectrum" was the column of the text file the program began reading. "Number of Spectra" was how many columns there are in the .txt file to read into the MATLAB workspace. "Number of Cells" was how many spectroscopic cells were simultaneously measured in the text file.

The box labeled "Method" determined whether the file to be loaded is a text file from the spectrometer, or a .mat file saved from a previous run of this GUI. When spoiled spectra are

removed an amended dataset is saved in the workspace as a .mat file. This .mat could be loaded using the same method as the .txt file.

An example of loading a .txt file has been shown in Figure A1-2. The information would be filled in the text boxes and then "Choose .txt" would be clicked. This allowed the browsing of files for the correct text file. Then the "Load" button in the "Method" box was clicked. At this point the data of the text file is saved in the workspace of MATLAB.

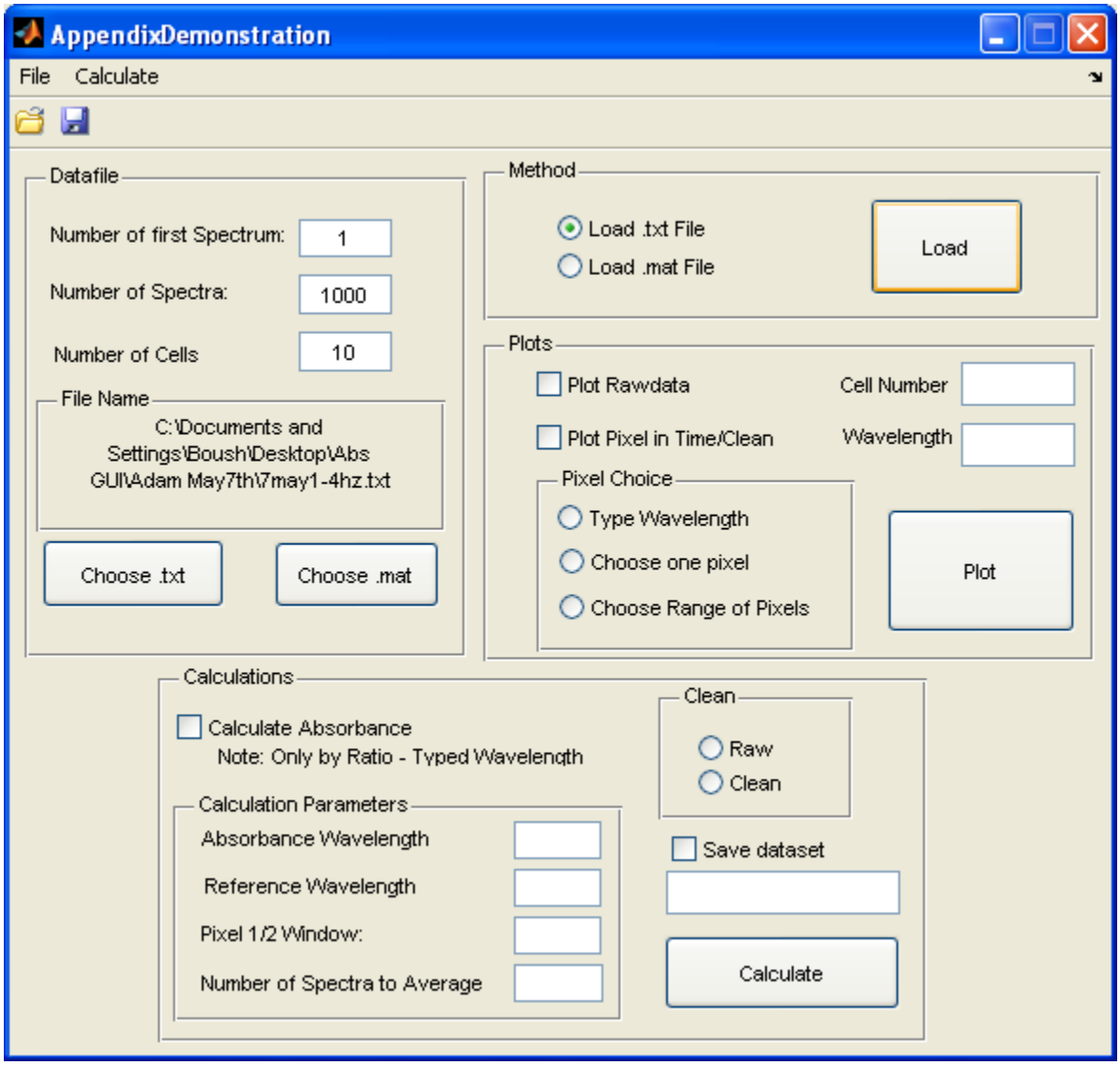


**Figure A1-2. Selecting and loading .txt file**

The file was stored in the workspace as a cell array. This array can then be parsed and used for plotting or for calculating absorbance. As shown in A1-2, there were 10 cells of data in the text file. When using the plotting function in the "Plots" box, the "Cell Number" selected for which cell's data will be plotted. In Figure A1-3, cell number 7 was selected to plot, by checking "Plot Rawdata" and clicking the "Plot" button.

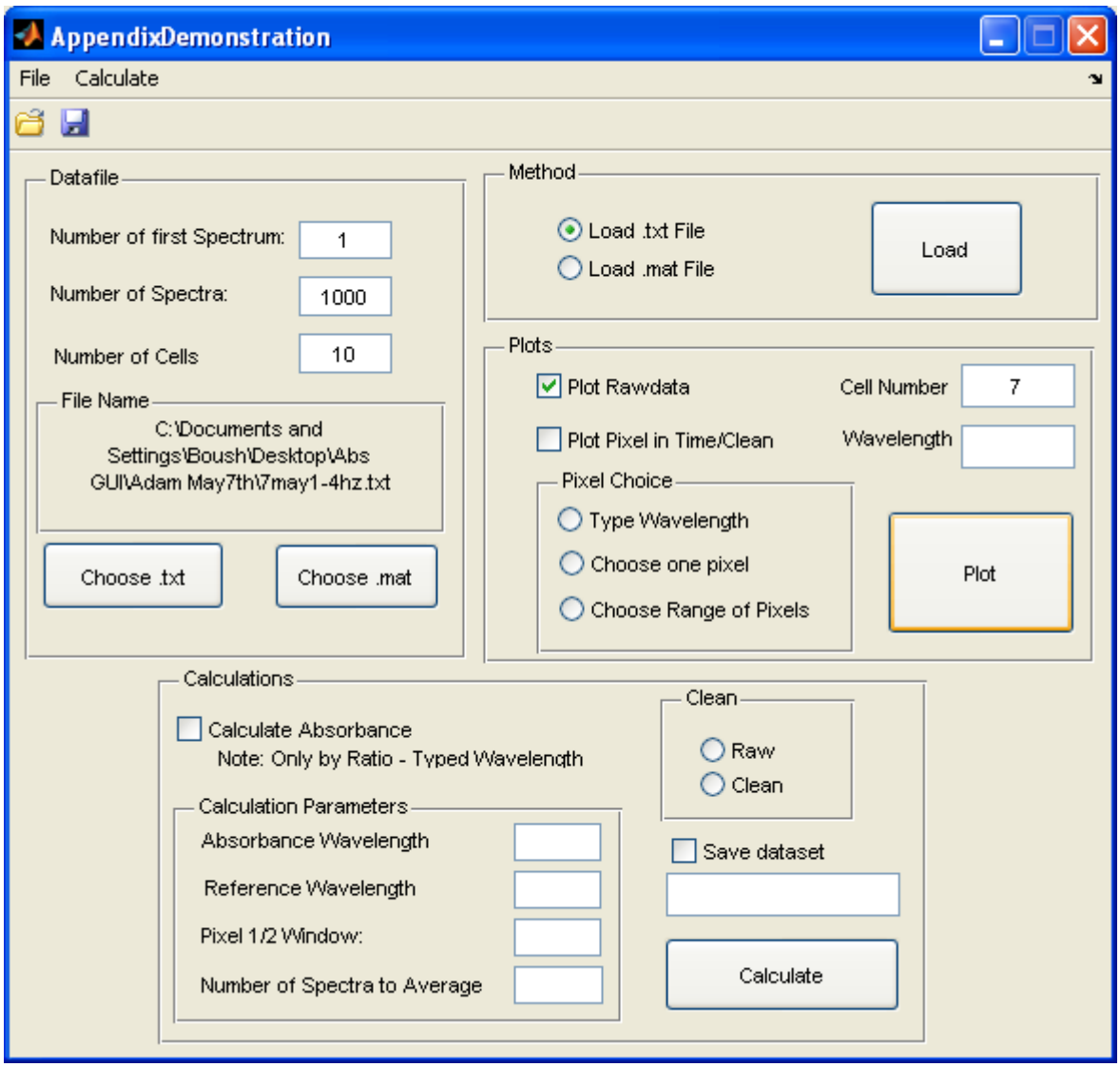


**Figure A1-3. Plotting the raw data of cell number 7**

The figure that is generated by the input of Figure A1-3 is shown in Figure A1-4 with the wavelength on the x-axis and the intensity in counts on the y-axis. The title is listed as the file location. As described in Chapter 2, there are spoiled spectra that must be removed.

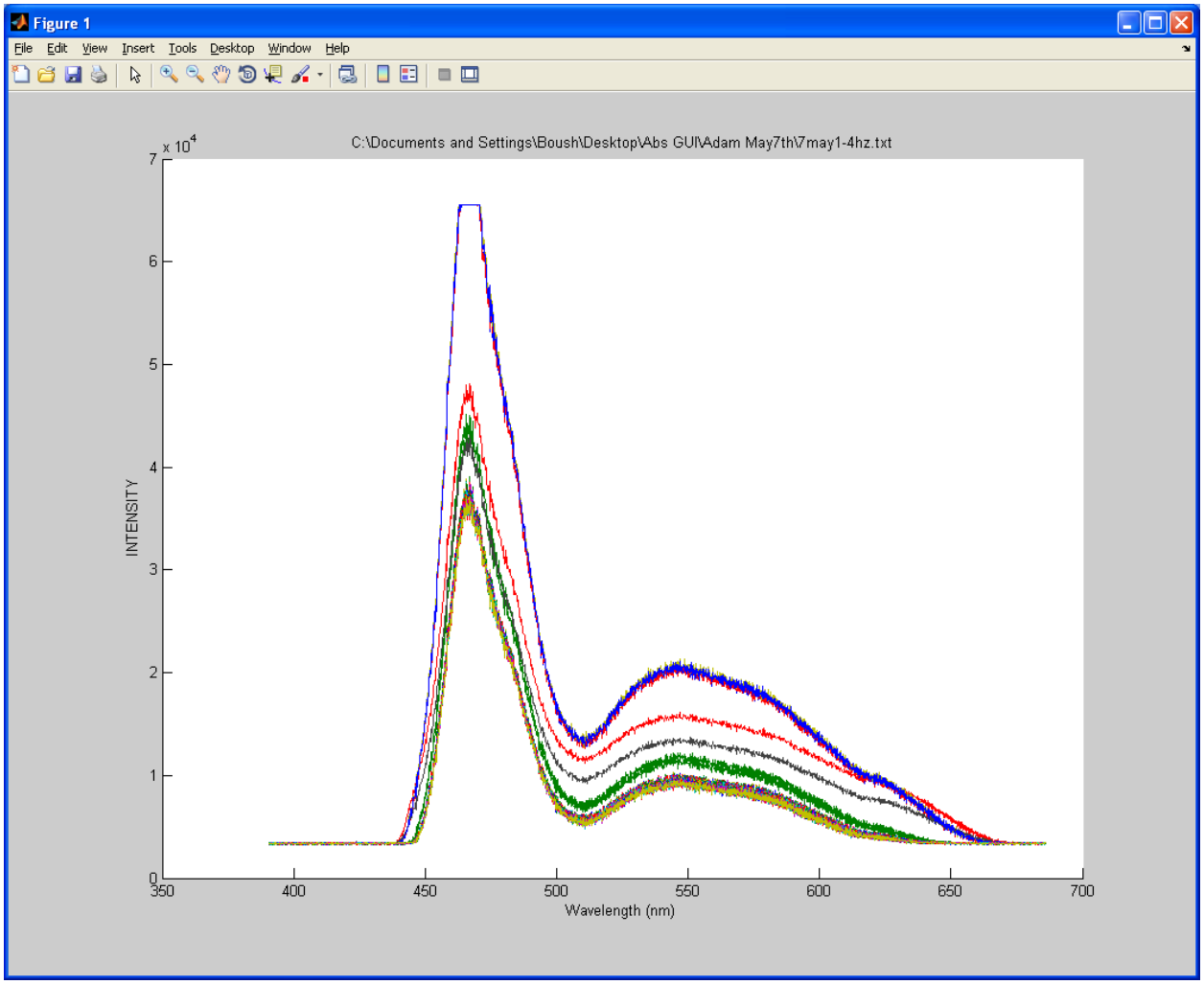


**Figure A1-4. Raw data plot of cell number 7**

The "Plots" box also has a selection for "Plot Pixel in Time/Clean". Five different cells are plotted in time using that setting and shown in Figure A1-5. By typing "1 2 5 7 10" into the text box for "Cell Number" the Cells 1, 2, 5, 7 and 10 were plotted in time. The radio button "Type

Wavelength" was selected in the box "Pixel Choice". The wavelength of interest, 466 nm, is then typed into the text box "Wavelength". This selects this pixel that will be plotted in time.

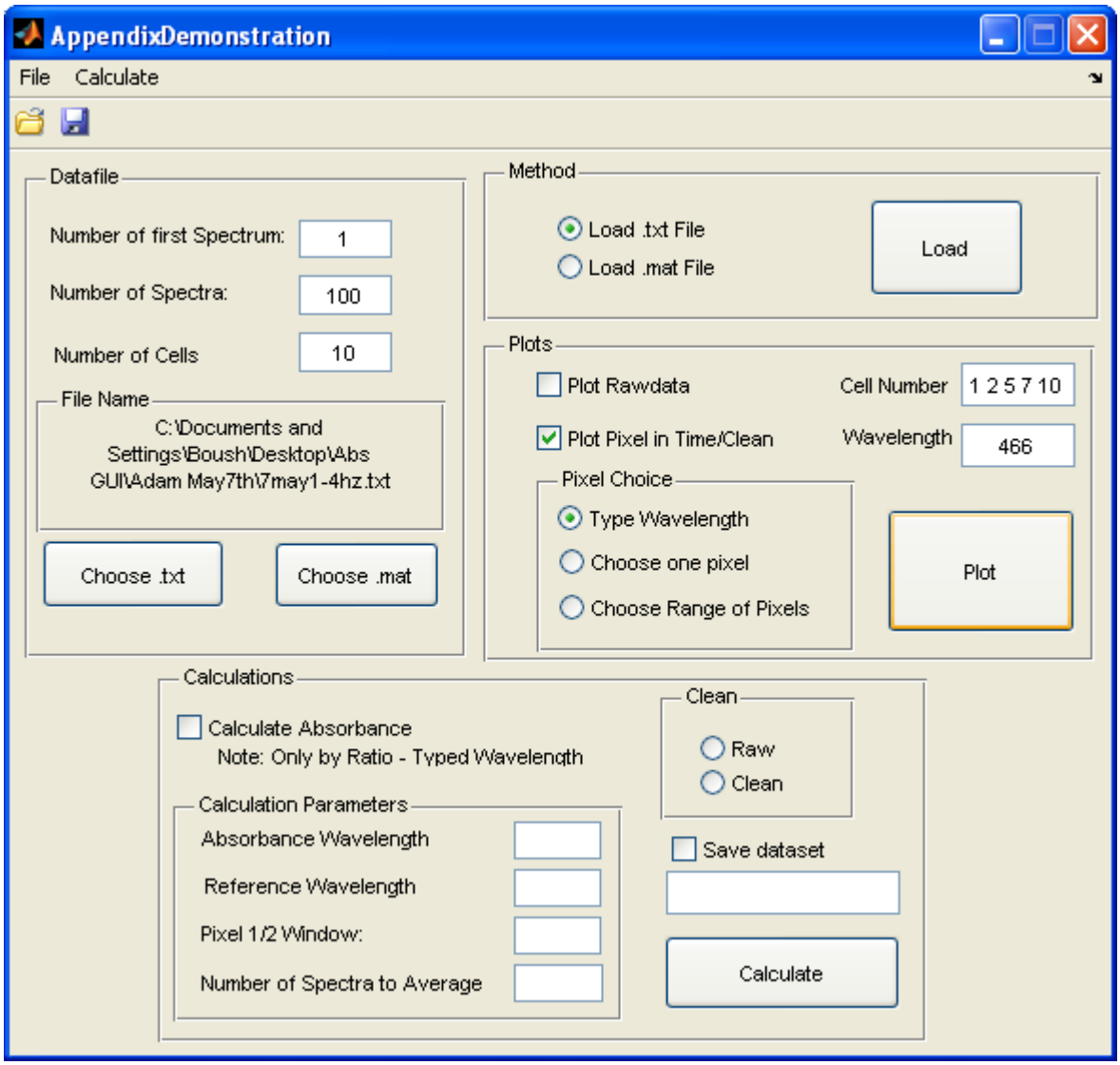


**Figure A1-5. Plotting a wavelength in time**
The input box for Cell Number will split the input string using the space character (i.e. " ") as a delimiter in order to plot multiple cells at the same time.

The plot that was generated by the input of Figure A1-5 is shown in Figure A1-6 with time as the x-axis in seconds and intensity on the y-axis in counts. The cells 1, 2, 5, 7 and 10 are shown. The spoiled spectra are as the outliers from the five lines between 3.5 and 4.5 x $10^4$ counts.

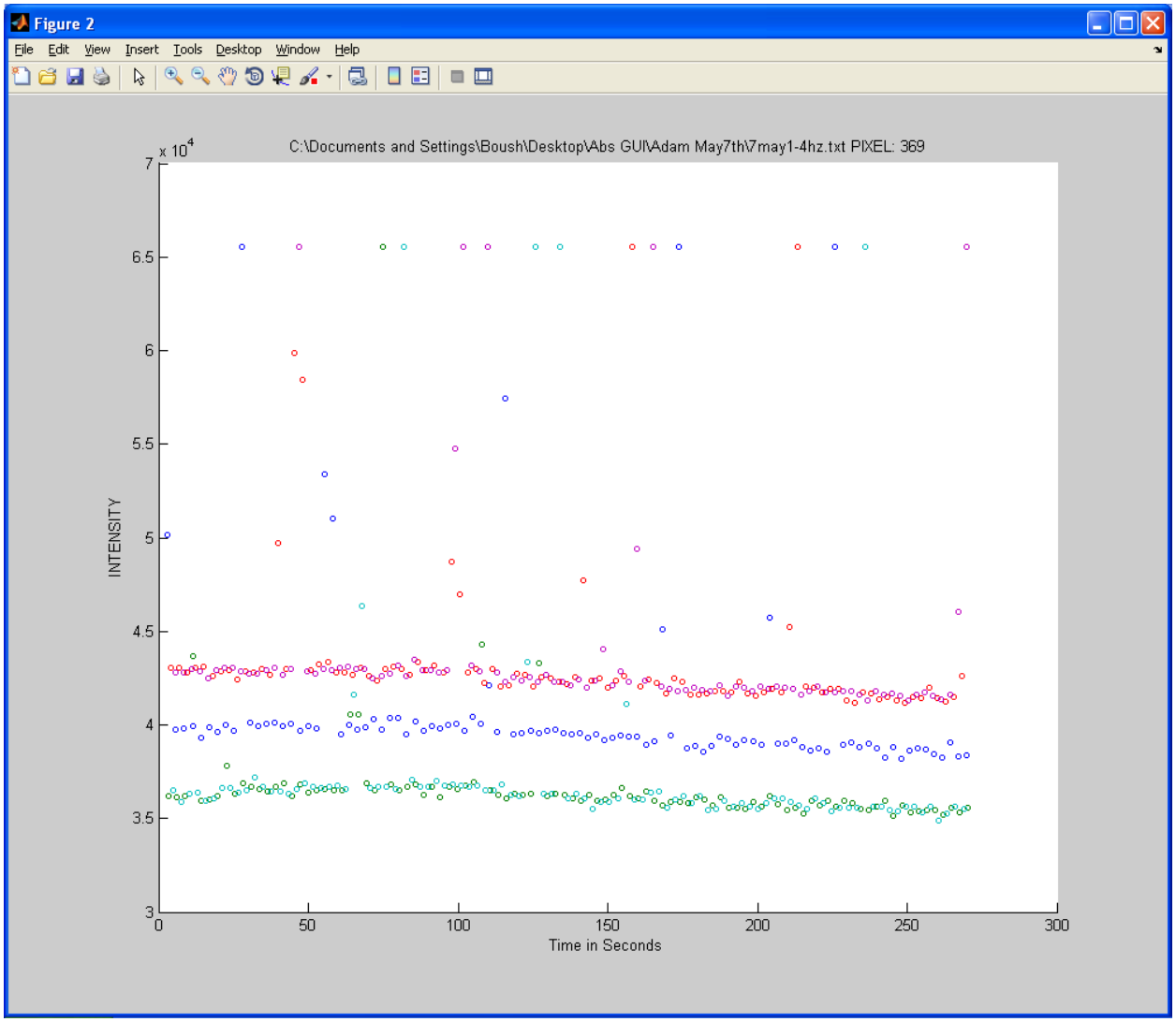


**Figure A1-6. Plotting cells 1, 2, 5, 7, 10 in time at 466 nm**
466 nm wavelength corresponds to pixel 369 in the USB4000 spectrometer. Thus the label in the title which contains the file location for this raw data set concatenated with "PIXEL: 369".

In order to remove spoiled spectra, the "Calculations" box is used and "Calculate Absorbance" is selected. In the box "Calculation Parameters", "Absorbance Wavelength" is the wavelength of interest. The setup as described in this thesis used an absorbing wavelength of 466 because it was the highest intensity wavelength of the LED white light source. The "Reference Wavelength" was the non-absorbing wavelength to use for the ratiometric method. The "Reference Wavelength" was also used to remove spoiled spectra by histogram. In the

demonstration for this appendix a reference wavelength of 550 nm was selected. However, any non-absorbing wavelength would return the same removal of spoiled spectra and calculated absorbance. In the earlier chapters of this thesis, multiple reference wavelengths were employed for different calculations. In Chapter 2, the calculation for the dilution of yellow dye used a wavelength of 542 nm and the calculations for the bromothymol blue used reference wavelengths of 600 and 640 nm. In Chapter 3, the calculation of absorbance was done with a reference wavelength of 545 nm.

In the box "Calculation Parameters", "Pixel ½ Window" determines how many pixels will be averaged together for the calculation. If "0" (zero) is entered into the text box then it will use only the pixel of the absorbing wavelength. If "1" (one) is entered into the text box then it will use a three pixel bandpass. If "2" (two) is entered then it will use a five pixel bandpass. "Number of Spectra to Average" determines for how many spectra to average for the calculation of absorbance.

In the box "Clean" the radio button "Clean" must be selected in order to remove spoiled spectra. If "Raw" was selected then there would be no removal of spoiled spectra for the calculation of absorbance. The removal of spoiled spectra was performed using the reference wavelength input in the calculation parameters and executed when the "Calculate" button is clicked. The setup for calculations can be seen in Figure A1-7.

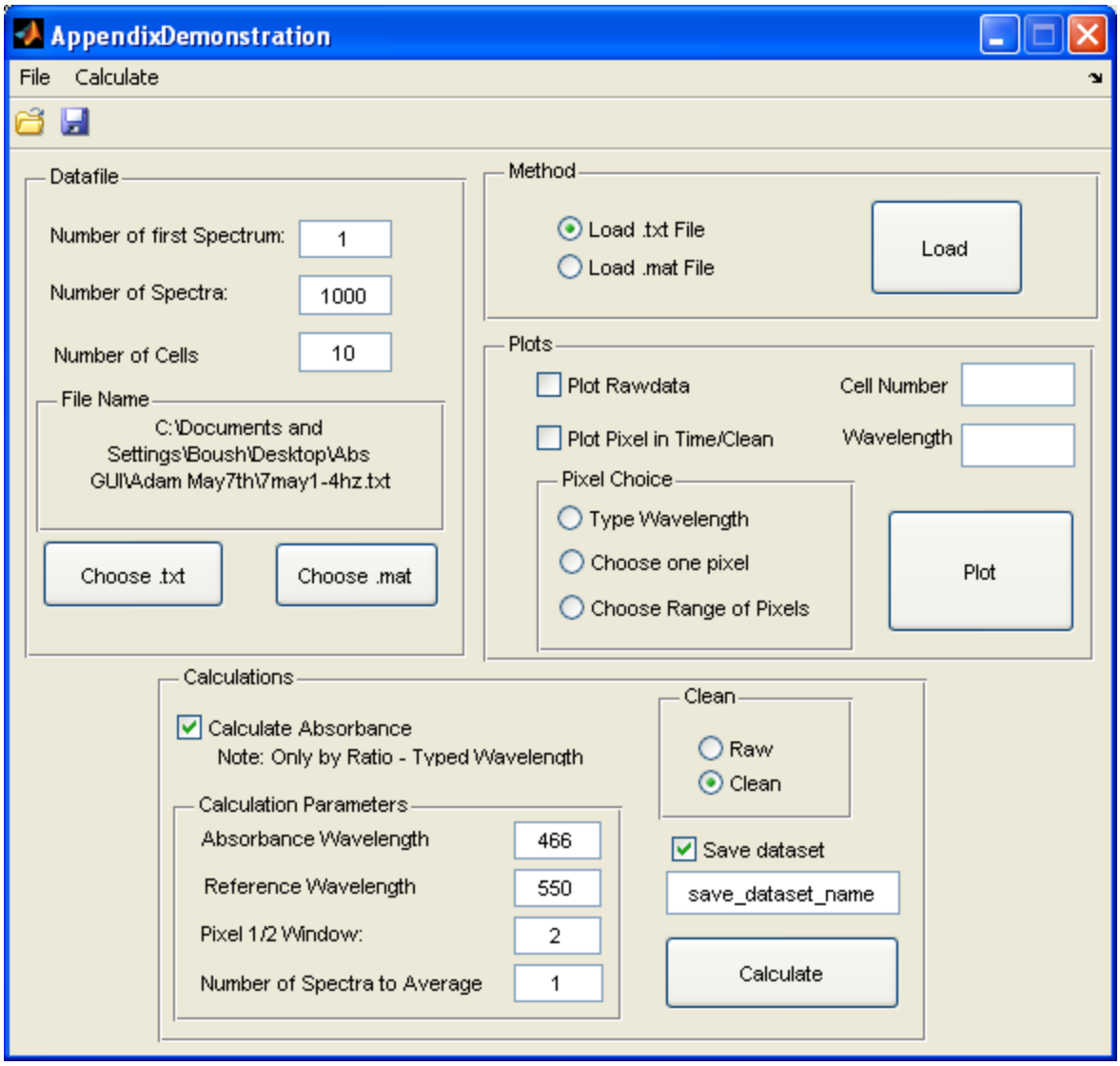


**Figure A1-7. GUI inputs for the removal of spoiled spectra and calculation of absorbance**

The resulting spectra from the calculation set up in Figure A1-7 can be seen in Figure A1-8. There are two plots of the data array; (1) pre-removal of spoiled spectra and (2) post-removal of spoiled spectra. In the MATLAB workspace, the data array is replaced when it is modified by calculations. Also, there are two histogram plots which show the distribution of light intensity in cell number 7 at the reference wavelength.

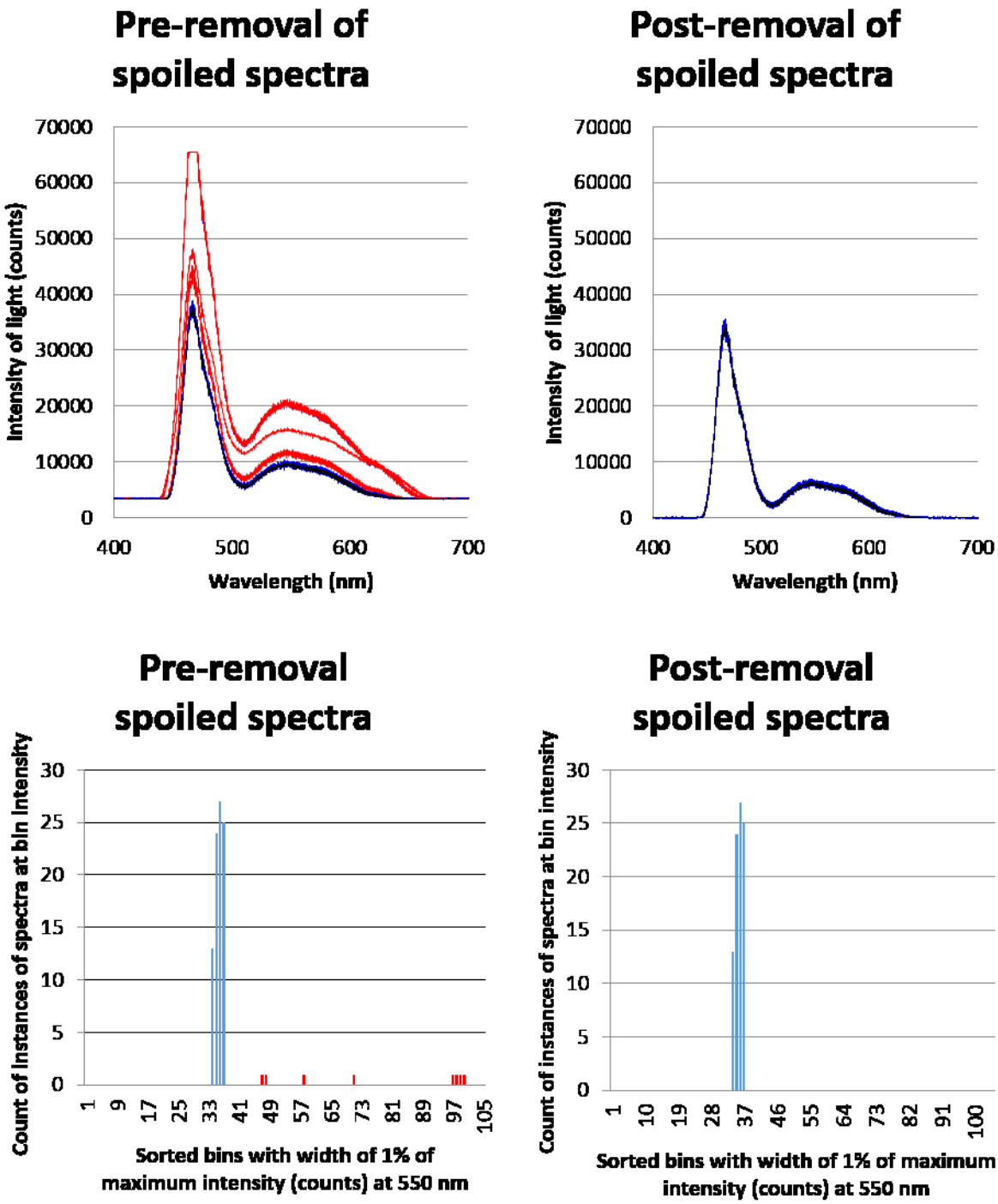


**Figure A1-8. Plot of spectra before and after the removal of spoiled spectra by histogram**
The spoiled spectra that will be removed by the histogram removal are marked as red in the plots. The spectra that will remain in the dataset are marked in blue. The program removed eight spoiled spectra from cell number 7 using the histogram plot.

The calculation of absorbance would be done when “Save dataset” was selected and a file name typed into the adjacent empty text field. Without the “Save dataset” checkbox selected the code executed on pressing “Calculate” would only remove spoiled spectra. The saved data was an array with the number of removed spoiled spectra, the absorbance at the absorbing wavelength, the standard deviation of the absorbance and the signal to noise ratio. This data was saved for every cell in the dataset. The output of the array was input into Excel worksheets for subsequent calculations as seen in Chapters 2 and 3 of this thesis. Additionally, when troubleshooting the system, or preparing figures such as Figure A1-8, the MATLAB code was supplemented with the function “xlswrite” to save data of interest to an excel template.

# Appendix 2 – Complete MATLAB code

## Interface 48

```
function varargout = interface48(varargin)
% INTERFACE48 MATLAB code for interface48.fig
%      INTERFACE48, by itself, creates a new INTERFACE48 or raises the
existing
%      singleton*.
%
%      H = INTERFACE48 returns the handle to a new INTERFACE48 or the handle
to
%      the existing singleton*.
%
%      INTERFACE48('CALLBACK',hObject,eventData,handles,...) calls the local
%      function named CALLBACK in INTERFACE48.M with the given input
arguments.
%
%      INTERFACE48('Property','Value',...) creates a new INTERFACE48 or
raises the
%      existing singleton*.  Starting from the left, property value pairs are
%      applied to the GUI before interface48_OpeningFcn gets called.  An
%      unrecognized property name or invalid value makes property application
%      stop.  All inputs are passed to interface48_OpeningFcn via varargin.
%
%      *See GUI Options on GUIDE's Tools menu.  Choose "GUI allows only one
%      instance to run (singleton)".
%
% See also: GUIDE, GUIDATA, GUIHANDLES

% Edit the above text to modify the response to help interface48

% Last Modified by GUIDE v2.5 23-May-2013 12:10:07

% Begin initialization code - DO NOT EDIT
gui_Singleton = 1;
gui_State = struct('gui_Name',       mfilename, ...
    'gui_Singleton',  gui_Singleton, ...
    'gui_OpeningFcn', @interface48_OpeningFcn, ...
    'gui_OutputFcn',  @interface48_OutputFcn, ...
    'gui_LayoutFcn',  [] , ...
    'gui_Callback',   []);
if nargin && ischar(varargin{1})
    gui_State.gui_Callback = str2func(varargin{1});
end

if nargout
    [varargout{1:nargout}] = gui_mainfcn(gui_State, varargin{:});
else
    gui_mainfcn(gui_State, varargin{:});
end
% End initialization code - DO NOT EDIT
```

```
% --- Executes just before interface48 is made visible.
function interface48_OpeningFcn(hObject, eventdata, handles, varargin)
% This function has no output args, see OutputFcn.
% hObject    handle to figure
% eventdata  reserved - to be defined in a future version of MATLAB
% handles    structure with handles and user data (see GUIDATA)
% varargin   command line arguments to interface48 (see VARARGIN)

% Choose default command line output for interface48
handles.output = hObject;
handles.percentage = 0;
handles.remove_percentage = 0;
handles.firstime = 0;
handles. = 0;
handles.samplingrate = 0;

% Update handles structure
guidata(hObject, handles);

% UIWAIT makes interface48 wait for user response (see UIRESUME)
% uiwait(handles.figure1);

% --- Outputs from this function are returned to the command line.
function varargout = interface48_OutputFcn(hObject, eventdata, handles)
% varargout  cell array for returning output args (see VARARGOUT);
% hObject    handle to figure
% eventdata  reserved - to be defined in a future version of MATLAB
% handles    structure with handles and user data (see GUIDATA)

% Get default command line output from handles structure
varargout{1} = handles.output;

% --- Executes during object creation, after setting all properties.
function abswavelength_box_CreateFcn(hObject, eventdata, handles)
% hObject    handle to abswavelength (see GCBO)
% eventdata  reserved - to be defined in a future version of MATLAB
% handles    empty - handles not created until after all CreateFcns called

% Hint: edit controls usually have a white background on Windows.
%       See ISPC and COMPUTER.
if ispc && isequal(get(hObject,'BackgroundColor'),
get(0,'defaultUicontrolBackgroundColor'))
    set(hObject,'BackgroundColor','white');
end

% --- Executes during object creation, after setting all properties.
function rawdata_CreateFcn(hObject, eventdata, handles)
% hObject    handle to rawdata (see GCBO)
% eventdata  reserved - to be defined in a future version of MATLAB
% handles    empty - handles not created until after all CreateFcns called

function firstspectrum_Callback(hObject, eventdata, handles)
% hObject    handle to firstspectrum (see GCBO)
% eventdata  reserved - to be defined in a future version of MATLAB
% handles    structure with handles and user data (see GUIDATA)
```

```
% Hints: get(hObject,'String') returns contents of firstspectrum as text
%        str2double(get(hObject,'String')) returns contents of firstspectrum
as a double

firstspectrum = str2double(get(hObject, 'String'));
if isnan(firstspectrum)
    set(hObject, 'String', 0);
    errordlg('Input must be a number','Error');
end

handles.firstspectrum = firstspectrum;
guidata(hObject,handles)

% --- Executes during object creation, after setting all properties.
function firstspectrum_CreateFcn(hObject, eventdata, handles)
% hObject    handle to firstspectrum (see GCBO)
% eventdata  reserved - to be defined in a future version of MATLAB
% handles    empty - handles not created until after all CreateFcns called

% Hint: edit controls usually have a white background on Windows.
%       See ISPC and COMPUTER.
if ispc && isequal(get(hObject,'BackgroundColor'),
get(0,'defaultUicontrolBackgroundColor'))
    set(hObject,'BackgroundColor','white');
end

function numspectra_box_Callback(hObject, eventdata, handles)
% hObject    handle to numspectra_box (see GCBO)
% eventdata  reserved - to be defined in a future version of MATLAB
% handles    structure with handles and user data (see GUIDATA)

% Hints: get(hObject,'String') returns contents of numspectra_box as text
%        str2double(get(hObject,'String')) returns contents of numspectra_box
as a double

numspectra = str2double(get(hObject, 'String'));
numspectra = numspectra+1;
if isnan(numspectra)
    set(hObject, 'String', 0);
    errordlg('Input must be a number','Error');
end

% Save the new numspectra value
handles.numspectra = numspectra;
guidata(hObject,handles)

% --- Executes during object creation, after setting all properties.
function numspectra_box_CreateFcn(hObject, eventdata, handles)
% hObject    handle to numspectra_box (see GCBO)
% eventdata  reserved - to be defined in a future version of MATLAB
% handles    empty - handles not created until after all CreateFcns called

% Hint: edit controls usually have a white background on Windows.
%       See ISPC and COMPUTER.
```

```
if ispc && isequal(get(hObject,'BackgroundColor'),
get(0,'defaultUicontrolBackgroundColor'))
    set(hObject,'BackgroundColor','white');
end

% --- Executes during object creation, after setting all properties.
function numcells_box_CreateFcn(hObject, eventdata, handles)
% hObject    handle to numcells_box (see GCBO)
% eventdata  reserved - to be defined in a future version of MATLAB
% handles    empty - handles not created until after all CreateFcns called

% Hint: edit controls usually have a white background on Windows.
%       See ISPC and COMPUTER.
if ispc && isequal(get(hObject,'BackgroundColor'),
get(0,'defaultUicontrolBackgroundColor'))
    set(hObject,'BackgroundColor','white');
end

function numcells_box_Callback(hObject, eventdata, handles)
% hObject    handle to numcells_box (see GCBO)
% eventdata  reserved - to be defined in a future version of MATLAB
% handles    structure with handles and user data (see GUIDATA)

% Hints: get(hObject,'String') returns contents of numcells_box as text
%        str2double(get(hObject,'String')) returns contents of numcells_box
as a double
numcells = str2double(get(hObject, 'String'));
if isnan(numcells)
    set(hObject, 'String', 0);
    errordlg('Input must be a number','Error');
end

% Save the new numcells value
handles.numcells = numcells;
guidata(hObject,handles)


% --- Executes during object creation, after setting all properties.
function loadfastspectra_CreateFcn(hObject, eventdata, handles)
% hObject    handle to loadfastspectra (see GCBO)
% eventdata  reserved - to be defined in a future version of MATLAB
% handles    empty - handles not created until after all CreateFcns called

% --- Executes on button press in loadfastspectra.
function loadfastspectra_Callback(hObject, eventdata, handles)
% hObject    handle to loadfastspectra (see GCBO)
% eventdata  reserved - to be defined in a future version of MATLAB
% handles    structure with handles and user data (see GUIDATA)

handles.firstime = handles.firstime + 1;

if handles.method == 1

    %numspectra = handles.numspectra;
    q = handles.numcells;
    q = handles.numspectra;
```

```
    [rawdata, wavelengths, timestamps] =
loadfastspectra(handles.firstspectrum,
handles.numspectra,handles.choosefile);

    [rawdata, timestamps] = deletedoubles(rawdata, timestamps);

    %save ('zrawdatafile', 'rawdata')
    %save ('ztimestamps', 'timestamps')

    [rawdata] = cellseparation(rawdata, handles.numcells);
    [timestamps] = cellseparation(timestamps, handles.numcells);

    %save ('zcellsrawdata', 'rawdata')
    %save ('zcellstimestamps', 'timestamps')

    %SAVING ALL THE UPCOMING VARIABLES
    %initialize = 1;
    %save('z_numdeleted' , 'initialize')

    % Save the new rawdata value
    handles.wavelengths = wavelengths;
    handles.rawdata = rawdata;
    handles.timestamps = timestamps;

elseif handles.method ==2

    %x = load( fullfile(handles.choosefile2))
    load(handles.choosefile2);
    x = rawdata_variable{1};

    handles.abswavelength = x(1);
    set(handles.abswavelength_box, 'String', x(1))
    handles.refwavelength = x(2);
    set(handles.refwavelength_box, 'String', x(2))
    handles.windowpixels = x(3);
    set(handles.windowpixels_box, 'String', x(3))
    handles.num_to_average = x(4);
    set(handles.num_to_average_box, 'String', x(4))
    handles.percentage = x(5); %Statitical Clean Value
    set(handles.percentage_box, 'String', x(5))
    handles.cellnumber2 = x(6);  %Which cell was the blank
    set(handles.cellnumber2_box, 'String', x(6))
    handles.numcells = x(7); %How many cells on the disk
    set(handles.numcells_box, 'String', x(7))
    handles.numspectra = x(8);
    disp_numspectra = x(8) - 1;
    set(handles.numspectra_box, 'String', disp_numspectra)
    handles.samplingrate = x(9);
    set(handles.samplingrate_box, 'String', x(9))
    handles.rpm = x(10);
    set(handles.rpm_box, 'String', x(10))

    handles.wavelengths = rawdata_variable{2};
    handles.timestamps = rawdata_variable{3};
```

```
    handles.rawdata = rawdata_variable{4};

    [handles.abswavelengths2] = calculationconditions2(handles.wavelengths,
handles.abswavelength ,handles.refwavelength, handles.windowpixels,
handles.num_to_average);

end

guidata(hObject,handles)

% --- Executes when selected object changed in method.
function method_SelectionChangeFcn(hObject, eventdata, handles)
% hObject    handle to the selected object in method
% eventdata  reserved - to be defined in a future version of MATLAB
% handles    structure with handles and user data (see GUIDATA)

if (hObject == handles.text_file_load)
    handles.method = 1;
    handles.text_file_load = 1;
elseif (hObject == handles.mat_file_load)
    handles.method = 2;
    handles.mat_file_load = 2;
end
guidata(hObject,handles)


%%%%%%%%%%%%%%%%%%%%%%%%%%%%%%%%%%%%%%%%%%%%%%%%%%%%%%%%%%%%%%%%%%%%%%%%%%%%
%ABSORBTION CODE BELOW
%%%%%%%%%%%%%%%%%%%%%%%%%%%%%%%%%%%%%%%%%%%%%%%%%%%%%%%%%%%%%%%%%%%%%%%%%%%%

function plotrawdatachoice_Callback(hObject, eventdata, handles)
% hObject    handle to plotrawdatachoice (see GCBO)
% eventdata  reserved - to be defined in a future version of MATLAB
% handles    structure with handles and user data (see GUIDATA)

% Hint: get(hObject,'Value') returns toggle state of plotrawdatachoice
handles.plotrawdatachoice = get(hObject, 'Value');

guidata(hObject,handles)

% --- Executes during object creation, after setting all properties.
function plot_CreateFcn(hObject, eventdata, handles)
% hObject    handle to plotrawdatachoice (see GCBO)
% eventdata  reserved - to be defined in a future version of MATLAB
% handles    empty - handles not created until after all CreateFcns called


% --- Executes on button press in plotrawdatachoice.
function plot_Callback(hObject, eventdata, handles)
% hObject    handle to plotrawdatachoice (see GCBO)
% eventdata  reserved - to be defined in a future version of MATLAB
% handles    structure with handles and user data (see GUIDATA)
if (handles.plotrawdatachoice == 1)
    plotspectra(handles.wavelengths, handles.rawdata, handles.choosefile,
handles.cellnumber);
```

```
end

if (handles.plotpixelintime == 1)
    pixel = 100;
    if (handles.pixelchoice == 1)
        plotspectra(handles.wavelengths, handles.rawdata, handles.choosefile,
handles.cellnumber);

        x = ginput(1);
        y = round(x);
        [pixel] = wavelength_to_pixel(handles.wavelengths, y(1,1));

        d = handles.rawdata{handles.cellnumber}(pixel,:);
        plotintime(handles.wavelengths, d, handles.choosefile, pixel,
handles.timestamps{handles.cellnumber});


    elseif (handles.pixelchoice == 2)
        plotspectra(handles.wavelengths, handles.rawdata, handles.choosefile,
handles.cellnumber);

        x = ginput(2);
        y = round(x);

        pixels = y(:,1);

        [pixel1] = wavelength_to_pixel(handles.wavelengths, y(1,1));
        [pixel2] = wavelength_to_pixel(handles.wavelengths, y(2,1));

        c = handles.rawdata{handles.cellnumber}([pixel1:pixel2],:) ;
        d = mean(c);

        plotintime(handles.wavelengths, d, handles.choosefile, pixel);
        %ACTIVATE THIS CODE IF YOU WOULD LIKE TO DELETE SPECTRA ABOVE A
        %CERTAIN LEVEL**************************************************

        x = ginput(1);
        y = round(x);
        threshold = y(1,2);

        cleanedindex = find(d < threshold);
        cleaned = handles.rawdata(:,cleanedindex);
        handles.rawdata = cleaned;

        plot(handles.wavelengths([1:1500],:),cleaned([1:1500],:))
        title([handles.choosefile ' PIXELS: ' num2str(pixels')])
        ylabel('INTENSITY')
        xlabel('Wavelength (nm)')

    elseif (handles.pixelchoice == 3)
        plotspectra(handles.wavelengths, handles.rawdata, handles.choosefile,
handles.cellnumber);

        [pixel] = wavelength_to_pixel(handles.wavelengths,
handles.wavelength_plotintime);
```

```
        % d = handles.rawdata{handles.cellnumber}(pixel,:);

        plotintime(handles.wavelengths, handles.rawdata, handles.choosefile,
pixel, handles.timestamps, handles.cellnumber);


    else
        figure
        plot(handles.rawdata(pixel,:))
        title([handles.choosefile ' PIXEL: ' num2str(pixel)])
        ylabel('INTENSITY')
        xlabel('SPECTRUM #')

        rounded = round(handles.wavelengths);
        set(gca,'XTick', [1:50:1500])
        set(gca,'XTickLabel', rounded(1:50:1500))
    end
end
guidata(hObject,handles)

% --- Executes during object creation, after setting all properties.
function plotpixelintime_CreateFcn(hObject, eventdata, handles)
% hObject    handle to plotpixelintime (see GCBO)
% eventdata  reserved - to be defined in a future version of MATLAB
% handles    empty - handles not created until after all CreateFcns called


% --- Executes on button press in plotpixelintime.
function plotpixelintime_Callback(hObject, eventdata, handles)
% hObject    handle to plotpixelintime (see GCBO)
% eventdata  reserved - to be defined in a future version of MATLAB
% handles    structure with handles and user data (see GUIDATA)

% Hint: get(hObject,'Value') returns toggle state of plotpixelintime

handles.plotpixelintime = get(hObject,'Value');
guidata(hObject,handles)


% --- Executes on button press in choosefile.
function choosefile_Callback(hObject, eventdata, handles)
% hObject    handle to choosefile (see GCBO)
% eventdata  reserved - to be defined in a future version of MATLAB
% handles    structure with handles and user data (see GUIDATA)
[files path] = getfiles('%/*.txt');
handles.choosefile = files{1};
handles.choosefilepath = path ;

set(handles.filename, 'String', handles.choosefile);
guidata(hObject,handles);

% --- Executes during object creation, after setting all properties.
function choosefile_CreateFcn(hObject, eventdata, handles)
% hObject    handle to choosefile (see GCBO)
```

```
% eventdata  reserved - to be defined in a future version of MATLAB
% handles    empty - handles not created until after all CreateFcns called


% --- Executes during object creation, after setting all properties.
function filename_CreateFcn(hObject, eventdata, handles)
% hObject    handle to filename (see GCBO)
% eventdata  reserved - to be defined in a future version of MATLAB
% handles    empty - handles not created until after all CreateFcns called

%************************************************************
%Menu Buttons
%************************************************************

% --------------------------------------------------------------------
function File_Callback(hObject, eventdata, handles)
% hObject    handle to File (see GCBO)
% eventdata  reserved - to be defined in a future version of MATLAB
% handles    structure with handles and user data (see GUIDATA)

% --------------------------------------------------------------------
function New_Callback(hObject, eventdata, handles)
% hObject    handle to New (see GCBO)
% eventdata  reserved - to be defined in a future version of MATLAB
% handles    structure with handles and user data (see GUIDATA)
interface8

% --------------------------------------------------------------------
function Save_Callback(hObject, eventdata, handles)
% hObject    handle to Save (see GCBO)
% eventdata  reserved - to be defined in a future version of MATLAB
% handles    structure with handles and user data (see GUIDATA)
save('saved', 'handles') ;
guidata(hObject,handles)

% --------------------------------------------------------------------
function load_Callback(hObject, eventdata, handles)
% hObject    handle to load (see GCBO)
% eventdata  reserved - to be defined in a future version of MATLAB
% handles    structure with handles and user data (see GUIDATA)
load('saved', 'handles');
guidata(hObject,handles)


%************************************************************
%CALCULATION BOX

% --- Executes on button press in calculateabsorbance.
function calculateabsorbance_Callback(hObject, eventdata, handles)
% hObject    handle to calculateabsorbance (see GCBO)
% eventdata  reserved - to be defined in a future version of MATLAB
% handles    structure with handles and user data (see GUIDATA)

% Hint: get(hObject,'Value') returns toggle state of calculateabsorbance
handles.calculateabsorbance = get(hObject,'Value');
guidata(hObject,handles)
```

```
% --- Executes on button press in calculateabsorbance2.
function calculateabsorbance2_Callback(hObject, eventdata, handles)
% hObject    handle to calculateabsorbance2 (see GCBO)
% eventdata  reserved - to be defined in a future version of MATLAB
% handles    structure with handles and user data (see GUIDATA)

% Hint: get(hObject,'Value') returns toggle state of calculateabsorbance2

handles.calculateabsorbance2 = get(hObject,'Value');
guidata(hObject,handles)

% --- Executes on button press in calculatebutton.
function calculatebutton_Callback(hObject, eventdata, handles)
% hObject    handle to calculatebutton (see GCBO)
% eventdata  reserved - to be defined in a future version of MATLAB
% handles    structure with handles and user data (see GUIDATA)

%CALCULATE TEXT_FILE_LOAD BY CLICKING ON TWO
WAVELENGTHS**********************
if (handles.calculateabsorbance == 1)

    if (handles.wavelengthinput == 1)

        plotspectra(handles.wavelengths, handles.rawdata, handles.choosefile,
handles.cellnumber2)

        x = ginput(2);
        y = round(x);
        [y(1,1)] = wavelength_to_pixel(handles.wavelengths, y(1,1));
        [y(2,1)] = wavelength_to_pixel(handles.wavelengths, y(2,1));

        handles.abswavelengths = y(:,1);
        handles.abswavelengths(3,1) = 0;
        handles.abswavelengths(4,1) = 1;

        [handles.blankspectrumavg, handles.ratio] =
calcratio(handles.abswavelengths,handles.rawdata, handles.cellnumber2);


    elseif (handles.wavelengthinput == 2)
        plotspectra(handles.wavelengths, handles.rawdata, handles.choosefile,
handles.cellnumber2)
        j = handles.plotabsorbancespectra;
        [handles.transmitance,handles.abscalculated,handles.absorbancedone] =
calcabsorbance(handles.ratio, handles.abswavelengths ,handles.rawdata,
handles.cellnumber2, j);
    end
end
%*************************************************************************
%CALCULATE TEXT_FILE_LOAD BY TYPING IN TWO WAVELENGTHS AND SUMMING VARIABLES

if handles.cleanselection == 1
    if (handles.calculateabsorbance2 == 1)
        if (handles.wavelengthinput2 == 1)
```

```
            plotspectra(handles.wavelengths, handles.rawdata,
handles.choosefile, handles.cellnumber2)
            [handles.abswavelengths2] =
calculationconditions2(handles.wavelengths, handles.abswavelength
,handles.refwavelength, handles.windowpixels, handles.num_to_average);

            i = 1;
            for x = [1:1: handles.numcells]
                [handles.rawdata{i}, handles.timestamps{i}] = sumspectra(
handles.rawdata{i}, handles.timestamps{i}, handles.abswavelengths2);
                i = i+1;
            end

            [handles.blankspectrumavg, handles.ratio] =
calcratio(handles.abswavelengths2,handles.rawdata, handles.cellnumber2);
            set(handles.blankratio_box, 'String', handles.ratio)

        elseif (handles.wavelengthinput2 == 2)

            i = 1;
            for x = [1:1: handles.numcells]
                [handles.rawdata{i}, handles.timestamps{i}] = sumspectra(
handles.rawdata{i}, handles.timestamps{i}, handles.abswavelengths2);
                i = i+1;
            end

            plotspectra(handles.wavelengths, handles.rawdata,
handles.choosefile, handles.cellnumber2);
            i=1;
            j = handles.plotabsorbancespectra;
            for x = [1:1:handles.numcells]

[handles.transmitance,handles.abscalculated{i},handles.absorbancedone] =
calcabsorbance(handles.ratio, handles.abswavelengths2 ,handles.rawdata, i,
j);
                i=i+1;
                j=0;
            end
            pixel = 0;
        end
    end
    set(handles.numcleaned,'string',num2str(0));

elseif handles.cleanselection == 2 %IF THE CHOICE CLEAN IS MADE DO IT HERE
    if (handles.calculateabsorbance2 == 1)
        if (handles.wavelengthinput2 == 1)
            plotspectra(handles.wavelengths, handles.rawdata,
handles.choosefile, handles.cellnumber2);
            [handles.abswavelengths2] =
calculationconditions2(handles.wavelengths, handles.abswavelength,
handles.refwavelength, handles.windowpixels, handles.num_to_average);
            %CLEANING FUNCTION**********************

            remove_percentage_Callback(hObject, eventdata, handles)
            i = 1;
            for x = [1:1:handles.numcells]
```

```
                [handles.rawdata{i}, numdeleted{i}, handles.timestamps{i}] =
cleaning(handles.rawdata, handles.wavelengths, handles.abswavelengths2, i,
handles.remove_percentage, handles.percentage, handles.timestamps);
                i = i+1;
            end

set(handles.numcleaned,'string',num2str(numdeleted{handles.cellnumber2}));

            i = 1;
            for x = [1:1: handles.numcells]
                [handles.rawdata{i}, handles.timestamps{i}] = sumspectra(
handles.rawdata{i}, handles.timestamps{i}, handles.abswavelengths2);
                i = i+1;
            end

            %**************************************
            plotspectra(handles.wavelengths, handles.rawdata,
handles.choosefile, handles.cellnumber2);
            i = 1;
            for x = [1:1:handles.numcells]
                [handles.blankspectrumavg, handles.ratio_cells{i}] =
calcratio(handles.abswavelengths2,handles.rawdata, i);
                i = i+1;
            end
            handles.ratio = handles.ratio_cells{handles.cellnumber2};
            set(handles.blankratio_box, 'String', handles.ratio)

        elseif (handles.wavelengthinput2 == 2)
            plotspectra(handles.wavelengths, handles.rawdata,
handles.choosefile, handles.cellnumber2)
            %CLEANING FUNCTION**********************
            i = 1;

            [handles.abswavelengths2] =
calculationconditions2(handles.wavelengths, handles.abswavelength
,handles.refwavelength, handles.windowpixels, handles.num_to_average);

            remove_percentage_Callback(hObject, eventdata, handles)

            for x = [1:1:handles.numcells]
                [handles.rawdata{i}, numdeleted{i}, handles.timestamps{i}] =
cleaning(handles.rawdata, handles.wavelengths, handles.abswavelengths2, i,
handles.remove_percentage, handles.percentage, handles.timestamps);
                i = i+1;
            end


set(handles.numcleaned,'string',num2str(numdeleted{handles.cellnumber2}));
            i = 1;

            for x = [1:1: handles.numcells]
                [handles.rawdata{i}, handles.timestamps{i}] = sumspectra(
handles.rawdata{i}, handles.timestamps{i}, handles.abswavelengths2);
                i = i+1;
            end
```

```
            %************************************
            i=1;
            j = handles.plotabsorbancespectra;

            for x = [1:1:handles.numcells]

[handles.transmitance{i},handles.abscalculated{i},handles.absorbancedone] =
calcabsorbance(handles.ratio, handles.abswavelengths2 ,handles.rawdata, i,
j);
                i = i+1;
                j=0;
            end
            pixel = 0;
        end
    end
  %  save ('z_numdeleted', 'numdeleted')
end

%CALCULATE AND SAVE THE AVG, STDEV AND S/N OF ALL CELL NUMBERS
if(handles.absorbancedone ==1)

    if (handles.store_avg_stdev_sn == 1)
        i = 1;
        for x = [1:1:handles.numcells]
            [all_cells_abs_sn2{i}] = calc_sn(handles.abscalculated{i},
handles.absavgdisplay, handles.stddevdisplay, handles.signoisedisplay,
numdeleted{i});
            i = i+1;
        end
        i = 1;

        for x = [1:1:handles.numcells]
            j = 1;
            for y = [1:1:4]
                all_cells_abs_sn(j,i) = all_cells_abs_sn2{i}(j,1);
                j = j+1;
            end
            i = i+1;
        end
        save (handles.savefile, 'all_cells_abs_sn')
    end
end

%CALCULATE AND DISPLAY THE TEXT_FILE_LOAD STANDARD DEVIATION AND S/N OF THE
%SELECTED CELL NUMBER.
if (handles.absorbancedone == 1)
    if (handles.calculatesn == 1)
        [one_cell_abs_sn] = calc_sn
(handles.abscalculated{handles.cellnumber2}, handles.absavgdisplay,
handles.stddevdisplay, handles.signoisedisplay,
handles.numdeleted{handle.scellnumber2});
    end
end
```

```
%PLOT THE TEXT_FILE_LOAD SPECTRUM WITH NO RATIO
if handles.plotabsorbancespectra ==1
    i = 1;
    for x = [1:1:handles.numcells]
        [absorbancespectra2{i}] = calcabsspectra(handles.rawdata,
handles.blankspectrumavg, i);
        i = i+1;
    end
    plotspectra(handles.wavelengths, absorbancespectra2, handles.choosefile,
handles.cellnumber2)
end

%Save the dataset
if handles.storedataset == 1
    initialize2 = 1;
    % save (handles.savedatasetname, 'initialize2')
    x = handles.abswavelength;
    y = handles.refwavelength;
    z = handles.windowpixels;
    m = handles.num_to_average;
    n = handles.percentage; %Statitical Clean Value
    o = handles.cellnumber2; %Which cell was the blank
    p = handles.numcells; %How many cells on the disk
    q = handles.numspectra;
    r = handles.samplingrate;
    s = handles.rpm;

    rawdata_variable{1} = [ x y z m n o p q r s];
    rawdata_variable{2} = handles.wavelengths;
    rawdata_variable{3} = handles.timestamps;
    rawdata_variable{4} = handles.rawdata;
    save (handles.savedatasetname, 'rawdata_variable')
end

if handles.plotFFT == 1
    i = 1;

    samplingrate = handles.samplingrate;
    rpm = handles.rpm;
    rpm_hz = rpm/60;
    numcells = handles.numcells;
    fraction_rotation = 1/numcells;

    corrected_samplingrate = samplingrate+(rpm_hz/fraction_rotation);

    [pixel] = wavelength_to_pixel(handles.wavelengths,
handles.abswavelength);

    for x = [1:1:handles.numcells]
        [handles.fftdata{i}, handles.f] =
simplefft(handles.rawdata{i}(pixel,:), corrected_samplingrate) ;
        i = i+1;
    end
end

handles.calculatebutton = get(hObject, 'Value');
```

```
guidata(hObject,handles)

% --- Executes when selected object is changed in wavelengthinput.
function wavelengthinput_SelectionChangeFcn(hObject, eventdata, handles)
% hObject    handle to the selected object in wavelengthinput
% eventdata  structure with the following fields (see UIBUTTONGROUP)
%   EventName: string 'SelectionChanged' (read only)
%   OldValue: handle of the previously selected object or empty if none was
selected
%   NewValue: handle of the currently selected object
% handles    structure with handles and user data (see GUIDATA)

if (hObject == handles.blank)
    handles.wavelengthinput = 1;
elseif (hObject == handles.sample)
    handles.wavelengthinput = 2;
end
guidata(hObject,handles)

% --- Executes when selected object is changed in wavelengthinput2.
function wavelengthinput2_SelectionChangeFcn(hObject, eventdata, handles)
% hObject    handle to the selected object in wavelengthinput2
% eventdata  structure with the following fields (see UIBUTTONGROUP)
%   EventName: string 'SelectionChanged' (read only)
%   OldValue: handle of the previously selected object or empty if none was
selected
%   NewValue: handle of the currently selected object
% handles    structure with handles and user data (see GUIDATA)

if (hObject == handles.blank2)
    handles.wavelengthinput2 = 1;
elseif (hObject == handles.sample2)
    handles.wavelengthinput2 = 2;
end

guidata(hObject,handles)

% --- Executes on button press in calculatesn.
function calculatesn_Callback(hObject, eventdata, handles)
% hObject    handle to calculatesn (see GCBO)
% eventdata  reserved - to be defined in a future version of MATLAB
% handles    structure with handles and user data (see GUIDATA)

% Hint: get(hObject,'Value') returns toggle state of calculatesn

handles.calculatesn = get(hObject, 'Value');
guidata(hObject,handles)

% --- Executes during object creation, after setting all properties.
function calculateabsorbance_CreateFcn(hObject, eventdata, handles)
% hObject    handle to calculateabsorbance (see GCBO)
% eventdata  reserved - to be defined in a future version of MATLAB
% handles    empty - handles not created until after all CreateFcns called

% --- Executes during object creation, after setting all properties.
function calculatebutton_CreateFcn(hObject, eventdata, handles)
```

```
% hObject    handle to calculatebutton (see GCBO)
% eventdata  reserved - to be defined in a future version of MATLAB
% handles    empty - handles not created until after all CreateFcns called

% --- Executes during object creation, after setting all properties.
function calculatesn_CreateFcn(hObject, eventdata, handles)
% hObject    handle to calculatesn (see GCBO)
% eventdata  reserved - to be defined in a future version of MATLAB
% handles    empty - handles not created until after all CreateFcns called

handles.absorbancedone = 0;

guidata(hObject,handles)

% --- Executes during object creation, after setting all properties.
function wavelengthinput_CreateFcn(hObject, eventdata, handles)
% hObject    handle to wavelengthinput (see GCBO)
% eventdata  reserved - to be defined in a future version of MATLAB
% handles    empty - handles not created until after all CreateFcns called

% --- Executes during object creation, after setting all properties.
function blank_CreateFcn(hObject, eventdata, handles)
% hObject    handle to blank (see GCBO)
% eventdata  reserved - to be defined in a future version of MATLAB
% handles    empty - handles not created until after all CreateFcns called

% --- Executes during object creation, after setting all properties.
function sample_CreateFcn(hObject, eventdata, handles)
% hObject    handle to sample (see GCBO)
% eventdata  reserved - to be defined in a future version of MATLAB
% handles    empty - handles not created until after all CreateFcns called


% --- Executes during object creation, after setting all properties.
function absavgdisplay_CreateFcn(hObject, eventdata, handles)
% hObject    handle to absavgdisplay (see GCBO)
% eventdata  reserved - to be defined in a future version of MATLAB
% handles    empty - handles not created until after all CreateFcns called


% --- Executes during object creation, after setting all properties.
function stddevdisplay_CreateFcn(hObject, eventdata, handles)
% hObject    handle to stddevdisplay (see GCBO)
% eventdata  reserved - to be defined in a future version of MATLAB
% handles    empty - handles not created until after all CreateFcns called


% --- Executes during object creation, after setting all properties.
function signoisedisplay_CreateFcn(hObject, eventdata, handles)
% hObject    handle to signoisedisplay (see GCBO)
% eventdata  reserved - to be defined in a future version of MATLAB
% handles    empty - handles not created until after all CreateFcns called


% --- Executes on button press in plotabsorbancespectra.
```

```
function plotabsorbancespectra_Callback(hObject, eventdata, handles)
% hObject    handle to plotabsorbancespectra (see GCBO)
% eventdata  reserved - to be defined in a future version of MATLAB
% handles    structure with handles and user data (see GUIDATA)

% Hint: get(hObject,'Value') returns toggle state of plotabsorbancespectra

handles.plotabsorbancespectra = get(hObject, 'Value');
guidata(hObject,handles)


% --- Executes during object creation, after setting all properties.
function plotabsorbancespectra_CreateFcn(hObject, eventdata, handles)
% hObject    handle to plotabsorbancespectra (see GCBO)
% eventdata  reserved - to be defined in a future version of MATLAB
% handles    empty - handles not created until after all CreateFcns called


% --- Executes when selected object is changed in cleanselection.
function cleanselection_SelectionChangeFcn(hObject, eventdata, handles)
% hObject    handle to the selected object in cleanselection
% eventdata  structure with the following fields (see UIBUTTONGROUP)
%   EventName: string 'SelectionChanged' (read only)
%   OldValue: handle of the previously selected object or empty if none was
selected
%   NewValue: handle of the currently selected object
% handles    structure with handles and user data (see GUIDATA)
if (hObject == handles.stayraw)
    handles.cleanselection = 1;
elseif (hObject == handles.cleanspectra)
    handles.cleanselection = 2;
end
handles.percentage_choosen = 0;
guidata(hObject,handles)


% --- Executes during object creation, after setting all properties.
function stayraw_CreateFcn(hObject, eventdata, handles)
% hObject    handle to stayraw (see GCBO)
% eventdata  reserved - to be defined in a future version of MATLAB
% handles    empty - handles not created until after all CreateFcns called


% --- Executes during object creation, after setting all properties.
function cleanspectra_CreateFcn(hObject, eventdata, handles)
% hObject    handle to cleanspectra (see GCBO)
% eventdata  reserved - to be defined in a future version of MATLAB
% handles    empty - handles not created until after all CreateFcns called


% --- Executes during object creation, after setting all properties.
function numcleaned_CreateFcn(hObject, eventdata, handles)
% hObject    handle to numcleaned (see GCBO)
% eventdata  reserved - to be defined in a future version of MATLAB
% handles    empty - handles not created until after all CreateFcns called
```

```
guidata(hObject,handles)



function cellnumber_Callback(hObject, eventdata, handles)
% hObject    handle to cellnumber (see GCBO)
% eventdata  reserved - to be defined in a future version of MATLAB
% handles    structure with handles and user data (see GUIDATA)

% Hints: get(hObject,'String') returns contents of cellnumber as text
%        str2double(get(hObject,'String')) returns contents of cellnumber as
a double

cellnumberstring = get(hObject, 'String');
%cellnumber = str2double(cellnumberstring)
cellnumber = str2num(cellnumberstring);

if isnan(cellnumber)
    set(hObject, 'String', 0);
    errordlg('Input must be a number','Error');
end

handles.cellnumber = cellnumber;
guidata(hObject,handles)


% --- Executes during object creation, after setting all properties.
function cellnumber_CreateFcn(hObject, eventdata, handles)
% hObject    handle to cellnumber (see GCBO)
% eventdata  reserved - to be defined in a future version of MATLAB
% handles    empty - handles not created until after all CreateFcns called

% Hint: edit controls usually have a white background on Windows.
%       See ISPC and COMPUTER.
if ispc && isequal(get(hObject,'BackgroundColor'),
get(0,'defaultUicontrolBackgroundColor'))
    set(hObject,'BackgroundColor','white');
end

% --- Executes during object creation, after setting all properties.
function pixelchoice_CreateFcn(hObject, eventdata, handles)
% hObject    handle to pixelchoice (see GCBO)
% eventdata  reserved - to be defined in a future version of MATLAB
% handles    empty - handles not created until after all CreateFcns called

function cellnumber2_box_Callback(hObject, eventdata, handles)
% hObject    handle to cellnumber2_box (see GCBO)
% eventdata  reserved - to be defined in a future version of MATLAB
% handles    structure with handles and user data (see GUIDATA)

% Hints: get(hObject,'String') returns contents of cellnumber2_box as text
%        str2double(get(hObject,'String')) returns contents of
cellnumber2_box as a double
cellnumber2 = str2double(get(hObject, 'String'));
```

```
if isnan(cellnumber2)
    set(hObject, 'String', 0);
    errordlg('Input must be a number','Error');
end

handles.cellnumber2 = cellnumber2;
guidata(hObject,handles)

% --- Executes during object creation, after setting all properties.
function cellnumber2_box_CreateFcn(hObject, eventdata, handles)
% hObject    handle to cellnumber2_box (see GCBO)
% eventdata  reserved - to be defined in a future version of MATLAB
% handles    empty - handles not created until after all CreateFcns called

% Hint: edit controls usually have a white background on Windows.
%       See ISPC and COMPUTER.
if ispc && isequal(get(hObject,'BackgroundColor'),
get(0,'defaultUicontrolBackgroundColor'))
    set(hObject,'BackgroundColor','white');
end

% --- Executes on button press in store_avg_stdev_sn.
function store_avg_stdev_sn_Callback(hObject, eventdata, handles)
% hObject    handle to store_avg_stdev_sn (see GCBO)
% eventdata  reserved - to be defined in a future version of MATLAB
% handles    structure with handles and user data (see GUIDATA)

% Hint: get(hObject,'Value') returns toggle state of store_avg_stdev_sn

handles.store_avg_stdev_sn = get(hObject, 'Value');
guidata(hObject,handles)

function refwavelength_box_Callback(hObject, eventdata, handles)
% hObject    handle to refwavelength_box (see GCBO)
% eventdata  reserved - to be defined in a future version of MATLAB
% handles    structure with handles and user data (see GUIDATA)

% Hints: get(hObject,'String') returns contents of refwavelength_box as text
%        str2double(get(hObject,'String')) returns contents of
refwavelength_box as a double

refwavelength = str2double(get(hObject, 'String'));
if isnan(refwavelength)
    set(hObject, 'String', 0);
    errordlg('Input must be a number','Error');
end

handles.refwavelength = refwavelength;
guidata(hObject,handles)


% --- Executes during object creation, after setting all properties.
function refwavelength_box_CreateFcn(hObject, eventdata, handles)
% hObject    handle to refwavelength_box (see GCBO)
% eventdata  reserved - to be defined in a future version of MATLAB
% handles    empty - handles not created until after all CreateFcns called
```

```
% Hint: edit controls usually have a white background on Windows.
%       See ISPC and COMPUTER.
if ispc && isequal(get(hObject,'BackgroundColor'),
get(0,'defaultUicontrolBackgroundColor'))
    set(hObject,'BackgroundColor','white');
end


function abswavelength_box_Callback(hObject, eventdata, handles)
% hObject    handle to abswavelength (see GCBO)
% eventdata  reserved - to be defined in a future version of MATLAB
% handles    structure with handles and user data (see GUIDATA)

% Hints: get(hObject,'String') returns contents of abswavelength as text
%        str2double(get(hObject,'String')) returns contents of abswavelength
as a double

abswavelength = str2double(get(hObject, 'String'));
if isnan(abswavelength)
    set(hObject, 'String', 0);
    errordlg('Input must be a number','Error');
end

handles.abswavelength = abswavelength;
guidata(hObject,handles)


function windowpixels_box_Callback(hObject, eventdata, handles)
% hObject    handle to windowpixels_box (see GCBO)
% eventdata  reserved - to be defined in a future version of MATLAB
% handles    structure with handles and user data (see GUIDATA)

% Hints: get(hObject,'String') returns contents of windowpixels_box as text
%        str2double(get(hObject,'String')) returns contents of
windowpixels_box as a double

windowpixels = str2double(get(hObject, 'String'));
if isnan(windowpixels)
    set(hObject, 'String', 0);
    errordlg('Input must be a number','Error');
end

handles.windowpixels = windowpixels;
guidata(hObject,handles)

% --- Executes during object creation, after setting all properties.
function windowpixels_box_CreateFcn(hObject, eventdata, handles)
% hObject    handle to windowpixels_box (see GCBO)
% eventdata  reserved - to be defined in a future version of MATLAB
% handles    empty - handles not created until after all CreateFcns called

% Hint: edit controls usually have a white background on Windows.
%       See ISPC and COMPUTER.
```

```
if ispc && isequal(get(hObject,'BackgroundColor'),
get(0,'defaultUicontrolBackgroundColor'))
    set(hObject,'BackgroundColor','white');
end


function num_to_average_box_Callback(hObject, eventdata, handles)
% hObject    handle to num_to_average_box (see GCBO)
% eventdata  reserved - to be defined in a future version of MATLAB
% handles    structure with handles and user data (see GUIDATA)

% Hints: get(hObject,'String') returns contents of num_to_average_box as text
%        str2double(get(hObject,'String')) returns contents of
num_to_average_box as a double
num_to_average = str2double(get(hObject, 'String'));
if isnan(num_to_average)
    set(hObject, 'String', 0);
    errordlg('Input must be a number','Error');
end

handles.num_to_average = num_to_average;
guidata(hObject,handles)

% --- Executes during object creation, after setting all properties.
function num_to_average_box_CreateFcn(hObject, eventdata, handles)
% hObject    handle to num_to_average_box (see GCBO)
% eventdata  reserved - to be defined in a future version of MATLAB
% handles    empty - handles not created until after all CreateFcns called

% Hint: edit controls usually have a white background on Windows.
%       See ISPC and COMPUTER.
if ispc && isequal(get(hObject,'BackgroundColor'),
get(0,'defaultUicontrolBackgroundColor'))
    set(hObject,'BackgroundColor','white');
end

% --- Executes when selected object is changed in pixelchoice.
function pixelchoice_SelectionChangeFcn(hObject, eventdata, handles)
% hObject    handle to the selected object in pixelchoice
% eventdata  structure with the following fields (see UIBUTTONGROUP)
%   EventName: string 'SelectionChanged' (read only)
%   OldValue: handle of the previously selected object or empty if none was
selected
%   NewValue: handle of the currently selected object
% handles    structure with handles and user data (see GUIDATA)

if (hObject == handles.choose1pixel)
    handles.pixelchoice = 1;
elseif (hObject == handles.chooserangepixel)
    handles.pixelchoice = 2;
elseif (hObject == handles.typewavelength)
    handles.pixelchoice = 3;
end

guidata(hObject,handles)
```

```
% --- Executes during object creation, after setting all properties.
function chooserangepixel_CreateFcn(hObject, eventdata, handles)
% hObject    handle to chooserangepixel (see GCBO)
% eventdata  reserved - to be defined in a future version of MATLAB
% handles    empty - handles not created until after all CreateFcns called


% --- Executes during object creation, after setting all properties.
function choose1pixel_CreateFcn(hObject, eventdata, handles)
% hObject    handle to choose1pixel (see GCBO)
% eventdata  reserved - to be defined in a future version of MATLAB
% handles    empty - handles not created until after all CreateFcns called



function savefile_Callback(hObject, eventdata, handles)
% hObject    handle to savefile (see GCBO)
% eventdata  reserved - to be defined in a future version of MATLAB
% handles    structure with handles and user data (see GUIDATA)

% Hints: get(hObject,'String') returns contents of savefile as text
%        str2double(get(hObject,'String')) returns contents of savefile as a
double
savefile = get(hObject, 'String');

handles.savefile = savefile;
guidata(hObject,handles)



% --- Executes during object creation, after setting all properties.
function savefile_CreateFcn(hObject, eventdata, handles)
% hObject    handle to savefile (see GCBO)
% eventdata  reserved - to be defined in a future version of MATLAB
% handles    empty - handles not created until after all CreateFcns called

% Hint: edit controls usually have a white background on Windows.
%       See ISPC and COMPUTER.
if ispc && isequal(get(hObject,'BackgroundColor'),
get(0,'defaultUicontrolBackgroundColor'))
    set(hObject,'BackgroundColor','white');
end


% --- Executes on button press in storedataset.
function storedataset_Callback(hObject, eventdata, handles)
% hObject    handle to storedataset (see GCBO)
% eventdata  reserved - to be defined in a future version of MATLAB
% handles    structure with handles and user data (see GUIDATA)

% Hint: get(hObject,'Value') returns toggle state of storedataset
handles.storedataset = get(hObject, 'Value');
guidata(hObject,handles)
```

```
function savedatasetname_Callback(hObject, eventdata, handles)
% hObject    handle to savedatasetname (see GCBO)
% eventdata  reserved - to be defined in a future version of MATLAB
% handles    structure with handles and user data (see GUIDATA)

% Hints: get(hObject,'String') returns contents of savedatasetname as text
%        str2double(get(hObject,'String')) returns contents of
savedatasetname as a double
savedatasetname = get(hObject, 'String');

handles.savedatasetname = savedatasetname;
guidata(hObject,handles)




% --- Executes during object creation, after setting all properties.
function savedatasetname_CreateFcn(hObject, eventdata, handles)
% hObject    handle to savedatasetname (see GCBO)
% eventdata  reserved - to be defined in a future version of MATLAB
% handles    empty - handles not created until after all CreateFcns called

% Hint: edit controls usually have a white background on Windows.
%       See ISPC and COMPUTER.
if ispc && isequal(get(hObject,'BackgroundColor'),
get(0,'defaultUicontrolBackgroundColor'))
    set(hObject,'BackgroundColor','white');
end



function wavelength_plotintime_Callback(hObject, eventdata, handles)
% hObject    handle to wavelength_plotintime (see GCBO)
% eventdata  reserved - to be defined in a future version of MATLAB
% handles    structure with handles and user data (see GUIDATA)

% Hints: get(hObject,'String') returns contents of wavelength_plotintime as
text
%        str2double(get(hObject,'String')) returns contents of
wavelength_plotintime as a double

wavelength_plotintime = str2double(get(hObject, 'String'));
if isnan(wavelength_plotintime)
    set(hObject, 'String', 0);
    errordlg('Input must be a number','Error');
end

handles.wavelength_plotintime = wavelength_plotintime;
guidata(hObject,handles)



% --- Executes during object creation, after setting all properties.
```

```
function wavelength_plotintime_CreateFcn(hObject, eventdata, handles)
% hObject    handle to wavelength_plotintime (see GCBO)
% eventdata  reserved - to be defined in a future version of MATLAB
% handles    empty - handles not created until after all CreateFcns called

% Hint: edit controls usually have a white background on Windows.
%       See ISPC and COMPUTER.
if ispc && isequal(get(hObject,'BackgroundColor'),
get(0,'defaultUicontrolBackgroundColor'))
    set(hObject,'BackgroundColor','white');
end


% --- Executes on button press in remove_percentage.
function remove_percentage_Callback(hObject, eventdata, handles)
% hObject    handle to remove_percentage (see GCBO)
% eventdata  reserved - to be defined in a future version of MATLAB
% handles    structure with handles and user data (see GUIDATA)

% Hint: get(hObject,'Value') returns toggle state of remove_percentage
remove_percentage = get(hObject, 'Value');

handles.remove_percentage = remove_percentage;
guidata(hObject,handles)


function percentage_box_Callback(hObject, eventdata, handles)
% hObject    handle to percentage_box (see GCBO)
% eventdata  reserved - to be defined in a future version of MATLAB
% handles    structure with handles and user data (see GUIDATA)

% Hints: get(hObject,'String') returns contents of percentage_box as text
%        str2double(get(hObject,'String')) returns contents of percentage_box
as a double
percentage = str2double(get(hObject, 'String'));
if isnan(percentage)
    set(hObject, 'String', 0);
    errordlg('Input must be a number','Error');
end

handles.percentage = percentage;
guidata(hObject,handles)

% --- Executes during object creation, after setting all properties.
function percentage_box_CreateFcn(hObject, eventdata, handles)
% hObject    handle to percentage_box (see GCBO)
% eventdata  reserved - to be defined in a future version of MATLAB
% handles    empty - handles not created until after all CreateFcns called

% Hint: edit controls usually have a white background on Windows.
%       See ISPC and COMPUTER.
if ispc && isequal(get(hObject,'BackgroundColor'),
get(0,'defaultUicontrolBackgroundColor'))
    set(hObject,'BackgroundColor','white');
end
```

```
% --- Executes on button press in choosefile2.
function choosefile2_Callback(hObject, eventdata, handles)
% hObject    handle to choosefile2 (see GCBO)
% eventdata  reserved - to be defined in a future version of MATLAB
% handles    structure with handles and user data (see GUIDATA)
[files path] = getfiles('%/*.mat');
handles.choosefile2 = files{1};
handles.choosefile2path = path;

set(handles.filename, 'String', handles.choosefile2);
guidata(hObject,handles);


% --- Executes on button press in plotFFT.
function plotFFT_Callback(hObject, eventdata, handles)
% hObject    handle to plotFFT (see GCBO)
% eventdata  reserved - to be defined in a future version of MATLAB
% handles    structure with handles and user data (see GUIDATA)

% Hint: get(hObject,'Value') returns toggle state of plotFFT
handles.plotFFT = get(hObject, 'Value');
guidata(hObject,handles)



function samplingrate_box_Callback(hObject, eventdata, handles)
% hObject    handle to samplingrate_box (see GCBO)
% eventdata  reserved - to be defined in a future version of MATLAB
% handles    structure with handles and user data (see GUIDATA)

% Hints: get(hObject,'String') returns contents of samplingrate_box as text
%        str2double(get(hObject,'String')) returns contents of
samplingrate_box as a double
samplingrate = str2double(get(hObject, 'String'));
if isnan(samplingrate)
    set(hObject, 'String', 0);
    errordlg('Input must be a number','Error');
end

handles.samplingrate = samplingrate;
guidata(hObject,handles)


% --- Executes during object creation, after setting all properties.
function samplingrate_box_CreateFcn(hObject, eventdata, handles)
% hObject    handle to samplingrate_box (see GCBO)
% eventdata  reserved - to be defined in a future version of MATLAB
% handles    empty - handles not created until after all CreateFcns called

% Hint: edit controls usually have a white background on Windows.
%       See ISPC and COMPUTER.
if ispc && isequal(get(hObject,'BackgroundColor'),
get(0,'defaultUicontrolBackgroundColor'))
    set(hObject,'BackgroundColor','white');
end
```

```
function rpm_box_Callback(hObject, eventdata, handles)
% hObject    handle to rpm_box (see GCBO)
% eventdata  reserved - to be defined in a future version of MATLAB
% handles    structure with handles and user data (see GUIDATA)

% Hints: get(hObject,'String') returns contents of rpm_box as text
%        str2double(get(hObject,'String')) returns contents of rpm_box as a
double
rpm = str2double(get(hObject, 'String'));
if isnan(rpm)
    set(hObject, 'String', 0);
    errordlg('Input must be a number','Error');
end

handles.rpm = rpm;
guidata(hObject,handles)

% --- Executes during object creation, after setting all properties.
function rpm_box_CreateFcn(hObject, eventdata, handles)
% hObject    handle to rpm_box (see GCBO)
% eventdata  reserved - to be defined in a future version of MATLAB
% handles    empty - handles not created until after all CreateFcns called

% Hint: edit controls usually have a white background on Windows.
%       See ISPC and COMPUTER.
if ispc && isequal(get(hObject,'BackgroundColor'),
get(0,'defaultUicontrolBackgroundColor'))
    set(hObject,'BackgroundColor','white');
end



function blankratio_box_Callback(hObject, eventdata, handles)
% hObject    handle to blankratio_box (see GCBO)
% eventdata  reserved - to be defined in a future version of MATLAB
% handles    structure with handles and user data (see GUIDATA)

% Hints: get(hObject,'String') returns contents of blankratio_box as text
%        str2double(get(hObject,'String')) returns contents of blankratio_box
as a double
blankratio = str2double(get(hObject, 'String'));
if isnan(blankratio)
    set(hObject, 'String', 0);
    errordlg('Input must be a number','Error');
end

handles.ratio = blankratio;
guidata(hObject,handles)


% --- Executes during object creation, after setting all properties.
function blankratio_box_CreateFcn(hObject, eventdata, handles)
```

```
% hObject    handle to blankratio_box (see GCBO)
% eventdata  reserved - to be defined in a future version of MATLAB
% handles    empty - handles not created until after all CreateFcns called

% Hint: edit controls usually have a white background on Windows.
%       See ISPC and COMPUTER.
if ispc && isequal(get(hObject,'BackgroundColor'),
get(0,'defaultUicontrolBackgroundColor'))
    set(hObject,'BackgroundColor','white');
end


% --- Executes during object creation, after setting all properties.
function firstime_box_CreateFcn(hObject, eventdata, handles)
% hObject    handle to firstime_box (see GCBO)
% eventdata  reserved - to be defined in a future version of MATLAB
% handles    empty - handles not created until after all CreateFcns called
```

# Function 1: averagepixels.m

```
function [q1, q2] = averagepixels(abswavelengths ,rawdata, cellnumber)

w1 = [abswavelengths(1,1) - abswavelengths(3,1): abswavelengths(1,1) +
abswavelengths(3,1)];
w2 = [abswavelengths(2,1) - abswavelengths(3,1): abswavelengths(2,1) +
abswavelengths(3,1)];

if abswavelengths(3,1) == 0
    q1 = rawdata{cellnumber}(w1,:);
    q2 = rawdata{cellnumber}(w2,:);
else
    q1 = mean(rawdata{cellnumber}(w1,:));
    q2 = mean(rawdata{cellnumber}(w2,:));
end
```

# Function 2: calc_sn.m

```
function [A] = calc_sn(abscalculated, absavgdisplay, stddevdisplay,
signoisedisplay)

absavg = mean(abscalculated);
set(absavgdisplay,'string',num2str(absavg));
A(1,1) = absavg;

stdevabs = std(abscalculated);
set(stddevdisplay,'string',num2str(stdevabs));
A(2,1) = stdevabs;

signoise = absavg/stdevabs;
set(signoisedisplay,'string',num2str(signoise));
A(3,1) = signoise;
```

# Function 3: calcabsorbance.m

```
function [transmitance,abscalculated,absorbancedone] = calcabsorbance(ratio,
abswavelengths ,rawdata, cellnumber, plotabsorbancespectra)

dark = mean(mean(rawdata{cellnumber}([1700:1900],:)));

if abswavelengths(3,1) == 0
    if abswavelengths(4,1) == 1
        transmitance = ((rawdata{cellnumber}(abswavelengths(1,1),:))-
dark)./((ratio)*(rawdata{cellnumber}(abswavelengths(2,1),:)-dark));
    else
        [q1, q2] = averagepixels(abswavelengths ,rawdata, cellnumber);
        transmitance = (q1 - dark)./((ratio)*(q2-dark));
    end
else
    if abswavelengths(4,1) ==1
        [q1, q2] = averagepixels(abswavelengths ,rawdata, cellnumber);
        transmitance = (q1 - dark)./((ratio)*(q2-dark));
    else
        [q1,q2] = averagepixels(abswavelengths ,rawdata, cellnumber);
        [q1,q2] = sumspectra(q1, q2, abswavelengths);
        transmitance = (q1 - dark)./((ratio)*(q2-dark));
    end
end

d = transmitance;

abscalculated = -log10(d);

if plotabsorbancespectra ==1

    figure
    plot (abscalculated)
    title([abscalculated ' PIXELS: '])
    ylabel('Absorbance')
    xlabel('SPECTRUM #')

end

absorbancedone = 1;
```

# Function 4: calcratio.m

```
function [blankspectrumavg, ratio] = calcratio(abswavelengths ,rawdata,
cellnumber)

%if abswavelengths(4,1)~= 1
%    [q1,q2] = sumspectra(rawdata,timestamps, abswavelengths);
%end

[q1,q2] = averagepixels(abswavelengths ,rawdata, cellnumber);
```

```
dark = mean(mean(rawdata{cellnumber}([1700:1900],:)));

ratio = (mean(q1) - dark)/((mean(q2) - dark));

blankspectrumavg = mean(rawdata{cellnumber}');
```

## Function 5: calculationconditions2.m

```
function [y] = calculationconditions2(wavelengths, abswavelength,
refwavelength, windowpixel, num_to_average)

x = [abswavelength, refwavelength, windowpixel, num_to_average]';
y = round(x);

%change wavelength to pixel:
[y(1,1)] = wavelength_to_pixel(wavelengths, y(1,1));

[y(2,1)] = wavelength_to_pixel(wavelengths, y(2,1));
```

## Function 6: cellseparation.m

```
function [A] = cellseparation(original, numcells)
i = 1;
[m,n] = size(original);
for x = 1:1:numcells
    A{i} = original(:,[i:numcells:n]) ;
    [m,p] = size(A{i});
    A{i} = A{i}(:,[2:p]);
    i = i+1;
end
```

## Function 7: cleaning2.m

```
function [cleandata, numdeleted, cleanedtime] = cleaning(rawdata,
labelwavelengths, abswavelengths2, cellnumber, remove_percentage, percentage,
timestamps)

lngth = length(rawdata{cellnumber}(1,:));
wavelength = abswavelengths2(2,1);
numberpixels = abswavelengths2(3,1);

dark = mean(mean(rawdata{cellnumber}([1700:1900],:)));
rawdata{cellnumber} = rawdata{cellnumber}(:,:) - dark;

%WHERE I WILL BE DOING THE WAVELENGTH RANGE

if numberpixels == 0
    q = rawdata{cellnumber}(wavelength,:);
    w = wavelength;
else
    w = [wavelength - numberpixels: wavelength + numberpixels] ;
```

```
    q = mean(rawdata{cellnumber}(w,:));
end

boxwidth = max(rawdata{cellnumber}(wavelength,:))/100;

findbad = q;

maximum = max(findbad);

x = 0:boxwidth: (maximum+(boxwidth*5));
[histogramraw,xout] = hist(findbad,x);

figure
bar(histogramraw)
title('Histogram Rawdata')

maxhistogram = max(histogramraw);
[row,col] = find(histogramraw == maxhistogram);
i = col;
j = col;

i = i(1,1);
j = j(1,1);

test = 0;

while test==0;
    if histogramraw(i) ~=0;
        i = i +1;
    end
    if histogramraw(i) ==0;
        test = 1;
    end
end

while test==1;

    if histogramraw(j)==0
        test = 0;
    end
    if histogramraw(j)~=0
        if j <= 1 ;
            test = 0;
        end
        j = j-1;
    end
end

lowerindex = j;
upperindex = i-1;

lowintensity = (lowerindex*boxwidth+(boxwidth/2));
highintensity = (upperindex*boxwidth+(boxwidth/2));
%GOOD*********************************************
```

```
cleanedindex = find(findbad > lowintensity);
cleaned = rawdata{cellnumber}(:,cleanedindex);
rawdata{cellnumber} = cleaned;

cleanedtime = timestamps{cellnumber}(:,cleanedindex);
timestamps{cellnumber} = cleanedtime;


if numberpixels == 0
    findbad = rawdata{cellnumber}(w,:);
    w = wavelength;
else
    w = [wavelength - numberpixels: wavelength + numberpixels] ;
    findbad = mean(rawdata{cellnumber}(w,:));
end

cleanedindex = find(findbad <highintensity);

cleaned = rawdata{cellnumber}(:,cleanedindex);

rawdata{cellnumber} = cleaned;

cleandata = cleaned;

cleanedtime = timestamps{cellnumber}(:,cleanedindex);
timestamps{cellnumber} = cleanedtime;

cleanedtime = cleanedtime;

%figure
%plot(labelwavelengths, rawdata{cellnumber})
%title('Before t-test');
%************************************************************

if numberpixels == 0
    findbad = rawdata{cellnumber}(w,:);
    w = wavelength;
else
    w = [wavelength - numberpixels: wavelength + numberpixels] ;
    findbad = mean(rawdata{cellnumber}(w,:));
end
maximum = max(findbad);

[histogramclean,xout] = hist(findbad,x);

figure
bar(histogramclean)
title('Histogram cleandata')

%************************************************

standardeviation_of_the_blank = std(rawdata{cellnumber}(wavelength,:));

numdeleted = lngth - length(rawdata{cellnumber}(1,:));
```

# Function 8: deletedoubles.m

```
function [deleted_doubles_rawdata, deleted_doubles_timestamps] =
deletedoubles(rawdata, timestamps)

tooshort = 50;
numspectra = length(timestamps)-1;

for x = 3:1:numspectra
    test(1,x) = timestamps(1,x) - timestamps(1,x-1);
end

goodindexes = find(test > tooshort);
deleted_doubles_rawdata = rawdata(:,goodindexes);
deleted_doubles_timestamps = timestamps(1,goodindexes);
```

# Function 9: getfiles.m (By Alexei Kazarine)

```
function [ files path] = getfiles(filetype)
%Opens a dialog box for file selection and returns the path/name of all
%selected files.

%By Alexei Kazarine. Last updated 16/11/2012

%'%/*.txt'

   [files path] = uigetfile(filetype,'MultiSelect','on');

        if iscell(files) ==0
            temp = files;
            clear files;
            files{1}=temp;
        end


        for i =1:length(files)
            files{i} = [path files{i}] ;
        end


end
```

# Function 10: loadfastspectra.m

```
function
[alldata,wavelengths,timestamps]=loadfastspectra(start,numcolumns,filename);
%g=strcat(filename,'.txt');
g = filename;
m = start;
n1 = numcolumns;
```

```
n2 = n1+m;
a(:,[1:n1-1])=dlmread(g,'\t',[1000 m 3200 n2-2]);
alldata = a;

wavelengths = dlmread(g,'\t',[1000 0 3200 0]);
timestamps = dlmread(g,'\t',[0 0 0 n2-2]);
```

## Function 11: LoadingData.m

```
%LoadingData

x = importdata('data.txt', '\t');

y = x.textdata;

y(cellfun(@(y) any(isnan(y)),y)) = [];
```

## Function 12: plotintime.m

```
function plotintime(wavelengths, data, name, pixel, timestamps, cellnumber)

if pixel ~= 0

    figure
    hold on
    i = 1;
    while i <= length(cellnumber)
        x = timestamps{cellnumber(i)};
        x = x ./(10^3);
        y = data{cellnumber(i)}(pixel,:);

        scatter(x,y,3)

        title([name ' PIXEL: ' num2str(pixel)])
        ylabel('INTENSITY')
        xlabel('Time in Seconds')

        i = i+1;
    end

end
```

## Function 13: plotspectra.m

```
function plotspectra(wavelengths, data, name, cellnumber)

range = 1500;

figure
hold on
i = 1;
```

```
while i <= length(cellnumber)

    x = wavelengths([1:range],:);
    y = data{cellnumber(i)}([1:range],:);

    plot(x, y)
    ylabel('INTENSITY')
    xlabel('Wavelength (nm)')
    title(name)

    i = i+1;
end

hold off
```

## Function 14: plotting.m

```
function plotintime(wavelengths, data, name, pixel)

range = 1500;

figure
plot(wavelengths([1:range],:), data([1:range],:))
ylabel('INTENSITY')
xlabel('Wavelength (nm)')
title(name)
```

## Function 15: sumspectra.m

```
function [rawdata_summed, timestamps_summed] = sumspectra(q1, q2, y)
%q1 = rawdata
%q2 = timestamps

%summing up the number of spectra
lengthq2 = length(q2);
q1sm = [];
q2sm = [];
for count = 1:y(4,1):floor(lengthq2/y(4,1))*y(4,1)
    q1sm(:,end+1) = sum(q1(:,[count:(count+y(4,1)-1)]),2);
    q2sm(:,end+1) = sum(q2(:,[count:(count+y(4,1)-1)]),2);
end

rawdata_summed = q1sm;
timestamps_summed = q2sm;
```

## Function 16: wavelength_to_pixel.m

```
function [pixel] = wavelength_to_pixel(wavelengths, lambda)

roundedwavelength = round(wavelengths);
ind1 = find(roundedwavelength == lambda);
pixel = ind1(3,1);
```